# BENDING BEHAVIOR OF INSULATED FRP-CONFINED CONCRETE SANDWICH PANELS WITH FRP PLATE SHEAR CONNECTORS

A Thesis

Presented in Partial Fulfillment of the Requirements for the

Degree of Master of Science

with a

Major in Civil Engineering

in the

College of Graduate Studies

University of Idaho

by

Thomas G. Norris

May 2014

Major Professor: An Chen, Ph.D.

# AUTHORIZATION TO SUBMIT THESIS

This thesis of Thomas G. Norris, submitted for the degree of Master of Science with a Major in Civil Engineering and titled "Bending Behavior of Insulated FRP-Confined Concrete Sandwich Panels with FRP Plate Shear Connectors," has been reviewed in final form. Permission, as indicated by the signatures and dates below, is now granted to submit final copies to the College of Graduate Studies for approval.

Major Professor: _____ Date: _____
An Chen, Ph.D.

Committee Members: _____ Date: _____
Richard Nielsen, Ph.D.

_____ Date: _____
Pizhong Qiao, Ph.D.

_____ Date: _____
Fouad Bayomy, Ph.D.

Department Administrator: _____ Date: _____
Richard Nielsen, Ph.D.

Discipline's College Dean: _____ Date: _____
Larry Stauffer, Ph.D.

Final Approval and Acceptance

Dean of the College of Graduate Studies: _____ Date: _____
Jie Chen, Ph.D.

# ABSTRACT

Insulated concrete sandwich panels are composed of two concrete wythes separated by a layer of foam insulation, providing the dual function of load transferring and insulation. Extensive studies have been conducted on the effectiveness of the sandwich panels as structural wall elements using different shear connectors including steel wires, solid concrete zones, FRP ties, FRP shear grid, etc. Those studies have shown that the behavior of panels depends upon the composite action between the two concrete wythe provided by the shear connectors. The objective of the study is to study the bending behavior of sandwich panels, in terms of stiffness and strength, with FRP plate shear connectors (both with and without FRP plates externally bonded) and their applicability for roof/floor constructions, as well as their behavior with respect to creep when a sustained load is applied.

The following document will show that FRP plate shear connectors are a feasible option for sandwich panel application. Additionally, the application of external FRP plates provide a confining effect which results in a higher degree of composite action, supplies a water barrier to protect the concrete, and even limits creep deflection over time to a level below that of a typical solid concrete slab.

# ACKNOWLEDGEMENTS

I would like to thank the following individuals, groups, and organizations for their support and assistance in the completion of this study:

- Financial support from Higher Education Research Council (HERC), Idaho State Board of Education
- Technical support from Missouri Structural Composites, LLC.
- Material donation from Crane Composites, Inc.
- Dr. An Chen for encouraging, directing, and motivating me towards the completion of this thesis
- The CE 441: Reinforced Concrete Students—Fall 2012, University of Idaho, for their help in the production and testing of several specimens at the beginning of this study
- Nicolas Peña for all his work in helping to produce, test, analyze and interpret the results of this study

Without those mentioned above, this study would not have been possible.

# DEDICATION

I would like to dedicate this thesis to my mother and father, Sally & Rick, and my brothers, Stefan & Paul, for their unwavering love and support. Without their encouragement and motivating words & gestures during this process, I would not be where I am now.

I would also like to thank all of my friends for their highbrow humor and playful jabs, which helped me to relax and gain perspective when everything seemed overwhelming. Without them, this chapter in my life would have been infinitely more difficult.

# TABLE OF CONTENTS

# LIST OF FIGURES

# LIST OF TABLES

# LIST OF DEFINITIONS

ACI—American Concrete Institute

CE—Civil Engineering

DCA—Degree of Composite Action

E—Young's Modulus

EPS—Expanded Polystyrene

$f'_c$—Compressive Strength of Concrete

FPCS Panel—FRP-confined Precast Concrete Sandwich Panel

FRP—Fiber Reinforced Polymer

I—Moment of Inertia

LVDT—Linear Variable Differential Transformer

O.C.—On Center

$R^2$—Measure of how well data points fit a line or curve

RCSP—Reinforced Concrete Sandwich Panel

UI—University of Idaho

w/c—Water/Cement Ratio

Wet Bond—Applying concrete onto adhesive prior to the adhesive curing

XPS—Extruded Polystyrene

Ω—Ohm

# CHAPTER 1: INTRODUCTION

Insulated concrete sandwich panels are composed of two concrete wythes separated by a layer of foam insulation, providing the dual function of load transferring and insulation. Extensive studies have been conducted on the effectiveness of the sandwich panels as structural wall elements using different shear connectors including steel wires, solid concrete zones, FRP ties, FRP shear grid, etc. Those studies have shown that the behavior of panels depends upon the composite action between the two concrete wythe provided by the shear connectors. Additionally, these studies have shown that insulated concrete sandwich panels have a variety of benefits both during construction and throughout the life of the structure. Some of these benefits are:

- Reduction in quantities of concrete required, thus reducing the weight of the slab; benefitting both transportation as well as constructability with strength comparable to that of a solid slab of concrete.
- Reduced $CO_2$ emissions due to a reduction in the quantity of required cement.
- Reduced heating and cooling costs due to insulation within the panels.
- Reduced structural footprint due to lighter weight and less negative space required for adding internal insulation.

As stated, the key to a strong panel is to develop a high Degree of Composite Action (DCA) between the two wythe through the application of shear connectors. Some shear connectors, namely steel and solid concrete zones, defeat the purpose of the insulation, as they provide thermal bridges. The use of FRP, which does not readily conduct heat, is a far superior connector in this regard. By using the FRP, the issue of thermal heating is eliminated, however, the DCA between the wythe is still an issue. Until now, no study has been conducted using FRP plate shear connectors. Additionally, the application of these panels as floor/roof panels has received little attention. By applying these panels to a structure as both floor/roof and wall elements, the benefits as described above would be further amplified. Furthermore, by bonding external FRP plates to the panels, a water barrier would be produced, which would be beneficial with regard to the application of a green roof.

With these gaps in knowledge, the objectives of this study are:

1) To develop innovative FRP plate shear connectors for insulated concrete sandwich panels.
2) To develop FRP-confined precast concrete sandwich (FPCS) panels.
3) To study the flexural behavior of scaled and full-scale FPCS panels.
4) To study the creep behavior of FPCS panels.

Chapter 2 provides information important to this study that has been gathered through the review of literature written based on studies done by other professionals. Using this information, Chapter 3 details the development of innovative FRP plate shear connectors. Following the development of these shear connectors, the effect of eliminating the compression reinforcement and the application of external FRP top plates compared to the application of external FRP top and side plates is presented in Chapter 4. With the findings from Chapter 4, full-scale specimens were then produced and tested, as shown in Chapter 5. The final area of study presented in Chapter 6 details the effect of sustained loads on the creep of various panels. Once all results have been presented, final conclusions, as well as recommendations for future study and application of these panels, are presented in Chapter 7.

# CHAPTER 2: LITERATURE REVIEW

## 2.1 INTRODUCTION

The purpose of this study is to develop innovative FRP plate shear connectors, calculate the bending stiffness and strength of concrete sandwich panels using said FRP plate shear connectors, both with and without external FRP plates, and to determine the effect of a sustained load on the creep of such panels. The following literature review focuses on the relevant subjects pertinent to this study

## 2.2 REINFORCED CONCRETE SANDWICH PANELS

Reinforced concrete sandwich panels have been in use for several decades, first appearing in North America more than 50 years ago [1][2]. Interest in these panels has recently increased due to the publication of the state-of-the-art report by PCI [2][8]. There are many variations to their designs which are primarily regarded as trade secrets. As such, there are not many guidelines to the design and implication of these panels. Generally, these panels are composed of two layers of concrete, known as wythes, separated by a layer of rigid foam plastic insulation [2][8]. The two wythes are connected by some form of shear mechanism, generally concrete webs, metal connectors, plastic connectors, or a combination of these elements [8].

The panels provide the dual function of transferring load and insulating the structure among other desirable characteristics of normal concrete panels. These include durability, economy, fire resistance, large vertical spaces between supports, and use as shear walls, bearing walls, retaining walls, beams, and general structural cladding [2]. The slabs also have been shown to provide superior structural efficiency, allowing for a smaller structural footprint due to the light weight of the slabs which require less supporting superstructure and the incorporation of insulation within the slab such that further insulation is unnecessary [6][8].

### 2.2.1 DEGREE OF COMPOSITE ACTION

Early sandwich panels were designed as non-composite panels, generally with a thick, structural wythe and another non-structural wythe [2]. A wythe is considered structural if it significantly contributes to the resistance of the load being applied to the panel. As such, in the case of non-composite panels, either one of the wythes is structural and the other wythe

is non-structural, or each wythe can independently resist the applied load, such that they are both structural [8]. In the latter case, each wythe will exhibit its own neutral axis, which is a characteristic of non-composite behavior [9].

It has been determined that increasing the degree of composite action between the wythes will increase the structural capacity of a given panel [1]. As such, partially composite panels are significantly superior to fully non-composite panels with regard to structural efficiency [1]. These partially composite panels possess a bending stiffness and strength between the stiffness and strength of fully composite panels (like a solid concrete slab) and non-composite panels [2].

The DCA of the panels has been determined to be the best and most reliable way to determine the strength and effectiveness of reinforced concrete sandwich panels. With a higher degree of composite action, a greater overall strength and comparing to a solid slab is achieved; the goal being to achieve a fully composite sandwich panel. Such a panel acts as a single unit in bending, accomplished by full shear transfer between the two wythes [2].

### 2.2.2 SHEAR CONNECTORS

Studies have shown that the ultimate strength and DCA of a panel depend largely on the stiffness of the shear connectors [9]. The purpose of the shear connectors within these reinforced concrete sandwich panels is to transfer the longitudinal shear, resulting from flexure in the panel, from one wythe to the other [8].

Many different types of connectors have been used in the past. These connectors include steel ties, wire trusses, bent wires, truss- shaped connectors, and solid concrete zones [1][4][5][8]. These connectors have been proven to establish exceptional connections between the wythe; however, they can result in a thermal bridge (an area where a temperature gradient increases substantially with respect to other insulated areas), developing at the locations of the connectors, thus negating, or at least limiting the insulating benefits that could be gained through the use of the foam core.

For this reason, carbon fibers have begun to be incorporated as members, as they have a thermal conductivity about 14% that of steel, and reduce thermal bridging [1][4][5]. These connectors have generally been constructed with fiber reinforced polymers (FRP). They

have been used in both truss and mesh orientations as shear connectors. Additionally, FRP exhibits high strength at low weight compared to steel and concrete. Although the initial material cost is comparatively higher than steel or concrete connectors, the use of FRP can reduce the long term building heating/cooling cost due to the elimination of thermal bridges. It should be noted that some form of mechanical anchorage should be provided for the FRP elements as their adhesion to concrete is not as high as that of steel[1][5].

### 2.2.3 INSULATION

At this time, the strength in stiffness and shear of the foam insulation has not been established by test and is generally ignored and assumed to be zero [2][6]. Having stated this, tests have shown that the panel stiffness is affected by the type of foam used. These studies have shown that a higher percentage of composite action can be achieved using expanded polystyrene (EPS) rather than extruded polystyrene (XPS) [1].

The primary benefits of the insulation are that of weight reduction and improved thermal performance. The reduction in weight has a substantial effect on the cost associated with these panels. Initially, there is a reduction in the amount of concrete required to produce one of these panels as compared to a solid slab, with comparable strength. As expected, this material reduction results in lighter weight. This lighter weight is beneficial to both transport and construction. As these panels are pre-cast and much lighter, they are much easier to erect on site. Due to the insulation being included within each panel, and the panels being lighter, the overall envelope of the structure, and therefore carbon footprint, can be reduced. Studies have shown that R values of up to 12 can be attained which can reduce peak heating and cooling loads of up to 30 percent as compared to insulated stud-wall systems [1][6][8].

### 2.2.4 WYTHE THICKNESS AND REINFORCEMENT

Most sandwich panels are designed to be as thin as possible [2]. In the case of concrete sandwich panels, this thickness depends on the structural function, concrete cover, anchorage of connectors, stripping, and finish. The minimum recommended thickness of a structural wythe is 2 inches if prestressed and 3 inches if non-prestressed, however, a thickness as small as 3/4 inches has been used [8].

The concrete wythes can be reinforced in several ways. These generally include prestressing strands, longitudinal reinforcing bars, wire mesh, or a combination thereof [8]. This reinforcement is generally located at the centroid of the wythe in order to minimize the tendency of the wythe to camber [2].

## 2.3 CREEP

Creep refers to the gradual increase in the deflection of a structural element as it supports a load for an extended period of time. It is a topic of study which has presented much difficulty to not only sandwich panels, but to concrete construction in general. Most experimental data for creep is limited to load magnitudes within the low service range [11]. This range is generally 15-45% of the maximum load for the test specimen [14][15].

The key conclusion is that the rate of deflection decreases over time, with the initial rate of deflection being extremely high [11][16]. At the present time though, an empirical formula to determine the change in the rate of deflection over time is unavailable. ACI-318 provides the following calculation to estimate a correction factor for expected long term deflections:

$$\lambda = \frac{\xi}{1 + 50\rho'}$$

where $\xi$ is a variable based on the amount of time that the sustained load is expected to be applied and $\rho'$ is the ratio of compression steel area ($A_s$) to the product of the depth (d) and width (b) of the specimen in question. This correction factor is then applied to the deflection produced by the initial application of the sustained load.

Ultimately, creep is a topic of study that requires more research. This is especially true with regard to reinforced concrete sandwich panels, as they are rarely implemented as roof/floor elements which are expected to sustain constant loads.

## 2.4 CONCLUSIONS

Much study has been done on reinforced concrete sandwich panels, but knowledge and standards are still lacking. This lack of knowledge is due to the high cost of full-scale testing and extreme difficulty in fabrication of small-scale models [9]. What is known though, is encouraging and the study of these panels and their variations should be continued.

# CHAPTER 3: DEVELOPMENT OF FRP PLATE SHEAR CONNECTORS

## 3.1 INTRODUCTION

Reinforced concrete sandwich panels consist of two layers of concrete wythe separated by foam insulation; generally ESP or XPS. This allows for greater thermal performance, lighter weight, decreased superstructure footprint, and increased ease of construction.

Research has shown that concrete sandwich panels are capable of performing at a level comparable with solid concrete slabs of equal dimension. This is dependent on the degree of composite action between the two concrete wythe. To achieve composite action, the two wythe must be connected through the foam insulation by shear connectors. Past shear connectors have included solid zones of concrete, steel, and fiber reinforced polymer (FRP) grid/truss elements. However, the solid concrete zones and steel provide a thermal bridge, negating the thermal properties of the foam insulation, while FRP does not transfer heat readily.

The objective of this study was to determine the feasibility of using FRP plate shear connectors in roof/floor panel application. The effects of three different shear connector configurations will be studied and compared with a solid concrete control slab. The optimum connector will be used in following studies.

## 3.2 EXPERIMENTAL PROGRAM

### 3.2.1 SPECIMEN DETAILS

A group of solid panels with depths of 10” were prepared as controls for this study. Three groups of typical sandwich panels with reinforcement similar to the solid slabs (most sandwich panels use less temperature steel), a wythe configuration of 3”+4”+3” (top wythe thickness, EPS foam core thickness, bottom wythe thickness; see Figure 1), but with varying shear connector configurations.

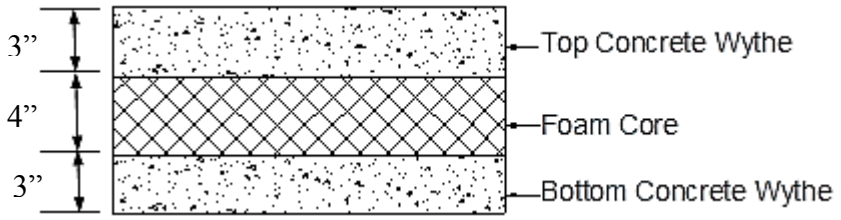


**Figure 1: Sandwich Panel**

All specimen were 2’x9’x10”. The reinforcement layout and specimen details can be seen in Table 1 and the dimensions of the specimen can be seen in Figure 2 through Figure 5.

**Table 1: Specimen Details**

| Group # | Compression Steel (#4 bars) | Tension Steel (#5 bars) | Top Temp. Steel (#4 bars) | Bottom Temp. Steel (#4 bars) | Load Condition | Shear Connectors |
|---|---|---|---|---|---|---|
| 1 | (2) @ 18" O.C. | (2) @ 12" O.C. | (6) @ 18" O.C. | (6) @ 18" O.C. | 4-pt Bending | Discrete 6" |
| | (2) @ 18" O.C. | (2) @ 12" O.C. | (6) @ 18" O.C. | (6) @ 18" O.C. | 4-pt Bending | Discrete 6" |
| 2 | (2) @ 18" O.C. | (2) @ 12" O.C. | (5) @ 18" O.C. | (5) @ 18" O.C. | 3-pt Bending | Segmental |
| | (2) @ 18" O.C. | (2) @ 12" O.C. | (5) @ 18" O.C. | (5) @ 18" O.C. | 3-pt Bending | Segmental |
| 3 | (2) @ 18" O.C. | (2) @ 12" O.C. | (5) @ 18" O.C. | (5) @ 18" O.C. | 3-pt Bending | Continuous |
| | (2) @ 18" O.C. | (2) @ 12" O.C. | (5) @ 18" O.C. | (5) @ 18" O.C. | 3-pt Bending | Continuous |
| 4 | (2) @ 18" O.C. | (2) @ 12" O.C. | (6) @ 18" O.C. | (6) @ 18" O.C. | 3-pt Bending | N/A |
| | (2) @ 18" O.C. | (2) @ 12" O.C. | (6) @ 18" O.C. | (6) @ 18" O.C. | 3-pt Bending | N/A |

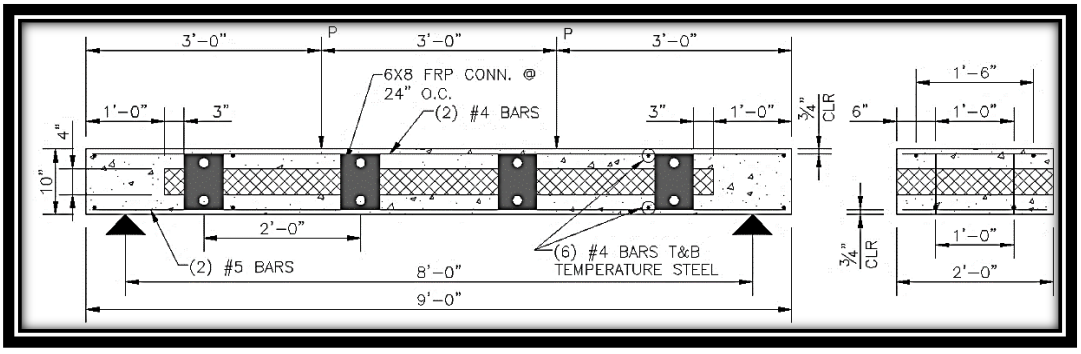


**Figure 2: Discrete Shear Connector Layout**

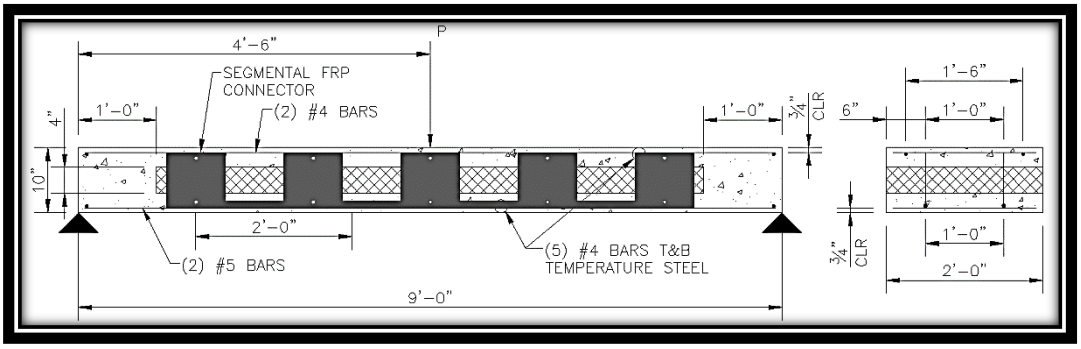


**Figure 3: Segmental Shear Connector Layout**

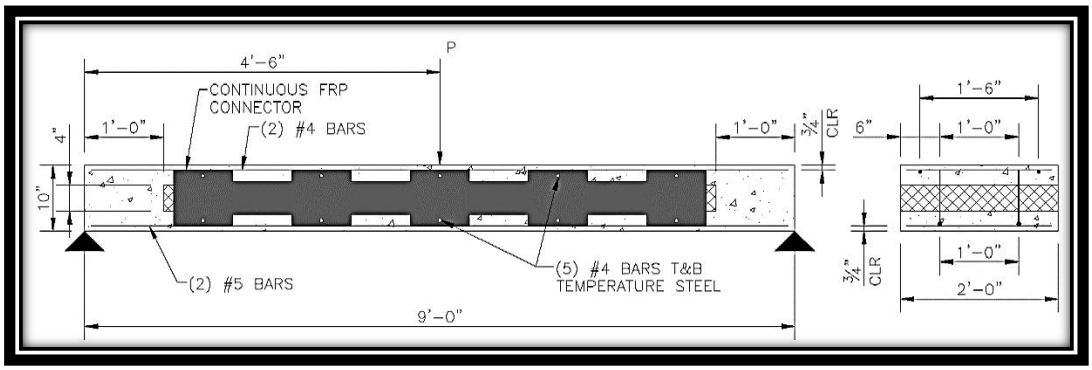


**Figure 4: Continuous Shear Connector Layout**

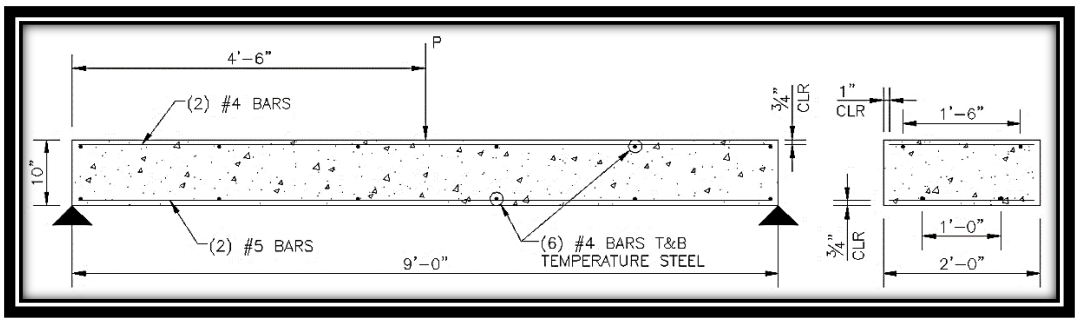


**Figure 5: Solid Control Slab Layout**

## 3.2.2 MATERIAL PROPERTIES

Table 2 presents the material properties of the concrete, foam core, and FRP shear connectors used in this study. Cylinder crushing tests were conducted among four 6"x12" specimens and the average compressive strength was calculated. Figure 6 displays the load-strain curves for the cylinder tests. The compressive strength of the concrete was averaged to be 4120psi with a standard deviation of 426psi.

**Table 2: Material Properties**

| | Expanded Polystyrene | 4120 psi Concrete |
|---|---|---|
| Mass Density (r) | 1.871 x $10^{-6}$ (lbf $s^2$)/$in^4$ | 2.246 x $10^{-6}$ (lbf $s^2$)/$in^4$ |
| Young's Modulus (E) | 1,349 psi | 2.558 x $10^6$ psi |
| Poisson's Ratio (n) | 0.3 | 0.15 |

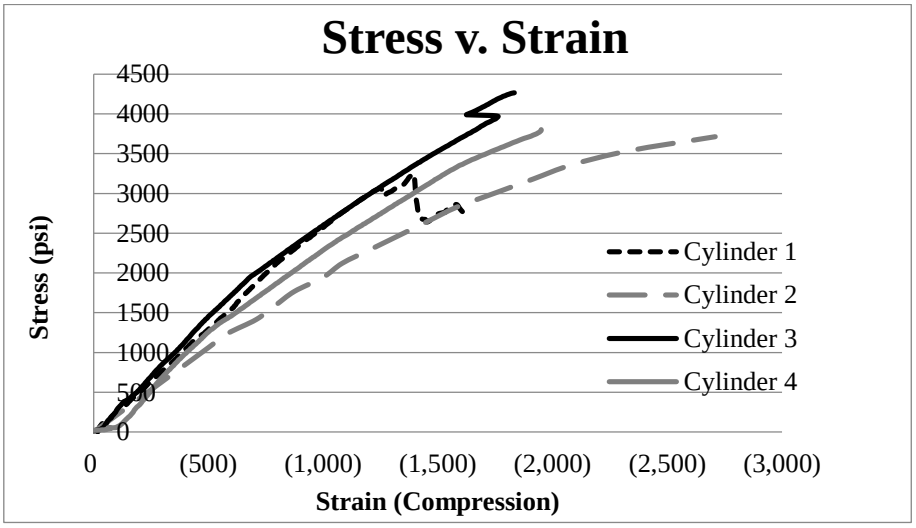


**Figure 6: Compressive Strength of Concrete**

Table 3 provides the material properties for the FRP used; both provided by CRANE Composites.

**Table 3: FRP Material Properties**

| Typical Values | | | |
|---|---|---|---|
| **Property** | **EATR .085" \| 2.2 mm** | | **Test Method** |
| Flexural Strength | 33 x $10^3$ psi | 228 MPa | ASTM - D790 |
| Flexural Modulus | 1.0 x $10^6$ psi | 6895 MPa | ASTM - D790 |
| Tensile Strength | 45 x $10^3$ psi | 310 MPa | ASTM - D638 |
| Tensile Modulus | 2.0 x $10^6$ psi | 13790 MPa | ASTM - D638 |
| Barcol Hardness | 45 | 45 | ASTM - D2583 |
| Coefficient of Linear Thermal Expansion | 0.8 x $10^{-5}$ in/in/°F | 14 µm/m/°C | ASTM - D696 |
| Thermal Conductivity | 0.4 Btu•in/hr•$ft^2$ °F | 5.0 cal•cm/hr•$m^2$ °C | ASTM - C177 |
| Water Absorption | 0.2%/24hrs@77°F | 0.2%/24hrs@77°F | ASTM - D570 |
| Specific Gravity | 1.75 | 1.75 | ASTM - D792 |

### 3.2.3 SPECIMEN FABRICATION

Wooden, concrete forms were constructed with 3/16” OSB and 2”x4” kiln dried Douglas fir. They were constructed with the assistance of University of Idaho’s Fall 2012 class of CE 441: Reinforced Concrete Design students, under the direction of Dr. An Chen. The inner dimensions of the forms were constructed to reflect the dimensions of the designed specimens, as seen in Figure 7.

**Figure 7: Wooden Concrete Form**

The shear connectors were designed with regard to their purpose and application. Figure 8 displays the 6” discrete connectors. The purpose of the 1 ½” holes is to allow concrete through the connector at the center of each wythe in order to promote the integration of the shear connector within the concrete.

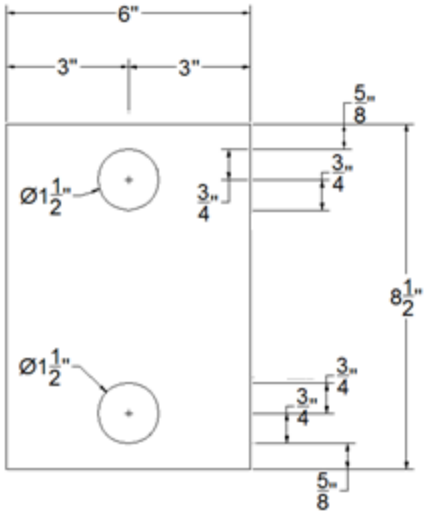


**Figure 8: 6" Discrete Shear Connector**

The segmental shear connectors for the sandwich are displayed in Figure 9. These connectors are designed to achieve 100% composite action. The small holes at the top and bottom of each segment allow for proper positioning of temperature steel, which doubles as an anchor for the shear connectors within the concrete.

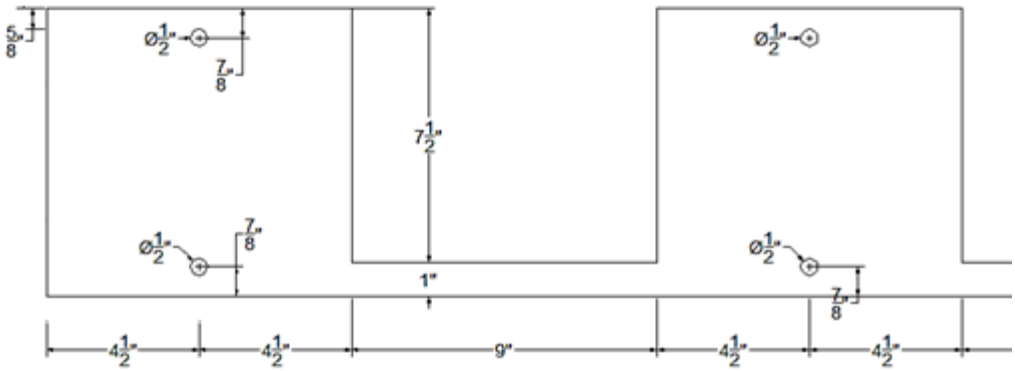


**Figure 9: Segmental Shear Connector**

Continuous shear connectors are displayed in Figure 10. The small holes at the top and bottom of each segment allow for proper positioning of temperature steel, which doubles as an anchor for the shear connectors within the concrete, in the same fashion as the segmental shear connectors.

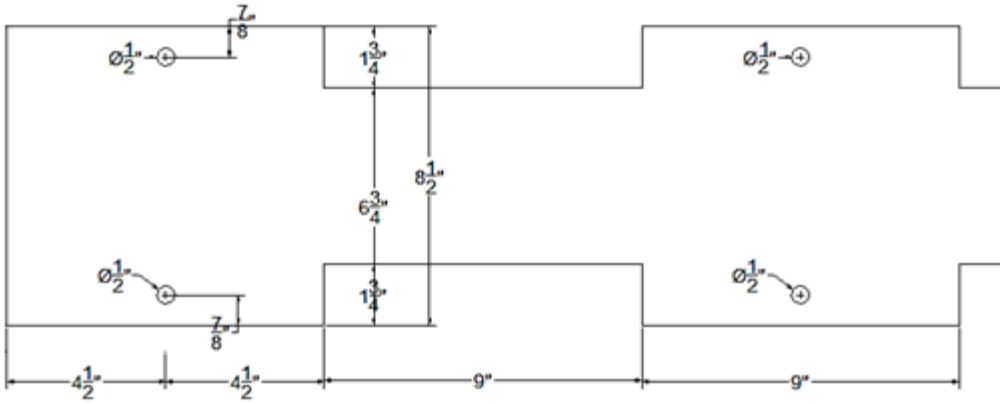


**Figure 10: Continuous Shear Connector**

## GROUP 1: DISCRETE SHEAR CONNECTORS

The tension and temperature steel were first tied together. Chairs were provided for the rebar to sit on such that proper clear distances were maintained. The form was then oiled to assist in the future stripping of the forms. After the tension reinforcement was placed, concrete was distributed throughout the form up to a level of 3". This layer of concrete was vibrated in order to eliminate voids. The foam core with the 6" discrete shear connectors was then lowered into position. Once the foam core was in position, the tension reinforcement was tied into place. The final layer of concrete was then added and vibrated. Special attention was taken to avoid the rebar and adequately vibrate in along the edges and corners of the slab. Once the form had been filled, the surface was smoothed and edged to allow for easier stripping.

**Figure 11: 6" Discrete Shear Connector Slab Fabrication**

**Figure 12: 6" Discrete Connector Slab Finishing**

## GROUP 2: SEGMENTAL SHEAR CONNECTORS

The foam cores were marked where the shear connectors would pass through. They were then cut with a knife along these marks and widened with a file in order to allow easier insertion of the shear connectors. The shear connectors were then inserted into the foam at which point the temperature reinforcement was passed through the holes in the connector. The tension and compression steel was then tied into place. Prior to positioning the reinforcement and foam, the first 3" lift of concrete was poured into the oiled form and vibrated. Next, the complete cage, including the foam core and corresponding shear connectors was lowered into position. It was placed such that the foam core, which was locked in place between the tension and compression reinforcement via shear connectors, could be seen to be properly positioned along the height of the form. When the foam core and cage were set, the final layer of concrete was added and vibrated. Once the form had been filled, the surface was smoothed and edged to allow for easier stripping.

**Figure 13: First Lift**

**Figure 14: Cage, Insulation, and Shear Connectors**

## GROUP 3: CONTINUOUS SHEAR CONNECTORS

The foam cores were partitioned to allow continuous shear connectors. A table saw segmented the original foam core into the following dimension (and quantities): (2) 6"x7'x4" & (1) 1'x7'x4". This allowed for the shear connectors to be properly positioned prior to the positioning of the foam core. The temperature steel for the bottom wythe first tied to the tension steel outside of the form. The tension steel and shear connectors were then placed within the oiled form. The first 3" lift of concrete was distributed throughout the form. This layer of concrete was the vibrated in order to eliminate voids. The three sections of the foam core were then positioned,

locking the shear connects vertically in place. Next, the top wythe temperature steel and compression reinforcement were tied in place. The final layer of concrete was then added and vibrated. Once the form had been filled, the surface was smoothed and edged to allow for easier stripping.

**Figure 15: Continuous Connectors**

## GROUP 4: SOLID SLAB

The rebar cage was cut and tied together. Spacers were provided for the rebar to sit on such that proper clear distances were maintained. The form was then oiled to assist in the future stripping of the forms. The cage was then positioned and the concrete added. The concrete was then vibrated, paying particular attention to the corners and to avoiding the rebar. As these were solid slabs, the concrete could be added in one 10” lift.

**Figure 16: Solid Slab Reinforcement**

All test specimens were allowed to cure under tarps for a week at which point the forms were stripped. The tarps were again placed over the specimens and were then allowed to cure for the remainder of the 28 days, prior to the beginning of testing.

## 3.3 TEST SETUP

### 3.3.1 TEST LAYOUT

Group 1 was the first group to be tested in four-point bending; however, due to unexpected shear failures at the edge between the foam core and the solid zones, this was changed to three-point bending and the effective length was increased to 9'. A schematic plan of the test setups is shown in **Error! Not a valid bookmark self-reference.** and Figure 19 with layouts represented in Figure 18 and Figure 20.

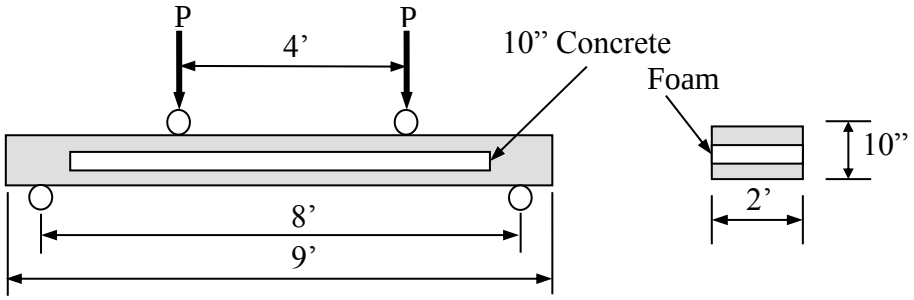


**Figure 17: Four-Point Bending Schematic**

**Figure 18: Four-Point Bending**

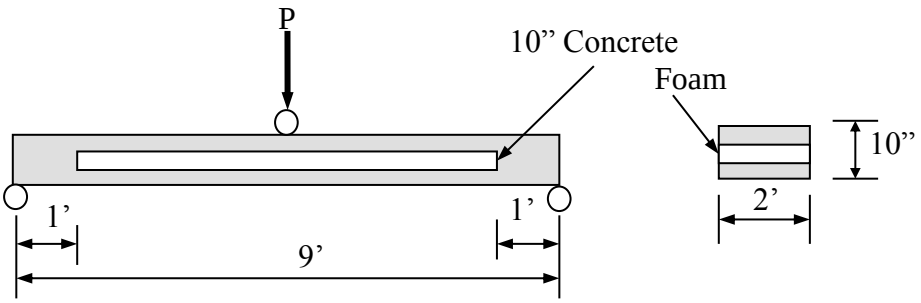


**Figure 19: Three-Point Bending Schematic**

**Figure 20: Three-Point Bending**

### 3.3.2 INSTRUMENTATION

In order to monitor the strain of the steel during testing, strain gages were needed on the tension reinforcement of each slab. As each slab contained (2) #5 rebar as tension reinforcement, both were prepared for strain gages, as a precaution, in the event that one gage failed or de-bonded prematurely. A small area at the mid-span of each bar was ground down smooth and cleaned such that the adhesive and gages would properly bond. After the adhesive had dried and the gages were securely bonded to each bar, the wires were soldered in place, and the gages tested to ensure functionality. The gages used were CEA-06-250UN-120 gages from VISHAY Precision Group.

After the specimens were cured, concrete strain gages were added. The surfaces to which they were added were first treated with an adhesive, in order to fill any gaps/air voids. Once the adhesive had dried, it was sanded down to a smooth surface and cleaned. The strain gage

was then bonded in place. Once the adhesive had dried, the wires were soldered on. The gages used were N2A-06-20CBW-120 gages from VISHAY Precision Group.

Each slab was monitored for its deflection along the centerline at three points along the length of the beam. The spacing between the LVDTs is based on the original 8’-0” effective length and was not altered after the switch to 9’-0” effective length, in order to maintain consistency. The strain gages were positioned at the top and bottom mid-spans along the center-line, and at the middle of the thicknesses of each wythe, also at mid-span. Their purpose is to determine the composite action between each concrete wythe. The FRP strain gages were placed in order to monitor the bond between the concrete and FRP plate. This schematic and layout are displayed in Figure 21 and Figure 22, respectively.

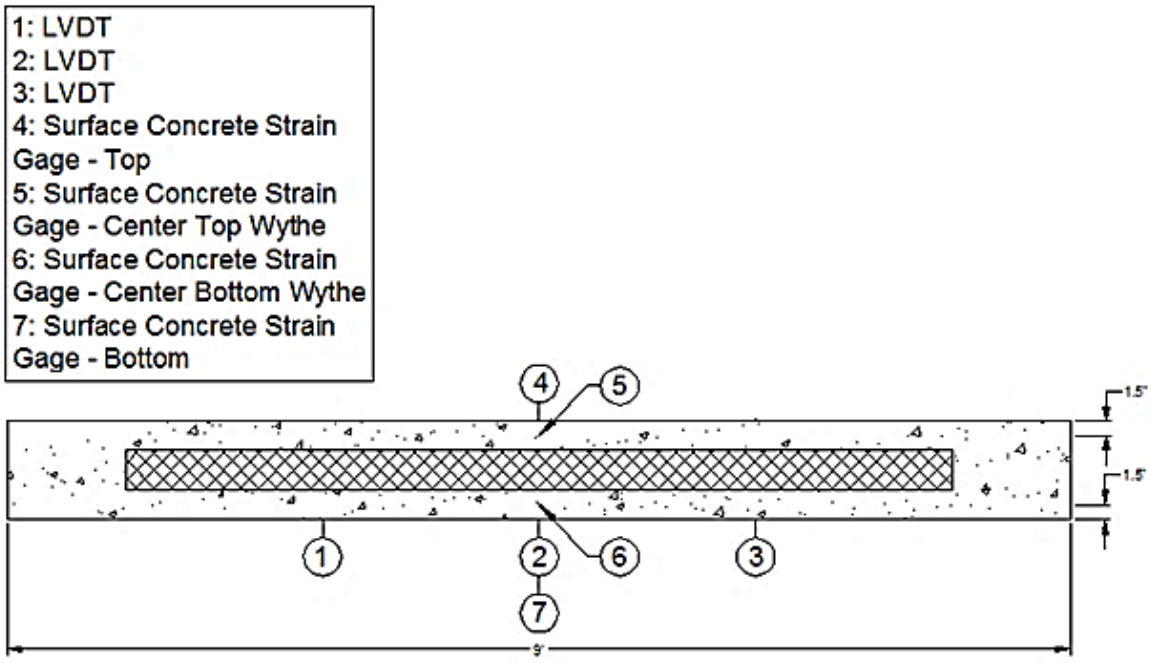


**Figure 21: Instrumentation Layout**

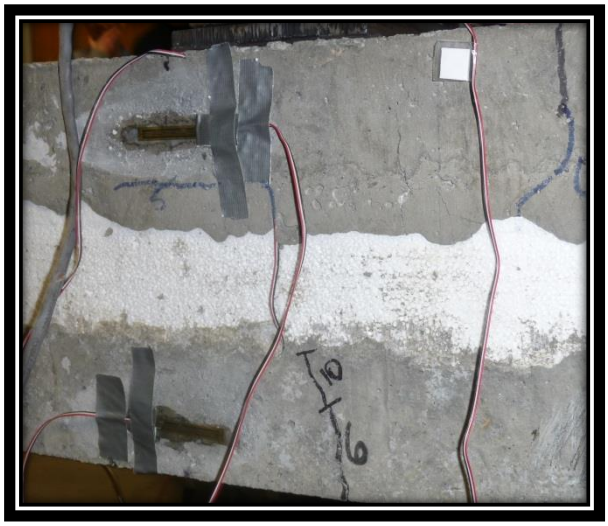

**Figure 22: Example Instrumentation**

## 3.4 TEST PROCEDURES

Each slab was positioned at described locations on the supports and centered with respect to the load cell. Each slab was then inspected for cracks prior to loading. If cracks existed, they were marked and noted. Load was then applied until a base-line load of two kips was reached using a ceiling mounted, hand pumped, hydraulic actuator with a capacity of 50,000lbs. The slab was then inspected for cracking with all new cracks or extensions of existing cracks being marked. After each inspection, the load was increased by one kip and the process repeated until significant cracking was apparent and failure was deemed imminent. At this point, the slab was steadily loaded until failure with no more inspection of cracks to ensure the safety of personnel.

## 3.5 EXPERIMENTAL RESULTS

During the tests, various crack initiation and propagation was observed. When cracking began at the border between the solid concrete zone and the insulation, a shear failure resulted. In this case, the cracks began both on the top and bottom of the specimen. When cracking began on the bottom surface of the specimen near mid-span, propagating in a generally straight line across the width of the specimen, a bending failure occurred. When both of these crack initiations and propagations were present in a specimen, it resulted in a mixed failure mode, characterized by mid-span cracking which propagated in an angular fashion as opposed to straight across the width of the specimen.

### 3.5.1 LOAD-DISPLACEMENT

The following figures display the load displacement curves recorded for the various specimens. Each group is compared to each other as can be seen. In some cases, which are addressed, corrections to the data had to be applied due to alterations to the testing procedure such that all data would be comparable. As these corrections are applied, it can be seen that the two specimen within each group exhibit similar behavior in the linear-elastic region, thus validating the data.

#### GROUP 1: DISCRETE SHEAR CONNECTORS

With group 1, the data acquisition system experienced an error which caused the system to cease collecting data; however, the second test exhibited a similar load-deflection trend and almost identical behavior in the linear-elastic region (See Figure 23). While the first specimen provides limited data, the initial loading of both specimens provides adequate data for later analysis.

Additionally, it was determined throughout testing that both four-point bending and the effective length of 8 feet resulted in shear failures, where bending failures were the goal. The change to a three-point load was implemented in later tests, but not for Group 1. For that reason, the displacements were adjusted to theoretically exhibit the deflections that would have occurred had they been tested in three-point bending with an effective length of 9 feet (see Figure 24). The details of this adjustment can be seen in APPENDICES

APPENDIX 1.

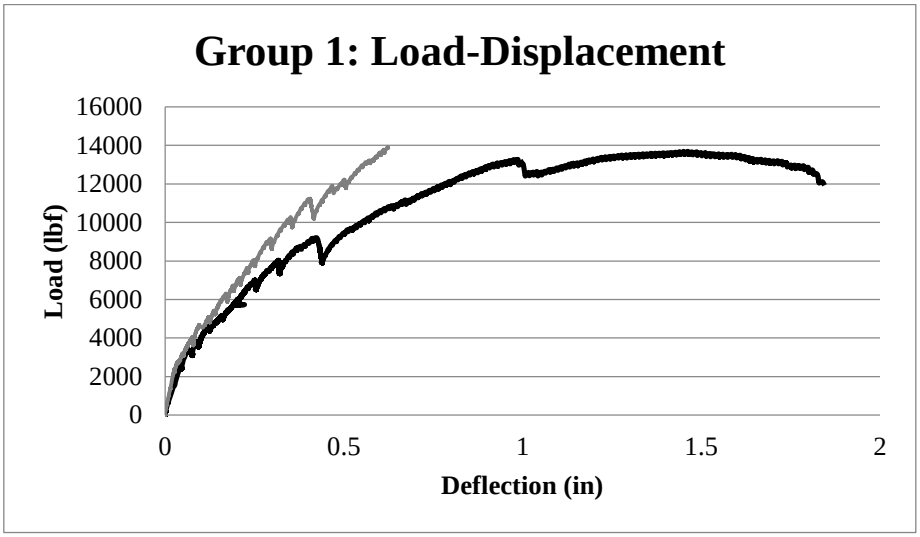


**Figure 23: Group 1 Load-Displacement Curves**

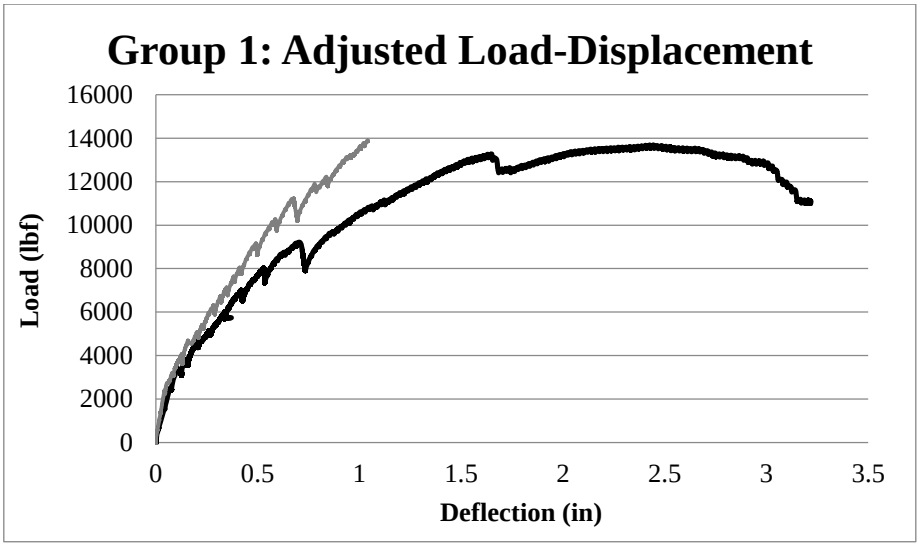


**Figure 24: Group 1 Adjusted Load Displacement Curves**

## GROUP 2: SEGMENTAL SHEAR CONNECTORS

Group 2 provided similar results. It can be seen that one specimen does not display the same degree of stiffness as the other initially (see Figure 25). As with Group 1, adjustments to the data were necessary. One specimen was tested in three-point bending with an effective length of 8 feet, while the other was tested with an effective length 9 feet. To account for this, the displacement of the specimen tested at 8 feet needed to be theoretically adjusted by applying a correction factor; calculated by comparing the theoretical deflections of a simply

supported beam in three-point bending at both effective lengths with all other variables equal. These adjustments can be seen in APPENDICES

APPENDIX 1. The results can be viewed in Figure 26. Once this correction factor was applied, it can be seen that both specimens behave more similarly, particularly in the linear elastic region.

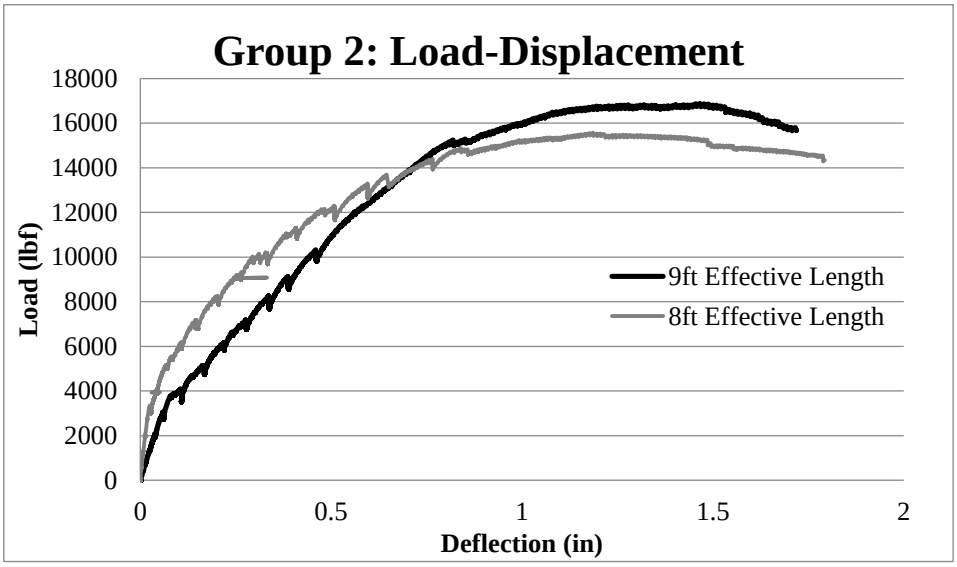


**Figure 25: Group 2 Load-Displacement Curves**

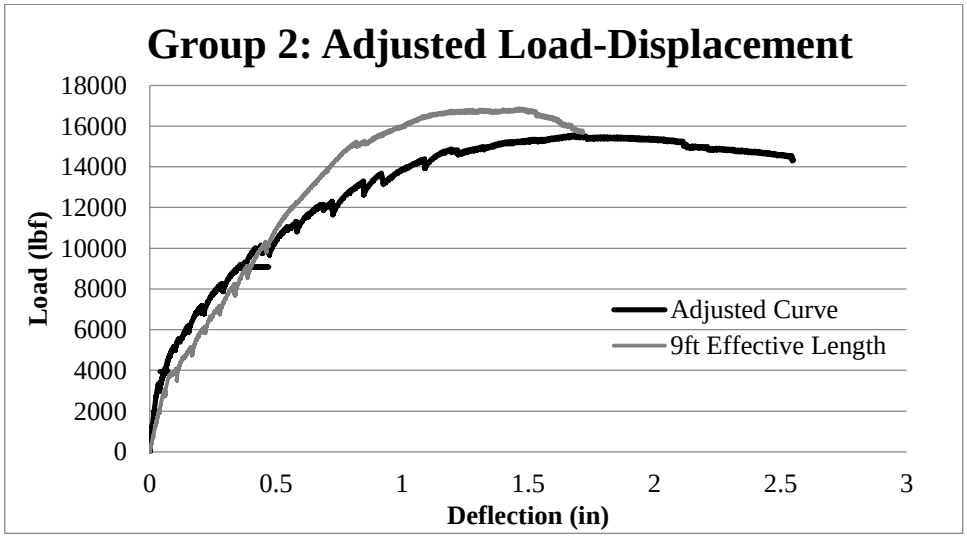


**Figure 26: Group 2 Adjusted Load-Displacement Curves**

## GROUP 3: CONTINUOUS SHEAR CONNECTORS

Both specimen with the continuous connectors exhibited almost identical elastic regions with one providing a greater overall stiffness and the other providing a greater overall strength (see Figure 27). These specimens provide similar results and will be used further analysis.

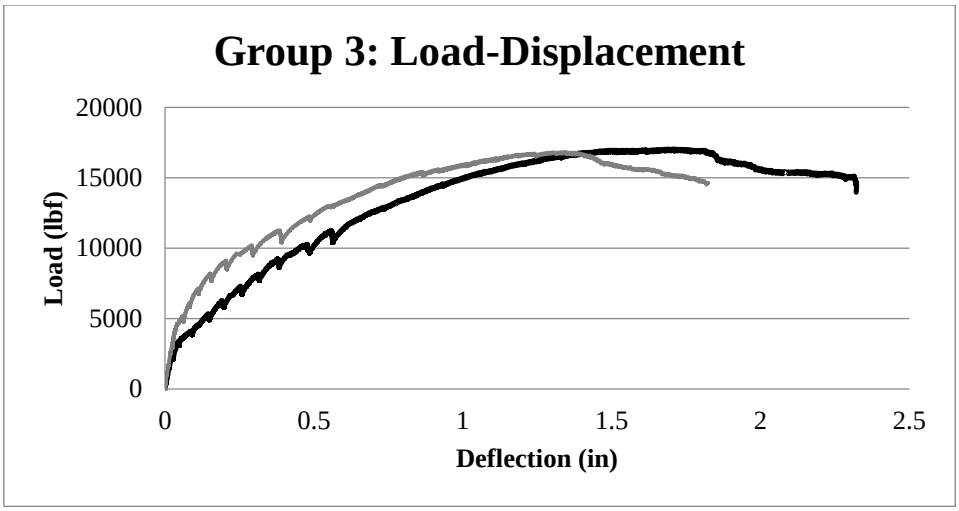


**Figure 27: Group 3 Load-Displacement Curves**

## GROUP 4: SOLID SLAB

As with the specimens with the continuous connectors, the solid slabs both exhibited the same initial linear-elastic region (see Figure 28). As with Group 3, these specimens both provide excellent data which can be used in further analysis.

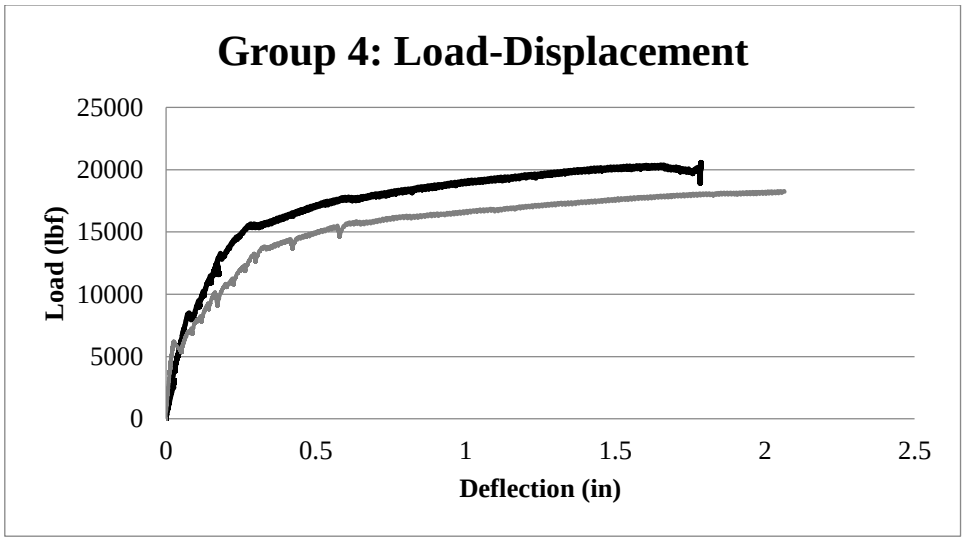


**Figure 28: Group 4 Load-Displacement Curves**

## COMPARISON:

Figure 29 presents the comparison of the load-displacement curves from each group. It can be seen that both of the continuous and segmental connector specimens exhibit similar strength while the discrete connectors exhibit lower strength as expected. Figure 30 represents the linear stage of all the slabs. It can be seen that the continuous and specimens

share a similar stiffness to one of the solid slab at the lower load. One of the segmental connector specimens has an almost identical slope to one of the solid slabs. The other exhibits a much lower stiffness, comparable to that of the discrete connector specimens. As anticipated, the discrete specimens do not exhibit stiffness as high as the majority of the other specimens. For reference, the load-deflection curves of 100% and 0% composite action have been added.

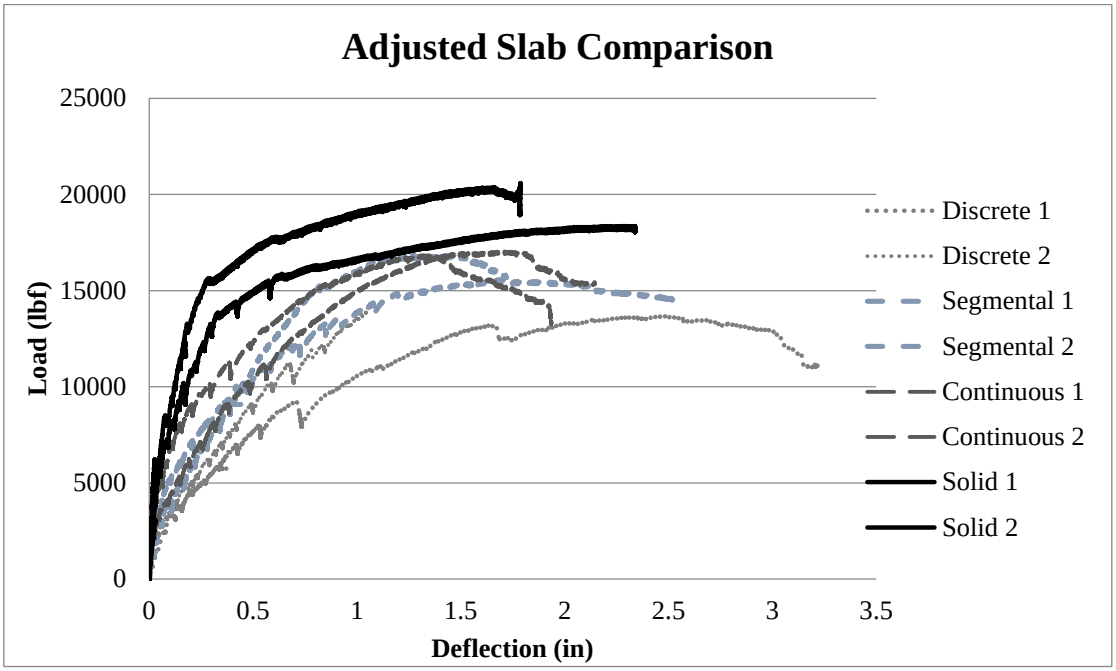


**Figure 29: Slab Comparison**

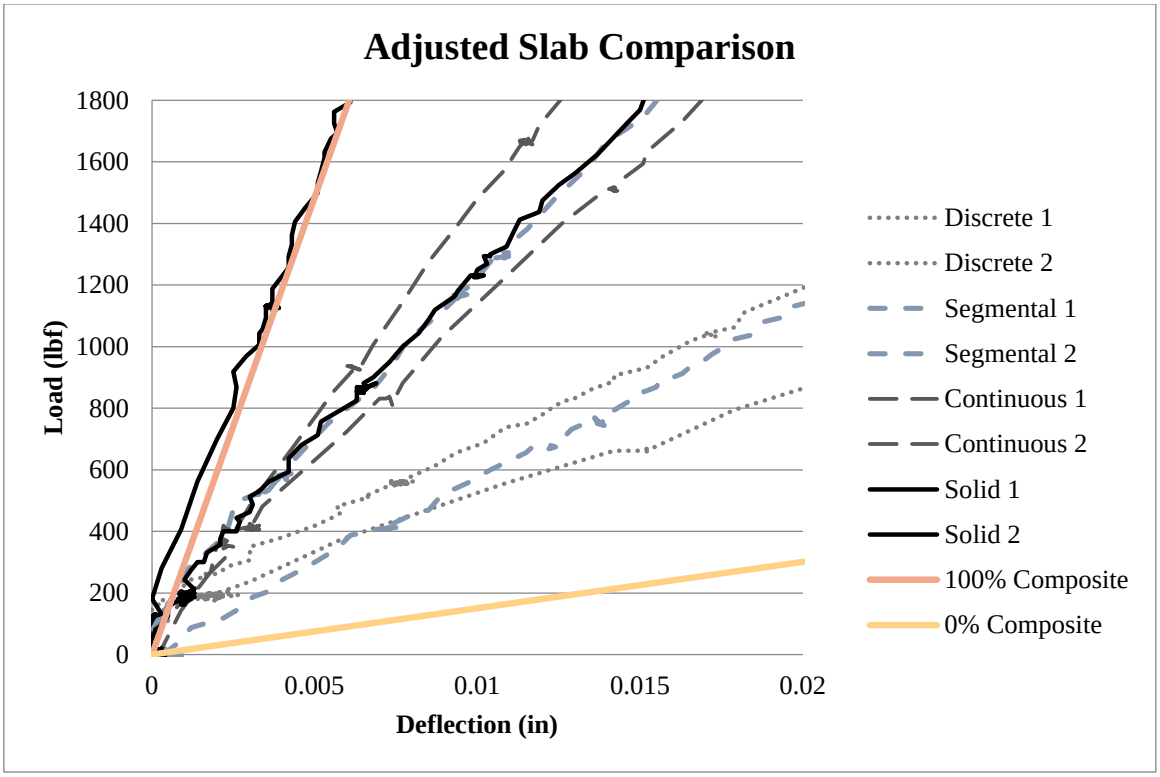


**Figure 30: Linear Region Comparison**

**Table 4: Ultimate Load Summary**

| Group | Effective Length (ft) | Bending Type | Moment Arm (ft) | Cracking Load (kip) | Cracking Moment (kip*ft) | Failure Load (kip) | Failure Moment (kip*ft) | Max Load Deflection (in) | Adjusted Max Load Deflection (in) |
|---|---|---|---|---|---|---|---|---|---|
| 1 | 8 | 4-pt | 1.3 | 3 | 1.95 | 13.694 | 17.802 | 1.451 | 2.425 |
| | 8 | 4-pt | 1.3 | 3 | 1.95 | 13.900 | 18.070 | 0.623 | 1.041 |
| 2 | 8 | 3-pt | 4 | 4 | 8.00 | 15.570 | 31.140 | 1.186 | 1.689 |
| | 9 | 3-pt | 4.5 | 3 | 6.75 | 16.875 | 37.969 | 1.466 | - |
| 3 | 9 | 3-pt | 4.5 | 3 | 6.75 | 17.000 | 38.250 | 1.710 | - |
| | 9 | 3-pt | 4.5 | 3 | 6.75 | 16.844 | 37.899 | 1.346 | - |
| 4 | 9 | 3-pt | 4.5 | 4 | 9.00 | 18.360 | 41.310 | 2.199 | - |
| | 9 | 3-pt | 4.5 | 3 | 6.75 | 20.600 | 46.350 | 2.140 | - |

In Table 4, the variations between bending type and effective length can be seen. The overall failure load in Group 2 can be seen to increase with the increase in effective length as bending becomes the failure type, rather than a sudden shear. As stated before, adjustments for this were applied to Groups 1 & 2 such that the results would be comparable to all others.

### 3.5.2 STRAIN

#### 3.5.2.1 LOAD-STRAIN

In some instances, a strain gage is damaged prior to testing. In others, a crack in the material that it is bonded to may render the gage useless. The load-strain curves of each were plotted to determine which gages to trust. By viewing the behavior of these curves, a judgment could be made as to which gages to use in later analysis, specifically, the development of strain profiles. This section presents the representative curves which were used.

**GROUP 1: DISCRETE SHEAR CONNECTORS**

Figure 31 & Figure 32 display typical load-strain curves for the top surface and tension reinforcement for a Group 1 specimen. As expected, the top surface experiences compression and the bottom wythe reinforcement experiences tension.

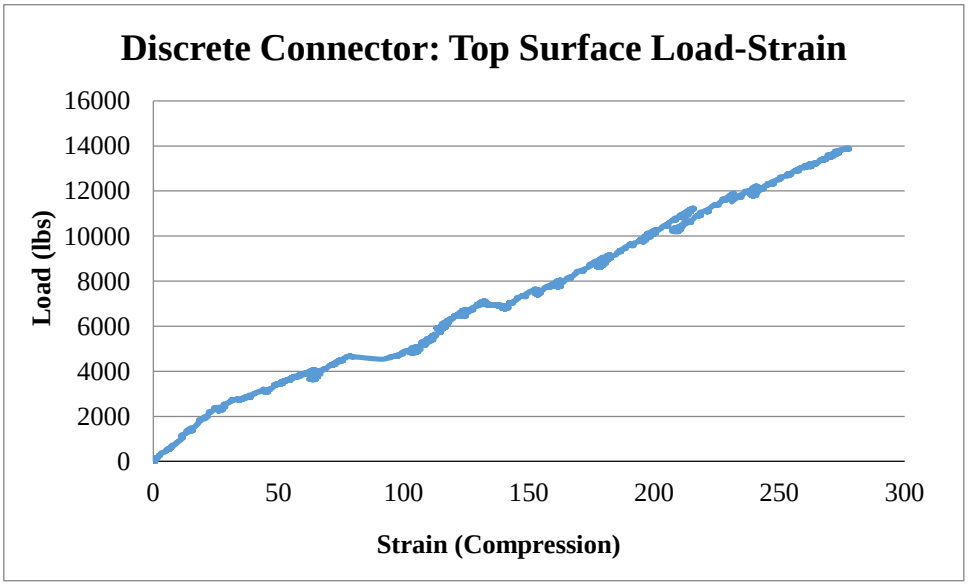


**Figure 31: Discrete Connectors--Top Surface Load-Strain**

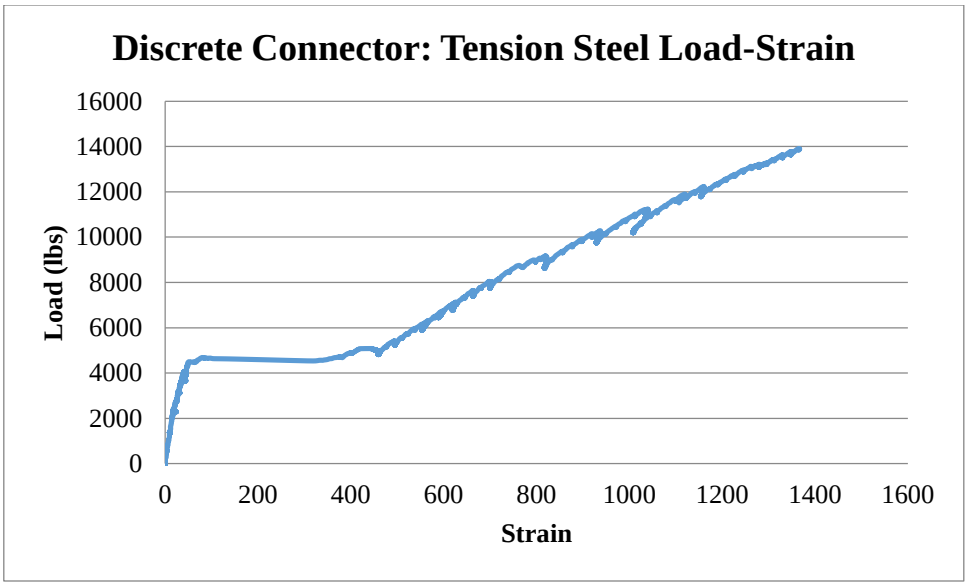


**Figure 32: Discrete Connectors--Tension Steel Load-Strain**

## GROUP 2: SEGMENTAL SHEAR CONNECTORS

Figure 33 & Figure 34 display typical load-strain curves for the top surface and tension reinforcement for a Group 2 specimen. As expected, the top surface experiences compression and the bottom wythe reinforcement experiences tension.

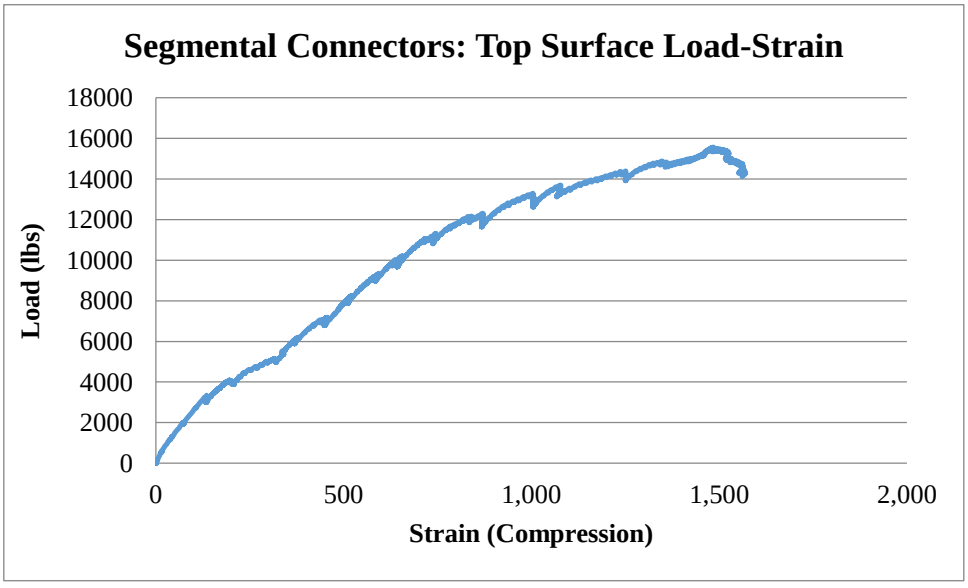


**Figure 33: Segmental Connectors--Top Surface Load-Strain**

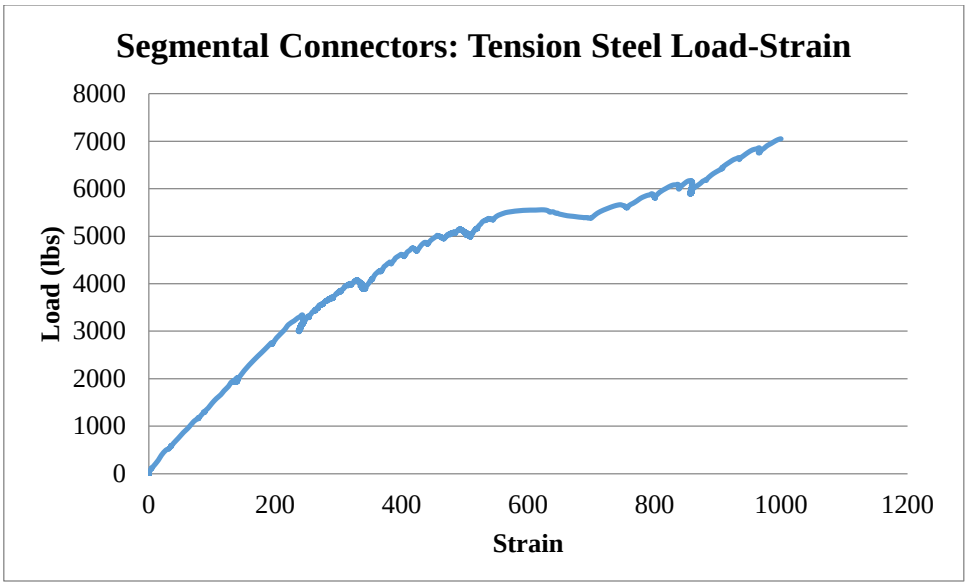


**Figure 34: Segmental Connectors--Tension Steel Load-Strain**

## GROUP 3: CONTINUOUS SHEAR CONNECTORS

Figure 35 & Figure 36 display typical load-strain curves for the top surface and tension reinforcement for a Group 3 specimen. As expected, the top surface experiences compression and the bottom wythe reinforcement experiences tension.

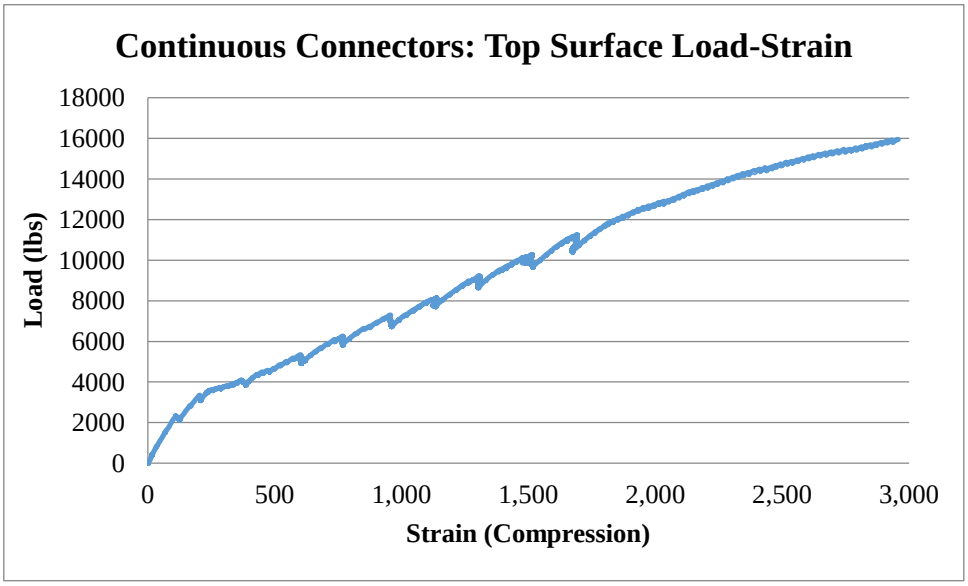


**Figure 35: Continuous Connectors--Top Surface Load-Strain**

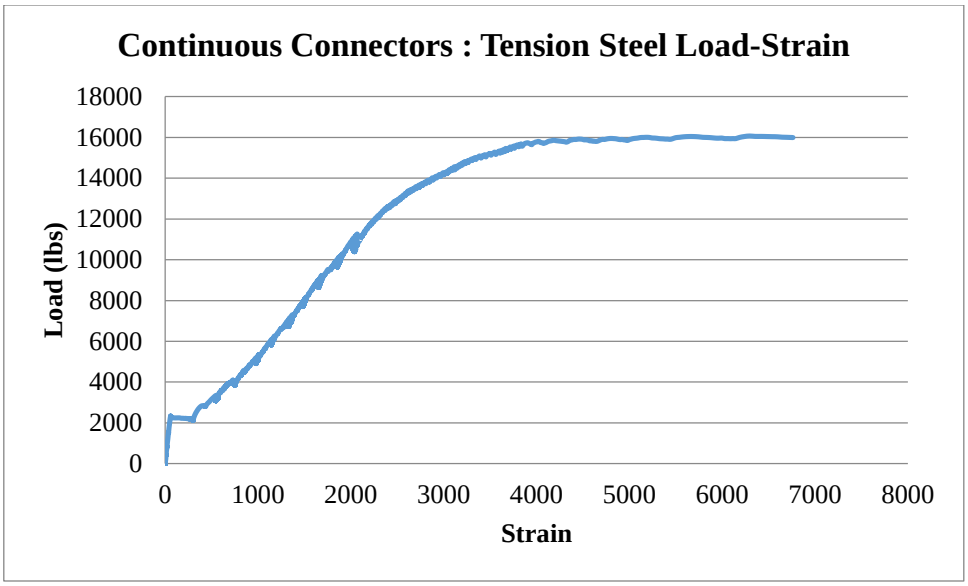


**Figure 36: Continuous Connectors--Tension Steel Load-Strain**

## GROUP 4: SOLID SLAB

Figure 37 & Figure 38 display typical load-strain curves for the top surface and tension reinforcement for a Group 4 specimen. As expected, the top surface experiences compression and the bottom wythe reinforcement experiences tension.

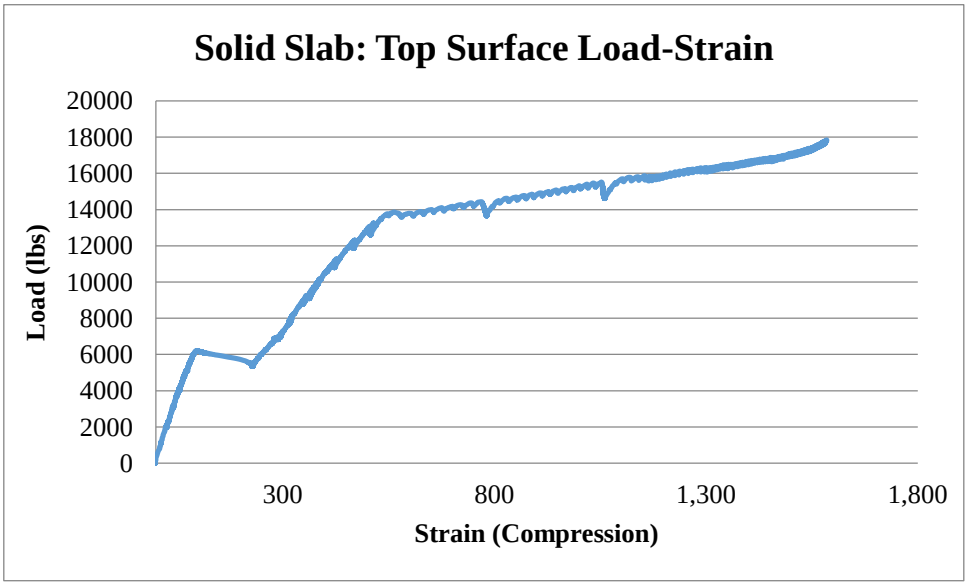


**Figure 37: Solid Slab--Top Surface Load-Strain**

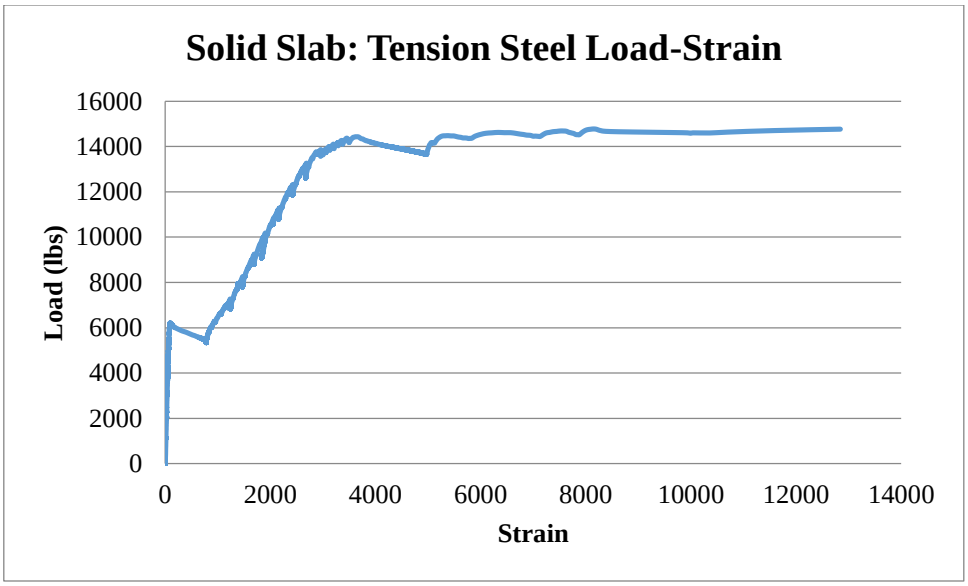


**Figure 38: Solid Slab--Tension Steel Load-Strain**

### 3.5.2.2 STRAIN DISTRIBUTION

The strain data collected was used to plot the distribution of strain across each slab to help determine DCA during the linear-elastic section of loading. In order to produce these strain distributions, it was necessary to have a minimum of two working strain gages on one wythe and a minimum of one other working strain gage on the opposite wythe. By satisfying these requirements, the slope of the strain distribution could be calculated in the wythe with two working strain gages and then applied to the other wythe, thus completing the strain distribution profile. Unfortunately, only one specimen from each group met these requirements.

In all cases, the slabs were analyzed at loads which produced identical moments at mid-span. This only affects the load at which the discrete connectors were analyzed as all other specimen providing strain data adequate for developing a strain profile were tested with an effective length of 9 feet in three-point bending. The following figures display the strain distribution across the various slabs. Notice that the $R^2$-value for the solid slab, which is a statistical measure of how well data points fit a statistical model; in this case a linear best-fit line for the collected strain data, displays 100% as it should, being the 100% composite control specimen (see Figure 39).

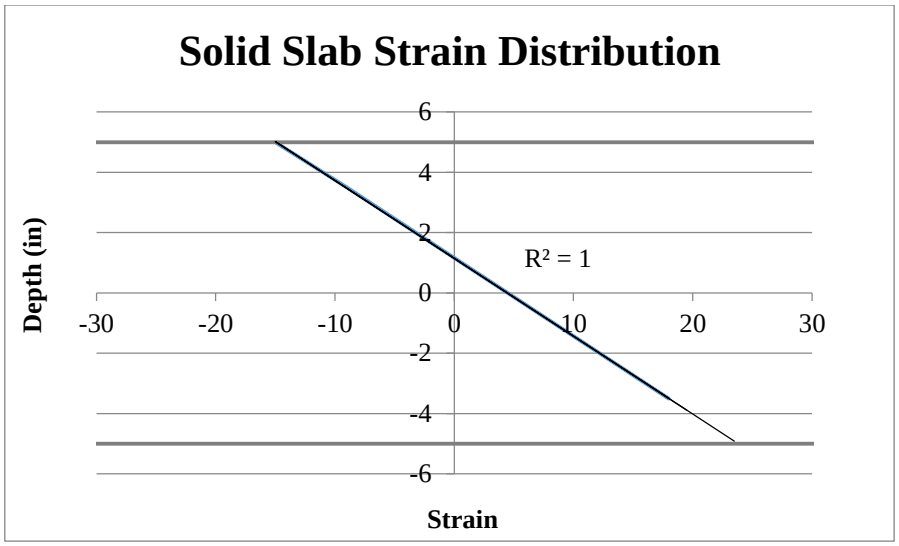


**Figure 39: Solid Slab Strain Distribution**

In the case of the discrete connectors (Figure 40), it can be seen that the strain profile crosses the neutral axis in each respective wythe. This behavior indicates non-composite action between the two wythes.

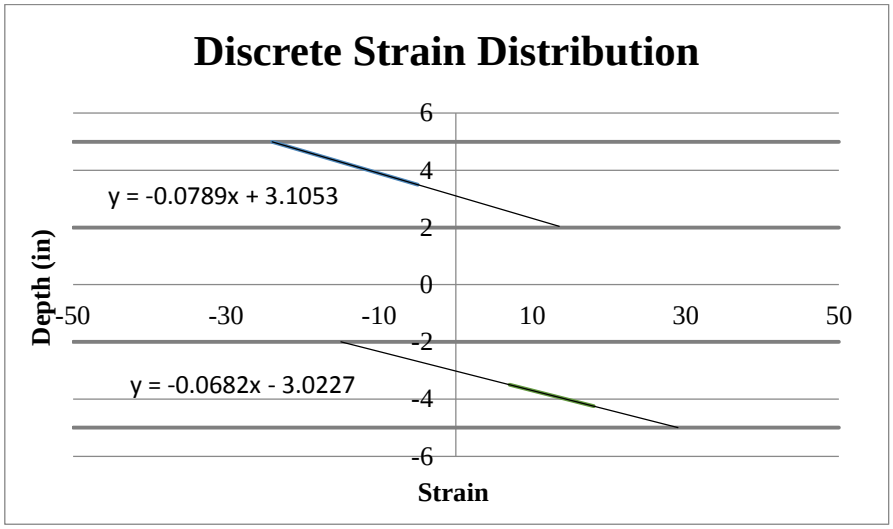


**Figure 40: Discrete Connector Strain Distribution**

In the case of both the segmental and continuous connectors (Figure 41 & Figure 42, respectively), the strain profile displays a strain distribution that does not cross the neutral axis within either wythe. This is a mark of composite action, but as the lines (if extrapolated) do not perfectly line up with each other, it can be concluded that the wythe are behaving in a partially composite manner.

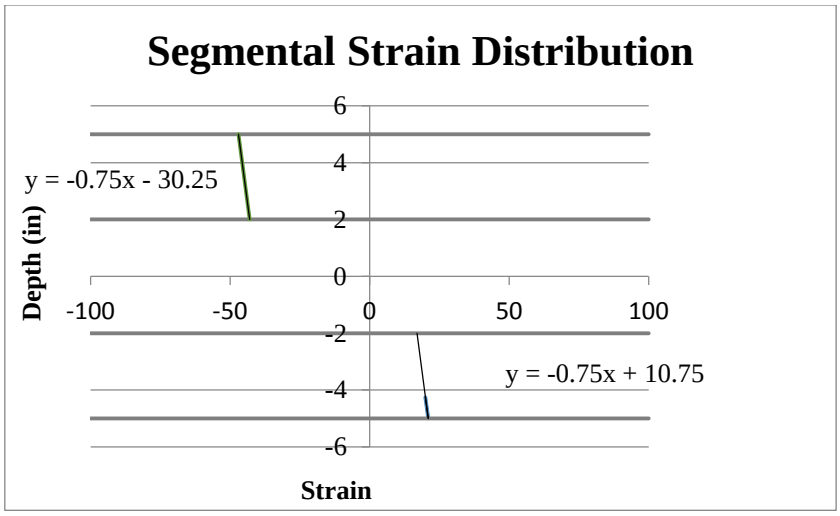


**Figure 41: Segmental Connector Strain Distribution**

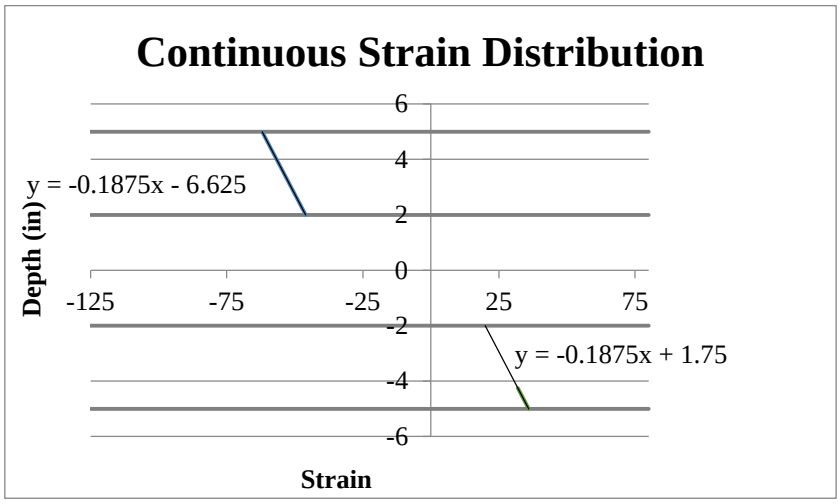


**Figure 42: Continuous Connector Strain Distribution**

### 3.5.3 FAILURE MODE

The failure mode experienced by each slab is presented in Table 5. Figure 43 & Figure 44 provide examples of shear and bending failure, respectively.

**Table 5: Failure Modes**

| Group | Connector Type | Initial Failure Mode | Secondary Failure Mode |
|---|---|---|---|
| **1** | 6" Discrete | End-zone Failure | - |
| | 6" Discrete | End-zone Failure | - |
| **2** | Segmental | Crushing | Shear |
| | Segmental | Bending | Shear |
| **3** | Continuous | Bending | Shear |
| | Continuous | Bending | Shear |
| **4** | N/A | Bending | - |
| | N/A | Bending | - |

**Figure 43: Shear Failure (Profile View)**

**Figure 44: Bending Failure (Bottom of Specimen)**

### 3.5.4 CRACK PATTERN

The expected crack pattern for each specimen was bending. While most failed in this manner, not all slabs exhibited this behavior. The following figures display the crack patterns (which are highlighted/traced where necessary) for the specimens from which the failure modes can be compared. Bending failures are exhibited by those slabs which crack along essentially straight lines from one side to the other. Any deviation or angle to the crack (using the edge of slab as a datum) displays shear cracking. This is also true when viewing the profile of these specimens.

**GROUP 1:**

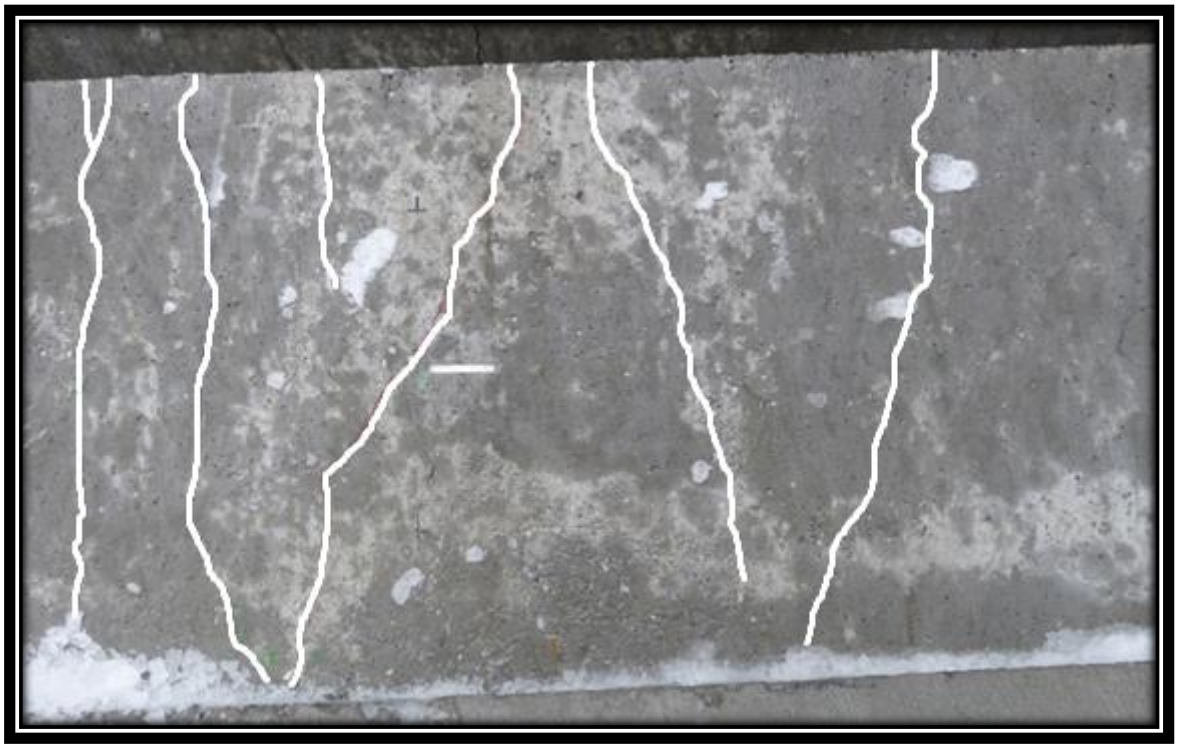

**Figure 45: Discrete Connector Specimen 1—Crack Pattern (Bottom of Specimen)**

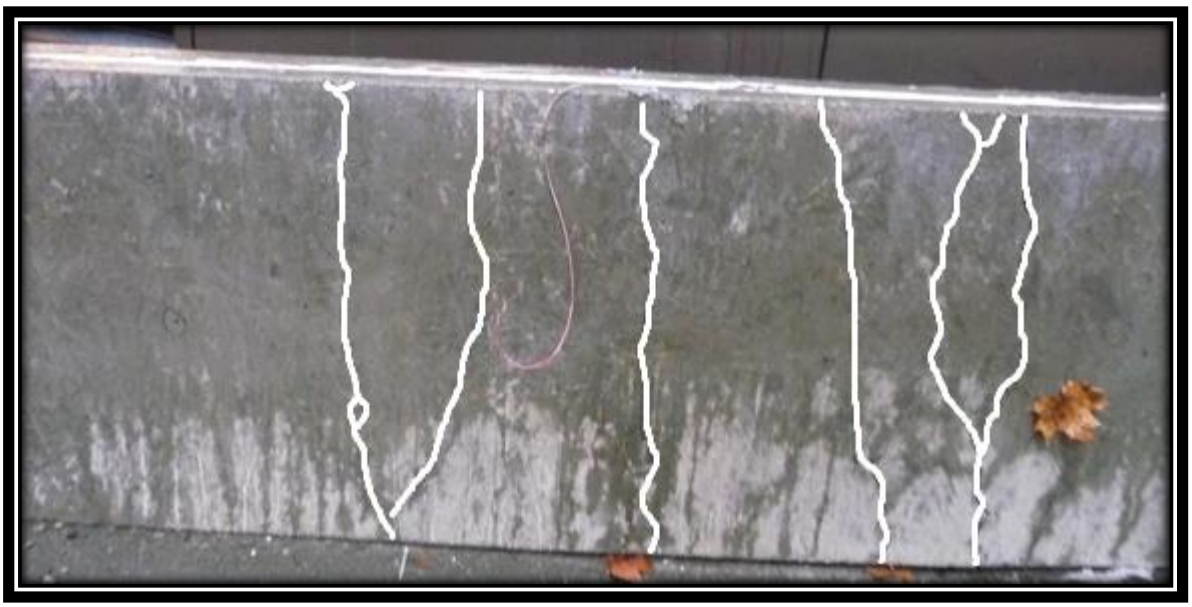

**Figure 46: Discrete Connector Specimen 2—Crack Pattern (Bottom of Specimen)**

The angle to the cracking patterns seen in Group 1 clearly shows a mix of bending and shear failure. Ultimately though, shear was the initial failure mode of these specimens.

## GROUP 2:

**Figure 47: Segmental Connector Specimen 1—Crack Pattern (Bottom of Specimen)**

**Figure 48: Segmental Connector Specimen 2—Crack Pattern (Bottom of Specimen)**

The first of the segmental specimen shows cracking at extreme angles, which fits with the shear failure of the specimen, as it was loaded with an effective length of 8-feet. The angles of the cracks in the second specimen are much less drastic, which corresponds with the bending failure that it experienced.

## GROUP 3:

**Figure 49: Continuous Connector Specimen 1—Crack Pattern (Bottom of Specimen)**

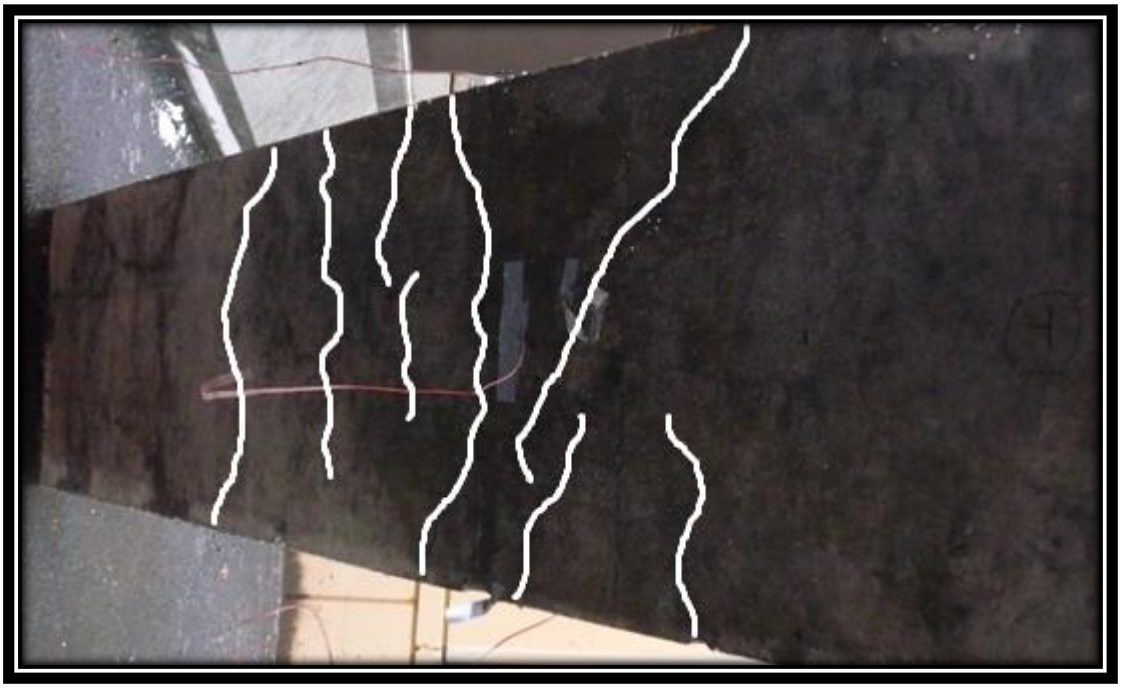

**Figure 50: Continuous Connector Specimen 2—Crack Pattern (Bottom of Specimen)**

Both of the continuous connector specimen experienced bending failures, but in both cases, the cracks still deviate in a manner that suggests secondary shear failure.

## GROUP 4:

**Figure 51: Solid Specimen 1—Crack Pattern (Bottom of Specimen)**

**Figure 52: Solid Specimen 2—Crack Pattern (Bottom of Specimen)**

Both solid specimen exhibit excellent shear failure as can be seen with the mostly straight cracks that cross from one edge of the slab to the other. In these situations, there was no secondary shear failure as is shown by the lack of deviation to the angle of the crack patterns.

## 3.6 DISCUSSION/RESULTS

### 3.6.1 DEGREE OF COMPOSITE ACTION

#### 3.6.1.1 LOAD-DEFLECTION METHOD

The degree of composite was first determined by the load and deflection of each specimen compared to that of the solid control specimens, given simply supported conditions. The degree of composite action was calculated using the following equation:

$$DCA = \frac{\left(\frac{1}{EI}\right)_{0\%} - \left(\frac{1}{EI}\right)_{Actual}}{\left(\frac{1}{EI}\right)_{0\%} - \left(\frac{1}{EI}\right)_{100\%}}(100\%)$$

where $\left(\frac{1}{EI}\right)_{0\%}$ represents that of the slab if acting with 0% composite action (non-composite), $\left(\frac{1}{EI}\right)_{Actual}$ represents the value calculated for the slab from test results based on load and

deflection, and $\left(\frac{1}{EI}\right)_{100\%}$ represents the value calculated for the solid control specimen, which is 100% composite. In order to determine $\left(\frac{1}{EI}\right)_{Actual}$, the following equation of a simply supported beam was applied:

$$\Delta = \frac{PL^3}{48EI}$$

For all calculations, the range of the load (P) was set as 0-1400lbs. By focusing on the data collected within this region, a best-fit line was applied, such that the slope would be equal to $\frac{P}{\Delta}$. Given that the load to deflection ratio, effective length, and modulus of elasticity (E) are all known values, it is possible to determine the moment of inertia (I) for each specimen. Using this information, the DCA for each was calculated. The results can be seen in Table 6. A more detailed explanation of these calculations can be seen in APPENDICES

APPENDIX 1 and an example calculation can be seen on the following page.

## Discrete Shear Connector DCA (Load-Displacement Method) Example:

Given: $f'_c := 4120psi$ $E := 57000\sqrt{f'_c \cdot psi} = 3.659 \times 10^3 ksi$

$\frac{P}{\Delta} = 36692 \frac{lbf}{in}$ $L := 9ft$ $\Delta = \frac{P \cdot L^3}{48EI}$

$b := 24in$ $I_{solid} := 2197.19in^4$ $h := 3in$

Required: Determine the DCA for the specimen.

## Solution:

Determine the Moment of Inertia for the specimen:

Based on the deflection equation for a simply supported beam, the following can be concluded:

$$I = \frac{P}{\Delta} \cdot \frac{L^3}{48E}$$

$$I_{ex} := \left(36692 \cdot \frac{lbf}{in}\right) \cdot \left(\frac{L^3}{48 \cdot E}\right) = 263.195\,in^4$$

Determine the Moment of Inertia for a fully non-composite specimen:

$$I_{nc} := 2 \cdot \left(\frac{b \cdot h^3}{12}\right) = 108\,in^4$$

Based on the following equation, the DCA can be calculated:

$$DCA := \frac{\left(\frac{1}{E \cdot I_{nc}}\right) - \left(\frac{1}{E \cdot I_{ex}}\right)}{\left(\frac{1}{E \cdot I_{nc}}\right) - \left(\frac{1}{E \cdot I_{solid}}\right)} \cdot (100\%)$$

DCA = 62.014 %

**Table 6: Degree of Composite Action (DCA)—Load-Deflection Method**

| Specimen | P/Δ | I | EI | 1/EI | DCA |
|---|---|---|---|---|---|
| Solid Slab | 306310 | 2197.190642 | 8038799640 | 1.24E-10 | 100.00% |
| | 129346 | 927.811109 | 3394556424 | 2.95E-10 | 92.93% |
| Discrete Connectors | 36692 | 263.1951913 | 962944848 | 1.04E-09 | 62.01% |
| | 92369 | 662.5715857 | 2424132036 | 4.13E-10 | 88.03% |
| Segmented Connectors | 110534 | 792.8708512 | 2900854296 | 3.45E-10 | 90.84% |
| | 55503 | 398.128276 | 1456620732 | 6.87E-10 | 76.64% |
| Continuous Connectors | 107414 | 770.4907957 | 2818973016 | 3.55E-10 | 90.43% |
| | 145932 | 1046.784058 | 3829839408 | 2.61E-10 | 94.32% |

Based on theory, the moment of inertia of a 24”x10” cross-section is 2129in$^4$. For this reason, the first solid slab was selected as the fully composite specimen due to the data showing 100% composite action, as a solid slab should theoretically exhibit, with the other (highlighted) being disregarded.

In the case of the discrete connectors, it can be seen that one specimen exhibits a DCA of 88%. This is exceptionally high for these specimens, particularly based on real-time test observations. Because of this and the fact that this is almost as high as the segmental and continuous connector specimens, it was decided to exclude this result.

With the segmental connector specimen, there is a large variance in the results. Based on further testing and analysis results (presented in Chapter 4), it was determined that the first specimen’s results were more reliable and that the other (highlighted) specimen’s results should be disregarded.

Because the continuous connector specimens exhibit similar results, neither specimen was discarded. The average of the two calculations for DCA (92.37%) will be used for further comparison.

It can be seen that the continuous shear connectors produced the highest DCA; however, the segmental shear connectors perform at a comparable level with a 26% reduction in material. It should be noted that as the EI-value for each specimen increases, as does the DCA.

#### 3.6.1.2 STRAIN DISTRIBUTION METHOD

In the case of a fully composite specimen, the strain distribution across the depth of the specimen should be completely linear. Likewise, when the specimen is fully non-composite,

each wythe of the specimen should exhibit a strain distribution that crosses the neutral axis in each wythe. To determine each specimen's DCA, the strain was analyzed at a time when all specimens were subject to the same moment. The following equation was used to determine the level of composite action of the various specimens.

$$DCA = \frac{\Delta x_{Actual} - \Delta x_{0\%}}{\Delta x_{100\%} - \Delta x_{0\%}}(100\%)$$

where $\Delta x_{0\%}$ represents the change in the calculated strain equation from one wythe to the other in a slab acting with 0% composite action (fully non-composite), $\Delta x_{Actual}$ represents the change in the calculated strain equation from one wythe to the other in a slab from test results based on load and deflection, and $\Delta x_{100\%}$ represents the strain difference calculated for the solid control specimen, which is 100% composite. As is expected for a specimen that is 100% composite, there is no variation in the strain distribution (refer to Figure 39). In the cases of the other specimen, equations were produced for the strain distribution across each wythe (refer back to Figure 40, Figure 41, & Figure 42). Using these equations and assuming an arbitrary datum, the x-value produced for each equation (both wythes) could be determined. From these values, a difference was calculated. In the case of $\Delta x_{0\%}$ , a more detailed explanation of the calculation is provided in APPENDICES

APPENDIX 1. On the following page, an example calculation using this method can be seen. A summary of the results using this method can be seen in Table 7.

**Table 7: Degree of Composite Action (DCA)—Strain Distribution Method**

| DCA - Strain Distribution Method | | | | | |
|---|---|---|---|---|---|
| **Specimen** | $\mathbf{X_{bot\text{-}ext}}$ | $\mathbf{X_{top}}$ | $\mathbf{X_{max}}$ | **ΔX** | **DCA** |
| Solid | - | - | - | 0 | 100% |
| Discrete | -117.6349 | -24.015209 | 669.6419 | 93.619688 | 86% |
| Segmental | 7.6666667 | -47 | 669.6419 | 54.666667 | 92% |
| Continuous | -17.333333 | -62 | 669.6419 | 44.666667 | 93% |

Again, the continuous shear connectors produce the highest DCA, but only by 1%. These results are extremely close to those calculated in the previous method, thus confirming the calculations. Note that in this method, a lower difference between strain distribution results in a greater DCA.

It should be noted that the specimen which supplied the strain data for the discrete specimen corresponds to the specimen which was excluded from the previous DCA calculation. As before, the DCA is far too high to be relied up and as such should be neglected again.

## Segmental Shear Connector DCA (Strain Distribution Method) Example:

Given: $y_1 = -0.75x - 30.25$ $\quad y_{bar1} := 1.5in$ $\quad y_{bar2} := 3in$ $\quad y := 5$

$y_2 = -0.75x + 10.75$ $\quad M := 18.9kip \cdot in$ $\quad b := 24in$ $\quad h := 3in$

$f'_c := 4120psi$ $\quad E := 57000\sqrt{f'_c \cdot psi} = 3.659 \times 10^3 ksi$

Required: Determine the DCA for the specimen.

## Solution:

Determine $\Delta x_{0\%}$:

By assuming different values of 'y' and using the following equation, the slope of the strain distribution for a fully non-composite specimen can be calculated. Assuming that this distribution crosses the neutral axis at the center of each wythe, the difference ($\Delta x_{0\%}$) can be calculated:

$$\varepsilon = \frac{M \cdot y}{E \cdot I} \qquad I := \frac{b \cdot h^3}{12} = 54 in^4$$

$$\varepsilon_1 := \left(\frac{M \cdot y_{bar1}}{E \cdot I}\right) \cdot 10^6 = 143.495 \qquad \varepsilon_2 := \left(\frac{M \cdot y_{bar2}}{E \cdot I}\right) \cdot 10^6 = 286.989$$

$$slope := \frac{y_{bar1} - y_{bar2}}{(\varepsilon_1 - \varepsilon_2) \cdot in} = 0.01$$

Assuming the top of the specimen to be the datum, use the distance between the top of the specimen and the center of each wythe to determine the values of 'x':

$$x1 := \frac{1.5}{slope} = 143.495 \qquad x2 := \frac{8.5}{slope} = 813.137$$

$$\Delta x_{0\%} := x2 - x1 = 669.642$$

Using the equations provided by the strain distribution and assuming an arbitrary datum, $\Delta$xex can be calculated:

$$x_1 := \left(\frac{y + 30.25}{-0.75}\right) = -47 \qquad x_2 := \left(\frac{y - 10.75}{-0.75}\right) = 7.667$$

$$\Delta x_{ex} := x_2 - x_1 = 54.667$$

Because a fully composite specimen would have no variance, $\Delta x1_{00\%} = 0$:

$$DCA := \left(\frac{\Delta x_{ex} - \Delta x_{0\%}}{0 - \Delta x_{0\%}}\right)(100\%)$$

DCA = 91.836 %

### 3.6.2 STRENGTH & STIFFNESS

The strength and stiffness effects of the various connectors as compared to a solid slab are presented in Table 8. The strength ratio (with respect to a solid slab) was calculated by dividing the maximum load applied to each specimen by the maximum load sustained by the solid slab. The stiffness is determined by dividing the EI-value experienced by the each specimen in the linear-elastic region by the EI-value experienced by the solid slab at an identical load (see Table 6 for values). The failure mode provided by these connectors is also provided.

$$Strength = \frac{P_{max}}{P_{solid}}$$

$$Stiffness = \frac{EI_{Actual}}{EI_{solid}}$$

**Table 8: Strength/Stiffness Comparison**

| Connector | Strength | Stiffness | Failure Mode |
|---|---|---|---|
| Discrete | 66.50% | 11.98% | Shear |
| Segmental | 82.04% | 36.58% | Bending |
| Continuous | 82.52% | 47.64% | Bending |

In both tables, it can be seen that a greater DCA results in a higher level of strength and stiffness with respect to solid slabs. For this reason the segmental and continuous connectors both could be used in further study, as they both provide a high level of strength and a comparable level of stiffness.

## 3.7 CONCLUSIONS

This study has shown the FRP plate shear connectors are feasible for reinforced concrete sandwich panels used in roof/floor applications. The level of composite action depends on the configuration of the shear connectors. With this level of composite action comes a variation in strength and stiffness. These variations also affect the failure mode of the panels. As high strength, stiffness, and bending failure are paramount for this study, the discrete connectors will not be used in further studies.

It was found that the segmental connectors present a large reduction (26%) in shear connector materials (FRP) compared to the continuous connectors and additionally provide comparable strength, stiffness, and acceptable failure modes. In both methods for calculating DCA, the segmental connectors performed almost as well as the continuous connector specimens. Due to exceptional performance and low material requirements, the segmental connectors have been selected to be used in further study; however, further tests with the continuous connectors will be presented in Chapter 4 as they were conducted simultaneously with the tests that have been presented in this chapter.

# CHAPTER 4: DEVELOPMENT OF FPCS PANELS

## 4.1 INTRODUCTION

The purpose of this chapter is to determine the effect of the application of external FRP plates on the sandwich panels. This chapter is divided into two sections as the initial testing took place simultaneously with the testing presented in Chapter 3. The subsequent testing took place several months later and incorporated modifications to the design, the details of which are described in this chapter. As before, the specimens were evaluated with respect to strength, stiffness, and DCA.

## 4.2 FPCS PANELS WITH FRP TOP PLATE

### 4.2.1 EXPERIMENTAL PROGRAM

#### 4.2.1.1 SPECIMEN DETAILS

Two groups of typical sandwich panels with a top FRP plate and wythe configuration of 3”+4”+3” (top wythe, EPS foam core, bottom wythe thickness; see Figure 53), but with varying shear connector configurations were then considered (segmental and continuous). Due to the application of the external FRP plate, no compression reinforcement or top wythe temperature steel was added. All other reinforcement remained identical to that described in Chapter 3.

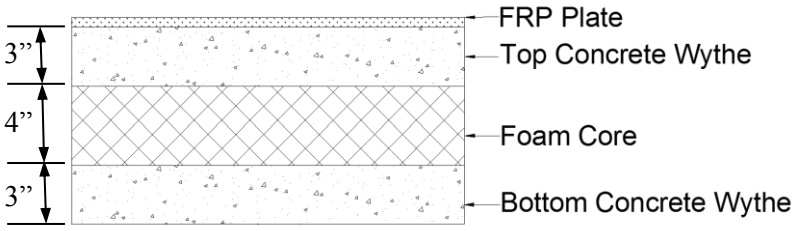


**Figure 53: Sandwich Panel with Top FRP Plate**

All specimen were 2’x9’x10”. The reinforcement layout can be seen in Table 1 and the dimensions of the specimen can be seen in Figure 54 & Figure 55.

**Table 9: Specimen Details**

| Group # | Compression Steel (#4 bars) | Tension Steel (#5 bars) | Top Temp. Steel (#4 bars) | Bottom Temp. Steel (#4 bars) | Load Condition | Shear Connectors |
|---|---|---|---|---|---|---|
| 1 | N/A | (2) @ 12" O.C. | N/A | (5) @ 18" O.C. | 3-pt Bending | Segmental |
| | N/A | (2) @ 12" O.C. | N/A | (5) @ 18" O.C. | 3-pt Bending | Segmental |
| 2 | N/A | (2) @ 12" O.C. | N/A | (5) @ 18" O.C. | 3-pt Bending | Continuous |
| | N/A | (2) @ 12" O.C. | N/A | (5) @ 18" O.C. | 3-pt Bending | Continuous |

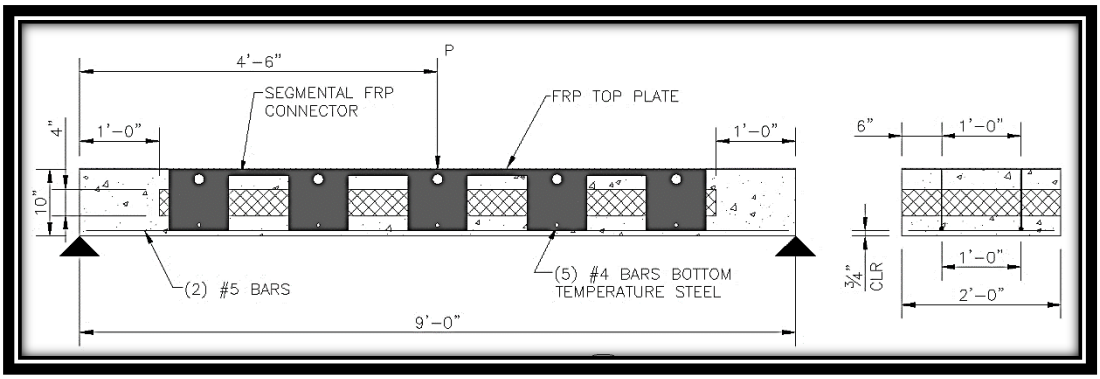


**Figure 54: Segmental Shear Connector w/FRP Plate Layout**

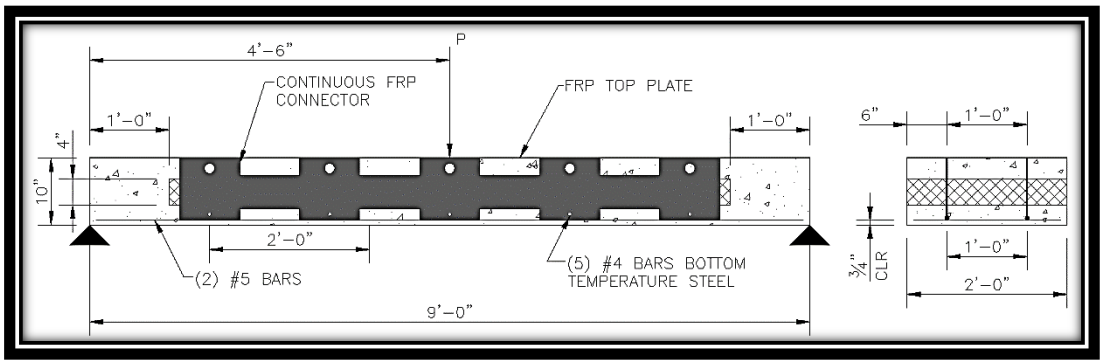


**Figure 55: Continuous Shear Connector w/FRP Plate Layout**

### 4.2.1.2 MATERIAL PROPERTIES

All concrete, foam insulation, and FRP material properties can be referred to in Chapter 3. The epoxy adhesive used to bond the external FRP plate to the concrete was the LORD® 312A/B epoxy adhesive, the material properties of which can be found in in APPENDIX 2.

### 4.2.1.3 SPECIMEN FABRICATION

Most procedures and techniques used in the fabrication of these slabs are identical to those presented in Chapter 3 with the exception of the details provided within this section.

#### 4.2.1.3.1 SHEAR CONNECTORS

The segmental and continuous connectors are similar to those presented in Chapter 3, with a few small differences. Where in Chapter 3, the connectors offered a ¾" clear distance at the top and bottom, the connectors for Chapter 4.1 only provide the ¾" clear distance on the bottom and extend all the way to the top FRP plate. Additionally, the holes which were originally used for the temperature steel in the top wythe have been increased in size. As there is no temperature steel in the top wythe to act as anchors, the larger holes provide an area for the concrete to flow through and develop a natural anchor within the shear connectors. These alterations and all other details for segmental and continuous shear connectors can be seen in Figure 56 & Figure 57, respectively.

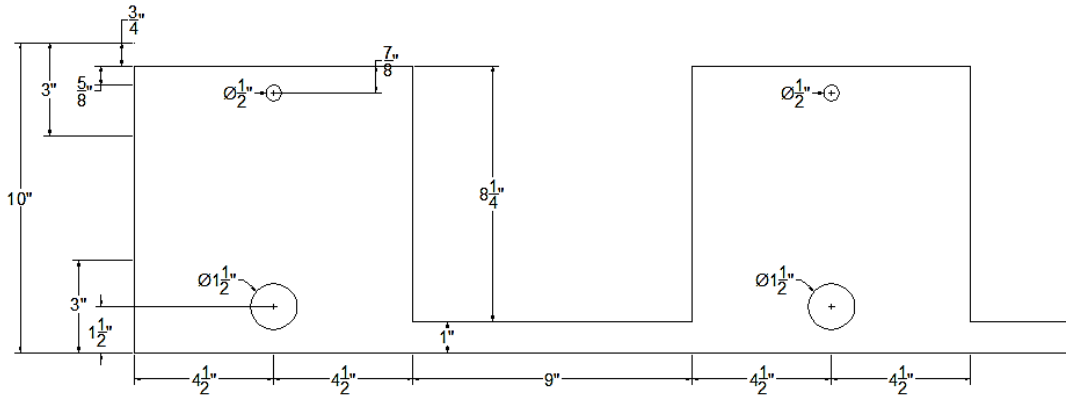


**Figure 56: Chapter 4.1 Segmental Shear Connector Detail**

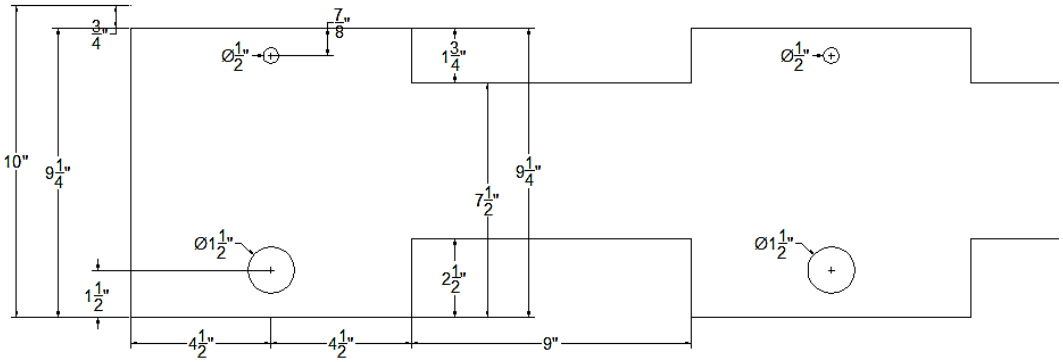


**Figure 57: Chapter 4.1 Continuous Shear Connector Detail**

#### 4.2.1.3.2 TOP FRP PLATE

The same FRP material was used for the top plate as was used to produce the shear connectors (see Table 3). They were cut into 9'x2' plates to be bonded to the slabs at the time of placement.

#### 4.2.1.3.3 POUR PROCEDURE

A wet bond (the direct application of uncured/wet concrete to uncured/wet adhesive) was implemented in order to properly bond the top FRP plate to the slabs as they cured. This required the slabs to be poured "upside-down" such that the top plate sat in the bottom of the wooden concrete forms as described in Chapter 3. Just prior to pouring the first layer of concrete, the FRP plates were placed in the forms and the adhesive added in order to develop a "wet bond" (see Figure 58). Once applied, the procedures for the segmental and continuous connector specimen described in Chapter 3 were repeated with the connectors and reinforcement inverted.

**Figure 58: Concrete Poured on FRP w/Adhesive (Wet Bond)**

## 4.2.2 TEST SETUP

### 4.2.2.1 TEST LAYOUT

The three-point bending test layout as described in Chapter 3 (refer to Figure 19 for schematic plan) was repeated for this chapter. The slab was positioned such that the FRP plate was on the top.

### 4.2.2.2 INSTRUMENTATION

The instrumentation is identical to that of Chapter 3, but for the top. Rather than using an N2A-06-20CBW-120 gage in position 4 (see Figure 59), a CEA-06-250UN-120 gage (same as used on the tension reinforcement) was applied to the top surface. This was done because the top surface was now FRP and not concrete. Two additional CEA-06-250UN-120 gages were also added to the top surface (positions 8 and 9 in Figure 59) in order to assist in monitoring de-bonding of the FRP plate.

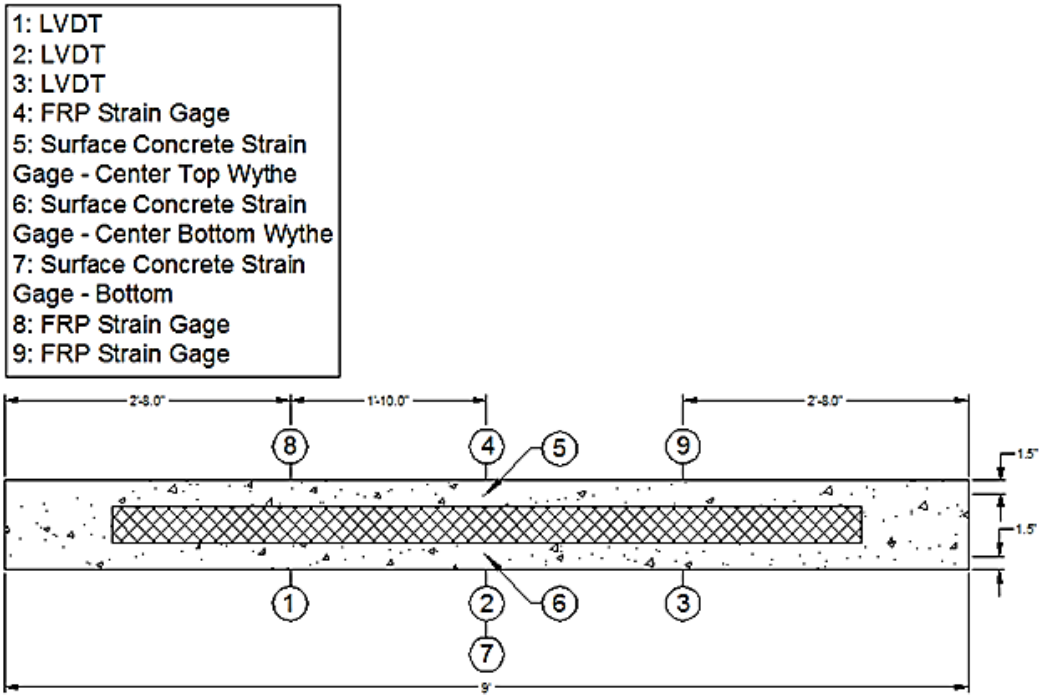


**Figure 59: Chapter 4.1 Instrumentation Layout**

### 4.2.3 TEST PROCEDURE

(Please refer back to Chapter 3)

### 4.2.4 EXPERIMENTAL RESULTS

Upon stripping the forms from the specimens, it was noticed that there were issues with the bonding of the FRP plate to the top of the specimens. The plates were cut slightly too large for the forms, thus causing them to ripple and not lie flat in the forms. Because of this, the FRP did not bond as well as was hoped. This poor bonding (see Figure 60) resulted in poor performance in some specimens, which will be noted later.

**Figure 60: Debonding of FRP Top Plate**

### 4.2.4.1 LOAD-DISPLACEMENT

With the first two specimens, a similar trend was noticed. The first slab exhibited a greater ultimate strength and flexibility, while the second exhibited a stiffer modulus of elasticity. In either case, their performance was fairly similar. It should be noted that the ultimate load sustained by both slabs is extremely similar (within 0.2kips).

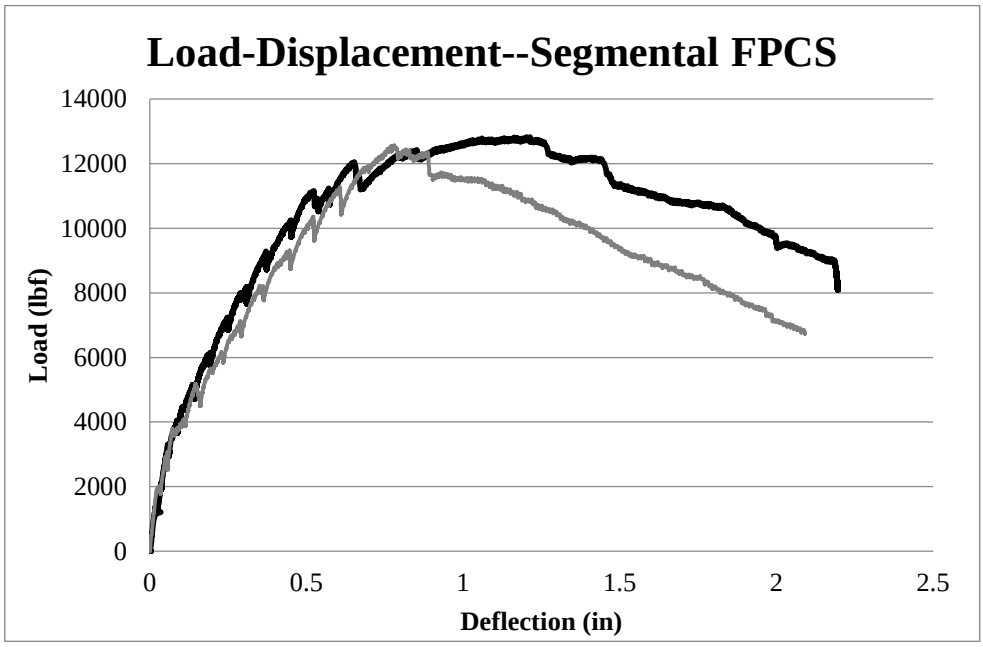


**Figure 61: Segmental FPCS Panels w/FRP Top Plate**

The specimens with the continuous connectors were extremely consistent in their linear-elastic regions (below 4000lbs) and also close in their ultimate load. The difference that can be seen is the rate of deflection in reaching these ultimate loads.

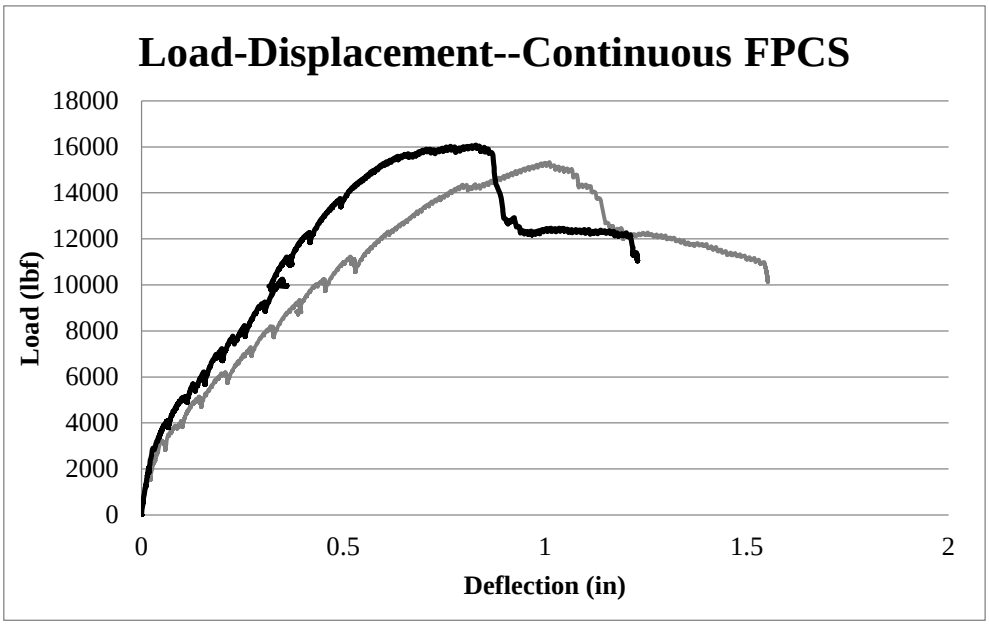


**Figure 62: Continuous FPCS Panels w/FRP Top Plate**

**Table 10: Ultimate Load Summary-FPCS Panels w/FRP Top Plate**

| Connector Type | Effective Length (ft) | Bending Type | Moment Arm (ft) | Cracking Load (kip) | Cracking Moment (kip*ft) | Failure Load (kip) | Failure Moment (kip*ft) | Max Load Deflection (in) |
|---|---|---|---|---|---|---|---|---|
| Segmental | 9 | 3-pt | 4.5 | 3 | 6.75 | 12.600 | 28.350 | 0.780 |
| | 9 | 3-pt | 4.5 | 2 | 4.50 | 12.800 | 28.800 | 1.202 |
| Continuous | 9 | 3-pt | 4.5 | 3 | 6.75 | 15.343 | 34.521 | 1.011 |
| | 9 | 3-pt | 4.5 | 3 | 6.75 | 16.000 | 36.000 | 0.779 |

### 4.2.4.2 STRAIN

#### 4.2.4.2.1 LOAD-STRAIN

SEGMENTAL CONNECTORS: FPCS PANELS

Figure 63 & Figure 64 display the load-strain curves for the top surface and tension reinforcement in the representative segmental connector specimen. As expected, the top surface experiences compression and the bottom wythe reinforcement experiences tension.

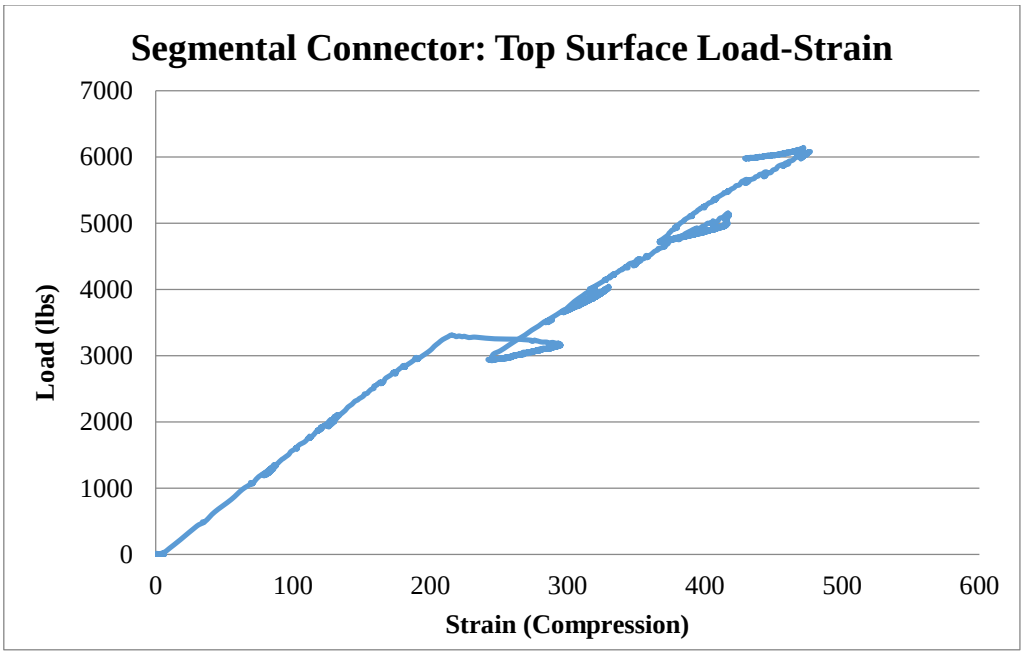


**Figure 63: FPCS Panel w/FRP Top Plate--Segmental Connector Top Surface Load-Strain**

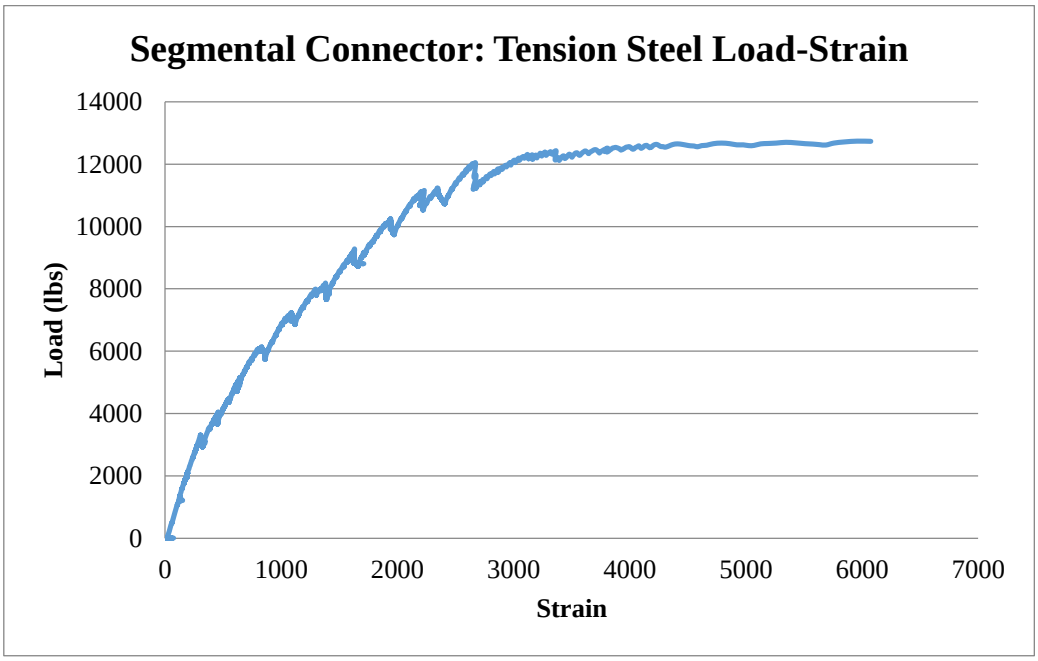


**Figure 64: FPCS Panel w/FRP Top Plate—Segmental Connector Tension Steel Load-Strain**

CONTINUOUS CONNECTORS: FPCS PANELS

Figure 65 & Figure 66 display the load-strain curves for the top surface and tension reinforcement in the representative continuous connector specimen. As expected, the top surface experiences compression and the bottom wythe reinforcement experiences tension.

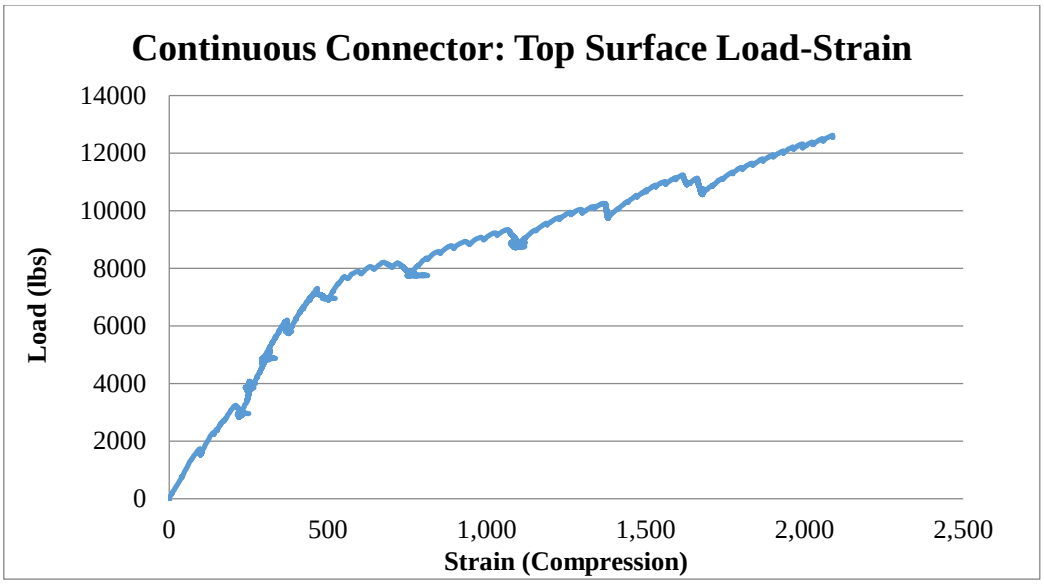


**Figure 65: FPCS Panel w/FRP Top Plate—Continuous Connector Top Surface Load-Strain**

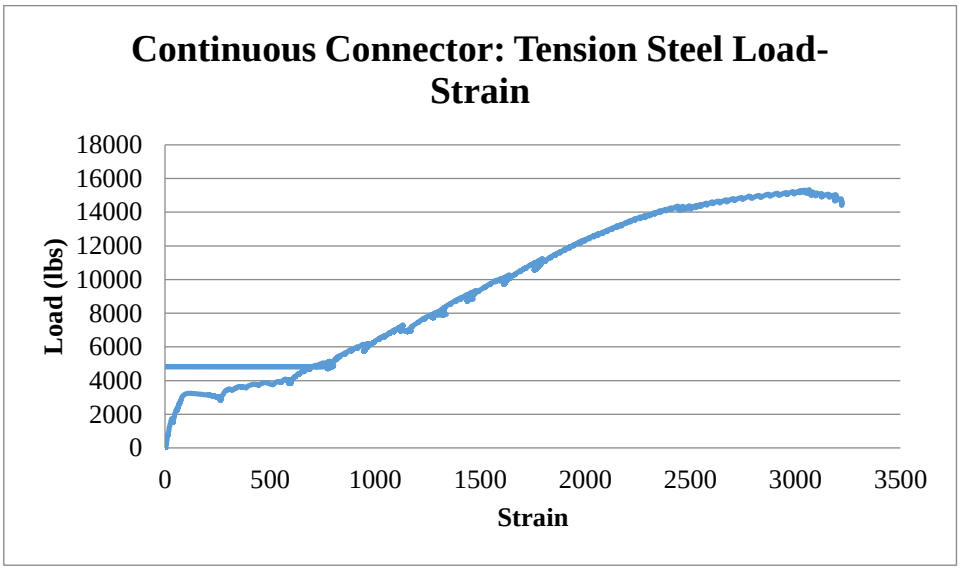


**Figure 66: FPCS Panel w/FRP Top Plate –Continuous Connector Tension Steel Load-Strain**

### 4.2.4.2.2 STRAIN DISTRIBUTION

In the case of both the segmental and continuous connectors (Figure 67 & Figure 68, respectively), the strain distribution exhibit high levels of composite action as evidenced by the lack of deviation of the calculated strain distribution equations from one wythe to the other. In both cases, each strain gage that was used to determine the distribution was monitored at the time that each gage experienced an equal moment, identically to those specimens analyzed in Chapter 3.

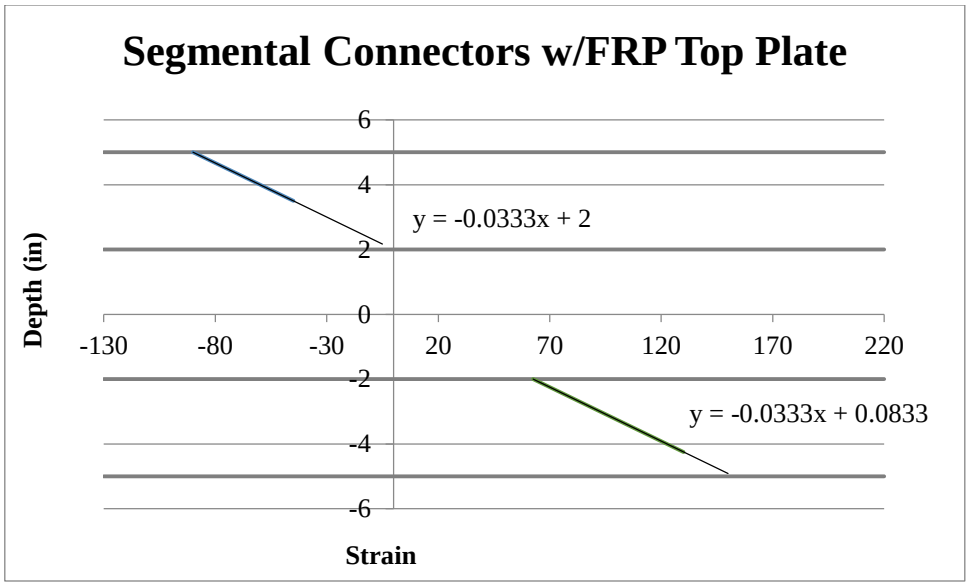


**Figure 67: Strain Distribution Across FPCS Panel w/Segmental Connectors**

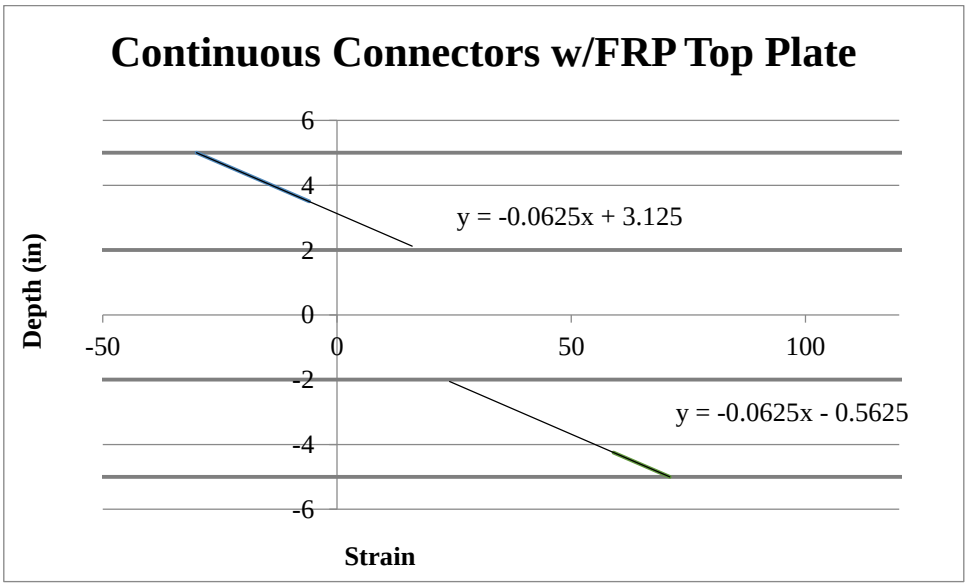


**Figure 68: Strain Distribution Across FPCS Panel w/Continuous Connectors**

### 4.2.4.2.3 FAILURE MODE

These specimens all initially failed in shear based on the crack patterns (presented in the next section) and the location of the failure (on the border between the solid concrete zone and the beginning of the insulation). Some specimens experienced secondary bending failure (see Table 11) which was noticed during testing. Figure 69 presents an example of the shear failure that these specimens experienced.

**Table 11: FPCS Panel w/FRP Top Plate—Failure Modes**

| Group | Connector Type | Initial Failure Mode | Secondary Failure Mode |
|---|---|---|---|
| 1 | Segmental | End-zone Failure | - |
| | Segmental | End-zone Failure | Bending |
| 2 | Continuous | End-zone Failure | - |
| | Continuous | End-zone Failure | Bending |


**Figure 69: Shear Failure Example (Profile View)**

### 4.2.4.3 CRACK PATTERN

#### GROUP 1:

The cracks seen on these two panels run straight across (from side-to-side), but the critical cracking occurs in areas which resulted in shear failures (notice the end of the specimen in Figure 70). These angled cracking patterns seen in the following figures, demonstrate shear failure.

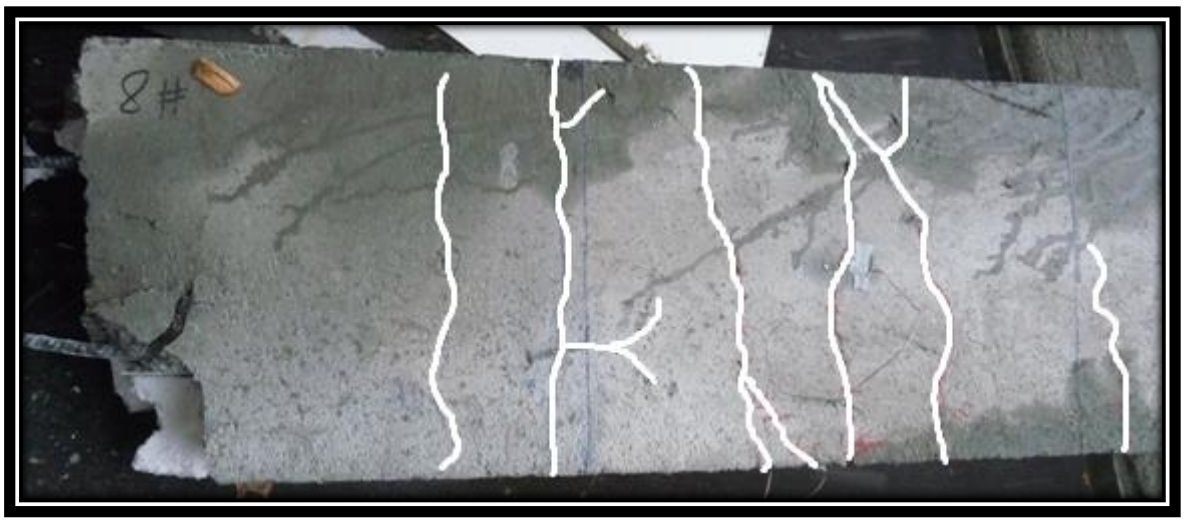


**Figure 70: Segmental FPCS Specimen 1—Crack Pattern (Bottom of Specimen)**

**Figure 71: Segmental FPCS Specimen 2—Crack Pattern (Bottom of Specimen)**

## GROUP 2:

Much like the preceding group of specimens, the critical cracking occurred at angles that were not straight across from one side to the other, which identify shear failure. As before, there are some cracks that are straight across from one side to the other, which identifies the secondary failure of the slabs as bending (see Figure 72 & Figure 73).

**Figure 72: Continuous FPCS Specimen 1—Crack Pattern (Bottom of Specimen)**

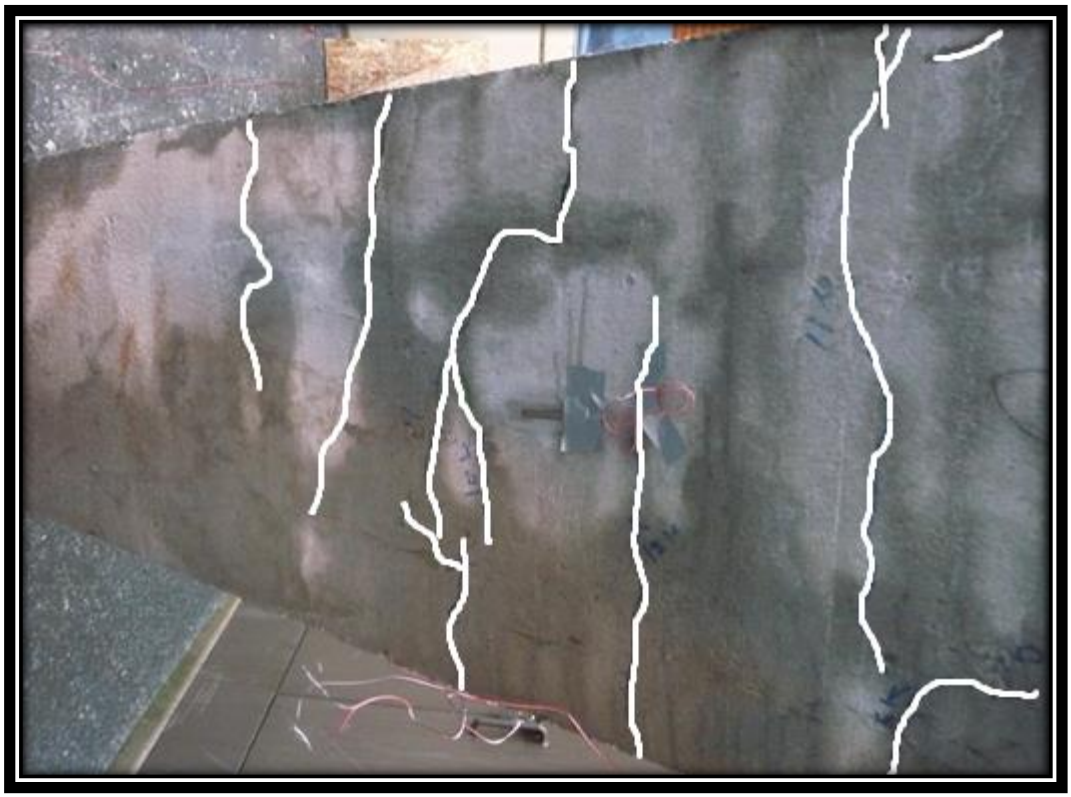

**Figure 73: Continuous FPCS Specimen 2—Crack Pattern (Bottom of Specimen)**

## 4.3 FPCS PANELS WITH TOP & SIDE FRP PLATES

### 4.3.1 EXPERIMENTAL PROGRAM

#### 4.3.1.1 ADHESIVE/AGGREGATE BONDING ANALYSIS

Due to poor bonding in the previous test (refer back to Figure 60), the decision was made to test a different adhesive (LORD® 305 Epoxy Adhesive; see APPENDIX 2 for properties) to determine whether or not better bonding was possible. Additionally, it was decided to test the bonding of aggregate to the FRP plates such that the wet concrete would bond more readily with the aggregate, which would be secured to the FRP plates via the adhesive.

Table 12 represents the optimum sizes and distributions of flint chips for bonding to FRP, determined through research [12].

**Table 12: Cho, et al**

| | Metric | US |
|---|---|---|
| **Optimum Aggregate Size** | 4 - 7 mm | 0.157 - 0.276 in |
| **Optimum Distribution** | 4 $kg/m^2$ | 0.82 $lb/ft^2$ |

Given the availability of materials, it was determined that flint chips would not be an option as they are primarily a product found on the east coast of the United States. For this reason, local concrete batch plants were contacted and Pre-Mix, Inc. agreed to supply a sample of their smallest aggregate, which was 3/4” minus. These samples were taken to Dr. Fouad Bayomy, PE (UI Professor of Pavement and Construction Material Engineering) to determine if they were of a sufficient quality and angulation for concrete bonding. He concluded that the material was suited for such an application due to adequate angularity for concrete bonding.

The next issue was producing enough aggregate in the appropriate size. Given limited oven space for drying the material and a limited number and size of shakers for grading, it quickly became evident that a new approach would be necessary in order to maintain the time frame that had been chosen.

#### 4.3.1.1.1 FINE AGGREGATE VS COARSE AGGREGATE

The solution was to compare the bonding specifications of aggregate within the size distribution as shown in Table 12 (Fine Aggregate). The second distribution (Coarse Aggregate) consisted of materials in the range of 1/4”—3/4”. In both cases, all fines and materials smaller than those specified in Table 12 were removed as they could cover the adhesive and not providing adequate surface area for the concrete to bond.

Two specimens with dimensions of 1’x3’x2.5” were constructed, one with “Fine-Aggregate” and one with “Course-Aggregate” bonded to their respective FRP plates. The distribution for each sample followed that specified by Table 12. The results can be seen in Figure 75.

The specimens were positioned in three point bending as seen in Figure 74. The FRP plate that was bonded to the specimen was positioned on the bottom of the specimen such that it would experience maximum tensile forces. The specimens were loaded slowly until failure, which in both cases was a violent shear failure roughly halfway between the load-cell and one of the supports.

**Figure 74: Adhesive Test Specimen**

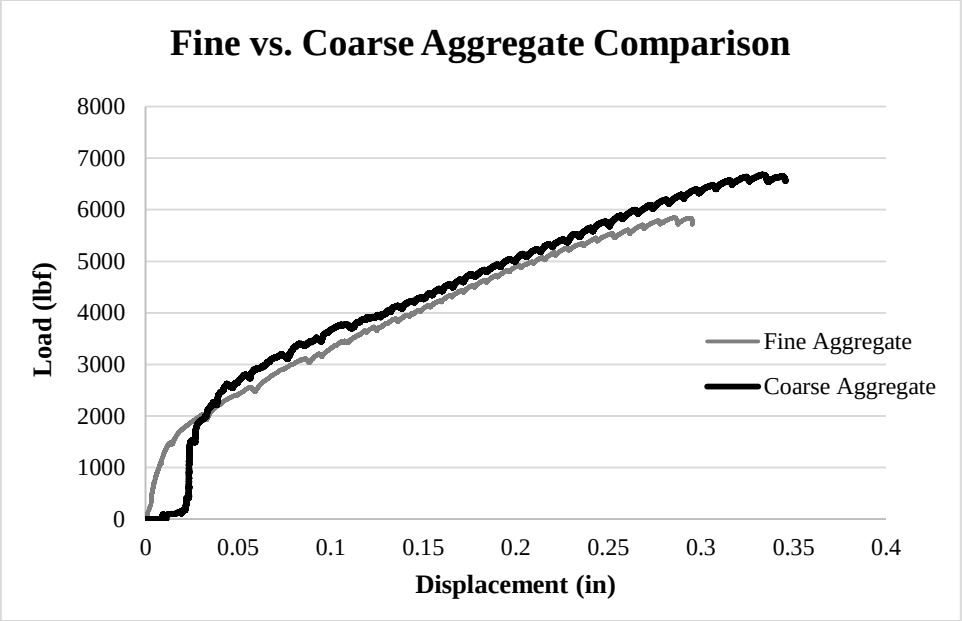


**Figure 75: Bonded Aggregate Analysis**

From this investigation, it was concluded that the material supplied by Pre-Mix, Inc. would be sufficient for our tests, in the range of 3/8”—3/4” as the coarse aggregate provided superior strength.

#### 4.3.1.1.2 MIXED AGGREGATE VS WET BOND

To be sure that aggregate bonding would provide optimum bonding of the FRP plates to the concrete; it had to be compared with a wet bond using the new adhesive. For this reason, four samples with identical dimensions to those in the previous aggregate test were constructed. Two specimens with the new aggregate blend (consisting of the same aggregate from the previous test) bonded to the FRP and two specimens were constructed with a wet bond and all four were tested as before. The results can be seen in Figure 76.

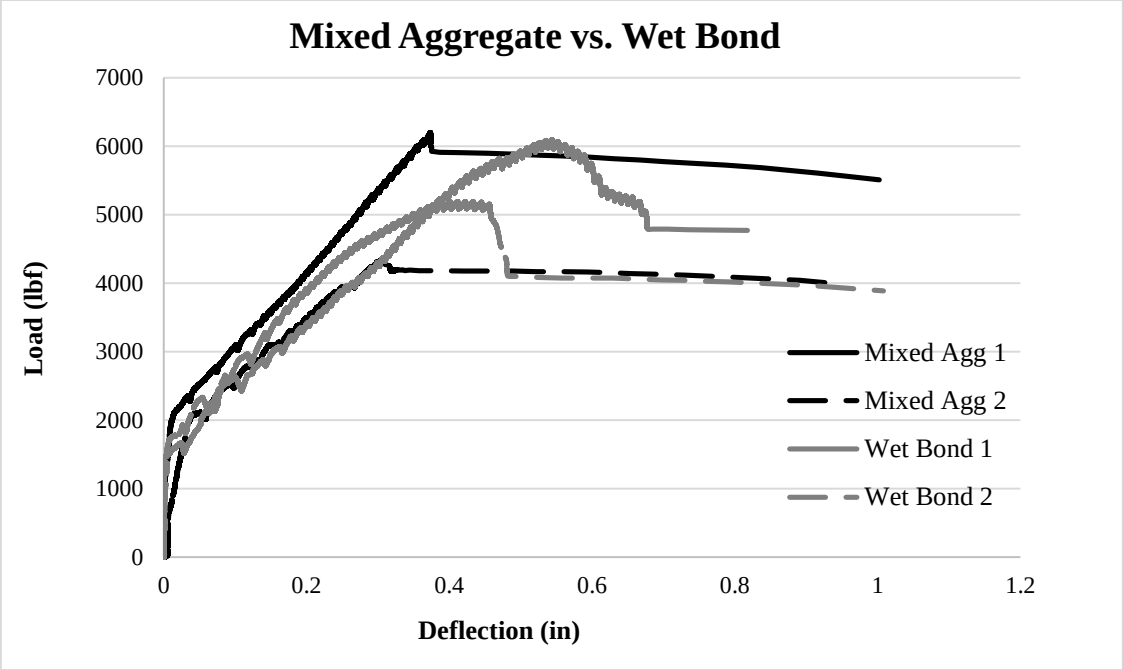


**Figure 76: Mixed Aggregate vs. Wet Bond**

From this investigation, it was seen that the mixed aggregate and the wet bond performed similarly. Considering the two strongest and stiffest of each group, note that the mixed aggregate specimen exhibits a superior stiffness compared to that of the wet bond specimen, as well as superior strength. Given this observation and the difficulty of applying the adhesive just prior to the concrete pour, knowing that the pour must be completed within a given time frame, the decision to bond aggregate to the external FRP-plates was determined to be superior.

### 4.3.1.2 SPECIMEN DETAILS

Two groups of FPCS panels with both top and side FRP external plates and varying wythe configuration (see Figure 77), were constructed. Due to the application of the external FRP plate, no compression reinforcement or top wythe temperature steel was added. All other reinforcement remained identical to that described in Chapter 3 (see Table 13).

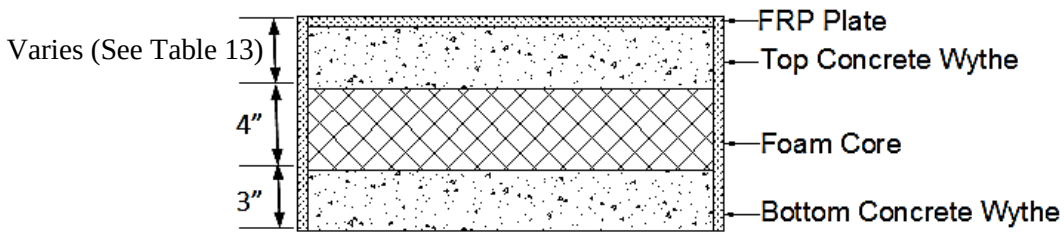


**Figure 77: FPCS Panels with Top and Side FRP Plates**

All specimen were 2’x9’x10”. The reinforcement layout can also be seen in Table 13 and the dimensions of the specimen can be seen in Figure 78 & Figure 79.

**Table 13: FPCS Panel Specimen Details**

| Wythe Configuration | Compression Steel (#4 bars) | Tension Steel (#5 bars) | Top Temp. Steel (#4 bars) | Bottom Temp. Steel (#4 bars) | Load Conditions | Shear Connectors |
|---|---|---|---|---|---|---|
| 3" - 4" - 3" | N/A | (2) @ 12" O.C. | N/A | (5) @ 18" O.C. | 3-pt Bending | Segmental |
| | N/A | (2) @ 12" O.C. | N/A | (5) @ 18" O.C. | 3-pt Bending | Segmental |
| 1" - 4" - 3" | N/A | (2) @ 12" O.C. | N/A | (5) @ 18" O.C. | 3-pt Bending | Segmental |
| | N/A | (2) @ 12" O.C. | N/A | (5) @ 18" O.C. | 3-pt Bending | Segmental |

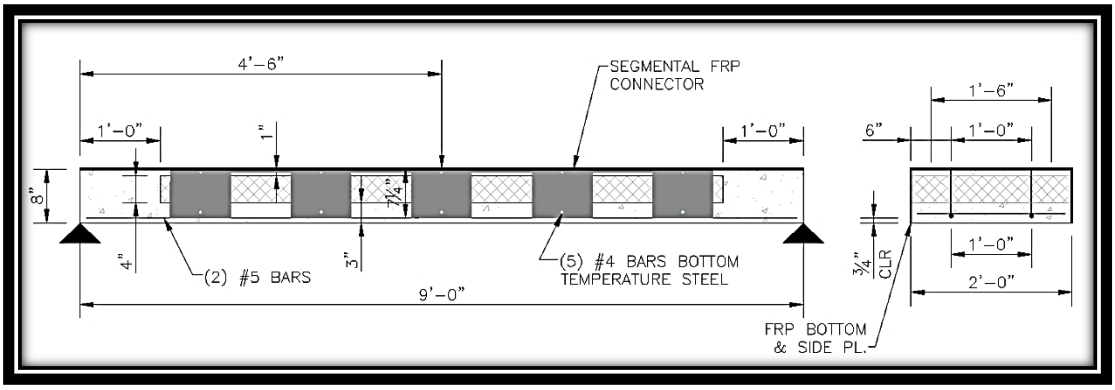


**Figure 78: 8" FPCS Shear Connector Layout**

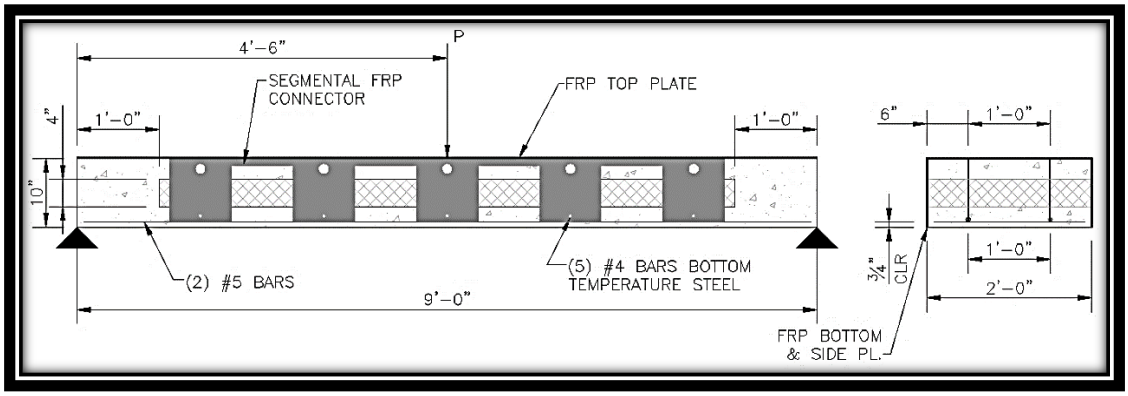


**Figure 79: 10" FPCS Shear Connector Layout**

### 4.3.1.3 MATERIAL PROPERTIES

All ESP properties are identical as have been presented in Chapter 3, as well as the shear connectors. The top and side plates, however, were produced using a thinner FRP as supplied by CRANE Composites (Table 15 & Table 16). The concrete pours for these two groups took place several days apart. For this reason, the compressive strength of concrete is different for each group. Table 14 presents the results of the compressive tests conducted for both concrete pours and the resulting strength used for later analysis.

**Table 14: Compressive Strength**

| Specimen | 10" FPCS Compressive Strength (psi) | 8" FPCS Compressive Strength (psi) |
|---|---|---|
| Cylinder 1 | 4675 | 2787 |
| Cylinder 2 | 4838 | 2818 |
| Cylinder 3 | 4648 | 2968 |
| Cylinder 4 | 5280 | 2687 |
| **Average** | **4860.25** | **2815** |

**Table 15: External FRP Plates**

| Table One: Physical Properties | | | |
|---|---|---|---|
| Typical Values | | | |
| Property | EARM | | Test Method |
| Flexural Strength | 30 x $10^3$ psi | 207 MPa | ASTM - D790 |
| Flexural Modulus | 0.7 x $10^6$ psi | 4826 MPa | ASTM - D790 |
| Tensile Strength | 47 x $10^3$ psi | 324 MPa | ASTM - D638 |
| Tensile Modulus | 2.0 x $10^6$ psi | 13,790 MPa | ASTM - D638 |
| Barcol Hardness | 35 | 35 | ASTM - D2583 |
| Coefficient of Linear Thermal Expansion | 0.80 x $10^{-5}$ in/in/°F | 14 µm/m/°C | ASTM - D696 |
| Thermal Conductivity | 0.4 Btu•in/hr•ft² °F | 5.0 cal•cm/hr•m² °C | ASTM - C177 |
| Water Absorption | 0.2%/24hrs@77°F | 0.2%/24hrs@25°C | ASTM - D570 |
| Specific Gravity | 1.75 | 1.75 | ASTM - D792 |

**Table 16: External FRP Plates (Continued)**

| Table Two: Physical Properties | | | | | |
|---|---|---|---|---|---|
| Product Code | Nominal Thickness | Nominal Weight | Finish | Size | Color |
| EARM | 0.07" 1.8 mm | 0.47 lbs/ft² 2.35 kg/m² | Embossed | Available up to 104" (2.64 m) wide and up to 300' (91 m) in length. Panels can be interlapped into packaged coils up to 700' (213 m) | White \| 85 |

As a precaution against strain gage damage and/or de-bonding, a protective coating called M-Bond J was applied at the location of strain gages within the concrete. The material properties of M-Coat J can be found in APPENDIX 2.

### 4.3.1.4 SPECIMEN FABRICATION

The fabrication of these specimen follows the same procedures described in the previous section, except where noted in the following sections.

#### 4.3.1.4.1 EXTERNAL FRP PLATE PREPARATION

The top FRP plates were cut 1/2" smaller than the dimensions of the final slab in order to allow easy insertion into the formwork, while the side FRP plates were cut 1/2" shorter in length, but to their required depth (8" or 10" depending on specimen).

The plates were then abraded with a belt sander in the regions which would receive resin. The plates were then cleaned using a heavy duty degreaser and clean gauze. Once this was completed, the resin was mixed and applied using a sharp bladed paint scraper in order to maintain thickness of resin as well as precise placement (only applying the resin where necessary on the side plates as no aggregate was required in the regions where EPS would be in contact; see Figure 80).

**Figure 80: Aggregate Bonding Location Example**

Upon the application of the resin and within the service time as specified (See APPENDIX 2) the aggregate that had been oven dried and graded was measured out and spread over the plates using the same distribution as described in Table 12. The aggregate and adhesive were then left to cure for 72 hours, in excess of the suggested 24-48 hours, in order to ensure full curing had occurred.

#### 4.3.1.4.2 TENSION STEEL PREPARATION

The tension steel was prepared and the strain gages were applied exactly as described in Chapter 3. In order to protect the strain gages though, a hydrophobic tape was applied around the bar at the location of the strain gage and M-Bond J added around the area as

specified (see APPENDIX 2) in order to protect the strain gages from damage due to water or de-bonding.

#### 4.3.1.4.3 SHEAR CONNECTOR PREPARATION

For the 10” FPCS panel, the same shear connectors were prepared as before (see Figure 56). In an attempt to gather further strain data from these slabs, strain gages were added to the central “tooth” of the strain gage (shown ahead in Figure 86). They were then covered in the same manner as the strain gages on the tension steel with the application of M-Bond J.

The 8” FPCS panel required a redesign of the segmental shear connector (shown below in Figure 81) due to the decreased depth. Once cut, strain gages were also added in the same fashion as the 10” FPCS panel (shown ahead in Figure 85) and protected with M-Bond J.

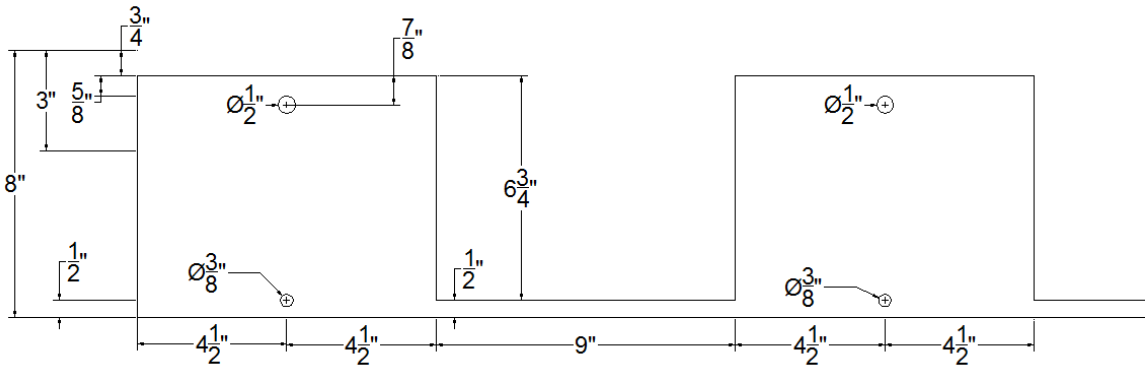


**Figure 81: 8" FPCS Segmental Shear Connector**

#### 4.3.1.4.4 CONCRETE POUR

The concrete pour began with the oiling of the forms as before. The top plate (with the aggregate facing upward) was then inserted followed by the side plates (with the aggregate facing inward) were set in place and secured with clamps.

The first lift of concrete was then added (3” or 1” depending on which specimen). At this point, the clamps were removed and the foam and shear connectors inserted, taking care to position them without getting caught on the side plates. Once the insulation was in place and all strain gage wires cleared, the final lift was added and the rest of the pour proceeded as all before it.

#### 4.3.1.4.5 PRE-TEST PREPARATION

In order for the FRP side plates to provide the confining effect that was intended, it was necessary for them to be bonded to the FRP top plate as well as to the individual wythe. In this way, the side plates would not only provide a confining effect in conjunction with the top plate, but would also serve as addition shear connectors.

The specimen were stripped and cured as described in Chapter 3. Once they had cured to their 28-day strength, they were flipped over to the position in which they would be tested, with the top FRP plate facing upwards. Once this was done, the plates were abraded and cleaned as before with heavy duty degreaser and clean gauze. Strips of chopped strand mat were then cut 6" wide, such that 3" would overlap the side plate and the top plate, and were then secured in place with duct tape. Resin was then mixed and applied liberally with a paint brush such that it would soak through the chopped strand mat and onto the abraded FRP surface. Once the resin had been applied, the coated areas were covered with cellophane wrap to prevent dirt from contaminating the resin. This was done to both edges of all panels and left to cure for one week to ensure ultimate strength. The following pictures depict this process.

**Figure 82: Abraded Surface Cleaning**

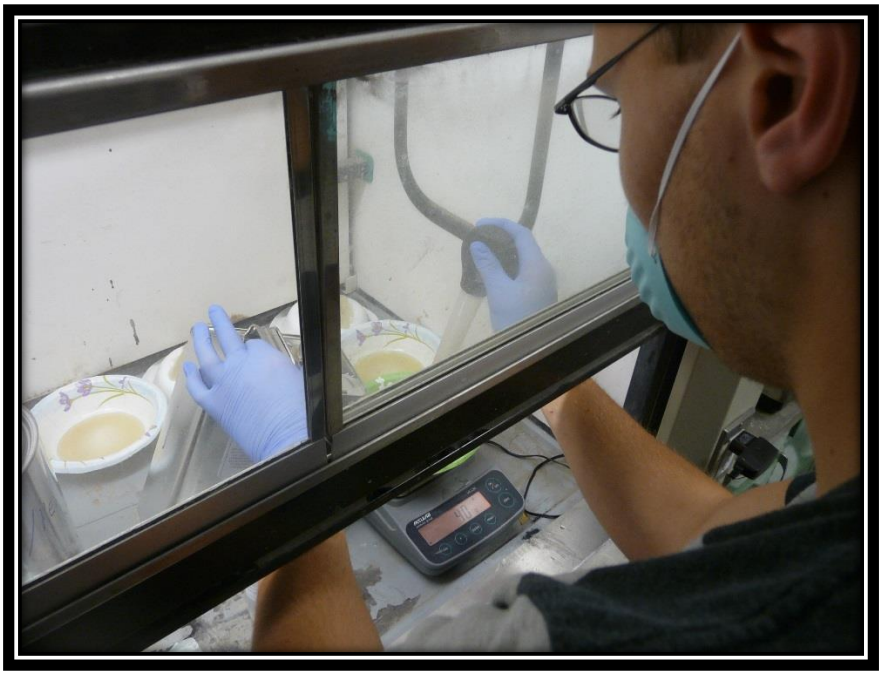

**Figure 83: Resin Mixing**

**Figure 84: Resin Application**

## 4.3.2 TEST SETUP

### 4.3.2.1 TEST LAYOUT

The three-point bending test layout as described in Chapter 3 (refer to Figure 19 for schematic plan) was repeated for this chapter. The slab was positioned such that the FRP plate was on the top.

### 4.3.2.2 INSTRUMENTATION

The instrumentation is identical to that described in Chapter 3 (regarding position). In addition, strain gages were added to both shear connectors for each specimen (see Figure 85 & Figure 86), rather than adding additional top surface strain gages as they did not provide the data that was anticipated. Similar to the first half of this chapter, an N2A-06-20CBW-120 gage at the bottom of each specimen as a concrete strain gage (see Figure 87 & Figure 88). However, due to availability with suppliers, the strain gages used for the shear connectors, FRP plates, and tension steel varied between CEA-06-250UN-120 and CEA-06-250UN-350 gages. The difference between the two is the ohms given by each (120Ω and 350Ω) and merely resulted in the need to adjust the data acquisition system. In each case of variation, the difference will be noted in the results.

The positioning of the shear connector strain gages can be seen in Figure 85 & Figure 86 and the position of the external strain gages/LVDTs can be seen in Figure 87 & Figure 88.

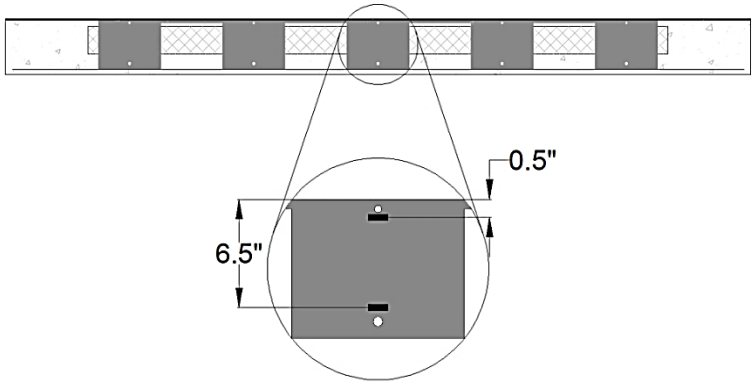


**Figure 85: 8" Shear Connector Strain Gage Positions**

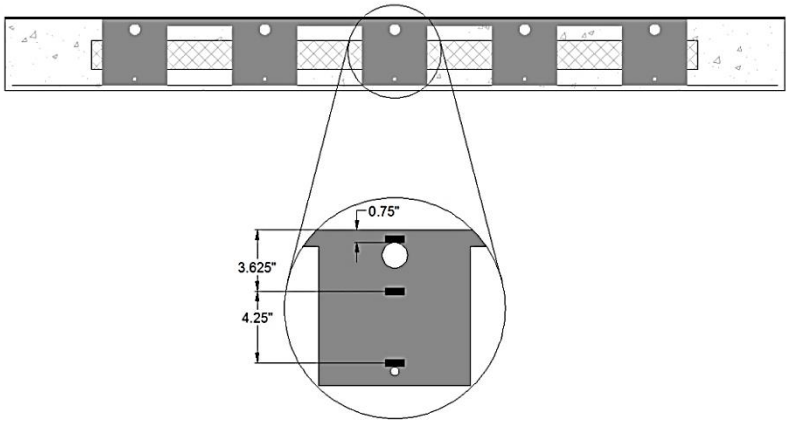


**Figure 86: 10" Shear Connector Strain Gage Positions**

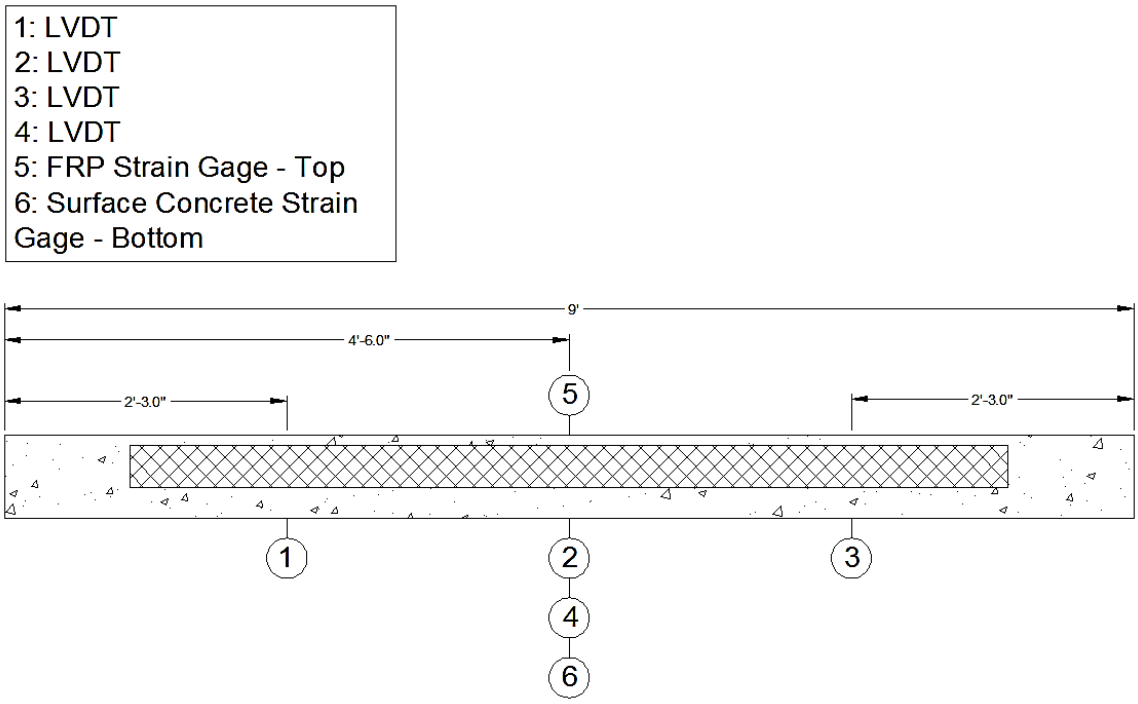


**Figure 87: 8" FPCS Panel External Instrumentation**

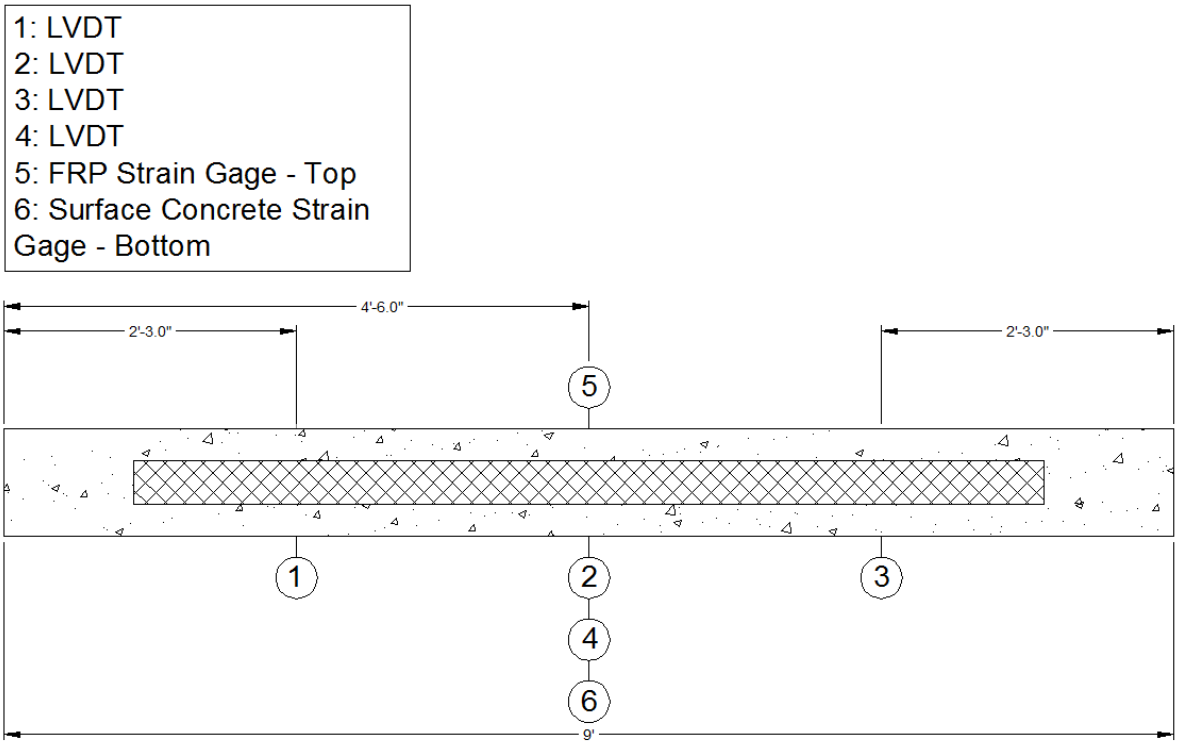


**Figure 88: 10" FPCS Panel External Instrumentation**

### 4.3.3 TEST PROCEDURE

(Please refer back to Chapter 3)

### 4.3.4 EXPERIMENTAL RESULTS

The 10” FPCS panels were well constructed and exhibited exceptional performance as will be demonstrated. The 8” FPCS panels had a much greater variation in performance. This is likely due to poor bonding of the FRP side plates to the specimen and poor vibrating techniques during the concrete pour as demonstrated in Figure 89.

**Figure 89: Debonding and Poor Concrete Vibration**

In the cases where debonding of FRP plates was noted as being a mode of failure, this refers primarily to the FRP side plates as the bond here seems to be weaker, possibly due to the

reduced bonding surface (no bonding occurs along the center where the insulation is present).

#### 4.3.4.1 LOAD-DISPLACEMENT

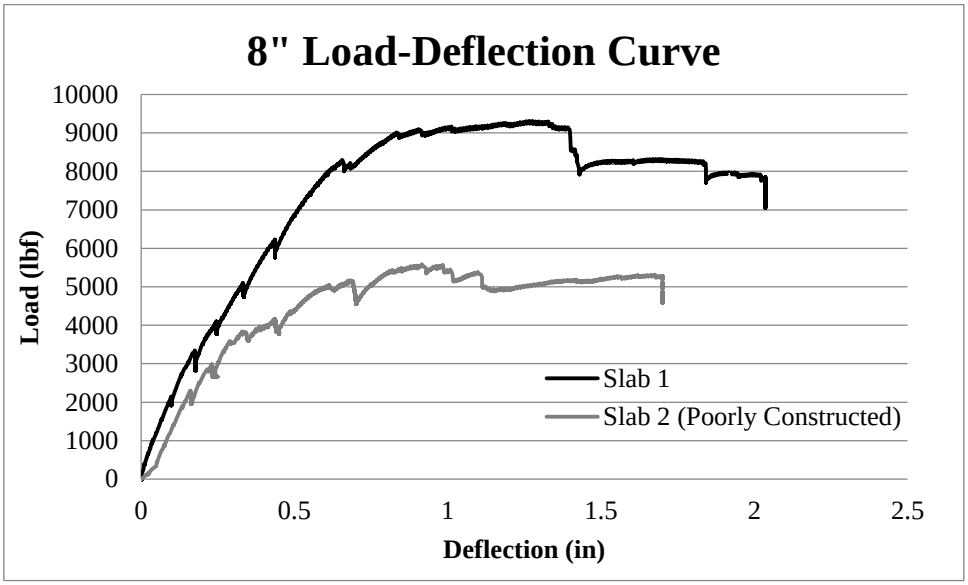


**Figure 90: 8" FPCS Panel Load-Displacement Curves**

There is a significant difference in the ultimate strength of these two specimens, which is likely due to poor construction practices, as noted before. It should be noted though that both specimens exhibit comparable behavior in the linear-elastic region.

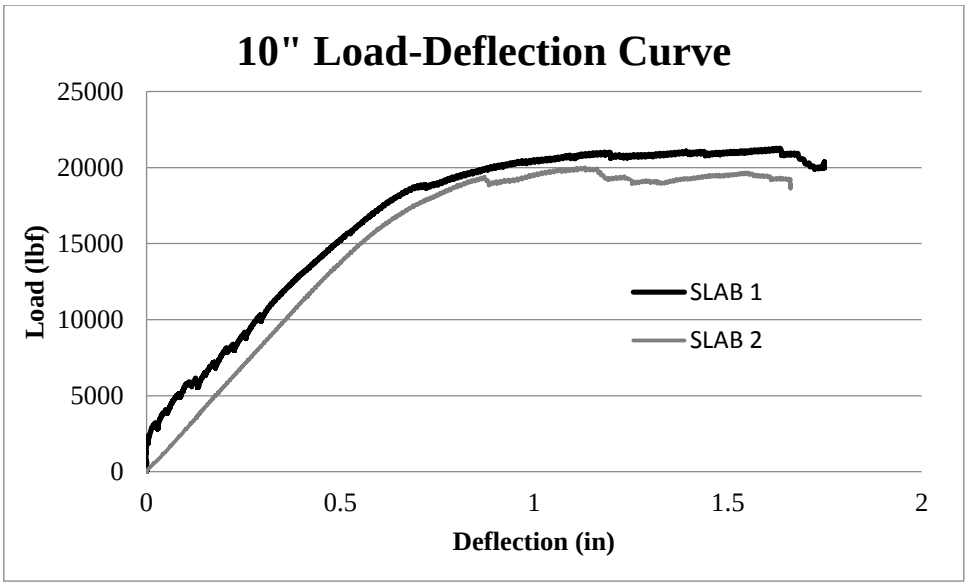


**Figure 91: 10" FPCS Panel Load-Displacement Curves**

**Table 17: FPCS Panel w/FRP Top & Side Plate—Ultimate Load Summary**

| Specimen Thickness | Effective Length (ft) | Bending Type | Moment Arm (ft) | Cracking Load (kip) | Cracking Moment (kip*ft) | Failure Load (kip) | Failure Moment (kip*ft) | Max Load Deflection (in) |
|---|---|---|---|---|---|---|---|---|
| 8" | 9 | 3-pt | 4.5 | 3 | 6.75 | 9.311 | 20.950 | 1.201 |
| | 9 | 3-pt | 4.5 | 3 | 6.75 | 5.581 | 12.557 | 0.916 |
| 10" | 9 | 3-pt | 4.5 | 2 | 4.50 | 21.280 | 47.880 | 1.634 |
| | 9 | 3-pt | 4.5 | 3 | 6.75 | 20.020 | 45.045 | 1.131 |

### 4.3.4.2 STRAIN

#### 4.3.4.2.1 LOAD-STRAIN

Figure 92 & Figure 93 display typical load-strain curves for the top surface and tension reinforcement for an 8" FPCS specimen. As expected, the top surface experiences compression and the bottom wythe reinforcement experiences tension.

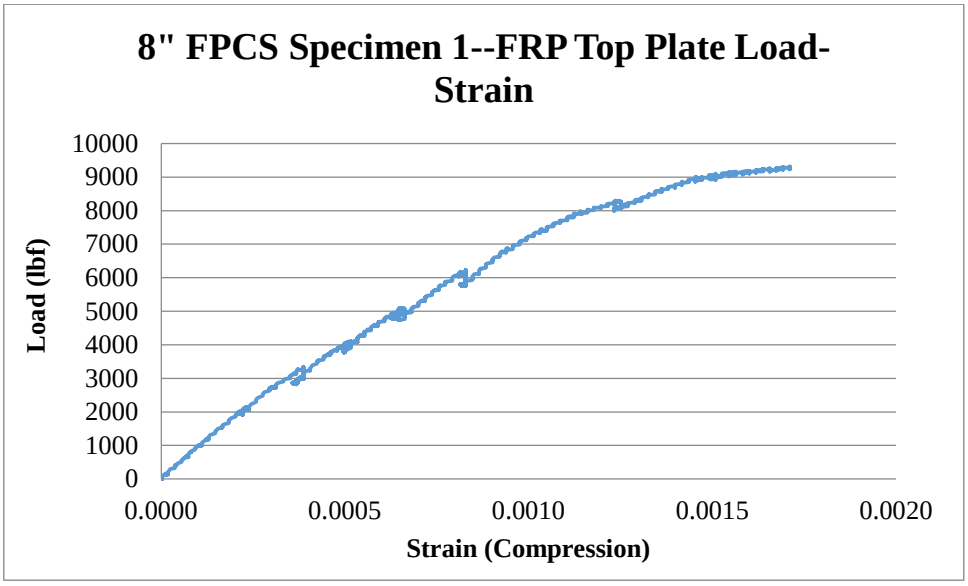


**Figure 92: 8" FPCS Specimen 1—FRP Top Plate Load-Strain**

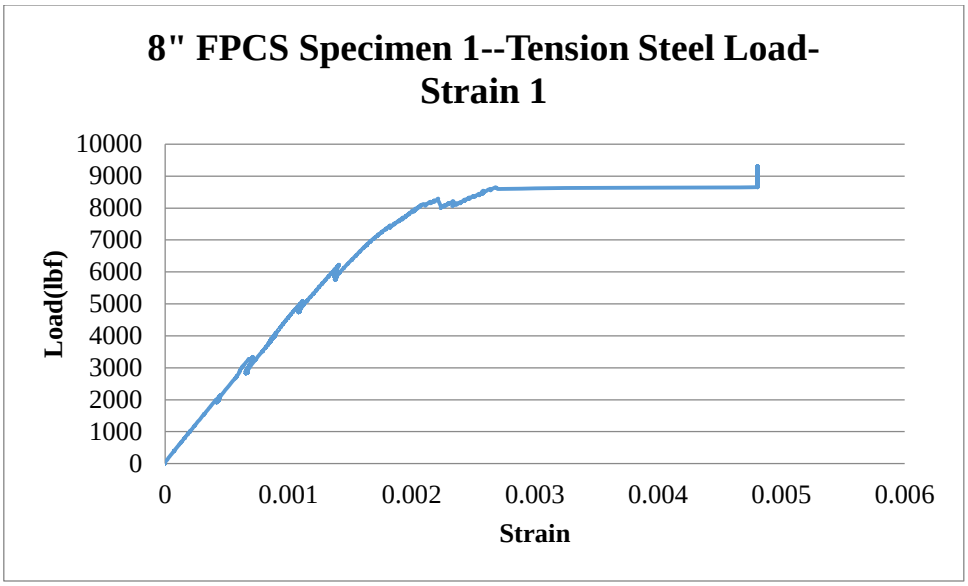


**Figure 93: 8" FPCS Specimen 1—Tension Steel Load-Strain 1**

Figure 94 & Figure 95 display typical load-strain curves for the top surface and tension reinforcement for an 8" FPCS specimen. As expected, the top surface experiences compression and the bottom wythe reinforcement experiences tension.

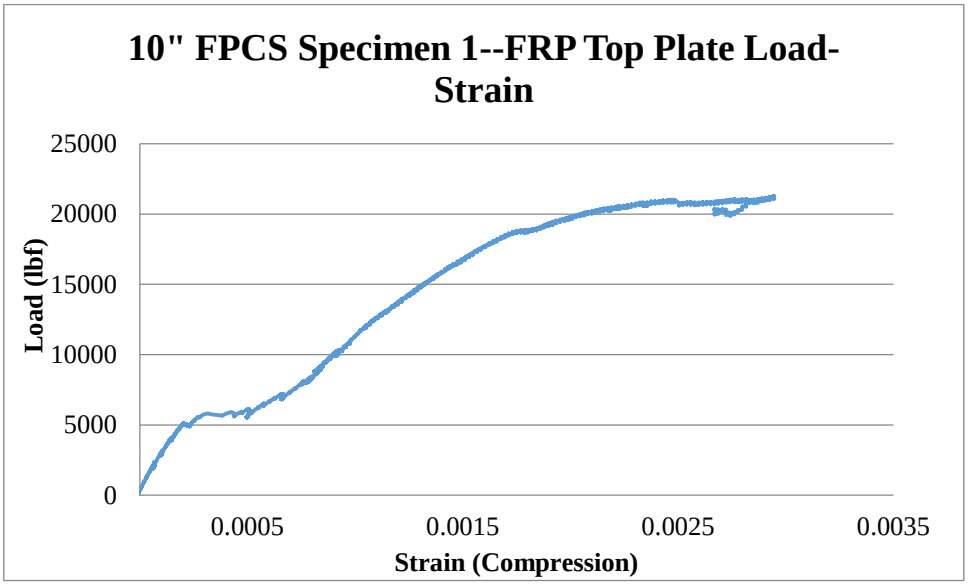


**Figure 94: 10" FPCS Specimen 1—FRP Top Plate Load-Strain**

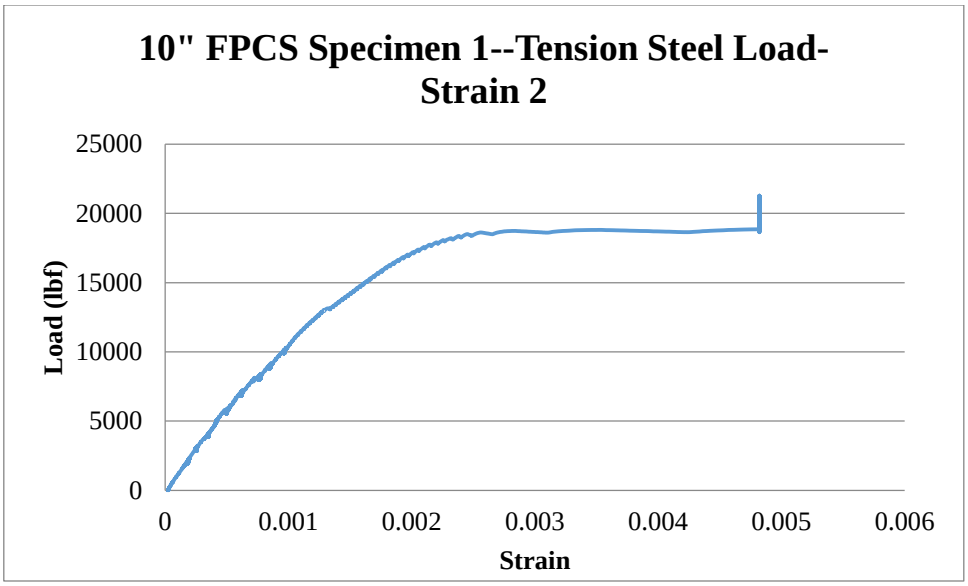


**Figure 95: 10" FPCS Specimen 1—Tension Steel Load-Strain 2**

### 4.3.4.2.2 STRAIN DISTRIBUTION

In order to construct a strain distribution, it is necessary to record the strain at various levels along the specimen's profile. As described in Chapter 3, this requires a minimum of three reliable strain gages. While the strain gages which were applied to the specimen did provide reliable strain data, they did not present the data needed to construct a strain distribution.

The reason for this is the gages which were attached to the shear connectors provided the strain within the shear connectors and not in the specimen as a whole. The connectors were constantly in tension (regardless of being monitored in the top or bottom wythe) and therefore did not show variation from compression to tension (top to bottom) as is expected for such loading. Due to a lack of other gages attached directly to the concrete as in previous tests (which was not an option due to the application of FRP side plates) there was not sufficient data to construct these strain distributions.

### 4.3.4.3 FAILURE MODE

The failure mode experienced by each slab is presented in Table 18.

**Table 18: FPCS Panel w/FRP Top Plate—Failure Modes**

| Slab Thickness | Connector Type | Initial Failure Mode | Secondary Failure Mode |
|---|---|---|---|
| 8" | Segmental | Bending | Crushing/Insulation Rupture |
| | Segmental | Bending | FRP Debond/Insulation Rupture |
| 10" | Segmental | Bending | FRP Debond |
| | Segmental | Bending | FRP Debond/Crushing |

### 4.3.4.4 CRACK PATTERN

### 10” FPCS PANELS

The first specimen (Figure 96) exhibits a typical bending failure cracking pattern, as was expected. The second specimen though, (Figure 97) demonstrates a mixture of bending and shear failure cracking. This can be explained by the fact that the bottom of the specimen was not level at the area of support and therefore resulted in a slight eccentricity (see Figure 98). Ultimately though, the failure mode was bending, which is demonstrated by the majority of the crack pattern.

**Figure 96: 10" FPCS Specimen 1—Crack Pattern (Bottom of Specimen)**

**Figure 97: 10" FPCS Specimen 2—Crack Pattern (Bottom of Specimen)**

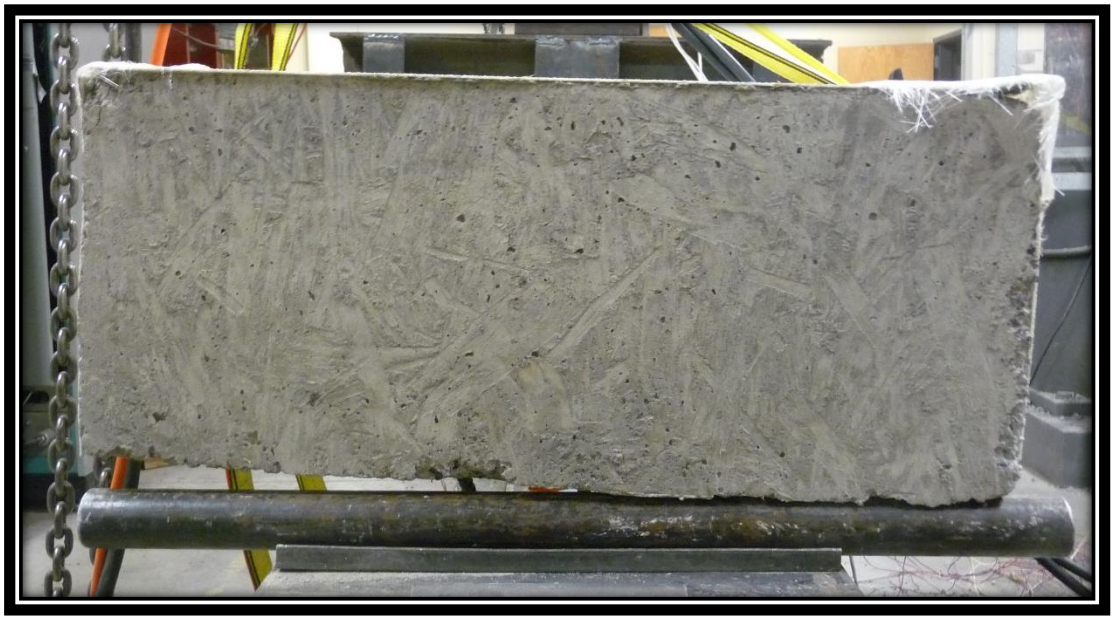

**Figure 98: Eccentricity at Support**

## 8” FRPCS PANELS

Both specimen 8” FPCS specimen experienced bending failure, as is evident in the crack patterns shown in the following figures by the clear lines that travel almost straight across from one edge to the other.

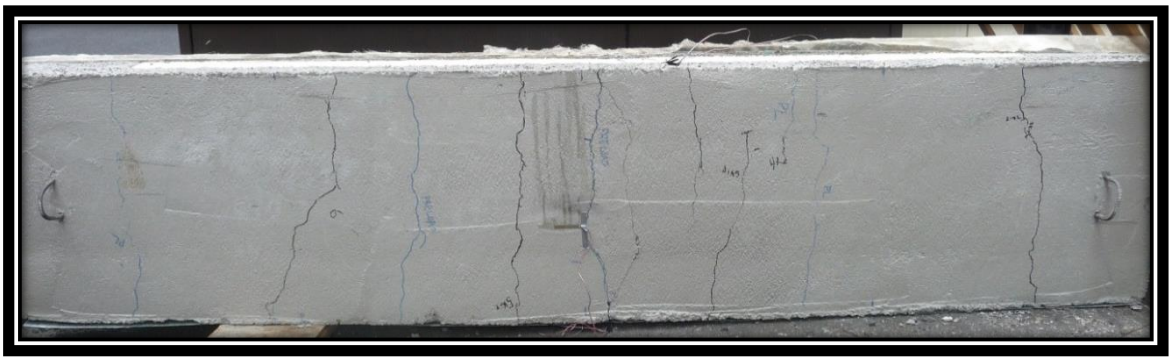

**Figure 99: 8" FPCS Specimen 1—Crack Pattern (Bottom of Specimen)**

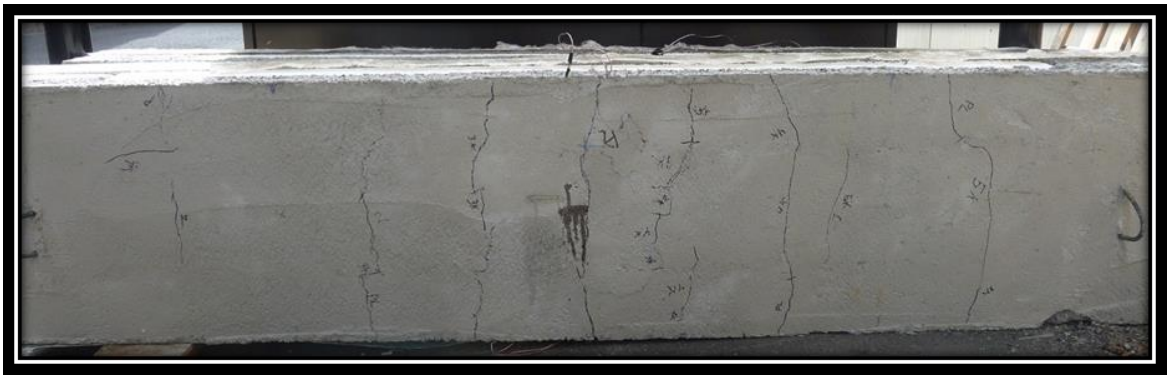

**Figure 100: 8" FPCS Specimen 2—Crack Pattern (Bottom of Specimen)**

## 4.4 DISCUSSIONS/RESULTS

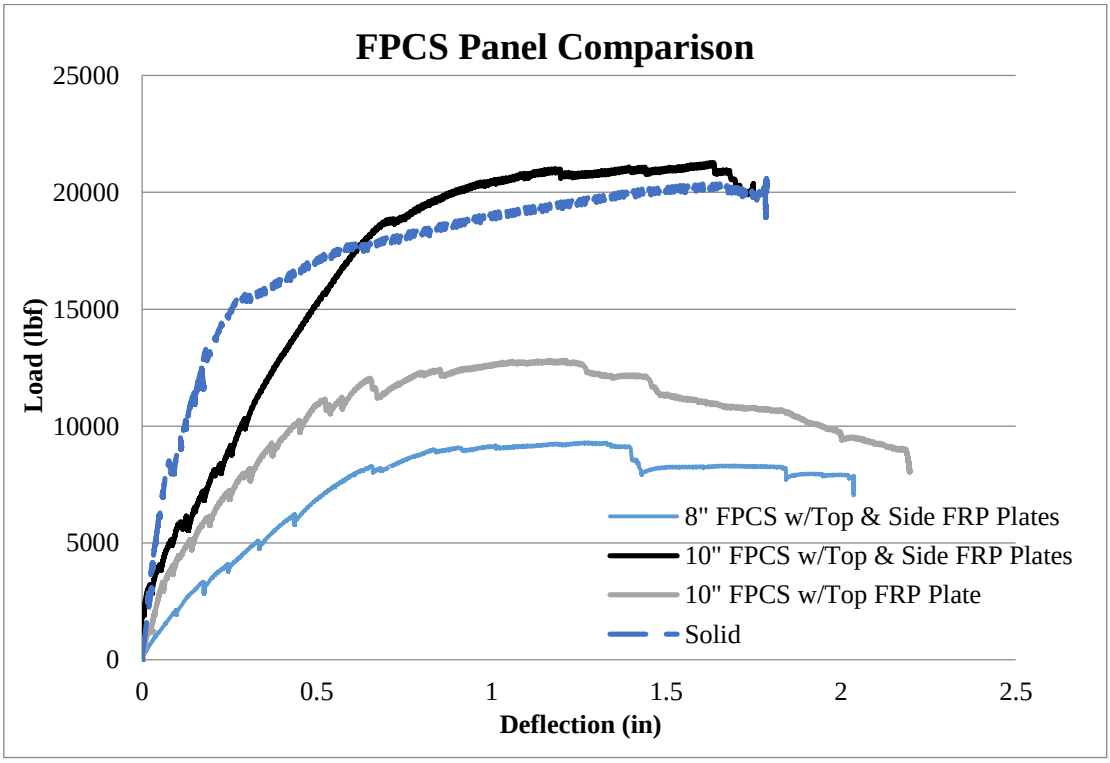


**Figure 101: FPCS Panel Comparison**

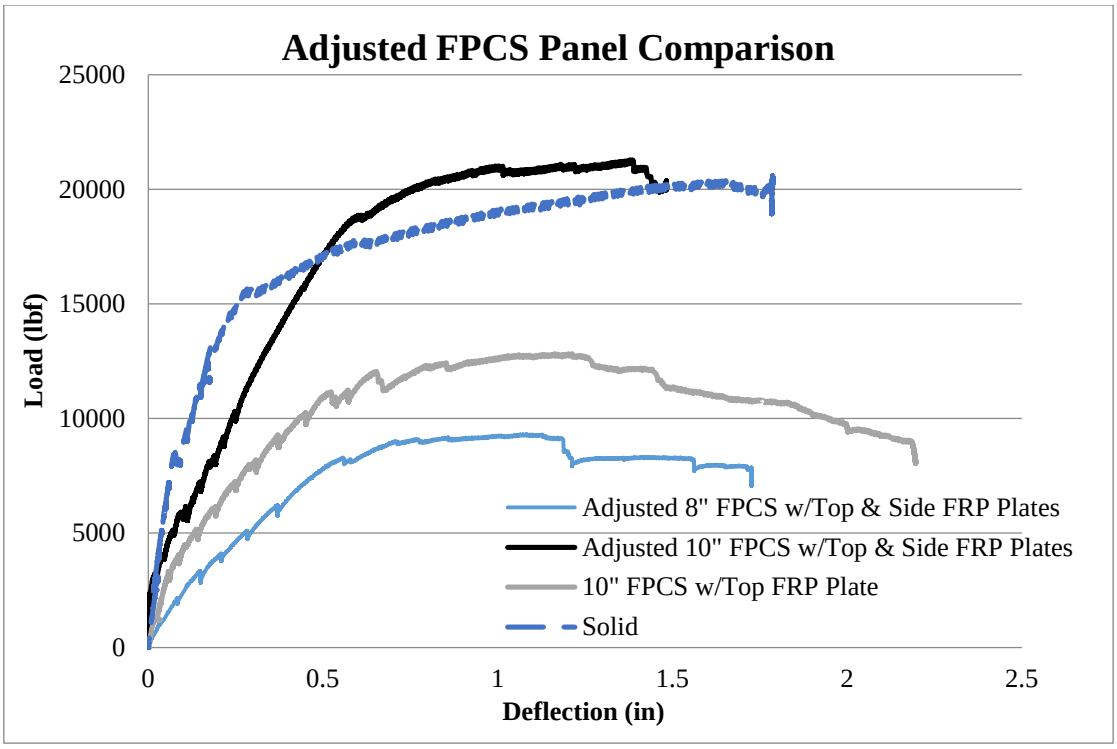


**Figure 102: Adjusted FPCS Panel Comparison**

It can be seen the adjusted 10” FPCS panel with top and side FRP plates has a greater initial modulus of elasticity; however, this does not continue whereas the solid slab maintains a high modulus to a load exceeding 15 kips. The ultimate strength of the 10” FPCS panel does reach a greater load than the solid slab though.

The 8” FPCS panel does not exhibit a very high ultimate strength in addition to having a much lower modulus of elasticity. It is likely that the 1” thick top wythe is too thin for such applications.

## 4.4.1 DEGREE OF COMPOSITE ACTION

### 4.4.1.1 LOAD-DEFLECTION METHOD

Following the same procedure described in Chapter 3, the DCA was calculated for the specimens presented in this chapter based on the deflection at the same load as before. To account for the difference in the compressive strength of concrete between tests, a correction factor was applied to the deflections of the specimen described in Chapter 4.2. The details of this can be seen in APPENDIX 2. Table 19 provides the results of these calculations, again,

following identical procedures as expressed in Chapter 3, as represented by the following example.

**Segmental Shear Connector DCA (Load-Displacement Method) Example:**

Given: $f'_c := 4120psi$ $E := 57000\sqrt{f'_c \cdot psi} = 3.659 \times 10^3 \cdot ksi$

$\frac{P}{\Delta} = 93070 \frac{lbf}{in}$ $L := 9ft$ $\Delta = \frac{P \cdot L^3}{48EI}$

$b := 24in$ $I_{solid} := 2197.19in^4$ $h := 3in$

Required: Determine the DCA for the specimen.

**Solution:**

Determine the Moment of Inertia for the specimen:

Based on the deflection equation for a simply supported beam, the following can be concluded:

$$I = \frac{P}{\Delta} \cdot \frac{L^3}{48E}$$

$$I_{ex} := \left(93070 \cdot \frac{lbf}{in}\right) \cdot \left(\frac{L^3}{48 \cdot E}\right) = 667.6 \cdot in^4$$

Determine the Moment of Inertia for a fully non-composite specimen:

$$I_{nc} := 2 \cdot \left(\frac{b \cdot h^3}{12}\right) = 108 \cdot in^4$$

Based on the following equation, the DCA can be calculated:

$$DCA := \frac{\left(\frac{1}{E \cdot I_{nc}}\right) - \left(\frac{1}{E \cdot I_{ex}}\right)}{\left(\frac{1}{E \cdot I_{nc}}\right) - \left(\frac{1}{E \cdot I_{solid}}\right)} \cdot (100\%)$$

$DCA = 88.156 \cdot \%$

**Table 19: Degree of Composite Action (DCA)—Load-Deflection Method-FPCS Panels**

| Specimen | P/Δ | I | EI | DCA |
|---|---|---|---|---|
| Segmental Connectors (FRP Top Plate) | 93070 | 667.5999251 | 2442529080 | 88.16% |
| | 84779 | 608.1277969 | 2224940076 | 86.49% |
| Continuous Connectors (FRP Top Plate) | 75233 | 539.6534347 | 1974414852 | 84.12% |
| | 107776 | 773.087456 | 2828473344 | 90.48% |
| 8" FPCS (FRP Top & Side Plate) | 25164 | 218.3713457 | 660404016 | 78.28% |
| | 20730 | 179.893419 | 544038120 | 72.51% |
| 10" FPCS (FRP Top & Side Plate) | 54005 | 356.6736361 | 1417307220 | 73.47% |
| | 44214 | 292.0094092 | 1160352216 | 66.40% |

As the 8” & 10” FPCS panels used segmental connectors, it can be seen that in the case of the 10” FPCS panel, an increase of composite action was recorded compared to that of the specimen with segmental connectors and only a top FRP plate. Additionally, the ultimate load and deflection at that point is far superior. Additionally, it can be seen that the 10” FPCS panel surpasses the DCA of the specimen with continuous connectors.

#### 4.4.1.2 STRAIN DISTRIBUTION METHOD

The following table provides the DCA of the specimen with only the top FRP plate because the strain distribution of the specimens with top and side FRP plates could not be established as has been discussed. Specimen with top and side FRP plates must rely on the DCA determined by the load-deflection method will have to be relied upon. For the specimens with only top FRP plates, one from each group provided sufficient data to accurately construct strain distribution profiles. These results were calculated following the same procedure as described in Chapter 3 and are shown in the following example. The results can be found in Table 20.

## Continuous Shear Connector DCA (Strain Distribution Method) Example:

Given: $y_1 = -0.0625x + 3.125$ $\quad y_{bar1} := 1.5in$ $\quad y_{bar2} := 3in$ $\quad y := 5$

$y_2 = -0.0625x - 0.5625$ $\quad M := 18.9kip \cdot in$ $\quad b := 24in$ $\quad h := 3in$

$f'_c := 4120psi$ $\quad E := 57000\sqrt{f'_c \cdot psi} = 3.659 \times 10^3 \cdot ksi$

Required: Determine the DCA for the specimen.

## Solution:

Determine $\Delta x_{0\%}$:

By assuming different values of 'y' and using the following equation, the slope of the strain distribution for a fully non-composite specimen can be calculated. Assuming that this distribution crosses the neutral axis at the center of each wythe, the difference ($\Delta x_{0\%}$) can be calculated:

$$\varepsilon = \frac{M \cdot y}{E \cdot I} \qquad I := \frac{b \cdot h^3}{12} = 54 \cdot in^4$$

$$\varepsilon_1 := \left(\frac{M \cdot y_{bar1}}{E \cdot I}\right) \cdot 10^6 = 143.495 \qquad \varepsilon_2 := \left(\frac{M \cdot y_{bar2}}{E \cdot I}\right) \cdot 10^6 = 286.989$$

$$slope := \frac{y_{bar1} - y_{bar2}}{(\varepsilon_1 - \varepsilon_2) \cdot in} = 0.01$$

Assuming the top of the specimen to be the datum, use the distance between the top of the specimen and the center of each wythe to determine the values of 'x':

$$x1 := \frac{1.5}{slope} = 143.495 \qquad x2 := \frac{8.5}{slope} = 813.137$$

$$\Delta x_{0\%} := x2 - x1 = 669.642$$

Using the equations provided by the strain distribution and assuming an arbitrary datum, $\Delta$xex can be calculated:

$$x_1 := \left(\frac{y + 0.5625}{-0.0625}\right) = -89 \qquad x_2 := \left(\frac{y - 3.125}{-0.0625}\right) = -30$$

$$\Delta x_{ex} := x_2 - x_1 = 59$$

Because a fully composite specimen would have no variance, $\Delta x1_{00\%} = 0$:

$$DCA := \left(\frac{\Delta x_{ex} - \Delta x_{0\%}}{0 - \Delta x_{0\%}}\right)(100\%)$$

$DCA = 91.189 \cdot \%$

**Table 20: Degree of Composite Action (DCA) w/Top FRP Plate—Strain Distribution Method**

| DCA - Strain Distribution Method | | | | | |
|---|---|---|---|---|---|
| **Specimen** | $X_{bot-ext}$ | $X_{top}$ | $X_{max}$ | **ΔX** | **DCA** |
| Segmental | -147.64865 | -90.09009 | 669.642 | 57.558559 | 91% |
| Continuous | -89 | -30 | 669.642 | 59 | 91% |

These results show that the segmental and continuous connectors produce identically degrees of composite action. Given the lower material requirements for the segmental connectors, it is again confirmed that they are the superior shear connector choice.

### 4.4.2 STRENGTH & STIFFNESS

The same procedure described in the previous Chapter 3.6.2 was used to determine the strength and stiffness of the specimen examined in this chapter, although correction factors were needed for the specimen with top and side FRP plates as no solid slab was tested with a concrete having a compressive strength equal to that of the composite slabs. A detailed explanation of the calculation of these correction factors can be seen in APPENDIX 2. The results can be seen in the following table.

**Table 21: Strength & Stiffness of Chapter 4 Specimens**

| Connector | Strength | Stiffness | Failure Mode |
|---|---|---|---|
| Segmental | 62.14% | 30.38% | Shear |
| Continuous | 77.67% | 35.19% | Shear |
| 8” FPCS | 51.26% | 19.56% | Bending |
| 10” FPCS | 88.98% | 16.86% | Bending |

## 4.5 CONCLUSIONS

This study has shown that the bond between the concrete and the external FRP plates is extremely important. While the study has shown that wet bonds can perform to the same level of strength and stiffness as initially bonding aggregate to the plates, it did result in severe debonding prior to the application of aggregate and FRP side plates. Additionally, wet bonds are more difficult to accomplish given the time and the intensive labor required to apply the adhesive. Therefore, for ease of construction and a more reliable bond, aggregate should be bonded to the plates prior to the pouring of concrete.

The addition of FRP side plates resulted in a greater ultimate load. This is due to the confining effect that they add to the panel in addition to behaving as pseudo shear connectors, thus adding improved shear transfer between wythe and restricting deformation.

# CHAPTER 5: FULL SCALE BENDING TEST OF FPCS PANELS

## 5.1 INTRODUCTION

The purpose of this chapter is to assess the performance of full-scale FPCS panels (16-feet long). The specimens were identical to the FPCS panels with top and side FRP plates, as presented in Chapter 4, with the exception of the increased length. As before, the specimens were evaluated with respect to strength, stiffness, and DCA.

## 5.2 EXPERIMENTAL PROGRAM

### 5.2.1 SPECIMEN DETAILS

Two groups of FPCS panels with both top and side FRP external plates and varying wythe configuration (see Figure 77), were constructed. Due to the application of the external FRP plate, no compression reinforcement or top wythe temperature steel was added as in Chapter 4. The length of these specimens has been increased from 9’ to 16’ and the reinforcement detail has altered to reflect this (see Table 22). The reinforcement layout and dimensions of the specimen can be seen in Figure 103 & Figure 104.

**Table 22: Full Scale FPCS Specimen Details**

| FPCS Panel Thickness | Compression Steel (#4 bars) | Tension Steel (#5 bars) | Top Temp. Steel (#4 bars) | Bottom Temp. Steel (#4 bars) | Load Conditions | Shear Connectors | Length |
|---|---|---|---|---|---|---|---|
| 8" | N/A | (2) @ 12" O.C. | N/A | (9) @ 18" O.C. | 3-pt Bending | Segmental | 16' |
| 10" | N/A | (2) @ 12" O.C. | N/A | (9) @ 18" O.C. | 3-pt Bending | Segmental | 16' |

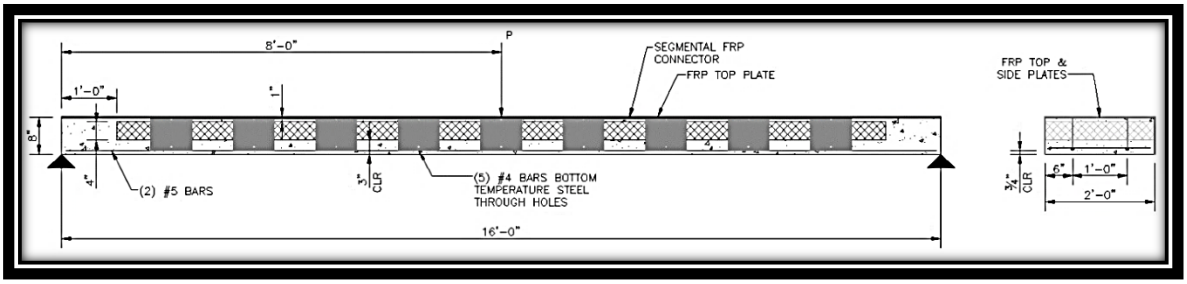


**Figure 103: Full Scale 8" FPCS Layout**

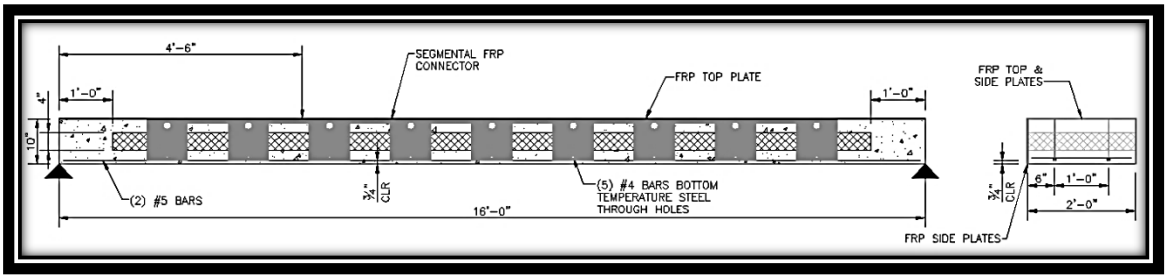


**Figure 104: Full Scale 10" FPCS Layout**

## 5.2.2 MATERIAL PROPERTIES

All material properties which apply to the specimen with both top and side FRP plates in Chapter 4 (i.e. FRP, adhesive, etc.) apply to this chapter, except for the compressive strength concrete which was calculated to be 4807.5 psi (see Table 23).

**Table 23: Compressive Strength**

| Specimen | Compressive Strength (psi) |
|---|---|
| Cylinder 1 | 4591 |
| Cylinder 2 | 5003 |
| Cylinder 3 | 4606 |
| Cylinder 4 | 5030 |
| **Average** | **4807.5** |

## 5.2.3 SPECIMEN FABRICATION

The same procedure as described for the 8" and 10" FPCS panels from Chapter 4 was followed during this study; the difference being the overall length of the specimen increasing from 9' to 16'. This resulted in two separate pieces of EPS insulation being required for each slab; however, they were slotted as before and the shear connectors were inserted through the gaps in the insulation prior to insertion into the forms. Further detail can be seen in the following figures.

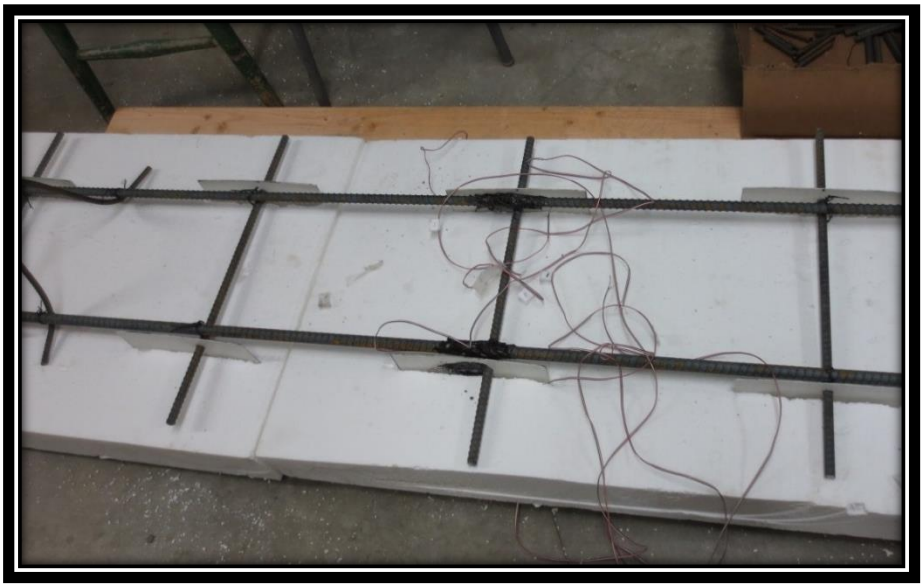

**Figure 105: Full Scale Insulation (2 Pieces) and Strain Gages**

**Figure 106: First Lift of Full Scale FPCS Panel**

**Figure 107: Insulation Installation**

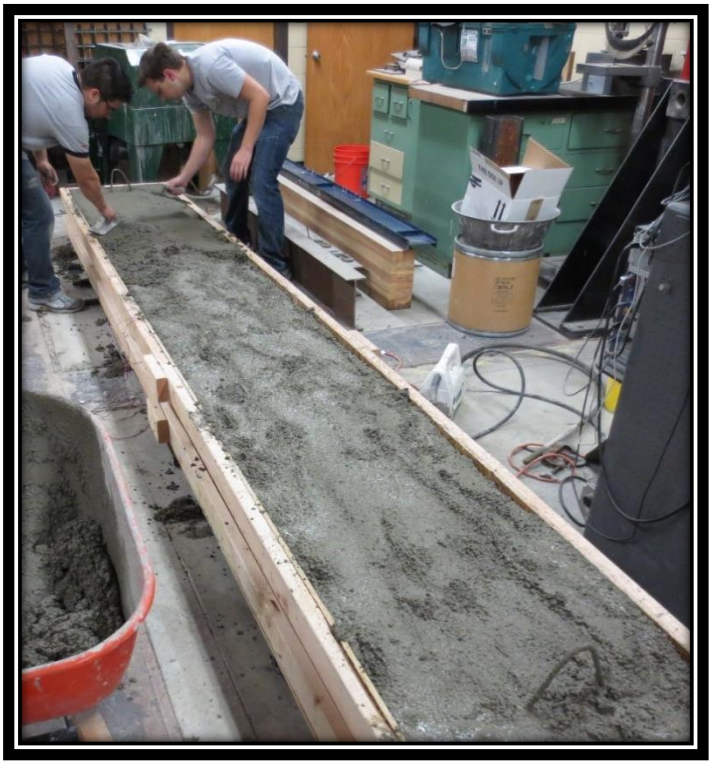

**Figure 108: Full Scale FPCS Panel Finishing**

**Figure 109: Cured and Stripped Full-Scale Specimens**

## 5.3 TEST SETUP

### 5.3.1 TEST LAYOUT

The test layout for the testing of the full scale specimens follows the same three-point bending layout as described in Chapter 3, except with an effective length of 16’ rather than 8’ or 9’. A schematic plan and live photo can be seen in Figure 110 & Figure 111, respectively.

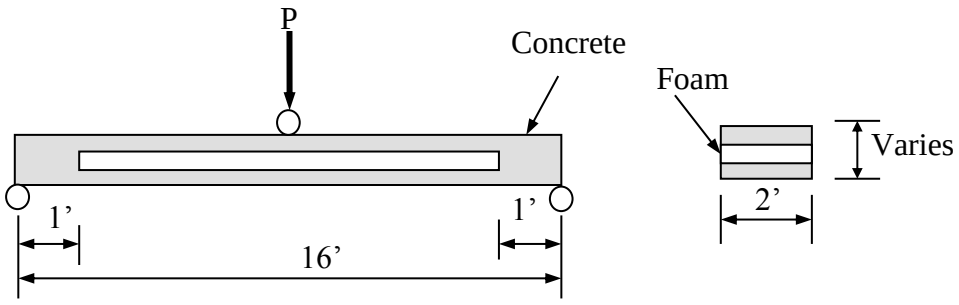


**Figure 110: Full Scale Test Schematic**

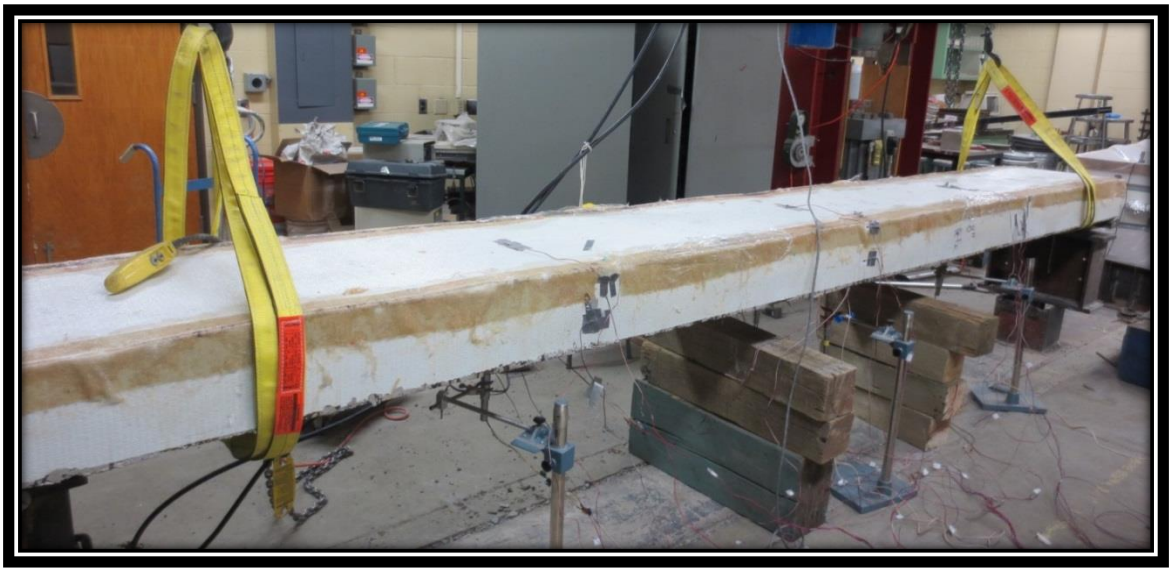

**Figure 111: Full Scale FPCS Panel Test**

## 5.3.2 INSTRUMENTATION

As in all other chapters, the strain gages used on the concrete are N2A-06-20CBW-120 and the strain gages used on the FRP (external plates and shear connectors) and the tension steel are CEA-06-250UN-350. The positioning of the shear connector strain gages can be seen in Figure 112 & Figure 113 and the position of external strain gages/LVDTs can be seen in Figure 114 & Figure 115.

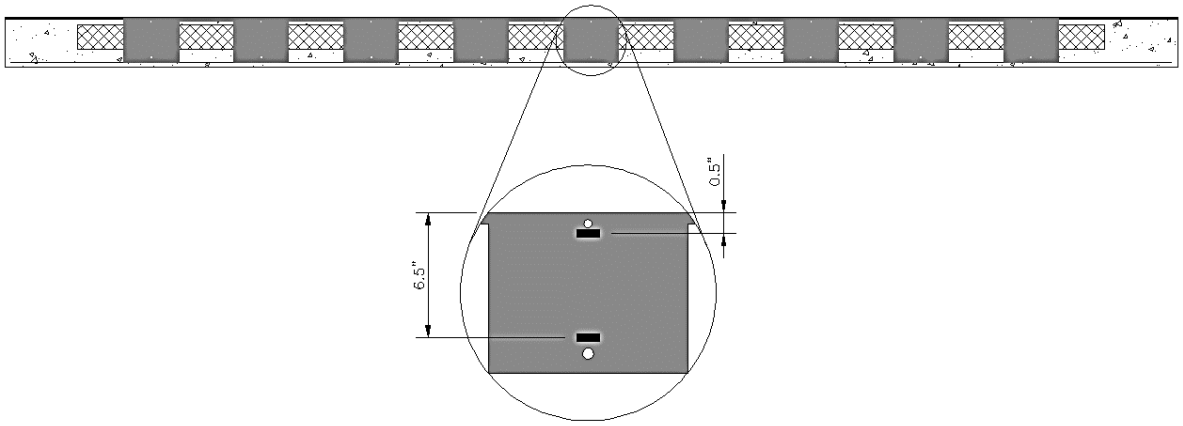


**Figure 112: Full Scale 8" Shear Connector Instrumentation**

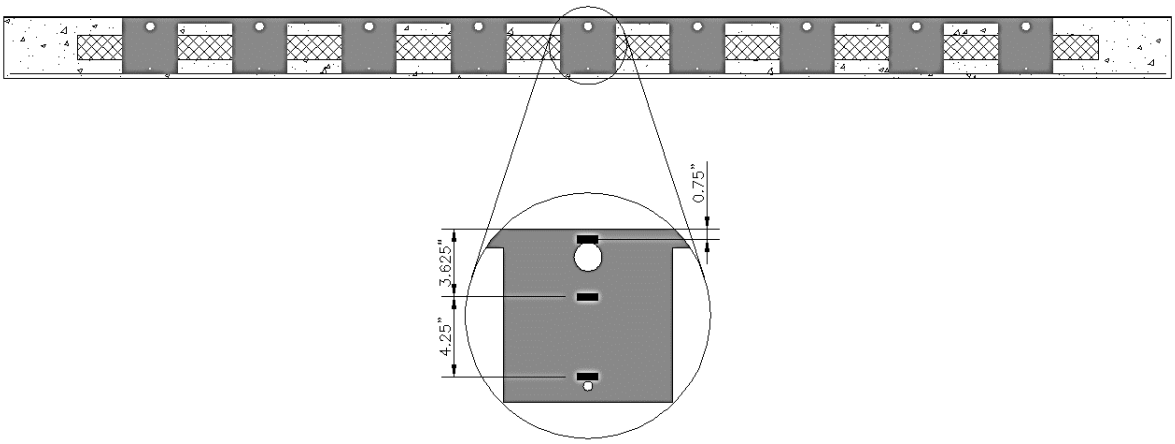


**Figure 113: Full Scale 10" Shear Connector Instrumentation**

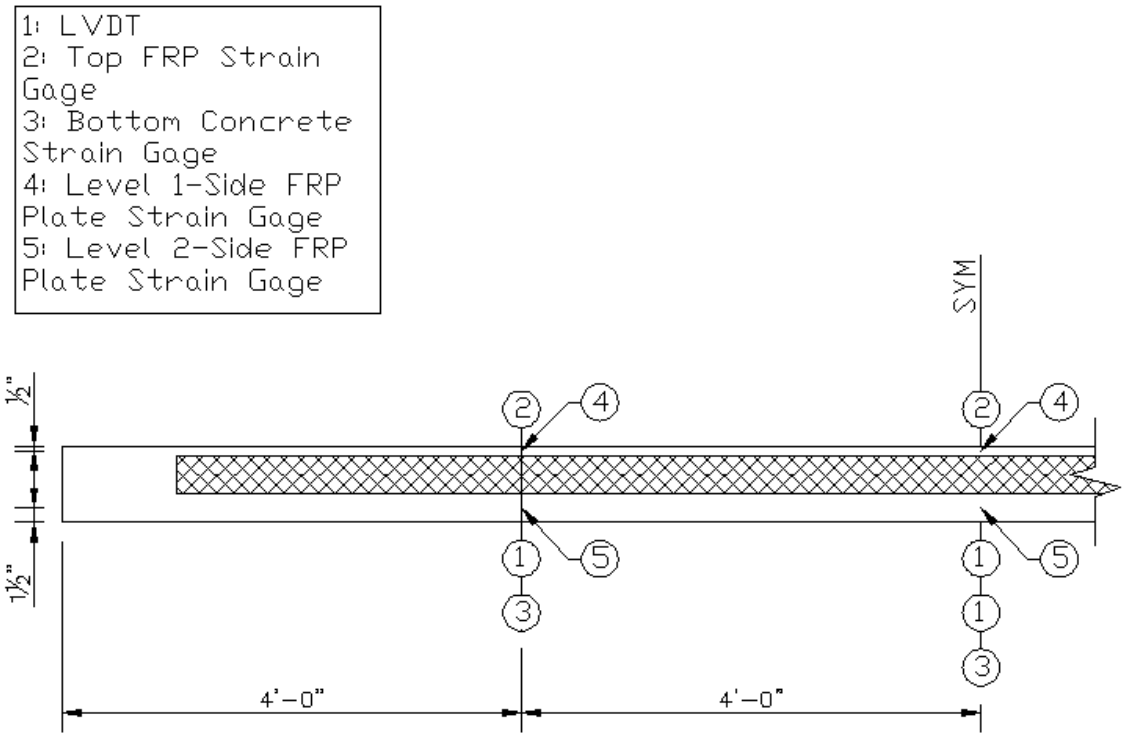


**Figure 114: Full Scale 8" FPCS External Instrumentation**

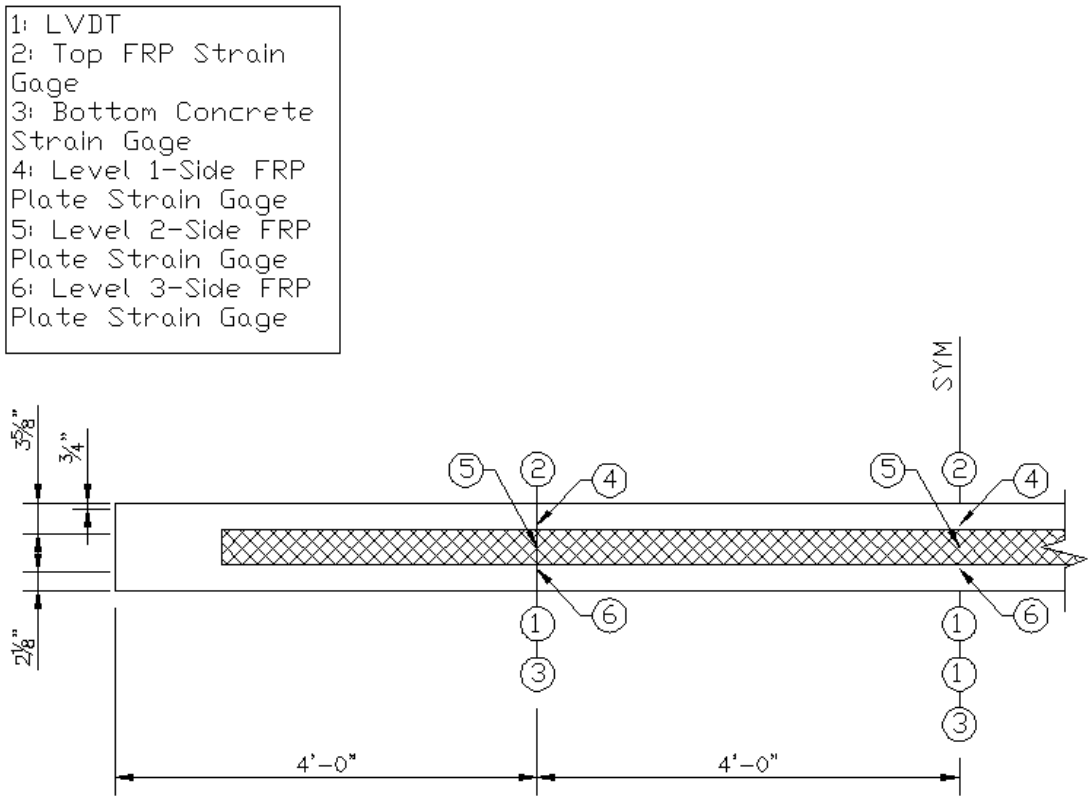


**Figure 115: Full Scale 10" FPCS External Instrumentation**

## 5.4 TEST PROCEDURE

(Please refer back to Chapter 3)

## 5.5 EXPERIMENTAL RESULTS

As with the smaller specimens, the full-scale specimens exhibited cracking consistent with bending failure. Also like the smaller specimens, the side FRP plates visibly and audibly debonded prior to ultimate failure.

### 5.5.1 LOAD-DISPLACEMENT

The two following graphs present the load-deflection curves for the 8” and 10” specimens, respectively. Table 24 provides the details of the tests including the failure load and the maximum deflection at that load.

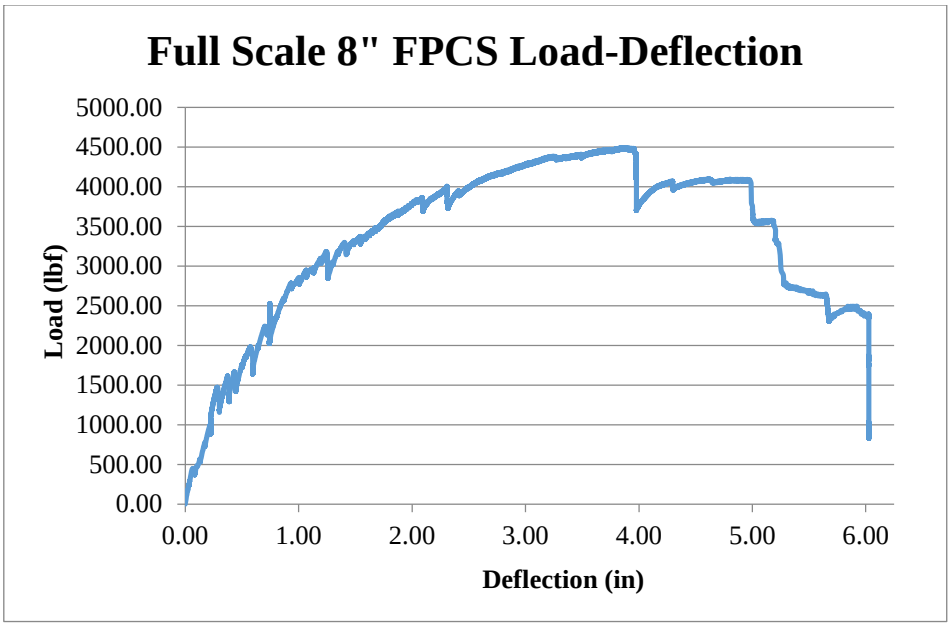


**Figure 116: 8" FPCS Load-Deflection Curve (Full Scale)**

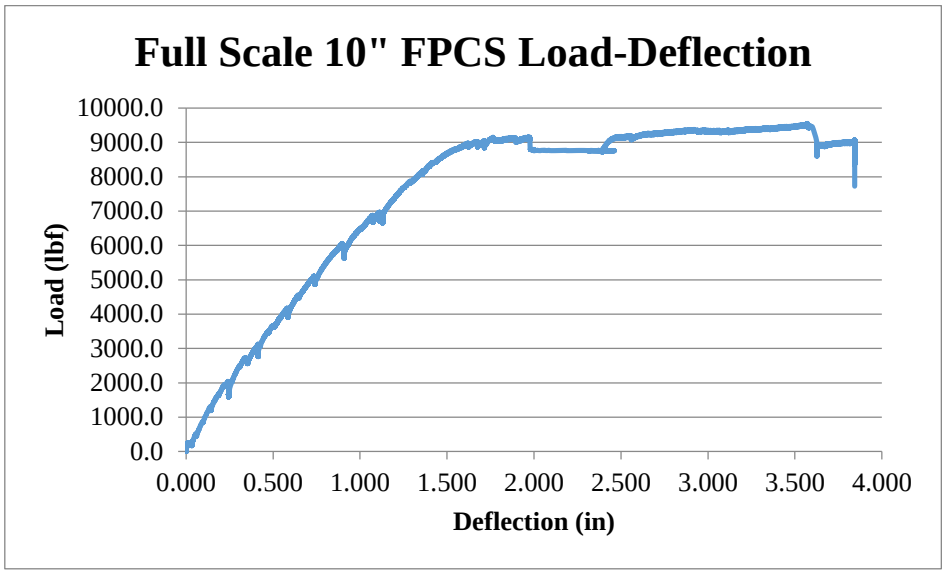


**Figure 117: 10" FPCS Load-Deflection Curve (Full Scale)**

**Table 24: Full Scale Ultimate Load Summary**

| Specimen Thickness | Effective Length (ft) | Bending Type | Moment Arm (ft) | Cracking Load (kip) | Cracking Moment (kip*ft) | Failure Load (kip) | Failure Moment (kip*ft) | Max Load Deflection (in) |
|---|---|---|---|---|---|---|---|---|
| 8" | 16 | 3-pt | 8 | 1 | 4.00 | 4.493 | 17.972 | 3.870 |
| 10" | 16 | 3-pt | 8 | 2 | 8.00 | 9.553 | 38.212 | 3.571 |

### 5.5.2 STRAIN

#### 5.5.2.1 LOAD-STRAIN

Figure 118 & Figure 119 display typical load-strain curves for the top surface and tension reinforcement for the full scale 8" FPCS specimen. As expected, the top surface experiences compression and the bottom wythe reinforcement experiences tension.

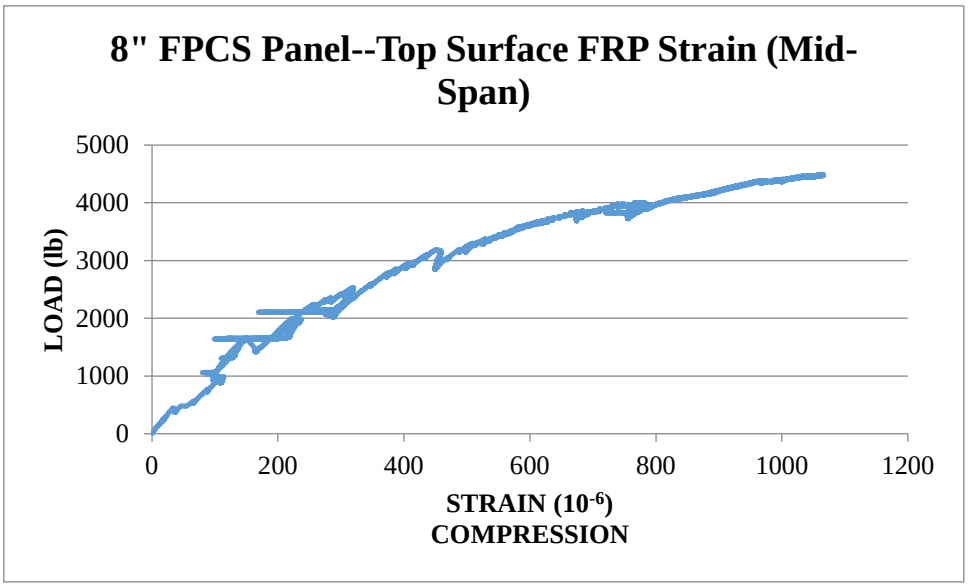


**Figure 118: 8" FPCS Panel--Top Surface FRP Strain (Mid-Span)**

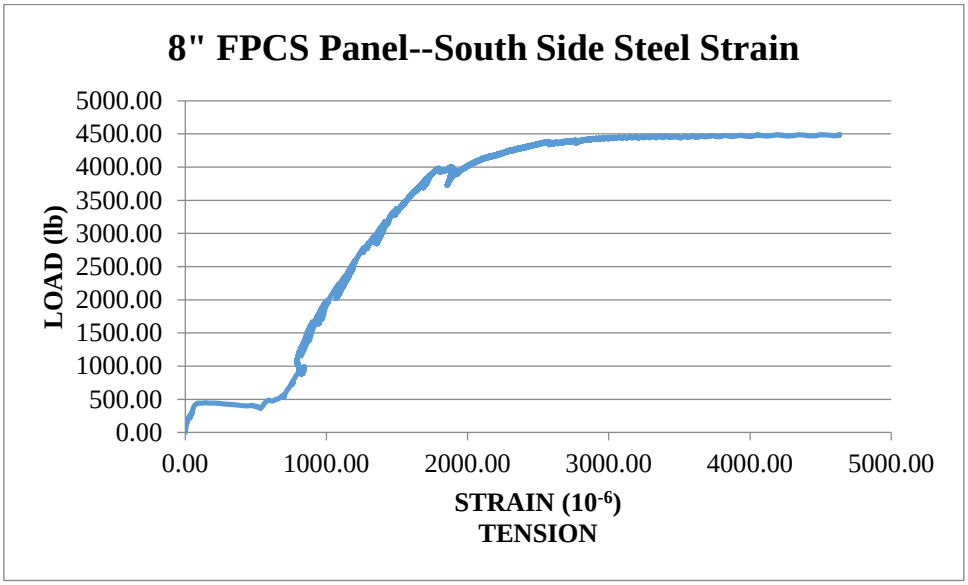


**Figure 119: 8" FPCS Panel--South Side Steel Strain**

Figure 120 & Figure 121display typical load-strain curves for the top surface and tension reinforcement for the full scale 10” FPCS specimen. As expected, the top surface experiences compression and the bottom wythe reinforcement experiences tension.

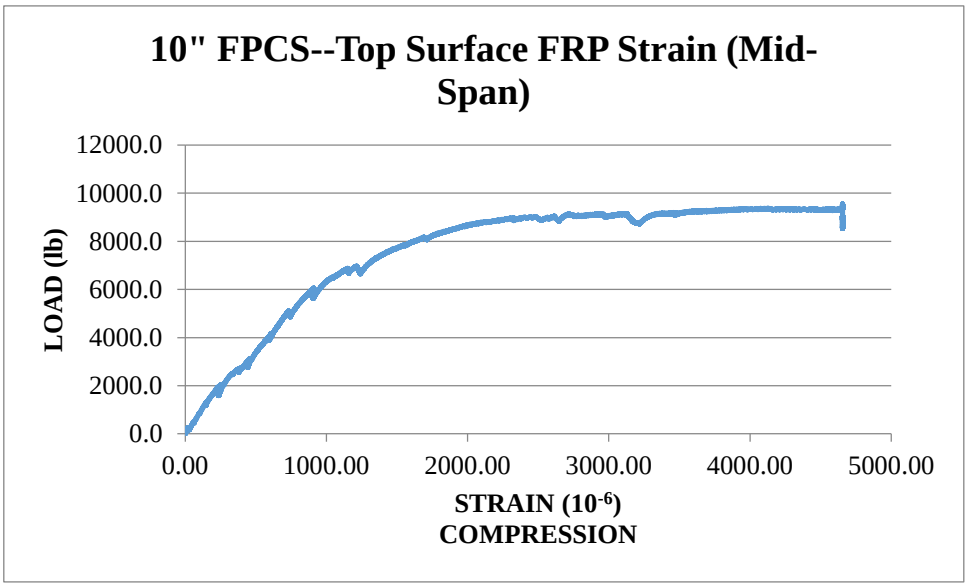


**Figure 120: 10" FPCS--Top Surface FRP Strain (Mid-Span)**

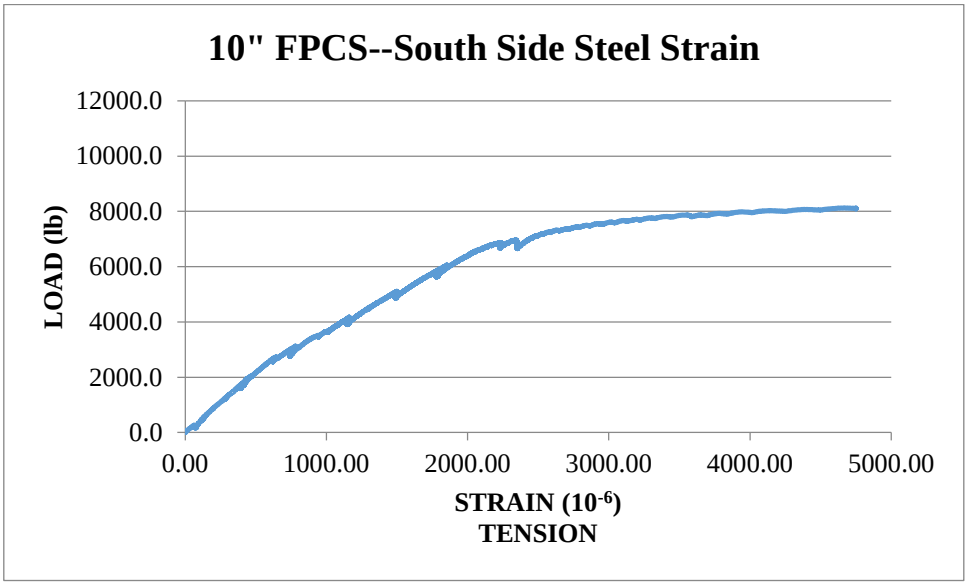


**Figure 121: 10" FPCS--South Side Steel Strain**

### 5.5.2.2 STRAIN DISTRIBUTION

In order to construct a strain distribution, it is necessary to record the strain at various levels along the specimen’s profile. As described in Chapter 3, this requires a minimum of three reliable strain gages. While the strain gages which were applied to the specimen did provide

reliable strain data, they did not provide the data needed to construct a strain distribution. As with the smaller samples in Chapter 4.3, the gages which were attached to the shear connectors provided the strain within the shear connectors and not in the specimen as a whole. The connectors were constantly in tension (regardless of being monitored in the top or bottom wythe) and therefore did not show variation from compression to tension (top to bottom) as expected for such loading. Due to a lack of other gages attached directly to the concrete as in previous tests (which was not an option due to the application of FRP side plates) there was not sufficient data to construct these strain distributions as was the case with the FPCS panels with top and side FRP plates in Chapter 4.

### 5.5.3 FAILURE MODE

The failure modes of the two full scaled specimens can be seen in Table 25.

**Table 25: Full Scale Specimens Failure Modes**

| Slab Thickness | Initial Failure Mode | Secondary Failure Mode |
|---|---|---|
| **8"** | Bending | Crushing/FRP Debond |
| **10"** | Bending | FRP Debond |

Both specimens failed in bending, as expected. The secondary failure for each involved the debonding of the side FRP plates. In the case of the 8" FPCS panel, the top wythe fractured in a manner that is consistent with crushing.

### 5.5.4 CRACK PATTERN

In Figure 122 &Figure 123, it can be seen that both full scale specimens experienced bending failure as shown by the vertical cracking through the wythe (pictures from the bottom were not available due to safety concerns).

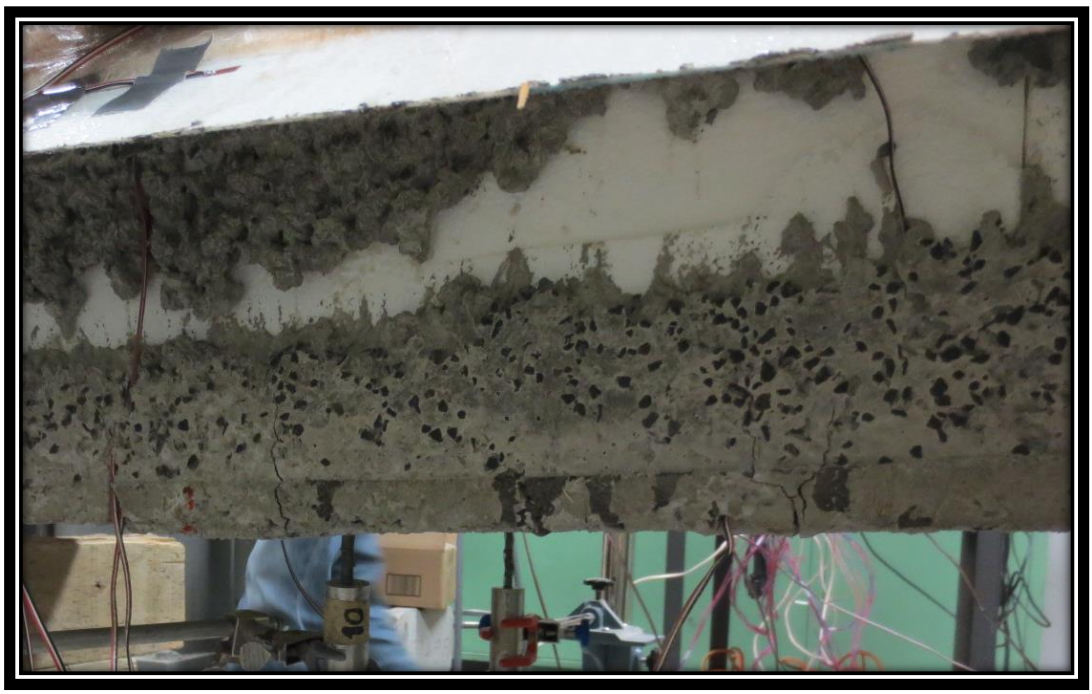

**Figure 122: Full Scale 8" FPCS Cracking**

**Figure 123: Full Scale 10" FPCS Cracking**

# 5.6 DISCUSSION/RESULTS

## 5.6.1 DEGREE OF COMPOSITE ACTION

### 5.6.1.2 LOAD-DEFLECTION METHOD

To determine the DCA for the full scale specimen, assumptions had to be made to equate the data to a theoretical solid specimen of like dimensions. The details of these calculations can be found in APPENDIX 3.

**Table 26: Degree of Composite Action (DCA)—Load-Deflection Method (Full Scale)**

| Specimen | P/Δ | I | EI | DCA |
|---|---|---|---|---|
| 8" FPCS (Full Scale) | 4503.1 | 168.0117046 | 664009113.6 | 70.27% |
| 10" FPCS (Full Scale) | 12543 | 467.9822368 | 1849540608 | 81.06% |

Due to the assumptions on which these values were based, the DCA cannot be confirmed. It is assumed that the theoretical approach is conservative and the specimen would likely have a higher DCA had data been collected from actual solid slabs. Additionally, given the increased effective length of the specimens, it is likely that the solid zones of concrete at each end provided much less composite action compared to the scaled tests.

### 5.6.1.2 STRAIN DISTRIBUTION METHOD

As stated before, the strain data that was collected provided information on the shear connectors and external FRP plates, but did not provide information regarding the strain across the depth of the slab, itself. For this reason, a strain distribution could not be constructed for either specimen and DCA could not be established using this method.

## 5.6.2 STRENGTH & STIFFNESS

The same procedure as described in Chapter 3.6.2 was used to determine the strength and stiffness of the specimen examined in this chapter, although correction factors were needed for the specimen with top and side FRP plates as no solid slab was tested with an equal compressive strength of concrete or effective length. The details to these corrections can be seen in APPENDIX 3. The results can be seen in the following table.

**Table 27: Strength/Stiffness of Full Scale Specimen**

| Connector | Strength | Stiffness | Failure Mode |
|---|---|---|---|
| 8” FPCS | 72.51% | 15.39% | Bending |
| 10” FPCS | 71.74% | 22.12% | Bending |

## 5.7 CONCLUSIONS

While these panels do not exhibit a high level of stiffness as compared to a solid slab, they exhibit an exceptionally high strength. As prescribed by ACI 318-11, the maximum deflection allowable for the given effective length is 0.533 inches. The loads which resulted in this displacement were taken from the collected data and equated first to an allowable distributed load and then to the allowable area load for both specimen (see APPENDIX 3). The ultimate loads were then analyzed in this same fashion. The results can be seen in Table 28.

**Table 28: Maximum Allowable/Failure Loads**

| Specimen | Allowable Distributed Load (lb/ft) | Allowable Area Load ($lb/ft^2$) | Failure Distributed Load (lb/ft) | Failure Area Load ($lb/ft^2$) |
|---|---|---|---|---|
| 8" FPCS | 186 | 93.2 | 449 | 224.65 |
| 10" FPCS | 385 | 192.25 | 955 | 477.65 |

It can be seen that both panels can withstand considerable loads, the 10” specimen being able to withstand over twice as much as the 8” specimen.

# CHAPTER 6: CREEP TEST OF SCALED SPECIMEN

## 6.1 INTRODUCTION

Creep has consistently been challenge when dealing with concrete. ACI318-11 has established conservative requirements for creep in solid concrete, but methods have not been developed for predicting creep in sandwich panels. Most literature shows that extensive research must still be done on this subject [11][13][14]15][16].

The purpose of this test is to study the creep behavior of the four test specimens: a sandwich panel with segmental shear connectors, an 8" FPCS panel, a 10" FPCS panel, and a 10" solid slab to act as control.

## 6.2 EXPERIMENTAL PROGRAM

### 6.2.1 SPECIMEN DETAILS

- Solid Slab (refer to Figure 5)
- Sandwich Panel—Segmental Shear Connectors (refer to Figure 3)
- 8" FPCS Panel (refer to Figure 78)
- 10" FPCS Panel (refer to Figure 79)

### 6.2.2 MATERIAL PROPERTIES

The solid slab, sandwich panel, and 10" FPCS panels were constructed as the 10" FPCS panels with top & side FRP plates as described in Chapter 4. Therefore, they have the same compressive strength (4860psi) as well as all other material properties. The 8" FPCS panel was constructed with the 8" FPCS panels with top & side FRP plates as presented in Chapter 4. Again all other material properties are identical, except for the compressive strength of concrete, which is 2815 psi (see Table 14).

### 6.2.3 SPECIMEN FABRICATION

- Solid Slab (refer to Chapter 3)
- Sandwich Panel—Segmental Shear Connectors (refer to Chapter 3)
    - Note that during the fabrication of this panel, the foam insulation fractured in half while positioning it.
- 10" FPCS Panel with Top & Side FRP Plates (refer to Chapter 4)

- 8’ FPCS Panel with Top & Side FRP Plates (refer to Chapter 4)

## 6.3 TEST SETUP

### 6.3.1 TEST LAYOUT

The four specimens were tested as simply supported beams. They were then loaded at mid-span with two Eco-blocks to simulate a sustained load (weights provided in Table 29) such as a piece of equipment or heavy furniture might place on these specimens. They all have an effective length of 9’. A schematic plan of the test setups is shown in Figure 124 with layouts represented in Figure 125.

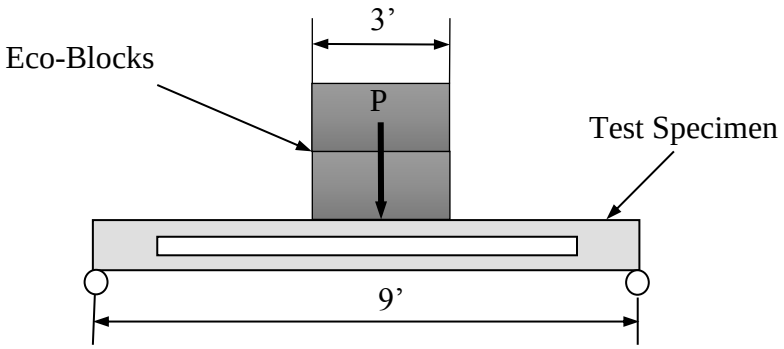


**Figure 124: Creep Loading Schematic**

**Figure 125: Creep Test Layout**

### 6.3.2 INSTRUMENTATION

Refer to Figure 85 for the shear connector instrumentation of the 8” FPCS panel. Refer to Figure 86 for the instrumentation of the shear connectors of the sandwich panel (10”) and the 10” FPCS panel.

The external instrumentation for each panel can be seen in Figure 126, Figure 127, and Figure 128:

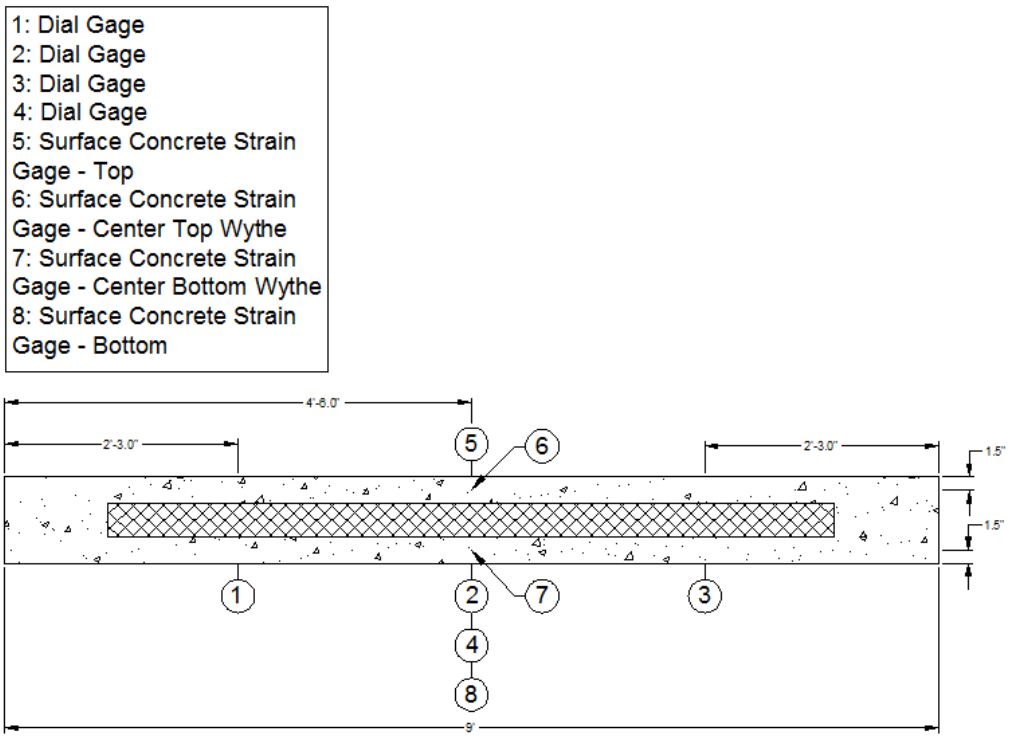


**Figure 126: Solid/Sandwich Panel External Creep Instrumentation**

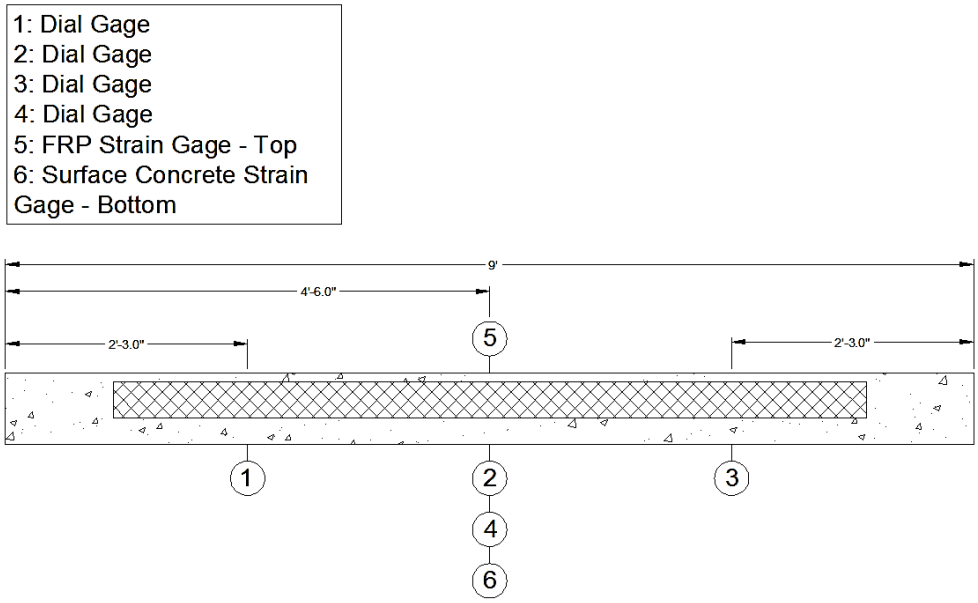


**Figure 127: 8" FPCS External Creep Instrumentation**

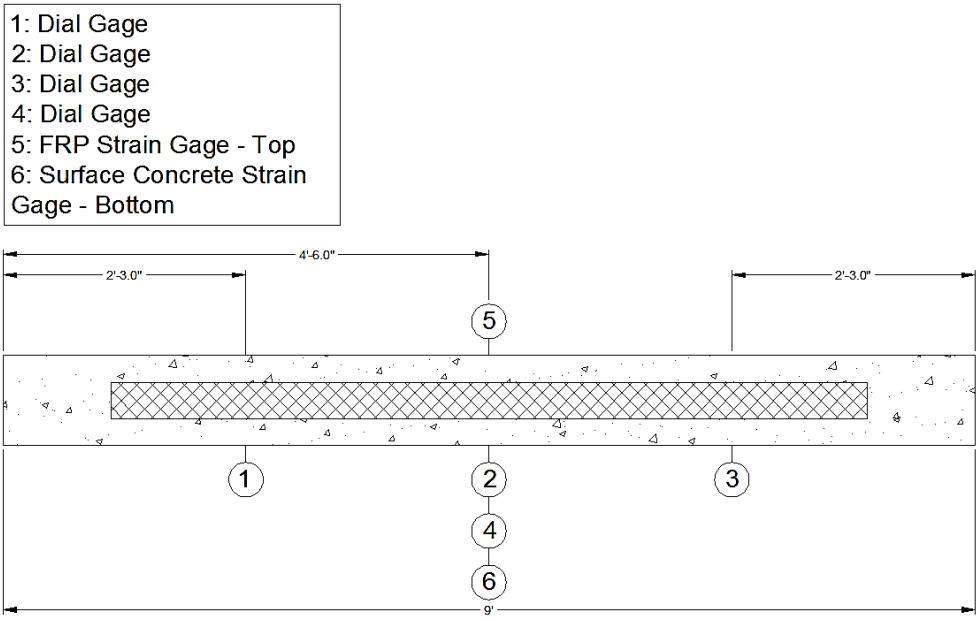


**Figure 128: 10" FPCS Panel External Creep Instrumentation**

While strain gages were applied at all locations as described in the above figures, not all were functional at the time of testing. The following table provides a list of all functioning and non-functioning strain gages.

## 6.4 TEST PROCEDURE

Supports were position and leveled such that they would support the slabs as simply supported beams. The specimens were then positioned on these supports. Once positioned, the instrumentation was set up, primarily the dial gages. Initial readings for both deflection and strain were then taken to act as the pre-load bench mark. The eco-blocks were then weighed individually and positioned, two to each specimen. As each specimen was loaded, additional readings for both deflection and strain were taken to determine the initial effect of the load. It should be noted that during the loading process, the loader which was positioning the blocks hit the 8” FPCS Panel with its tire and an audible crack was heard. This could be relevant when considering the result.

Once the loads had been placed and all initial readings taken the slabs were monitored twice a day, every day for one week in both strain and deflection. For the following three weeks, the measurements were taken once a day. From that point forward, measurements were taken roughly twice per week as the measurements began to exhibit a more gradual trend.

## 6.5 EXPERIMENTAL RESULTS

During the initial loading of these specimens, there were several occurrences which likely contributed to the issues experienced when analyzing the data such as the dial gage supports being disturbed during and after loading. Also, given the public nature of these tests, the specimens were subject to vandalism.

### 6.5.1 DISPLACEMENT OVER TIME

Table 29 represents the two individual and ultimate loads placed upon the creep specimens. Figure 129 depicts the creep at the mid-span of each specimen as time passes. Due to the limited testing areas available, these specimens were tested in an environment which could not be perfectly controlled as it was outdoors and open to the public. For this reason, several factors have affected the results; primarily with the solid slab, the sandwich panel, and the 8” FPCS panel, as they were most exposed. The 10” FPCS panel was more discretely

located and, therefore, experienced a more stable environment. In Figure 129, areas of note/concern are circled and numbered. The explanations for these numbers are as follows:

1.) The dial gages had been moved such that they no longer recorded any data. For that reason, deflection data acquisition at that location was halted.
2.) This illustrates the recovery of the deflection as the load was removed from the sandwich panel.
3.) This illustrates the recovery of the deflection as the load was removed from the solid slab.

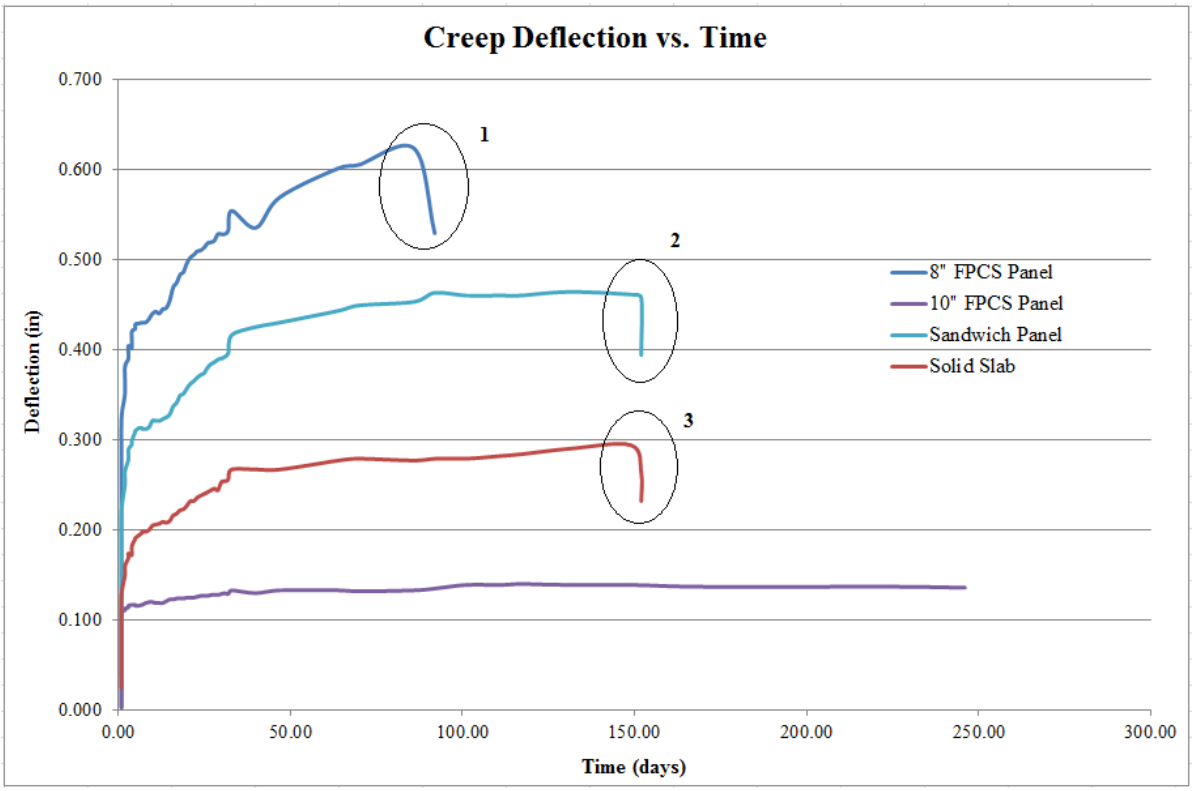


**Figure 129: Creep Deflection vs. Time**

To compare and confirm the nature of the deflection, the deflection at the quarter points of each specimen were reviewed. The results can be seen in Figure 130.

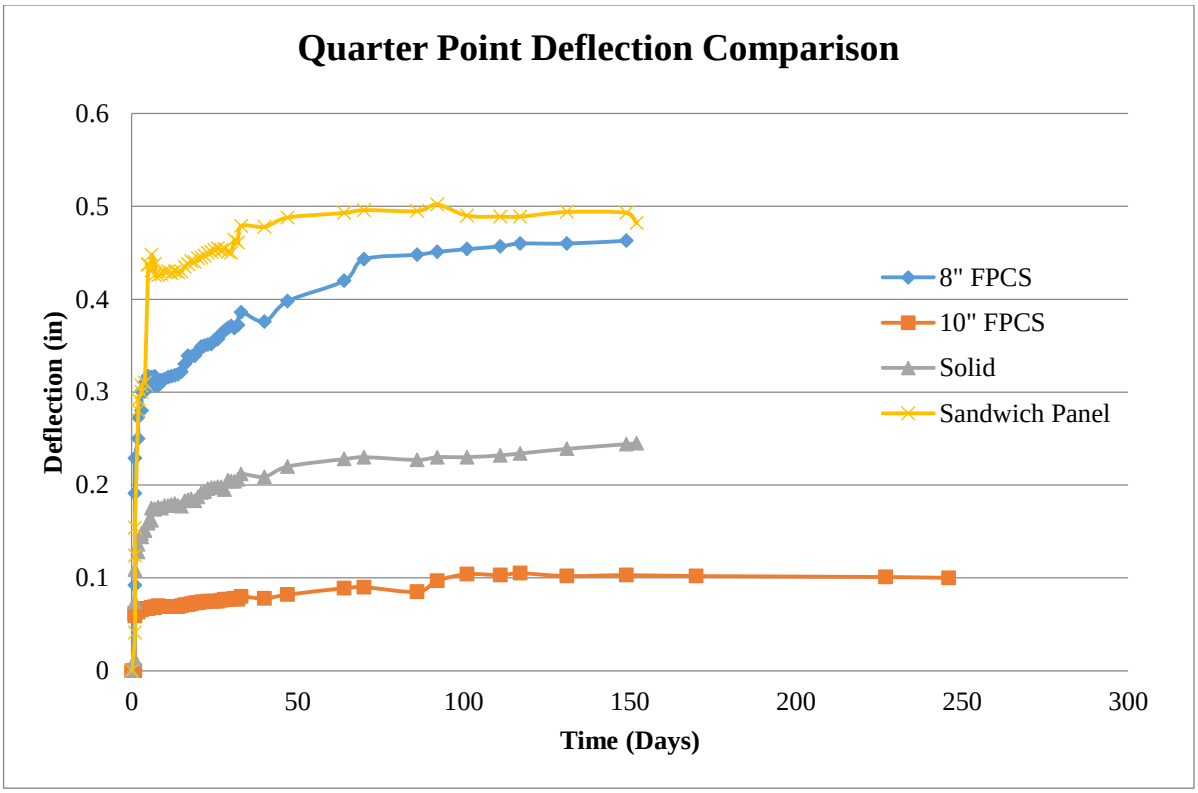


**Figure 130: Quarter Point Deflection vs. Time**

It can be seen in Figure 129 that each specimen experiences the greatest increase in deflection during the initial stages of testing (i.e. as soon as the loads were positioned). Over time, the increase to this deflection, which at first appears to increase vertically, begins to increase at a slower rate as time progresses. At this point, a plateau begins to appear with increasing small changes to the monitored deflection. These small increases in deflection represent creep.

It should be noted though, that the initial deflections of these specimens are extremely high over the first 24-48 hours of sustained loading, even for the solid slab. When compared with the deflection experienced by the solid slabs presented in Chapter 3, it is clear that the initial deflection is unreasonable. This is likely due to either disturbances to the dial gages, total system settlement experienced at the supports, or a combination of the two. By removing the initial deflection (over the first 24-hour period), the following figures were produced and they present a much more reasonable creep deflection.

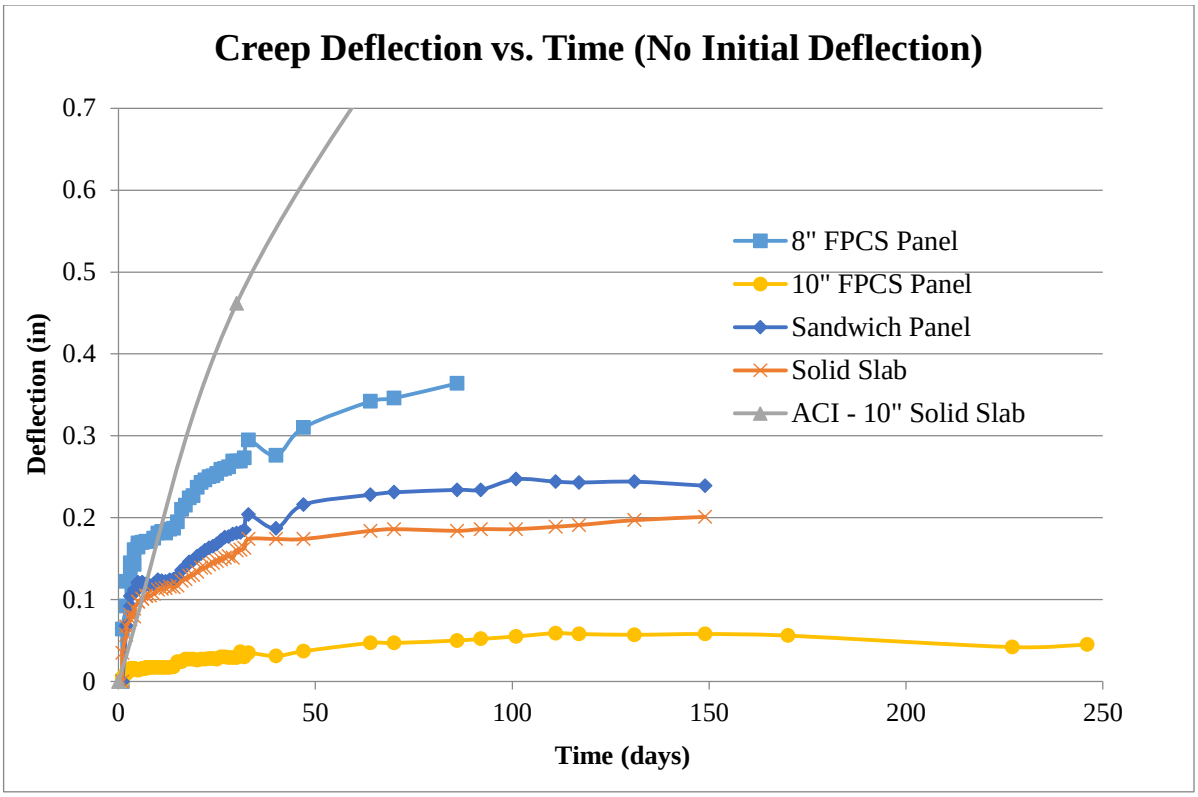


**Figure 131: Mid-Span Deflection vs. Time (No Initial Deflection)**

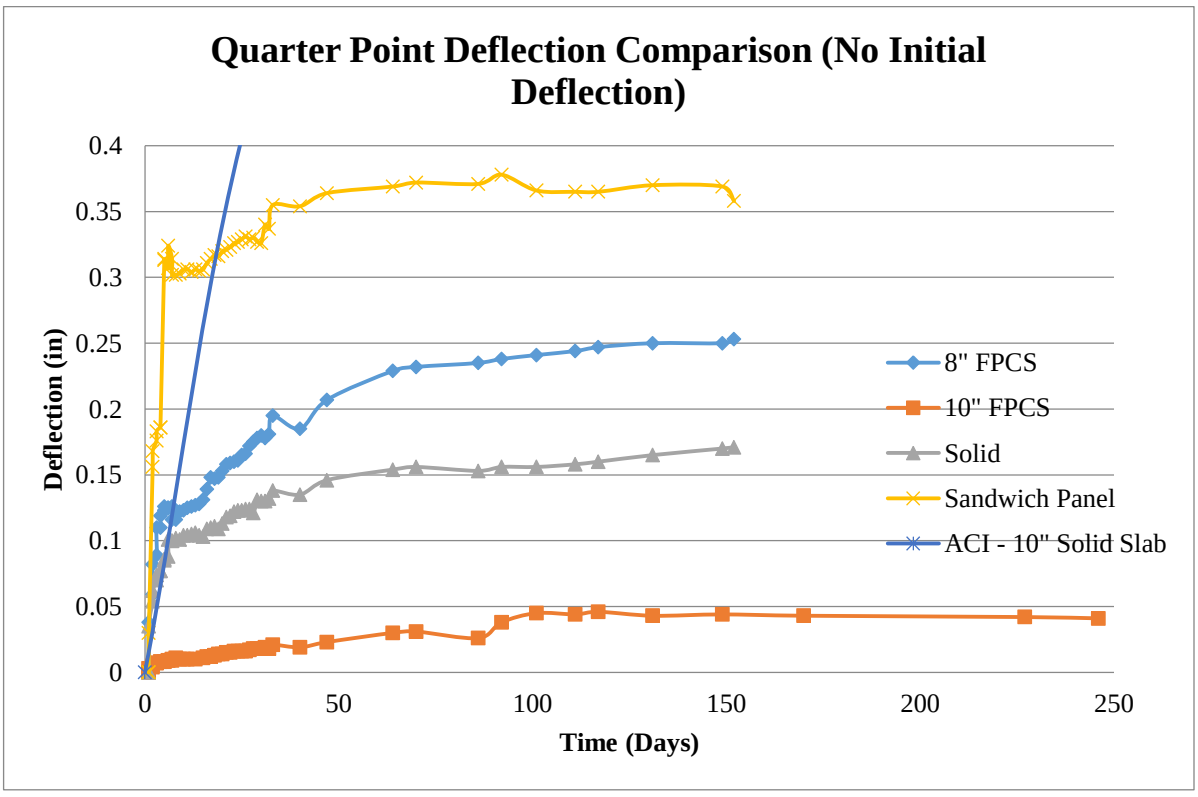


**Figure 132: Quarter Point Deflection vs. Time (No Initial Deflection)**

As the initial deflection of the specimens was compromised, the specimens were also compared with respect to secondary creep. Primary creep is the initial phase of creep which is characterized by an extremely high deformation rate and often resembles a curve. Secondary creep begins when the rate of deformation stabilized and appears linear. By focusing on this region of each specimen, a best-fit line can be plotted and the slope compared. The results can be seen in Figure 133.

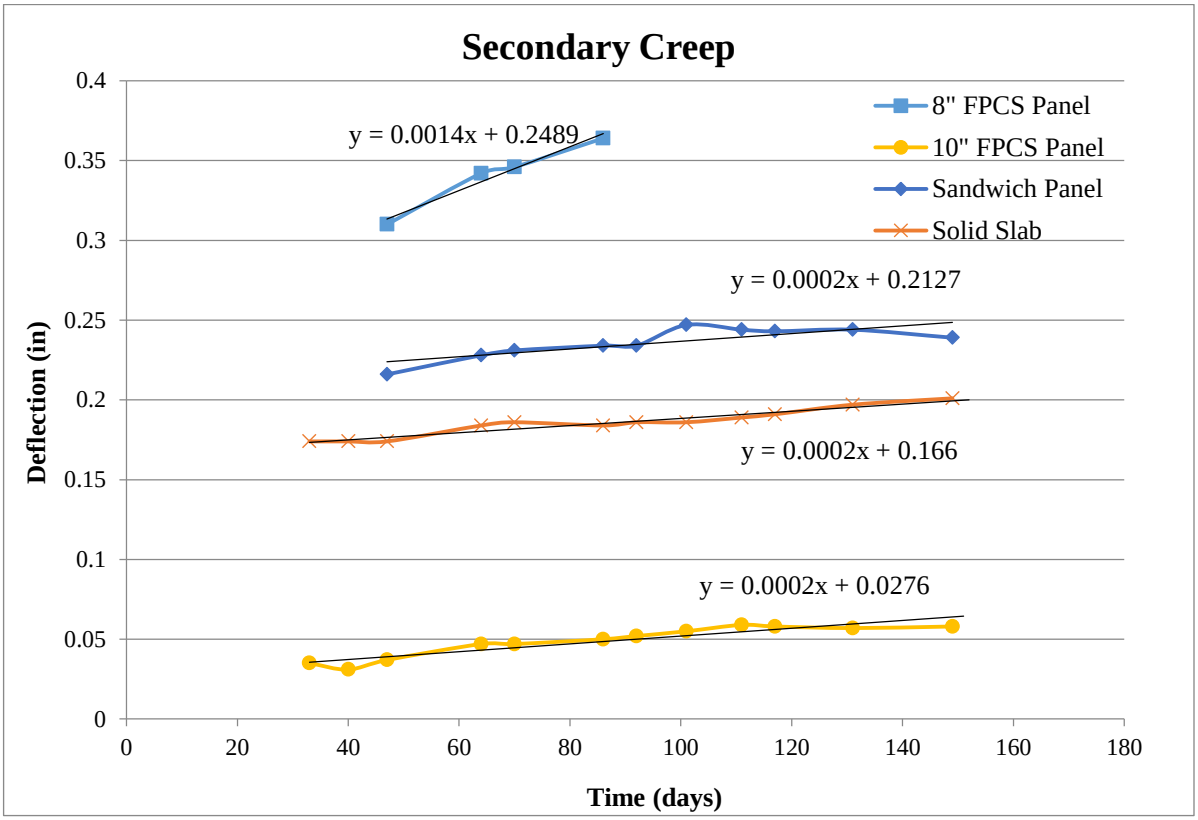


**Figure 133: Secondary Creep**

By focusing on the secondary creep, it can be seen that all 10" thick specimens exhibit a slope of 0.0002. The $\lambda_\Delta$ factor as calculated in accordance with ACI 318-11 presents a creep slope of 0.0007 in this time range. From this, it can be concluded that the solid, sandwich, and 10" FPCS panels all creep a rate lower than the maximum allowable rate.

Creep data continues to be collected from the 10" FPCS panel in order to determine long-term effects.

**Table 29: Creep Loading**

| Specimen | Weight of Block 1 (lbs) | Weight of Block 2 (lbs) | Total Load (lbs) |
|---|---|---|---|
| Solid Slab | 1552 | 1504 | 3056 |
| 10" Sandwich Panel | 1540 | 1542 | 3082 |
| 8" FPCS Panel | 1565 | 1572 | 3137 |
| 10" FPCS Panel | 1598 | 1576 | 3174 |

## 6.5.2 STRAIN

The following figures present typical strain-over-time graphs for the creep study. Usually, these distributions produce a smooth curve when plotted in a logarithmic scale [14][15]; however, this was not the case for the data collected. The remaining graphs can be found in APPENDIX 4. Variations beyond this point cannot be confirmed, although temperature and other environmental factors likely contributed.

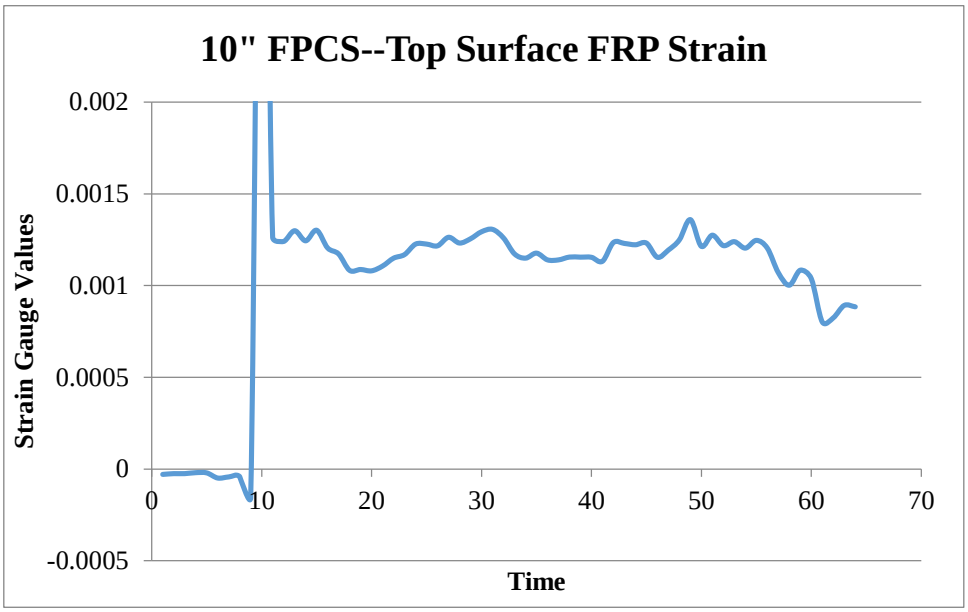


**Figure 134: 10" FPCS Surface—Top FRP Strain (Typical Strain)**

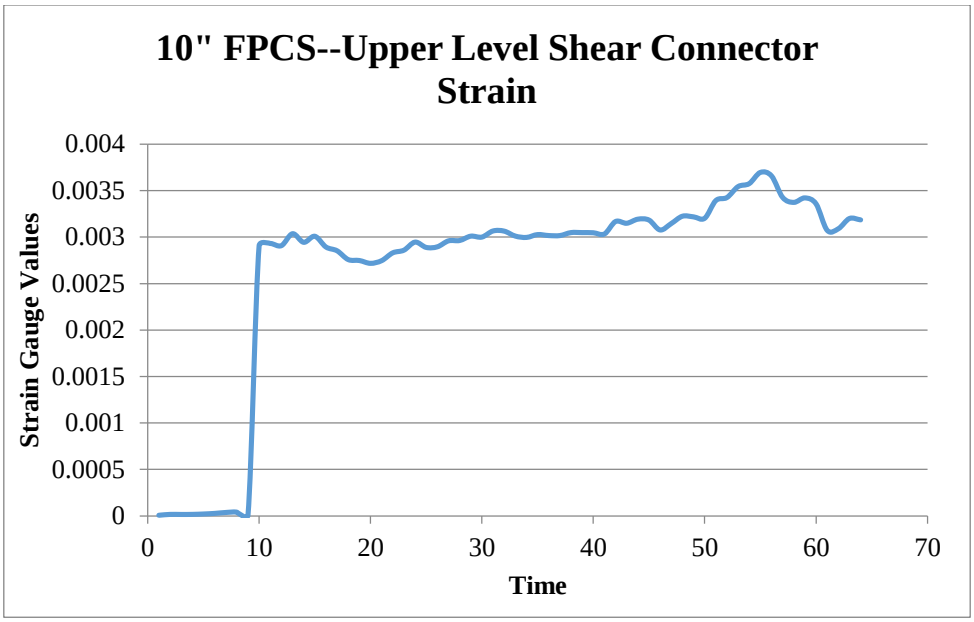


**Figure 135: 10" FPCS—Upper Level Shear Connector Strain (Typical Strain)**

## 6.6 CONCLUSIONS

Based on the recorded creep of all the panels, it can be concluded that the FRP top and side plates offer a confining effect that is beneficial to the reduction to the rate of creep. This is evident by the fact that the 10” FPCS panel deflected at a lower rate compared to the solid slab, even though it had 118 pounds more weight applied to it.

According to ACI 318-11, the solid slab and the 10” FPCS panel were the only two that satisfied requirements for creep deflection, given a six month time frame and using the recorded deflection values. However, by focusing on the secondary creep region of each specimen, the solid, sandwich, and 10” FPCS panels all creep at a rate lower than the maximum allowable rate specified by ACI 318-11. The maximum allowable deflection calculations can be seen in APPENDIX 4.

# CHAPTER 7: CONCLUSIONS/RECOMMENDATIONS

Several conclusions can be made from the study presented in this paper:

- FRP plate shear connectors are a feasible option as shear connectors in reinforced concrete sandwich panels.
- The wet bond method is a viable option for bonding FRP to concrete; however, it can be difficult to do within the time frame allowable for the concrete pour and the batch time of the adhesive.
- Bonding aggregate to the FRP ahead of time increases the speed and efficiency of the production of these panels at the time of the concrete pour without negatively affecting the strength of the FRP to concrete bond; however, it does require advanced planning, as the adhesive will need time to cure prior to the application of concrete.
- The confining effect produced by bonding both top and side FRP plates to the panels provides a high DCA, improved ultimate strength, while providing a resistance to creep that exceeds that of a solid concrete slab.
- These full-scaled FPCS panels have been confirmed to perform at the allowable deflection with area loads of 93 lb/ft$^2$ and 192 lb/ft$^2$ for the 8" and 10" FPCS panels, respectively, as per ACI 318-11.
- The scaled 10" FPCS panel has been confirmed to perform at the allowable deflection with respect to creep, as per ACI 318-11.
- The rate of secondary creep for the sandwich panel with segmental shear connectors and the 10" FPCS panel are all below the maximum specified by ACI 318-11 and equal to that of the solid panel. The primary difference is that the 10" FPCS panel reaches secondary creep sooner than the solid slab and sandwich panel, which is beneficial to total creep.

While this study has confirmed many of the ideas it set out to achieve, more research is still required. The effects of creep are a difficult topic to study due to the time required to conduct a test, and this issue is exacerbated by the time required to prepare these specimen with full instrumentation and the area required for testing. Additionally, it is recommended that separate supports be provided for each specimen being tested to avoid support settlement in future studies.

For this study, an initial concern was the ends of the slabs crushing at the supports, so for that reason, a solid zone was provided at each support, which can act as thermal bridges. With the full scale specimen, these zones provide much less strength and DCA; however, further testing should be conducted without these solid zones. This will optimize the thermal insulation provided by these panels and confirm the effectiveness of the internal and external FRP plates in providing strength and stiffness.

Finally, it is hoped that a FEM of these panels can be produced with the results of this data. This will assist in the optimization of these panels on a greater scale with regard to wythe thickness, shear connector spacing and insulation thickness/density. It will also allow for several theoretical tests such as thermal conduction.

# REFERENCES


1.) Frankl, Bernard A., Gregory W. Lucier, Tarek K. Hassan, and Sami H. Rizkalla. "Behavior of precast, prestressed concrete sandwich wall panles reinforced with CFRP shear grid." *PCI Journal*. Spring 2011. (2011): 42-54. Print.

2.) PCI Committee on Precast Sandwich Wall Panels. "State of the Art of Precast/Prestressed Concrete Sandwich Wall Panels." *PCI Committe Report*. Spring 2011. (2011): 131-142. Print.

3.) Bush, Jr., Thomas D., and Zhiqi Wu. "Flexural Analysis of Prestressed Concrete Sandwich Panels with Truss Connectors." *PCI Journal*. December 43.5 (1998): 76-86. Print.

4.) Salmon, David C., Amin Einea, et al. "Partially Composite Sandwich Panel Deflections." *Journal of Structural Engineering*. April 121.4 (1995): 778-783. Print.

5.) Einea, Amin, David C. Salmon, Maher K. Tardos, and Todd Culp. "A New Structurally and Thermally Efficient Precast Sandwich Panel System." *PCI Journal*. July-August 1994. (1994): 90-101. Print.

6.) Bush, Jr., Thomas D., and Gregory L. Stine. "Flexural Behavior of Composite Precast Concrete Sandwich Panels With Continuous Truss Connectors." *PCI Journal*. March-April 1994. (1994): 112-121. Print.

7.) Lorenz, Robert F., and Frank W. Stockwell. "Concrete Slab Stresses in Partially composite Beams and Girders." *AISC Engineering Journal*. 3rd Quarter 1984. (1984): 185-188. Print.

8.) Einea, Amin, David C. Salmon, Gyula J. Fogarasi, Todd D. Culp, and Maher K. Tardos. "State-of-the-Art of Precast Concrete Sandwich Panels." *PCI Journal*. November-December 1991. (1991): 78-98. Print.

9.) Benayoune, A., A.A. Abdul Samad, et al. "Flexural behaviour of pre-cast concrete sandwich composite panel - Experimental and theoretical investigations." *Construction and Building Materials*. April 22.4 (2008): 580-592. Print. <http://www.sciencedirect.com/science/article/pii/S095006180600300X>.

10.) Henin, Eliya, George Morcous, and Maher K. Tardos. "Precast Concrete Sandwich Panels For Floor and Roof Applications." *PCI Journal*. (2011): 1-11. Print.

11.) Al Chami, G., M. Theriault, and K.W. Neale. "Creep Behavior of CFRP-strengthened reinforced concrete beams." *Construction and Building Materials*. 23. (2009): 1640-1652. Print.

12.) Cho, Jeong-Rae, et al. "Bond characteristics of coarse sand coated interface between stay-in-place fibre-reinforced polymer formwork and concrete based on shear and tension tests." *NCR Research Press*. 37. (2010): 706-718. Print.

13.) Al-Salloum, Yousef A., and Tarek H. Almusallam. "Creep effect on the behavior of concrete beams reinforced with GFRP bars subjected to different environments." *Construction and Building Materials*. 21. (2007): 1510-1519. Web. 31 Mar. 2014.

14.) Guedes, R.M., C.M.L. Taveres, and A.J.M. Ferreira. "Experimental and theoretical study of the creep behavior of GFRP-reinforced polymer concrete." *Composites Science and Technology*. 64. (2004): 1251-1259. Print.

15.) Tavares, C.M.L., M.C.S. Ribeiro, A.J.M. Ferreira, and R.M. Guedes. "Creep behaviour of FRP-reinforced polymer concrete." *Composite Structures*. 57. (2002): 47-51. Print.

16.) Laoubi, Kader, Ehab El-Salakawy, and Brahim Benmokrane. "Creep and durability of sand-coated glass FRP bars in concrete elements under freeze/thaw cycling and sustained loads." *Cement & Concrete Composites*. 28. (2006): 869-878. Print.

# APPENDICES

# APPENDIX 1

This appendix presents all corrections, material properties, and additional graphs/figures pertaining to Chapter 3.

# CORRECTION CALCULATIONS

## Correction of Segmental Shear Connector Specimen:

***Adjusting effective length from 8-ft to 9-ft***

**Given:** $L_{8ft} := 96in$ $L_{9ft} := 108in$ EI = Constant P = Constant

**Required:** Assuming the same loading, develop and apply a correction to the deflection of the specimen.

## Solution

$$\Delta = \frac{P \cdot L^3}{48EI}$$

Assuming P and EI are constant, consider them as unit values:

$$\frac{P}{EI} = \frac{48 \cdot \Delta}{L^3}$$

As P/EI is constant, set the deflection equations for the 8-ft and 9-ft effective lengths equal to each other.

$$\frac{48\Delta_{8ft}}{L_{8ft}^3} = \frac{48 \cdot \Delta_{9ft}}{L_{9ft}^3}$$

$$\Delta_{9ft} = \frac{L_{9ft}^3 \cdot \Delta_{8ft}}{L_{8ft}^3} \text{ simplify } \rightarrow \Delta_{9ft} = \frac{729 \cdot \Delta_{8ft}}{512} \qquad \frac{729}{512} = 1.424$$

Therefore: $\Delta_{9ft} = 1.424\Delta_{8ft}$

## Correction of Discrete Shear Connector Specimen:

***Adjusting effective length from 8-ft to 9-ft and loading condition from 4-pt to 3-pt bending***

**Given:** $L_{8ft} := 96in$ $L_{9ft} := 108in$ $a := \frac{L}{3}$ EI = Constant P = Constant

**Required:** Assuming the same loading, develop and apply a correction to the deflection of the specimen.

## Solution

$$\Delta_{3pt} = \frac{P \cdot L^3}{48EI} \qquad \Delta_{4pt} = \frac{P \cdot a \cdot \left(3 \cdot L^2 - 4a^2\right)}{24EI}$$

Simplifying the equation for 4-pt bending:

$$\frac{P \cdot a \cdot \left(3 \cdot L^2 - 4a^2\right)}{24EI} \rightarrow \frac{23 \cdot L^3 \cdot P}{648 \cdot EI}$$

As the load, P, is distributed at two locations in 4-pt bending, the load must be halved to compare to 3-pt bending:

$$\Delta_{4pt} = \frac{23 \cdot L^3 \cdot \frac{P}{2}}{648 \cdot EI} \rightarrow \Delta_{4pt} = \frac{23 \cdot L^3 \cdot P}{1296 \cdot EI}$$

Assuming P and EI are constant, consider them as unit values:

$$\frac{P}{EI} = \frac{48 \cdot \Delta_{3pt}}{L_{9ft}^3} = \frac{1296 \cdot \Delta_{4pt}}{L_{8ft}^3}$$

As P/EI is constant, set the deflection equations for the 8-ft and 9-ft effective lengths equal to each other.

$$\frac{1}{\Delta_{3pt9ft}} = \left(\frac{48}{L_{9ft}^3}\right) \cdot \left(\frac{23 \cdot L_{8ft}^3}{1296 \cdot \Delta_{4pt8ft}}\right) \rightarrow \frac{1}{\Delta_{3pt9ft}} = \frac{11776}{19683 \cdot \Delta_{4pt8ft}} \qquad \frac{11776}{19683} = 0.598$$

Taking the reciprical to apply the correction:

Therefore: $\Delta_{9ft} = 1.67145 \cdot \Delta_{8ft}$

# DEFLECTION ACROSS SAMPLE LENGTH

## GROUP 1

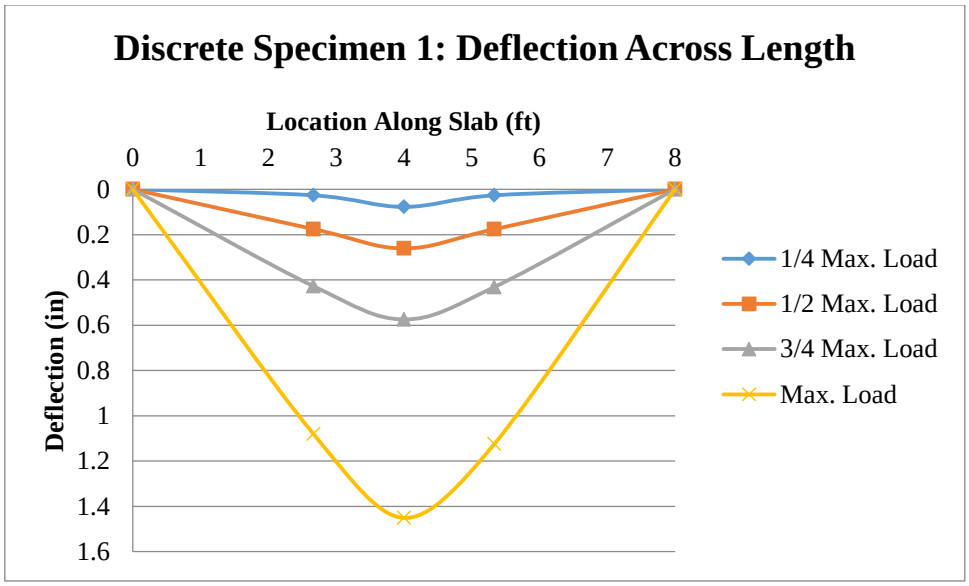


**Figure 136: Discrete Connector Specimen 1--Deflection Across Sample Length**

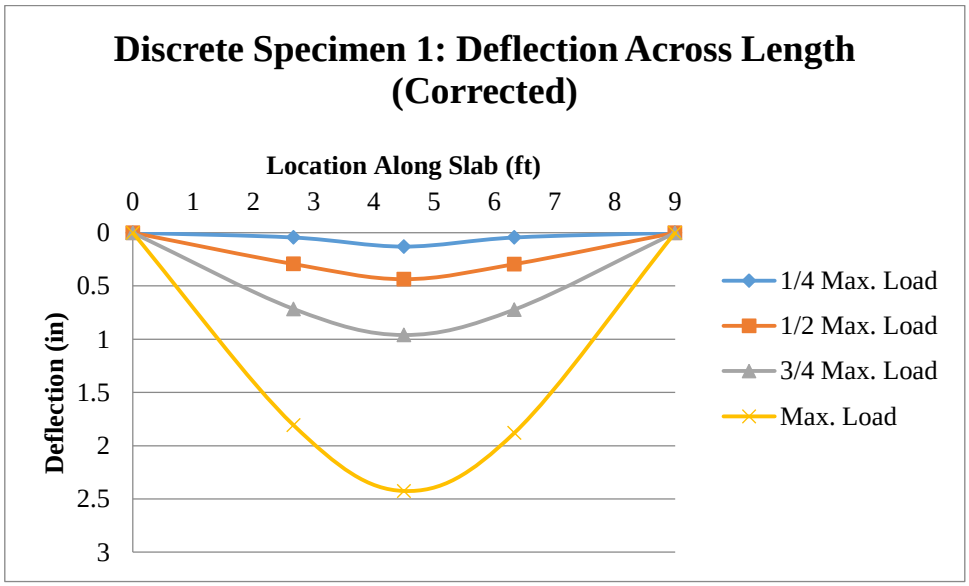


**Figure 137: Discrete Connector Specimen 1--Deflection Across Sample Length (Corrected)**

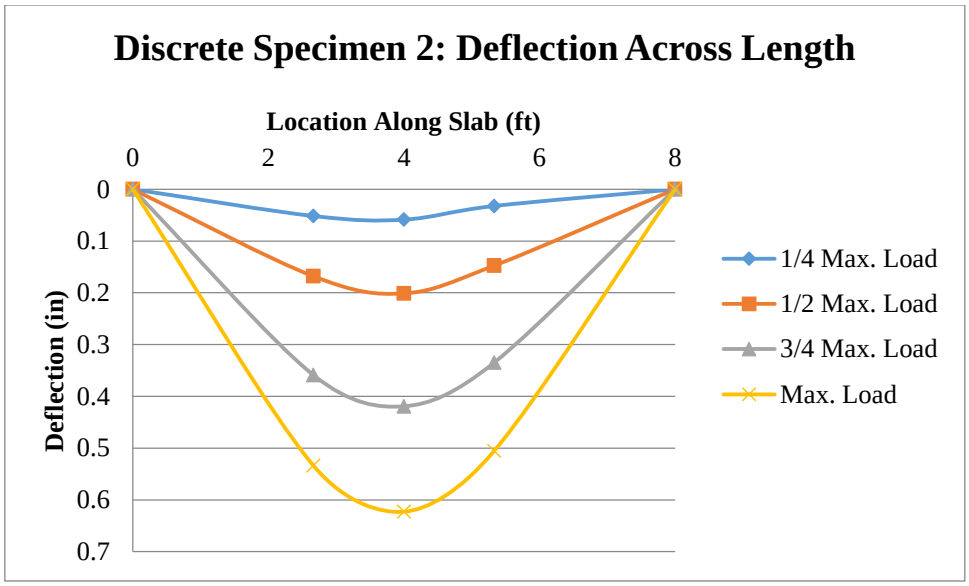


**Figure 138: Discrete Connector Specimen 2--Deflection Across Sample Length**

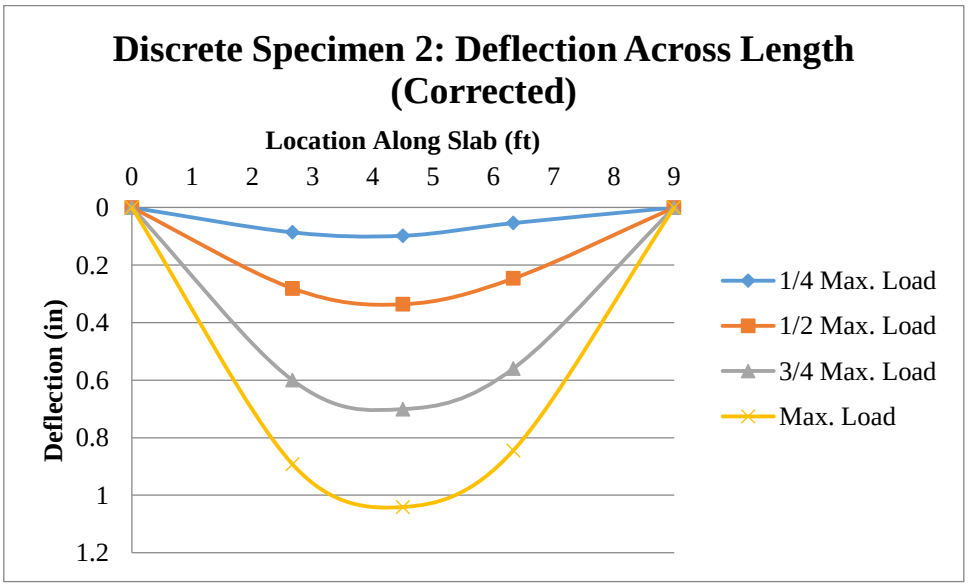


**Figure 139: Discrete Connector Specimen 2--Deflection Across Sample Length (Corrected)**

## GROUP 2

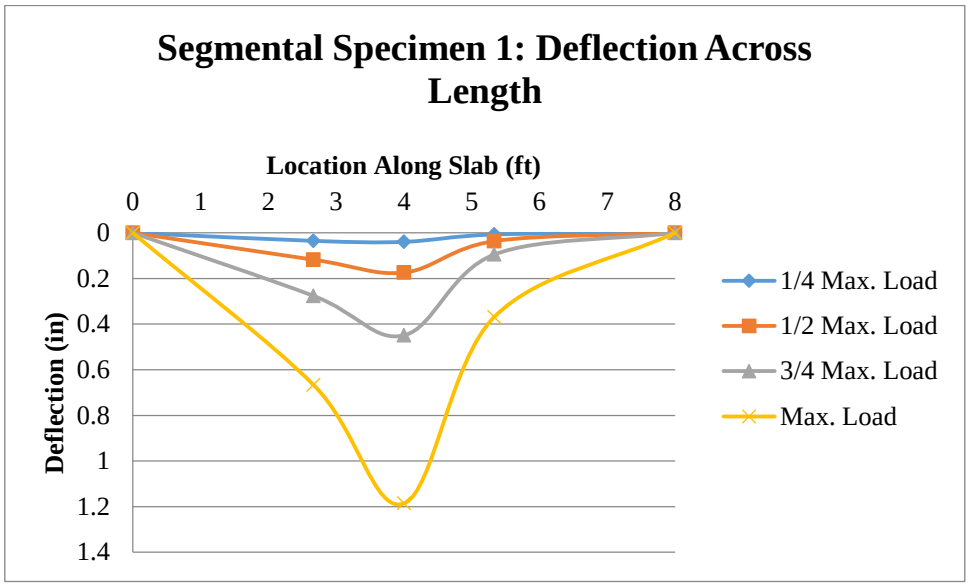


**Figure 140: Segmental Connector Specimen 1--Deflection Across Sample Length**

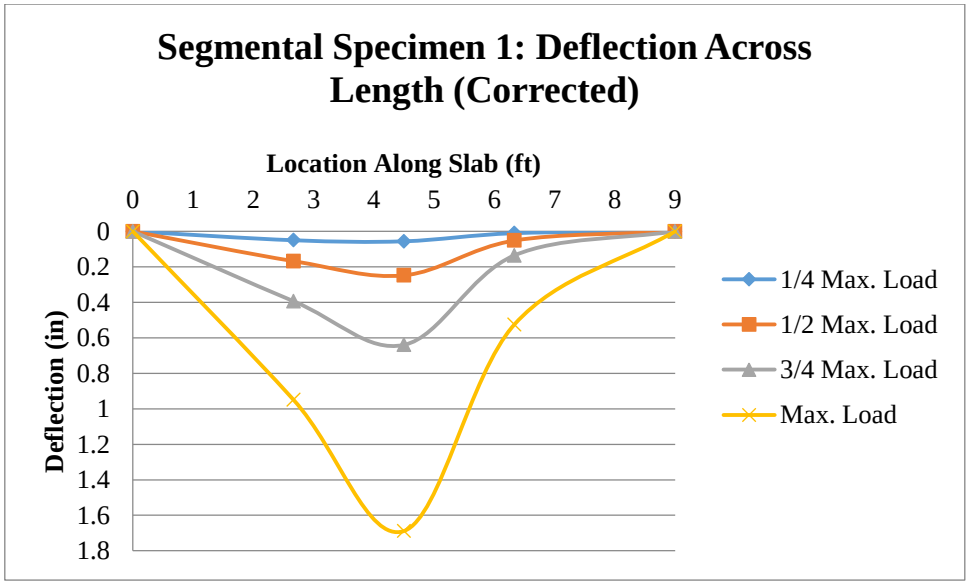


**Figure 141: Segmental Connector Specimen 1--Deflection Across Sample Length (Corrected)**

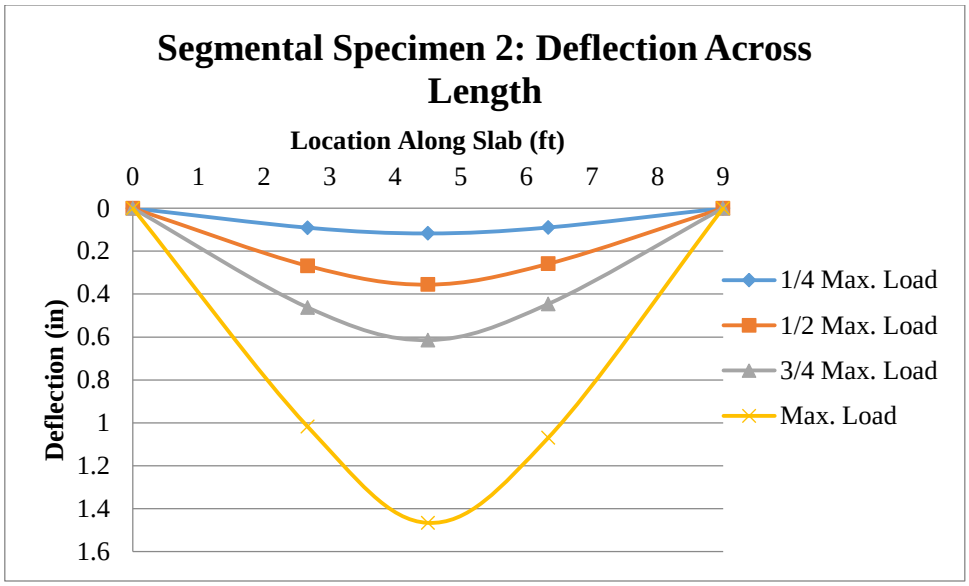


**Figure 142: Segmental Connector Specimen 2--Deflection Across Sample Length**

## GROUP 3

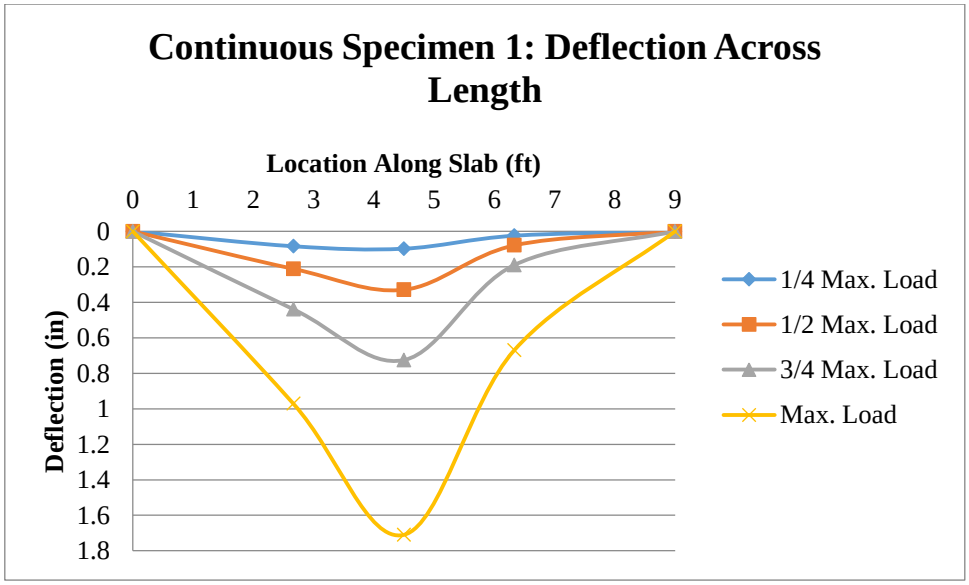


**Figure 143: Continuous Connector Specimen 1--Deflection Across Sample Length**

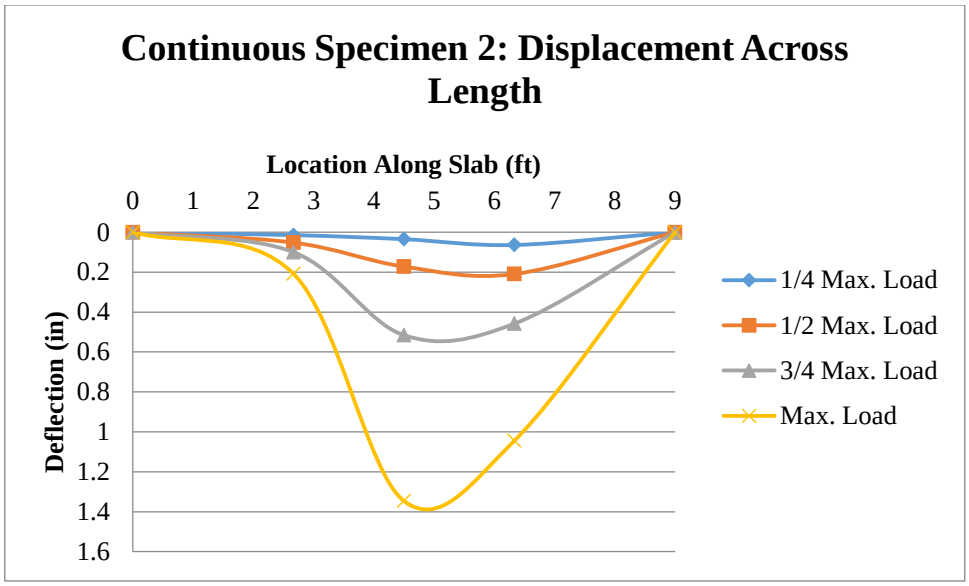


**Figure 144: Continuous Connector Specimen 2--Deflection Across Sample Length**

## GROUP 4

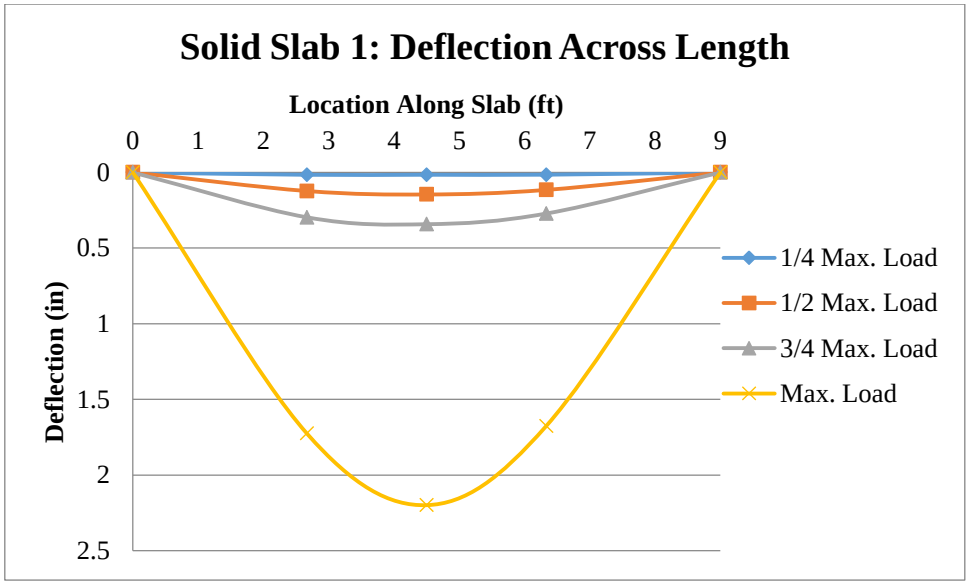


**Figure 145: Solid Specimen 1--Deflection Across Sample Length**

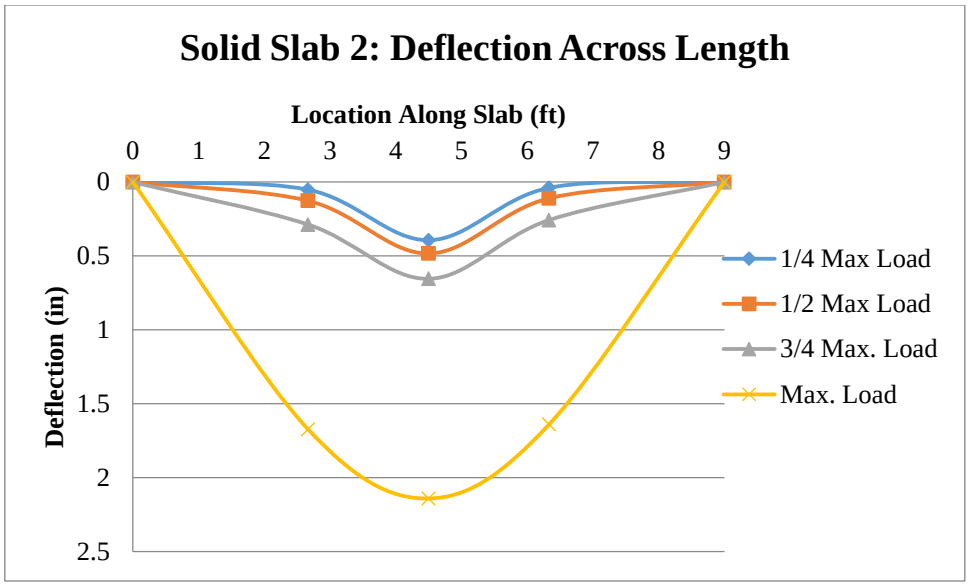


**Figure 146: Solid Specimen 2--Deflection Across Sample Length**

## ADDITIONAL STRAIN GAGE DATA

### GROUP 1

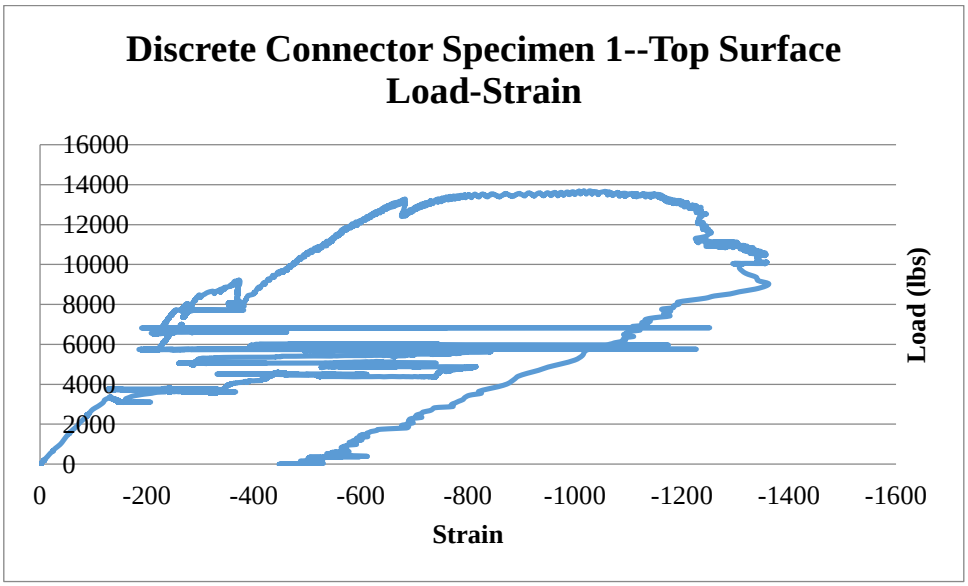


**Figure 147: Discrete Connector Specimen 1--Top Surface Load-Strain**

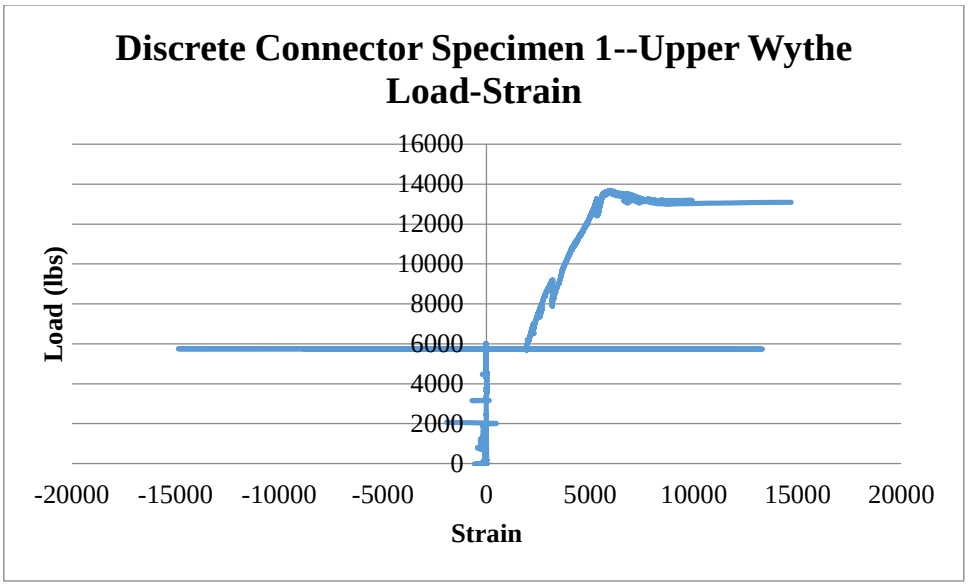


**Figure 148: Discrete Connector Specimen 1--Upper Wythe Load-Strain**

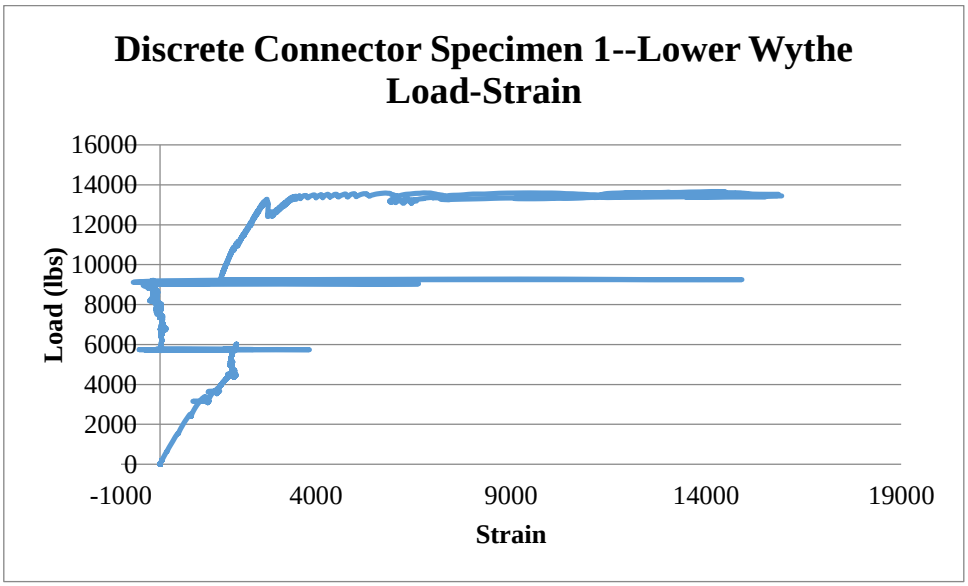


**Figure 149: Discrete Connector Specimen 1-- Lower Wythe Load-Strain**

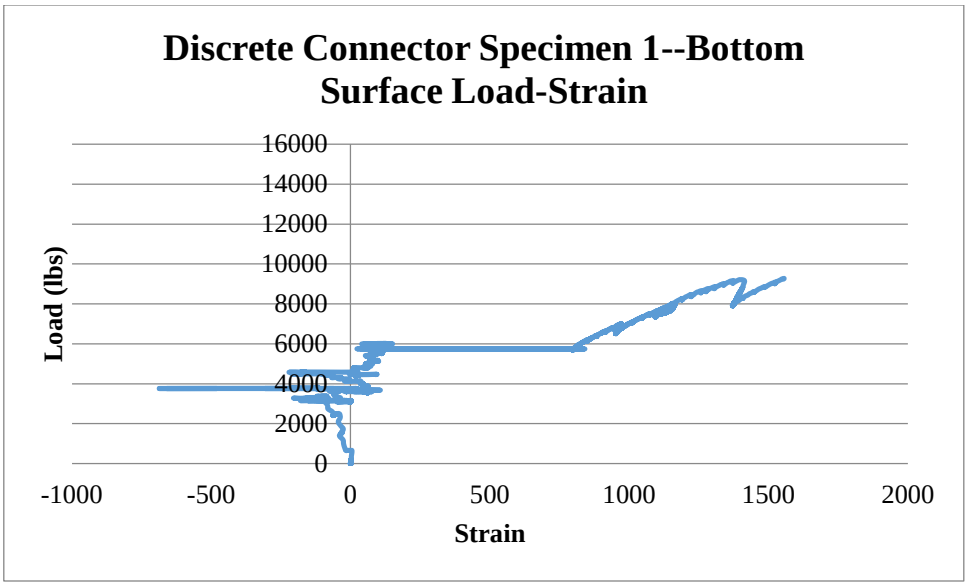


**Figure 150: Discrete Connector Specimen 1--Bottom Surface Load-Strain**

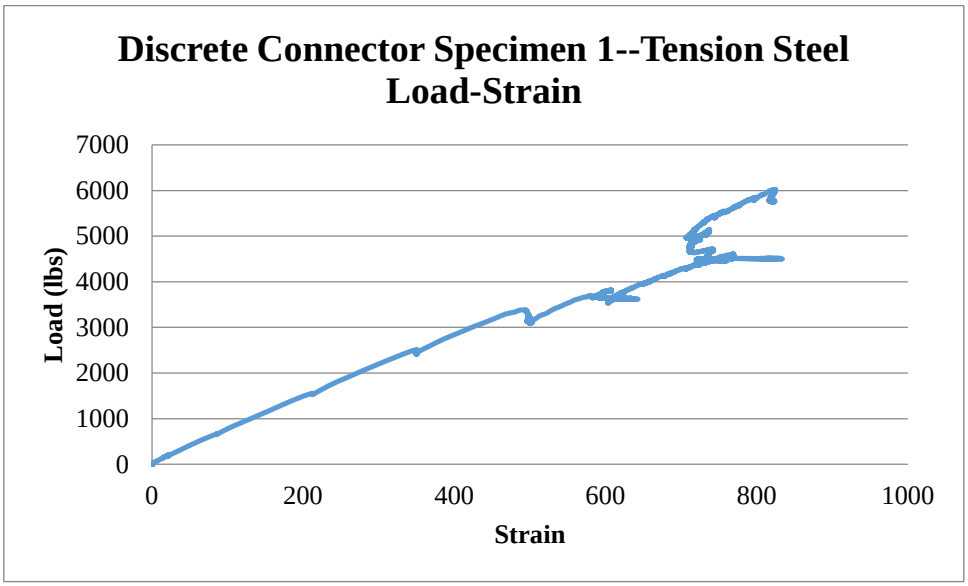


**Figure 151: Discrete Connector Specimen 1--Tension Steel Load-Strain**

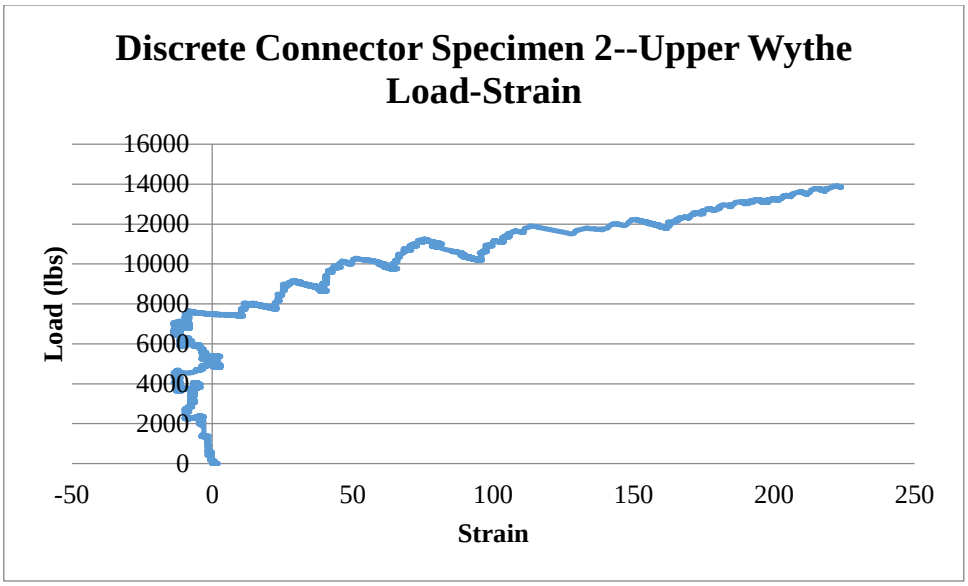


**Figure 152: Discrete Connector Specimen 2--Upper Wythe Load-Strain**

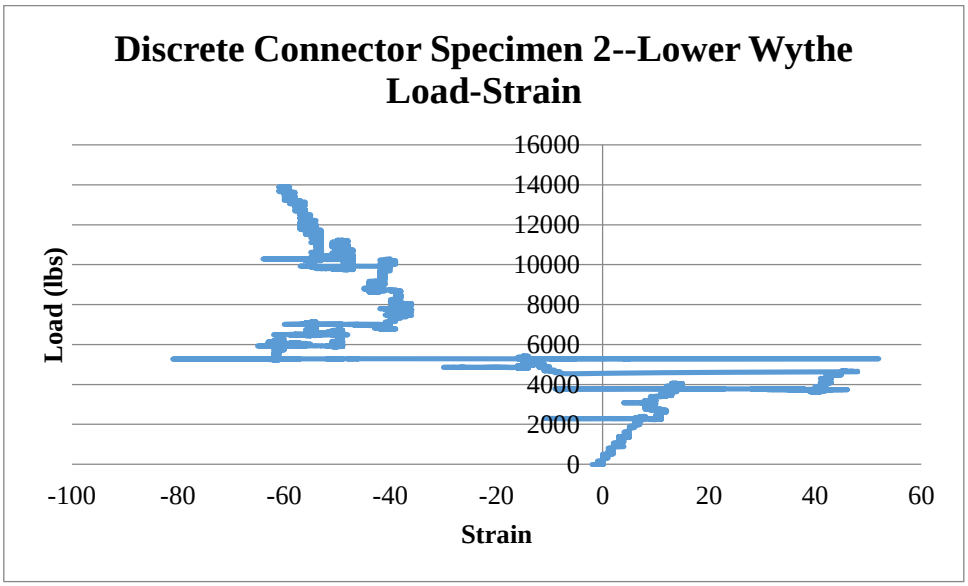


**Figure 153: Discrete Connector Specimen 2--Lower Wythe Load-Strain**

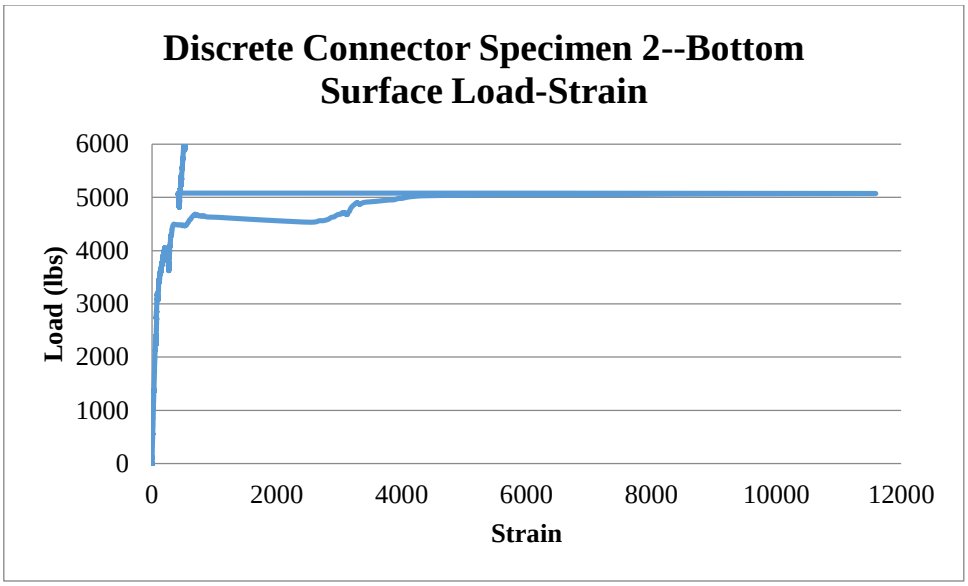


**Figure 154: Discrete Connector Specimen 2--Bottom Surface Load-Strain**

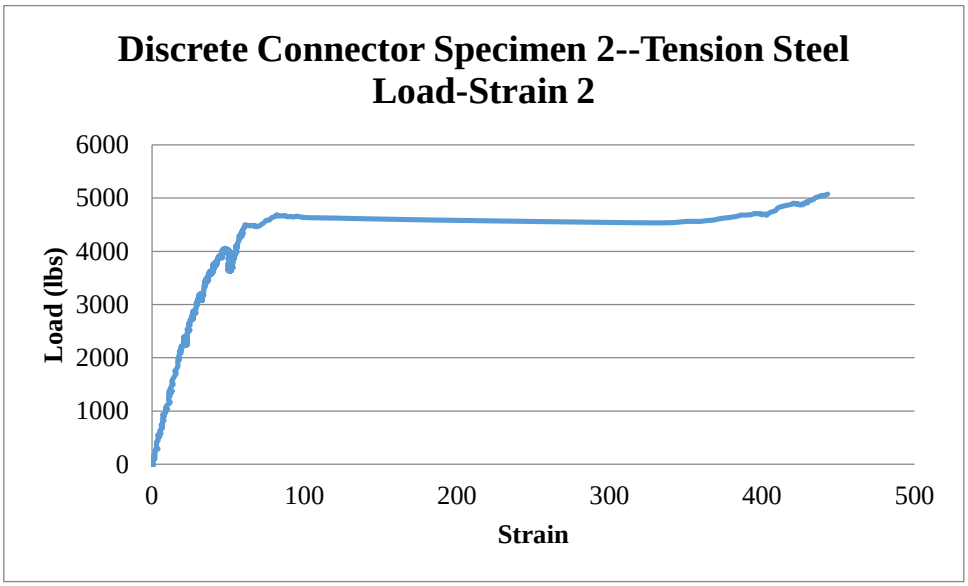


**Figure 155: Discrete Connector Specimen 2--Tension Steel Load-Strain 2**

## GROUP 2

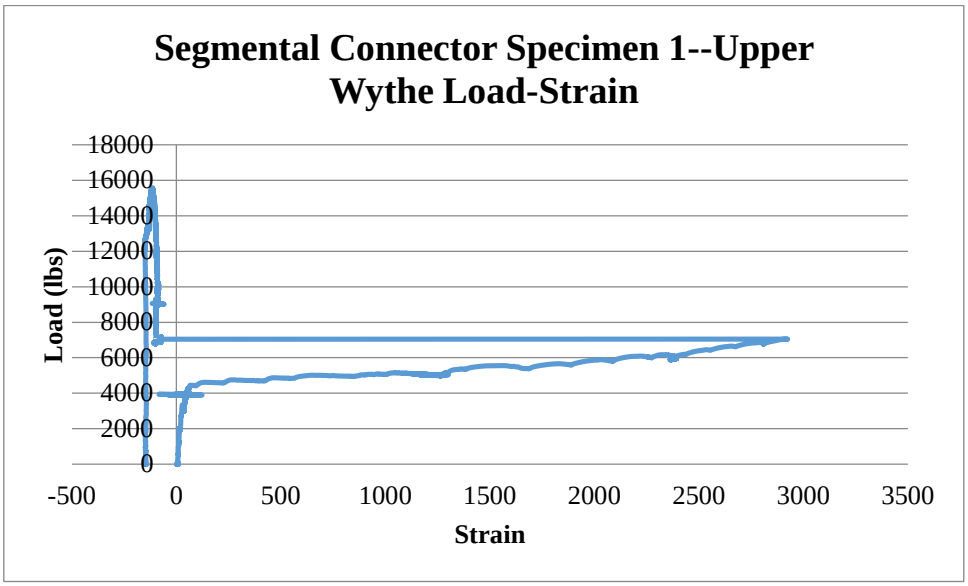


**Figure 156: Segmental Connector Specimen 1--Upper Wythe Load-Strain**

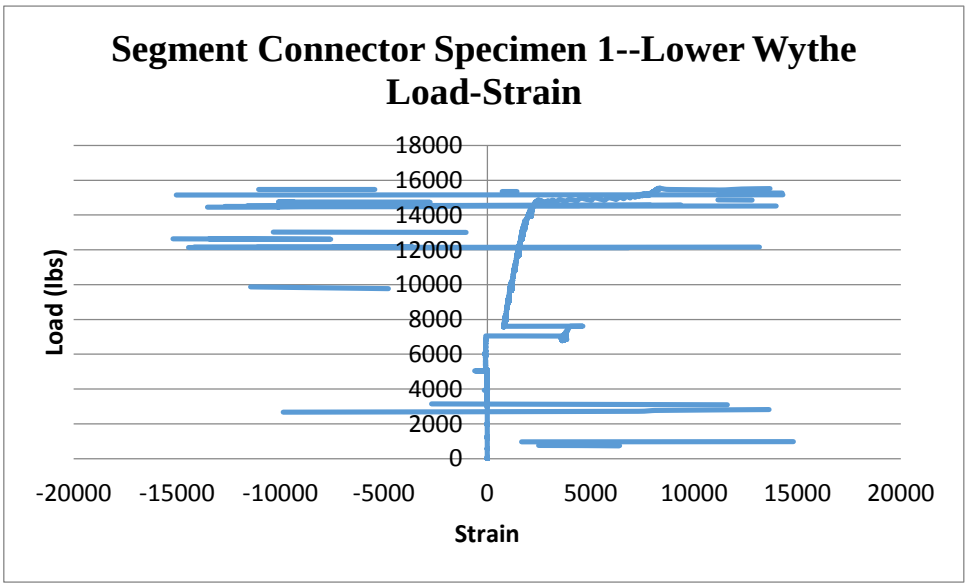


**Figure 157: Segmental Connector Specimen 1: Lower Wythe Load-Strain**

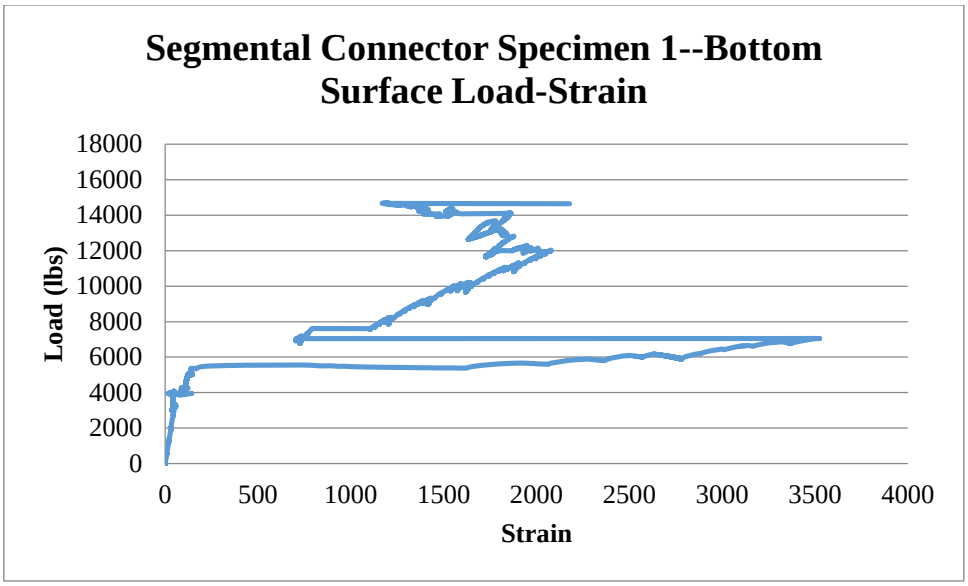


**Figure 158: Segmental Connector Specimen 1--Bottom Surface Load-Strain**

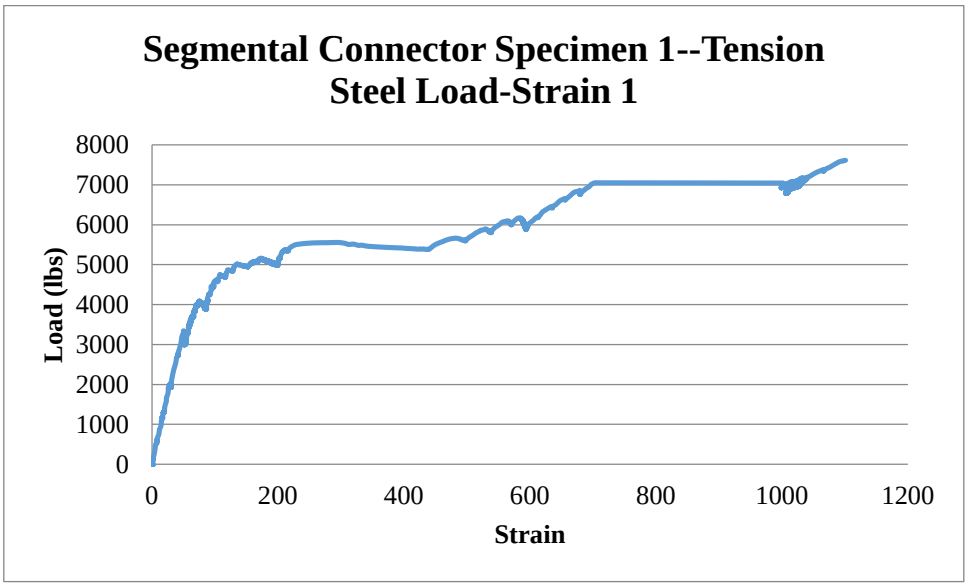


**Figure 159: Segmental Connector Specimen 1--Tension Steel Load-Strain 1**

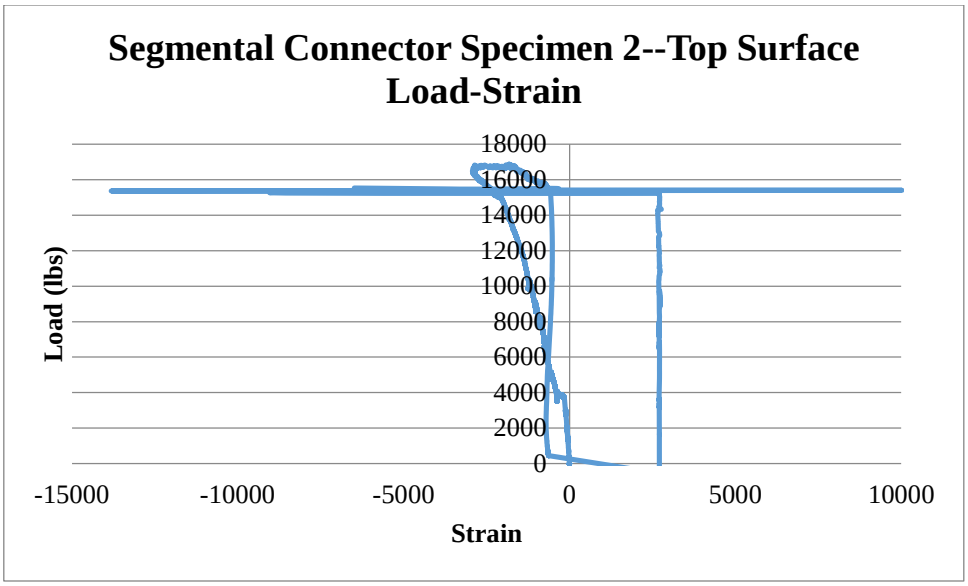


**Figure 160: Segmental Connector Specimen 2--Top Surface Load-Strain**

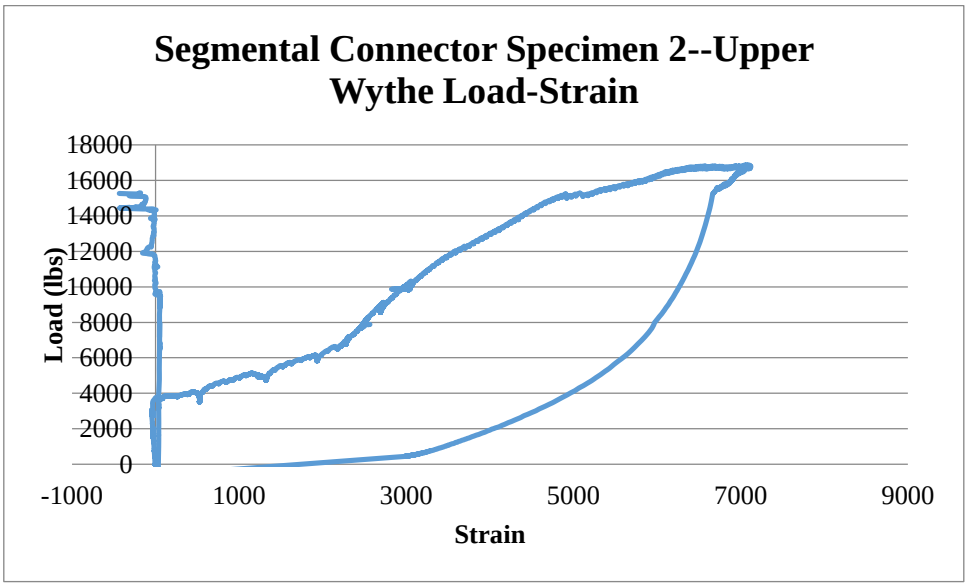


**Figure 161: Segmental Connector Specimen 2--Upper Wythe Load-Strain**

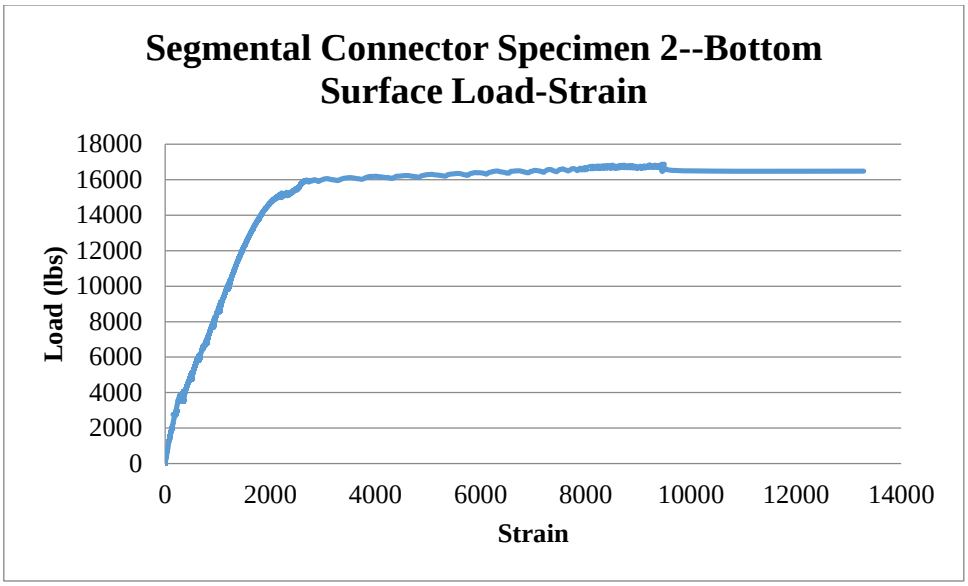


**Figure 162: Segmental Connector Specimen 2--Bottom Surface Load-Strain**

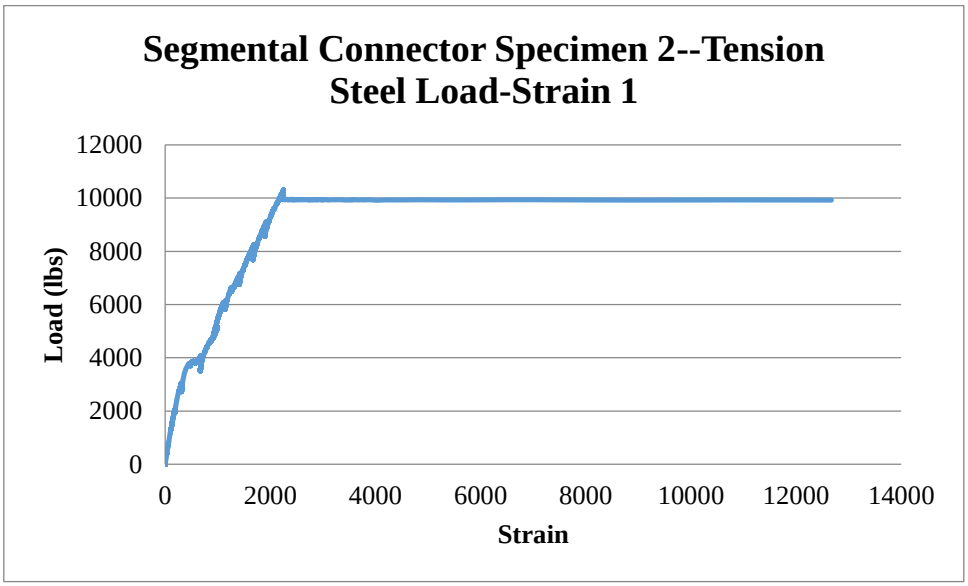


**Figure 163: Segmental Connector Specimen 2--Tension Steel Load-Strain 1**

## GROUP 3

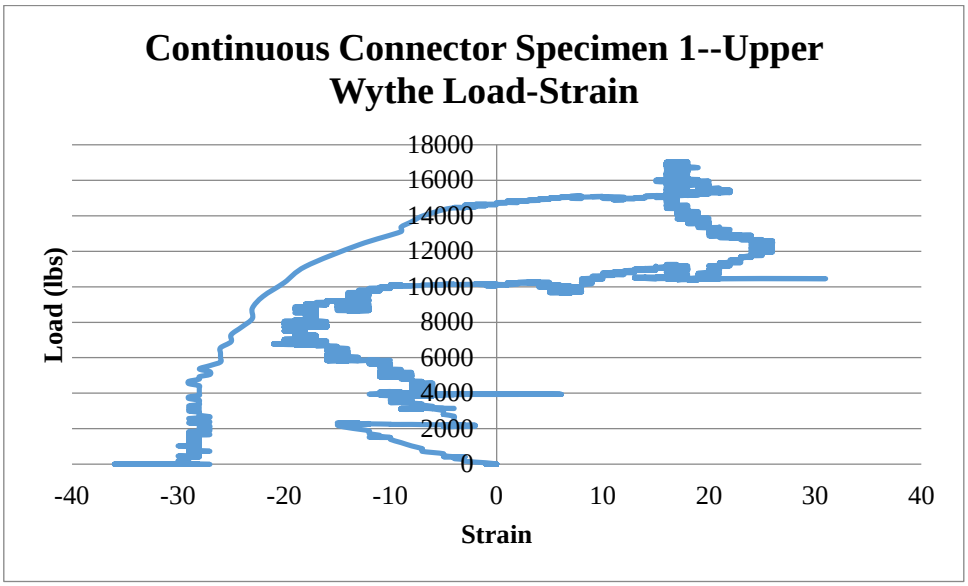


**Figure 164: Continuous Connector Specimen 1--Upper Wythe Load-Strain**

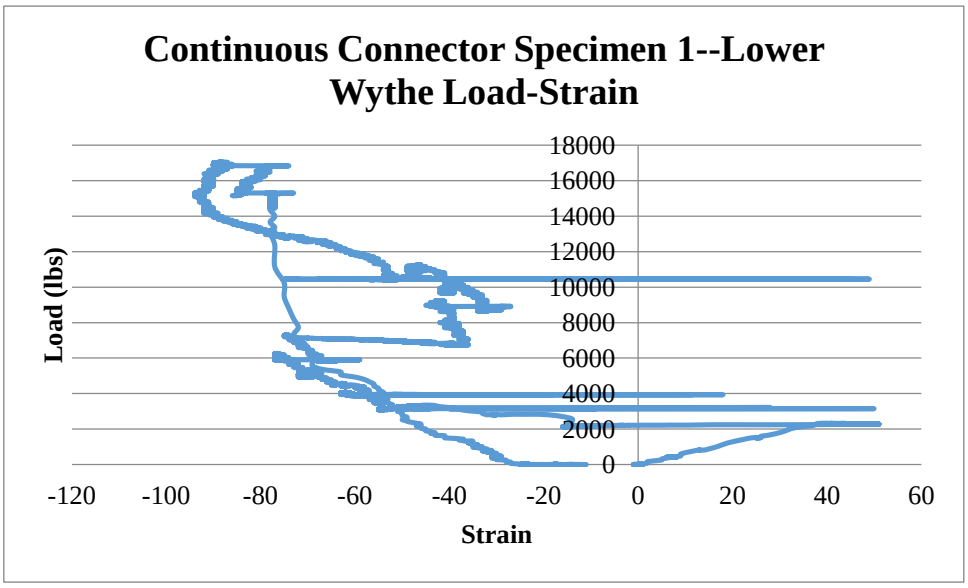


**Figure 165: Continuous Connector Specimen 1: Lower Wythe Load-Strain**

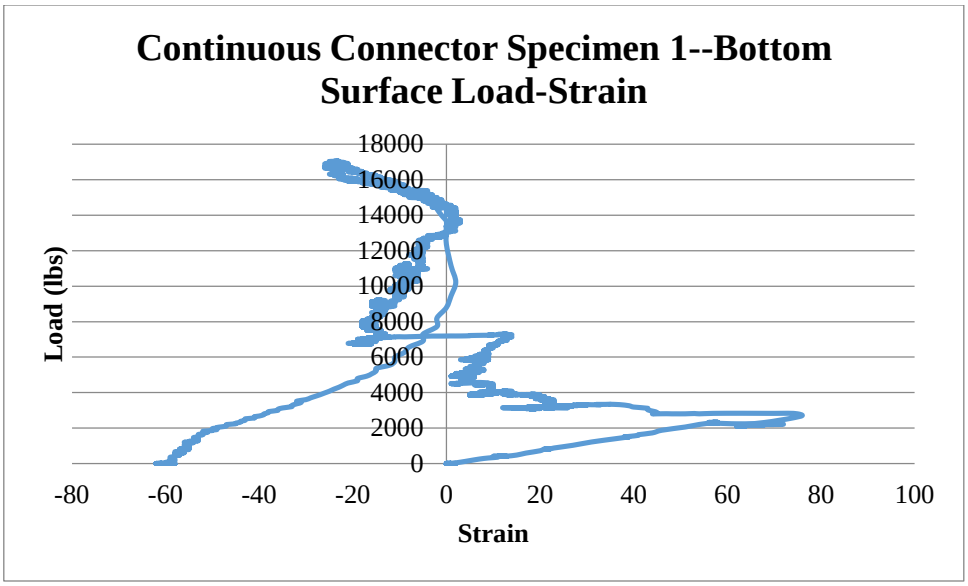


**Figure 166: Continuous Connector Specimen 1--Bottom Surface Load-Strain**

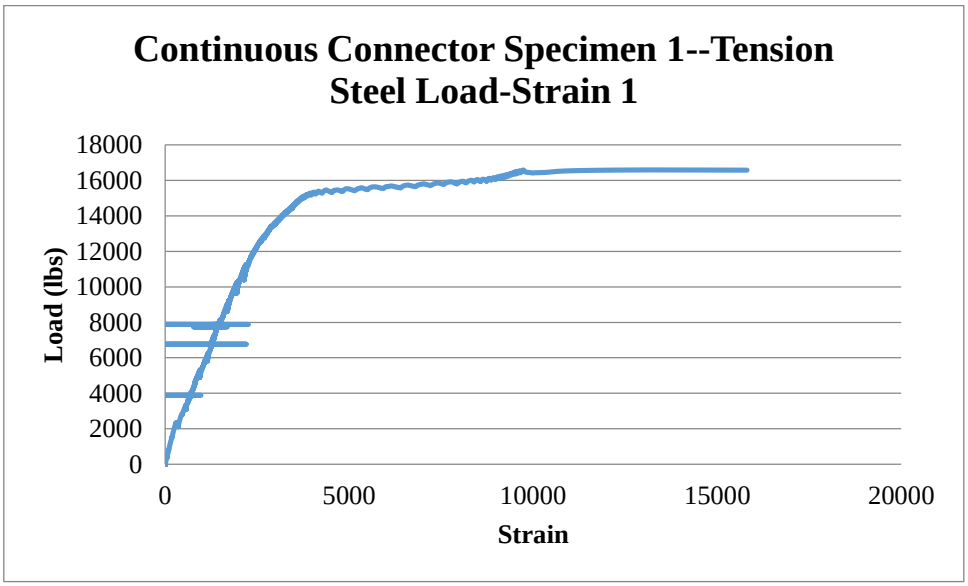


**Figure 167: Continuous Connector Specimen 1--Tension Steel Load-Strain 1**

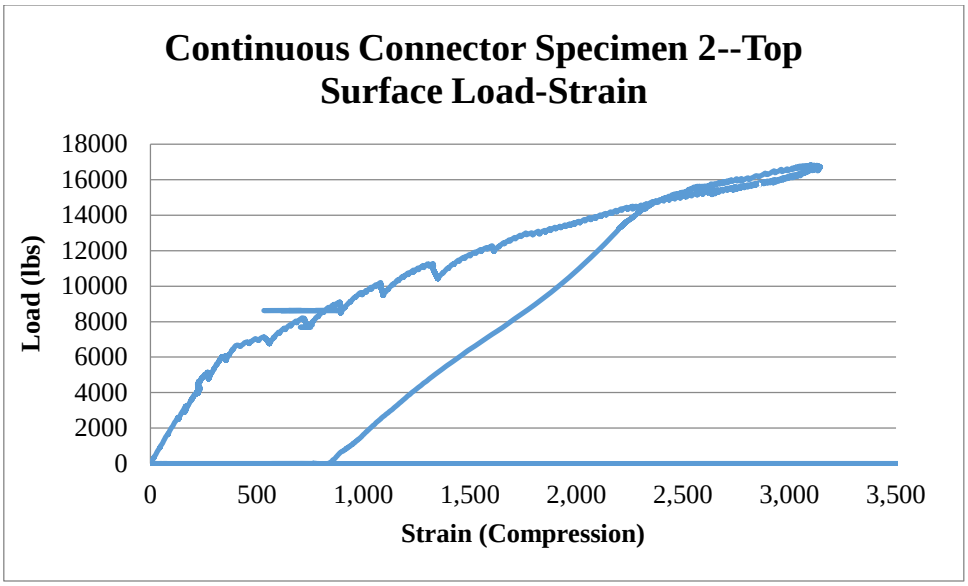


**Figure 168: Continuous Connector Specimen 2--Top Surface Load-Strain**

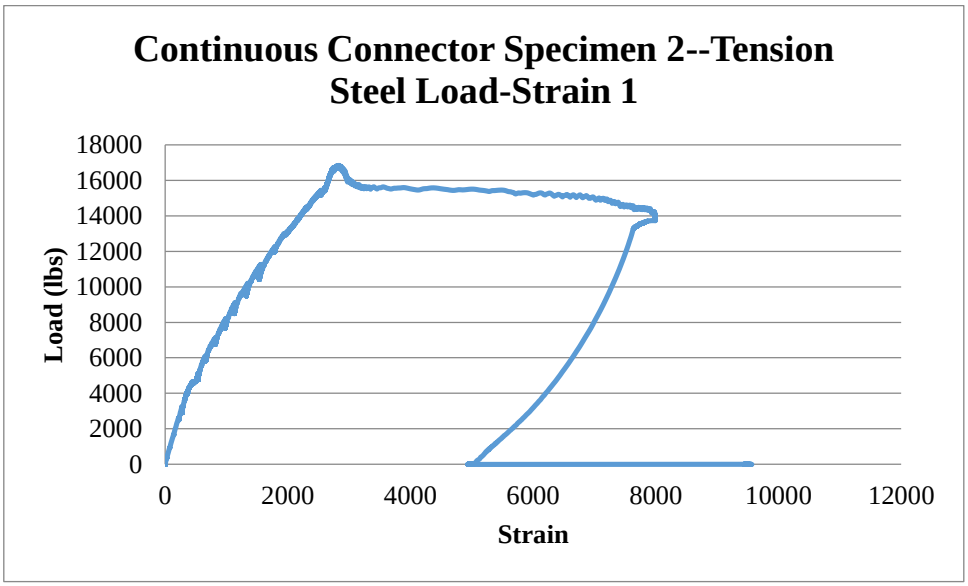


**Figure 169: Continuous Connector Specimen 2--Tension Steel Load-Strain 1**

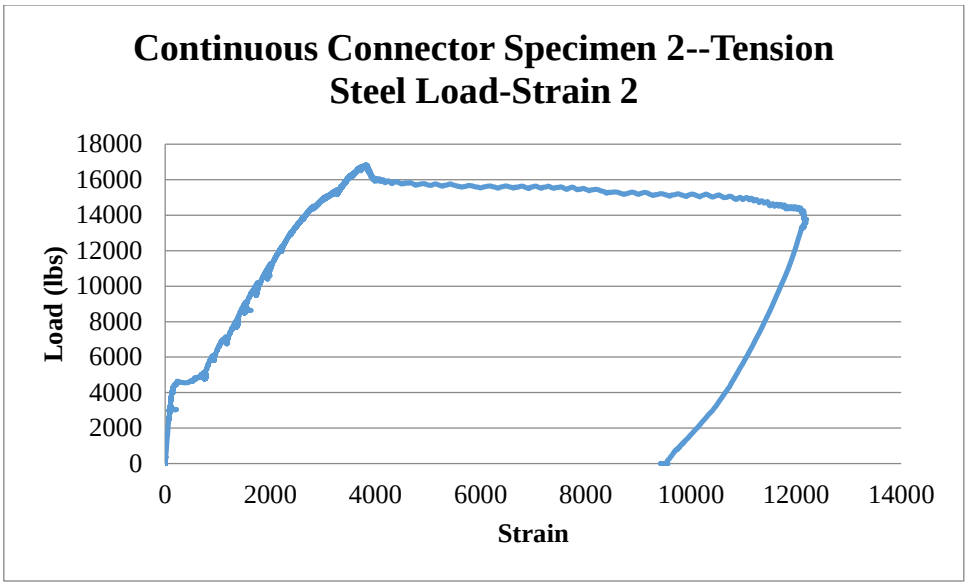


**Figure 170: Continuous Connector Specimen 2--Tension Steel Load-Strain 2**

## GROUP 4

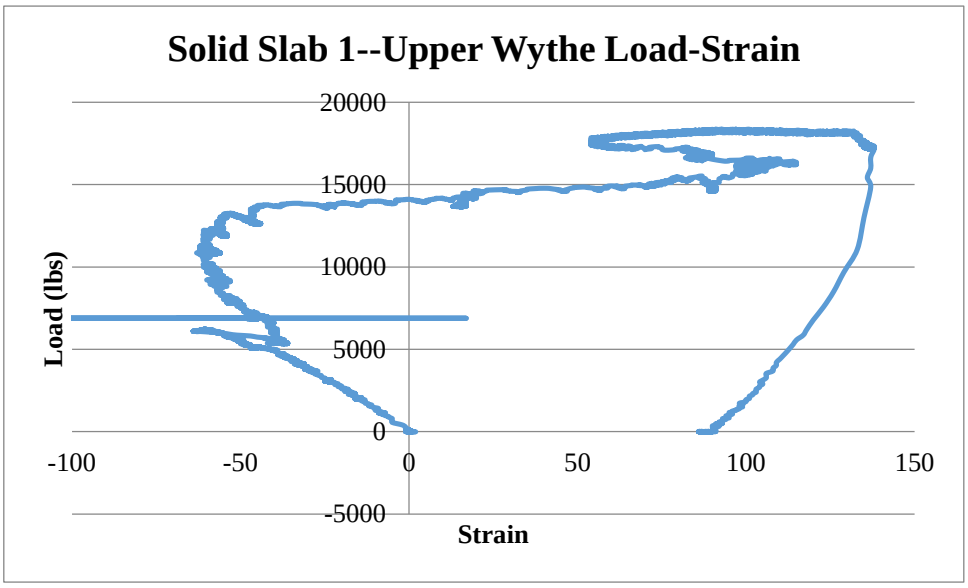


**Figure 171: Solid Slab 1--Upper Wythe Load-Strain**

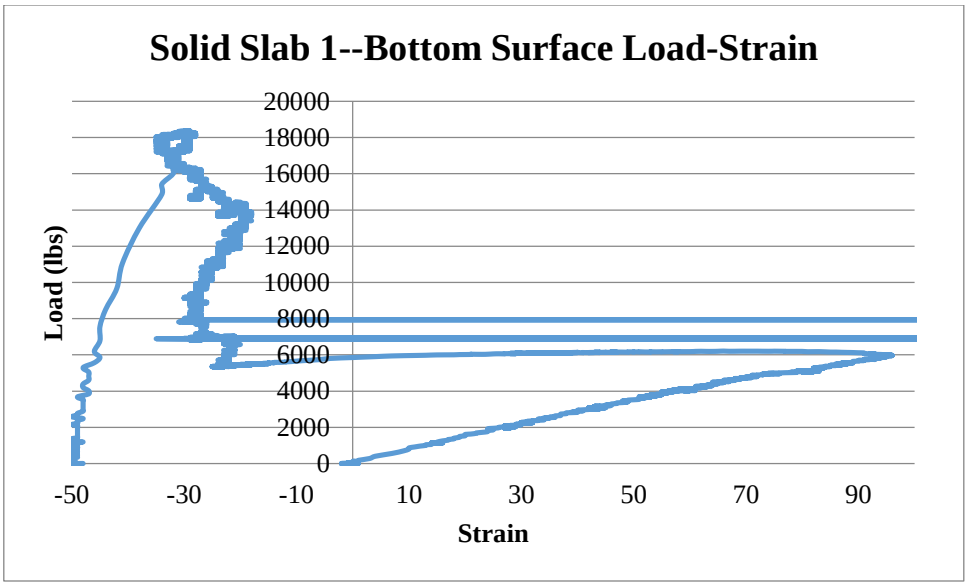


**Figure 172: Solid Slab 1--Bottom Surface Load-Strain**

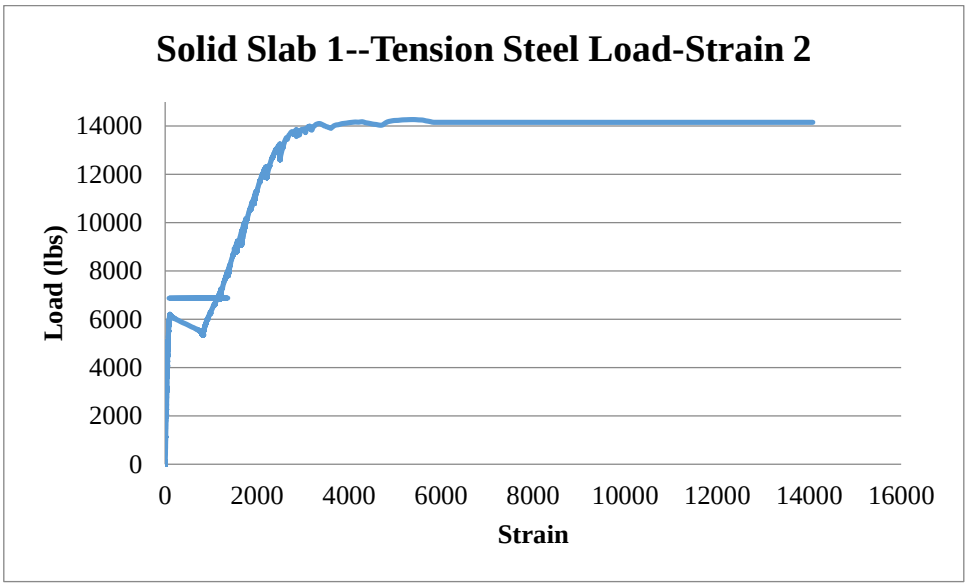


**Figure 173: Solid Slab 1--Tension Steel Load-Strain 2**

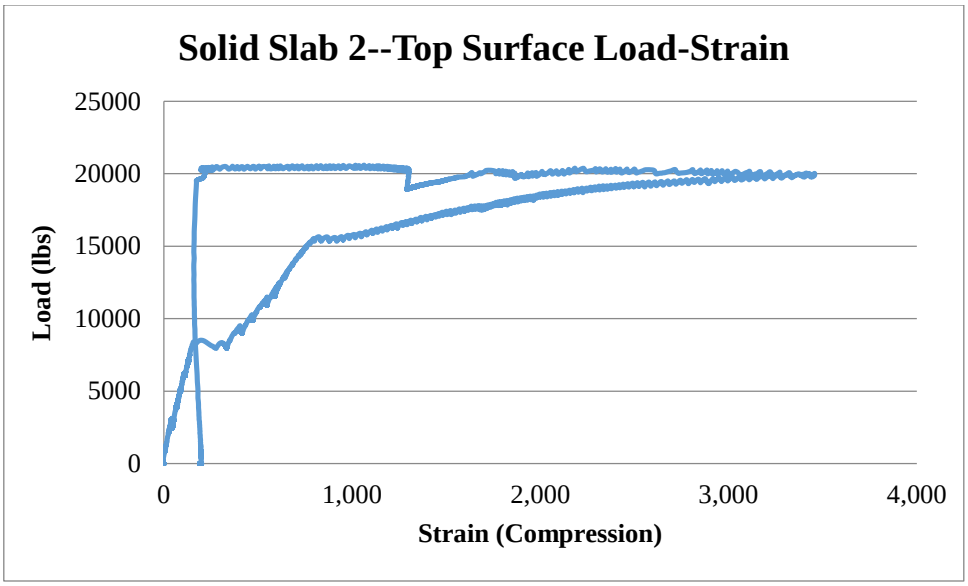


**Figure 174: Solid Slab 2--Top Surface Load-Strain**

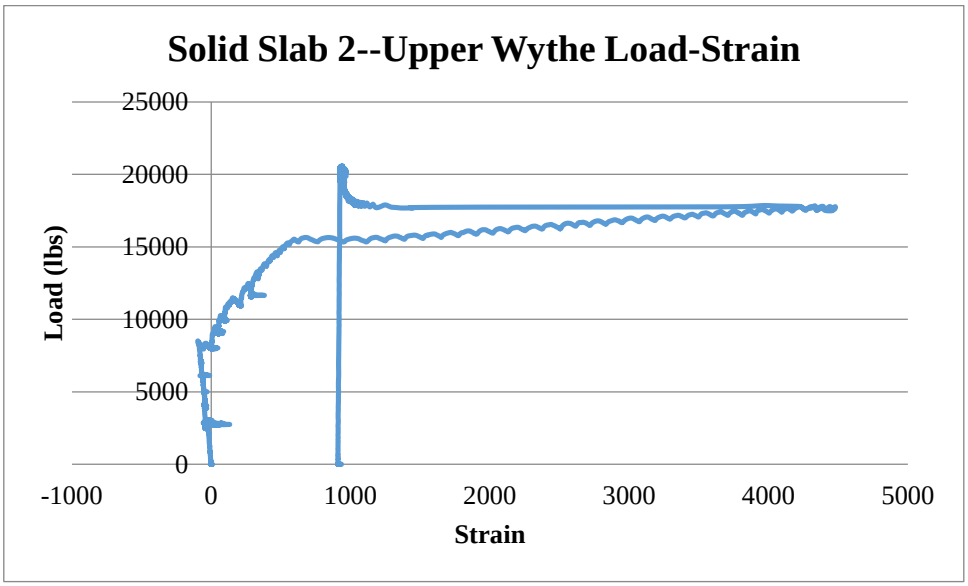


**Figure 175: Solid Slab 2--Upper Wythe Load-Strain**

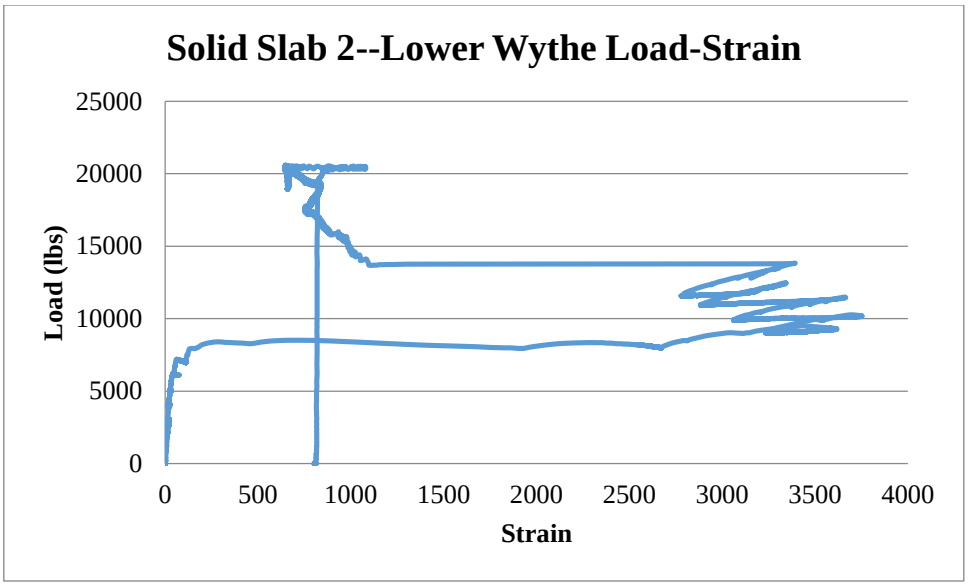


**Figure 176: Solid Slab 2--Lower Wythe Load-Strain**

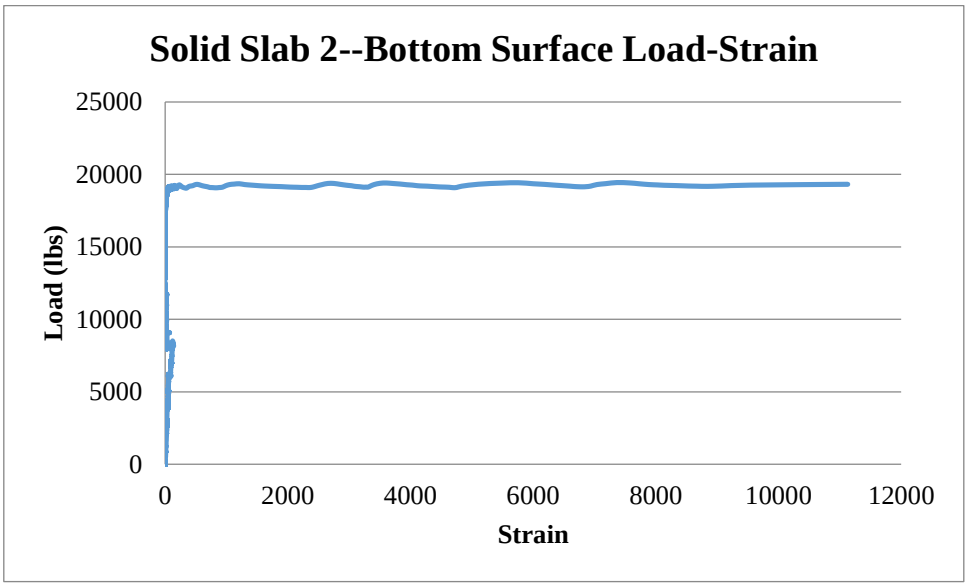


**Figure 177: Solid Slab 2--Bottom Surface Load-Strain**

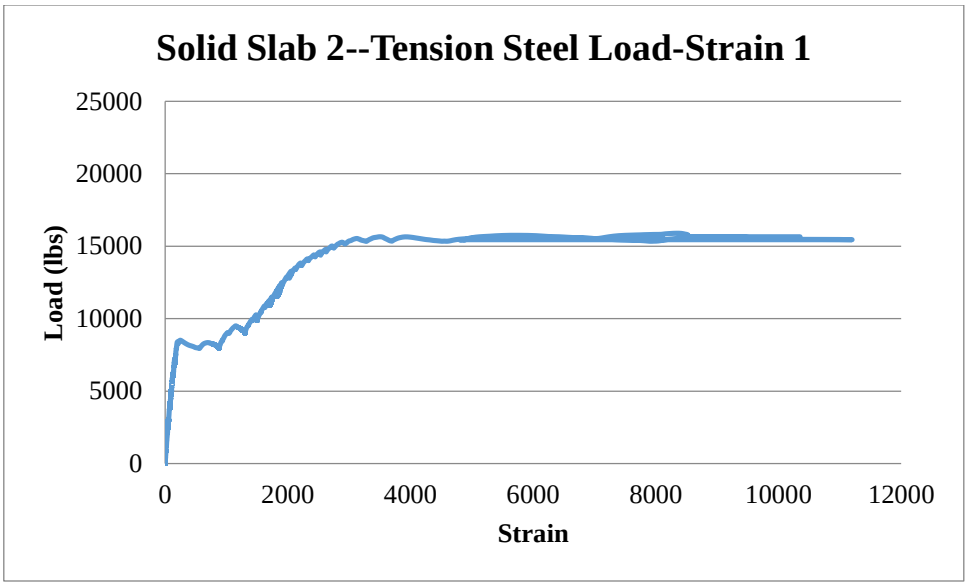


**Figure 178: Solid Slab 2--Tension Steel Load-Strain 1**

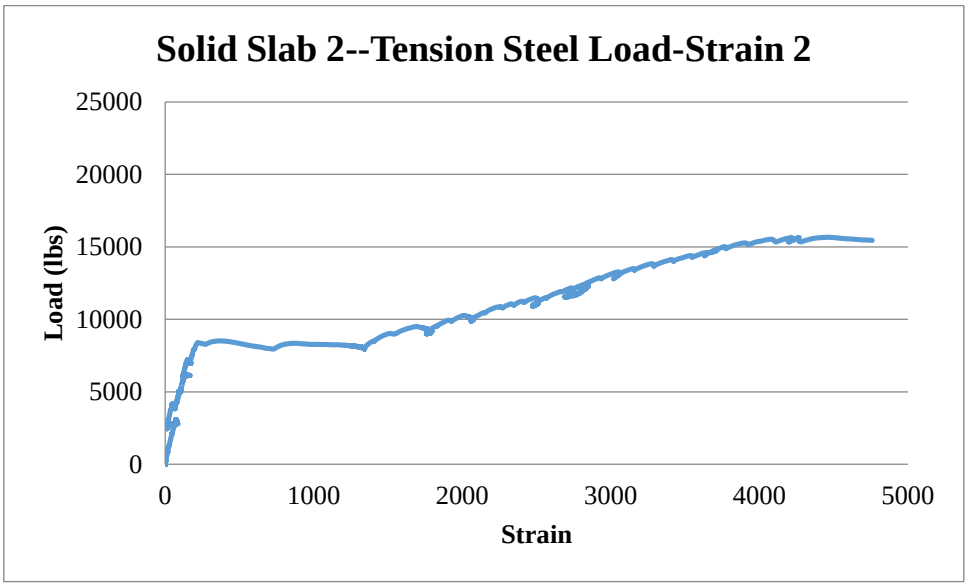


**Figure 179: Solid Slab 2--Tension Steel Load-Strain 2**

# DCA FORMULAS

## LOAD-DEFLECTION METHOD

Given: $b := 24in$ $h_1 := 3in$ $h_2 := 1in$ $h_{solid1} := 10in$ $h_{solid2} := 8in$

General Equation: $$DCA = \frac{\left(\frac{1}{E_c \cdot I_{nc}}\right) - \left(\frac{1}{E \cdot I_{exp}}\right)}{\left(\frac{1}{E \cdot I_{nc}}\right) - \left(\frac{1}{E \cdot I_{solid}}\right)} \cdot (100\%)$$

Where: $I_{nc}$ = moment of inertia of non-composite panels
$EI_{exp}$ = Calculated Experimental Values
$EI_{solid}$ = Calculated Solid Specimen Values = 100% Composite Action

Calculate Moment of Inertia of Fully Non-Composite Panel (10 inches):

$$I_{nc1} := 2 \cdot \left(\frac{b \cdot h_1^{\,3}}{12}\right) = 108 \cdot in^4$$

Calculate Moment of Inertia of Fully Non-Composite Panel (8 inches):

$$I_{nc1} := \left(\frac{b \cdot h_1^{\,3}}{12}\right) + \left(\frac{b \cdot h_2^{\,3}}{12}\right) = 56 \cdot in^4$$

Calculate Moment of Inertia of Fully Composite Panel (10 inches):

$$I_{solid} := \frac{b \cdot h_{solid1}^{\,3}}{12} = 2 \times 10^3 \cdot in^4$$

Calculate Moment of Inertia of Fully Composite Panel (8 inches):

$$I_{solid} := \frac{b \cdot h_{solid2}^{\,3}}{12} = 1.024 \times 10^3 \cdot in^4$$

Assuming Simply Supported Beam Theory:

$$\Delta = \frac{P \cdot L^3}{EI}$$

Because length (L) does not contribute to the modulus of elasticity or moment of inertia, assume it has at unit value.

$$\frac{P}{\Delta} = EI$$

In all cases, the load (P) was kept constant at 1400lbs, as this is within the linear-elastic range of all specimen. Additionally, due to the load being in the linear-elastic range, it can be assumed that the concrete has not cracked and therefore the modulus elasticity of the following equation can be applied as the compressive strength of concrete changes between tests.

$$E_c = 57000 \cdot \sqrt{f'_c}$$

Due to the only solid specimen (100% composite) tested occurred during the first test, the following correction was appied to the deflection where applicable, such that the DCA of each test would remain comparable.

$$\Delta_i = \left( \frac{E_{c0}}{E_{ci}} \right) \cdot \Delta_0$$

Where $\Delta_i$ is the adjusted experimental deflection; $\Delta_0$ is the original experimental deflection; $E_{c\,0}$ is the modulus of elasticity of concrete for the first test (only solid fully composite specimen); $E_{c\,i}$ is the modulus of elasticity of the specimen being analyzed.

Once this correction has been applied, the procedure as described above is followed.

# STRAIN DISTRIBUTION METHOD

Given: $\varepsilon = \frac{M \cdot y}{E \cdot I}$ $b := 24in$ $h := 3in$ $M_0$ = Applied Moment $x_{solid} := 0$

General Equation: $DCA = \frac{x_{nc} - x_{solid}}{x_{exp} - x_{solid}} \cdot (100\%)$

Where: $x_{nc}$ = Difference between strain distribution in non-composite specimen
$x_{exp}$ = Calculated Experimental Values
$x_{solid}$ = Calculated Solid Specimen Values = 100% Composite Action = 0 variance

Fully Non-Composite Specimen:

$M = \frac{M_0}{2}$ $y_1 := \frac{h}{2}$ $y_2 := h = 3 \cdot in$ $E = 57000 \cdot \sqrt{f'_c}$ $I := 2 \cdot \left( \frac{b \cdot h^3}{12} \right) = 108 \cdot in^4$

Find Slope of Fully Non-Composite Strain Distribution:

$\varepsilon_1 = \frac{M \cdot y_1}{E \cdot I}$ $\varepsilon_2 = \frac{M \cdot y_1}{E \cdot I}$ $Slope = \frac{(\varepsilon_1 - \varepsilon_2)}{(y_1 - y_2)}$

Assume this slope crosses the neutral axis at the center of each wythe, then extend the line formed by the equation through the entire specimen. The distance between the values at which each equation crosses an arbitrary datum is known as $x_{nc}$.

The difference between the experiment specimen is cacluated in the same fashion, except the slope produced by the experiment is used.

# APPENDIX 2

This appendix presents all corrections, material properties, calculations and additional graphs/figures pertaining to Chapter 4.

**LORD® 312 EPOXY ADHESIVE**

LORD TECHNICAL DATA

# LORD® 312 Epoxy Adhesive

## Description

LORD® 312 adhesive is a general purpose, low viscosity, two-component epoxy adhesive system used for applications, such as potting and thin film encapsulation, that require an adhesive with good flow characteristics. This adhesive system provides excellent adhesion to prepared metals, thermosets, wood, prepared rubber and other materials. LORD 312 adhesive can be either room temperature cured or heat cured for faster processing.

## Features and Benefits

***Durable*** – provides load bearing properties equal to or greater than the materials being bonded.

***Environmentally Friendly*** – contains no solvent, nonflammable and virtually odorless.

***Environmentally Resistant*** – resists moisture, sunlight and weathering.

***Temperature Resistant*** – performs at temperatures from -30 to +250°F (-34 to +121°C).

***Chemically Resistant*** – resists dilute acids, alkalis, solvents, greases and oils.

***Excellent Engineering Properties*** – provides low shrinkage, good creep properties, fully insulating and low water absorption.

## Application

***Surface Preparation*** – Remove soil, grease, oil, fingerprints, dust, mold release agents, rust and other contaminants from the surfaces to be bonded by solvent degreasing or alkaline cleaning.

On metal surfaces which are free of oxidation, use an isopropyl alcohol wipe. If necessary, use an abrasive material to remove tarnish. Always follow abrasion by a second cleaning to ensure removal of loose particles.

When bonding cured rubber, allow LORD 7701 adhesion enhancer/surface modifier to flash off before applying LORD 312 adhesive. Prime glass and ceramic surfaces with LORD AP-134 adhesion enhancer/surface modifier to promote adhesion.

Handle prepared surfaces carefully to avoid contamination. Assemble as soon as possible.

## Typical Properties*

| | 312-A Resin | 312-B Hardener |
|---|---|---|
| Appearance | Yellow Liquid | Yellow Liquid |
| Viscosity, cP @ 77°F (25°C)<br>Brookfield LVT<br>Spindle 2, 12 rpm | 650-1950 | 750-2500 |
| Density | | |
| lb/gal | 9.3-9.45 | 8.1-8.3 |
| (kg/m³) | (1114-1132) | (970-995) |
| Flash Point (Closed Cup), °F (°C) | >171 (>77) | >200 (>93) |

*Data is typical and not to be used for specification purposes.

LORD
Ask Us How™

# LORD TECHNICAL DATA

***Mixing*** – Thoroughly mix the proper amount of resin and hardener until uniform in color and consistency. Be careful not to whip excessive air into the adhesive system.

Heat buildup due to an exothermic reaction between the two components will shorten the working time of the adhesive. Mixing smaller quantities will minimize heat buildup. Do not use any adhesive that has begun to cure.

***Applying*** – Apply the mixed adhesive to bond surfaces using automatic meter/mix/dispense equipment or any convenient tool such as a stiff brush, spatula or trowel. For general use, a film thickness of approximately 0.02 inch (0.51 mm) is recommended. To control bond-line thickness, a small amount of solid glass beads can be added into the mixed adhesive.

Join the parts in such a way as to avoid entrapped air. Apply only enough pressure to ensure good wetting of the adhesive on both surfaces. Squeezing a little adhesive out at the edges is usually a sign of proper assembly. It is not necessary to clamp the assembly unless movement during adhesive cure is likely.

Maximum adhesion will occur only with parts which mate well without the need for excessive clamping pressure during cure. Excessive clamping may squeeze too much adhesive from the bond area which can result in a poor bond.

***Curing*** – LORD 312 adhesive will cure to full strength in 24-48 hours, provided that the adhesive, substrates and ambient temperature are 65°F (18°C) or higher.

Higher temperatures will provide faster cure times; however, the bondline temperature should not exceed 325°F (162°C). Elevated temperature cure produces the highest bond strengths and impact resistance. Firm recommendations of cure times and temperatures depend on material composition and heating methods.

Once the adhesive has cured, it can be filed, sanded, machined or otherwise handled in the same way as a light metal. Paint, lacquers, enamels and other coatings can be applied to cured adhesive.

## Typical Properties* of Resin Mixed with Hardener

| | |
|---|---|
| Mix Ratio, Resin to Hardener | |
| General Purpose, -30 to 250°F (-34 to 121°C) | |
| Mixed Stress Joint Design | |
| by Volume | 1.75:1 |
| by Weight | 2:1 |
| High Temperature, 50-250°F (10-121°C) | |
| Shear Stress Joint Design | |
| by Volume | 1.9:1 |
| by Weight | 2.2:1 |
| Low Temperature, -40 to 100°F (-40 to 38°C) | |
| Peel Stress Joint Design | |
| by Volume | 1.6:1 |
| by Weight | 1.8:1 |
| Solids Content, % | 100 |
| Working Time, hr @ 75°F (24°C) | 1.5-2.5 |
| 54 g mass | |
| Time to Handling Strength, hr | 8-16 |
| Mixed Appearance | Yellow Liquid |
| Cured Appearance | Straw to Honey-colored |

*Data is typical and not to be used for specification purposes.

# LORD TECHNICAL DATA

## Typical Cured Properties

| | |
|---|---|
| Tensile Strength at Break, psi (MPa)<br>ASTM D882-83A, modified | 1460 (10) |
| Elongation, %<br>ASTM D882-83A, modified | 56 |
| Young's Modulus, psi (MPa)<br>ASTM D882-83A, modified | 33,814 (233) |
| Glass Transition Temperature, °F (°C)<br>ASTM E1640-99, by DMA | 122 (50) |

## Bond Performance

| Subtrates | Cold Rolled Steel to Cold Rolled Steel<br>Lap Shear<br>psi (MPa) | Aluminum to Aluminum<br>Lap Shear<br>psi (MPa) | SMC to SMC<br>Lap Shear<br>psi (MPa) | Natural Rubber to Cold Rolled Steel<br>45° Peel<br>pli (N/mm) | SBR to SBR<br>T-Peel<br>pli (N/mm) |
|---|---|---|---|---|---|
| Test @ Room Temperature | 2080 (14.3) | 1860 (12.8) | 940 (6.5) | 43 (7.5) | 127 (22.2) |
| Failure Mode | A | A | 100FT | 62R/A | SB |
| Test @ Hot Strength, 180°F (82°C) | 340 (2.3) | 330 (2.3) | 160 (1.1) | — | — |
| Failure Mode | 10C/A | A | 10C/A | | |
| Test after 7 days in $H_2O$ @ 130°F (54°C)<br>Test after 24 hours | 2980 (20.5) | 2540 (17.5) | 690 (4.7) | 25 (4.4) | 70 (12.3) |
| Failure Mode | A | A | FT | A | 50R/C |
| Test after 14 days Salt Spray Exposure<br>Test Immediately | 2920 (20.1) | 2440 (16.8) | 840 (5.8) | 13 (2.3) | 122 (21.4) |
| Failure Mode | A | A | FT | A | SB |
| Test after 14 days @ 100°F (38°C), 100% RH<br>Test Immediately | 2510 (17.3) | 1690 (11.6) | 670 (4.6) | 34 (5.9) | 94 (16.5) |
| Failure Mode | A | A | 66FT/A | 34R/A | 16SB/42R/C |
| Test @ -30°F (-34°C) | 2440 (16.8) | 1310 (9.0) | 590 (4.0) | 66 (11.6) | 109 (19.1) |
| Failure Mode | A | A | FT | 90R/A | R |

| Substrate | Surface Treatment |
|---|---|
| Cold Rolled Steel and Alumimum | MEK Wipe, Grit Blast, MEK Wipe |
| Sheet Molded Compound (SMC) | 320-grit Sandpaper, Dry Rag Wipe |
| Styrene Butadiene Rubber (SBR) | Primed with LORD 7701 Surface Treatment |
| Natural Rubber | Primed with LORD 7701 Surface Treatment |

| Bonded Parameters | Bond Area | Film Thickness | Cure | Mix Ratio |
|---|---|---|---|---|
| Metal Lap Shears | 1.0"x0.5" | 0.010" | 72 hr @ RT | 1:1 by Weight |
| SMC Lap Shears | 1.0"x1.0" | 0.030" | 72 hr @ RT | 1:1 by Weight |
| T-Peels | 1.0"x3.0" | 0.020" | 72 hr @ RT | 1:1 by Weight |
| 45° Peels | 1.0"x1.0" | 0.020" | 72 hr @ RT | 1:1 by Weight |

| Failure Mode Definition | Abbreviation |
|---|---|
| Adhesive Failure | A |
| Cohesive Failure | C |
| Fiber Tear | FT |
| Rubber Failure | R |
| Stock Break | SB |

***Cleanup*** – Clean excess adhesive on the bonded assembly, as well as the equipment, prior to the adhesive cure with hot water and detergent or an organic solvent such as ketones. Once adhesive has cured, heat the adhesive to 400°F (204°C) or above to soften the cured adhesive. This allows the parts to be separated and the adhesive to be more easily removed. Some success may be achieved with commercial epoxy strippers.

## Shelf Life/Storage

Shelf life is two years from date of manufacture when stored at 40-80°F (4-27°C) in original, unopened container.

## Cautionary Information

Before using this or any LORD product, refer to the Material Safety Data Sheet (MSDS) and label for safe use and handling instructions.

*For industrial/commercial use only.* Must be applied by trained personnel only. Not to be used in household applications. Not for consumer use.



---

LORD provides valuable expertise in adhesives and coatings, vibration and motion control, and magnetically responsive technologies. Our people work in collaboration with our customers to help them increase the value of their products. Innovative and responsive in an ever-changing marketplace, we are focused on providing solutions for our customers worldwide ... Ask Us How.

**LORD Corporation**
**World Headquarters**
111 Lord Drive
Cary, NC 27511-7923
USA
**Customer Support Center** (In United States & Canada)
+1 877 ASK LORD (275 5673)
www.lord.com
For a listing of our worldwide locations, visit LORD.com/locations.



LORD Ask Us How™

# M-COAT J

## M-Coat J

Micro-Measurements

VISHAY PRECISION GROUP

## Protective Coating

### FEATURES

- Excellent resistance to moisture
- Good resistance to chemicals
- Good protection against mechanical damage
- Room-temperature cure

RoHS COMPLIANT

### DESCRIPTION

Two-part polysulfide liquid polymer compound. Can be applied in coating thickness of 1/8 in [3 mm] without flowing on vertical surfaces. Tough, flexible coating. No weighing required. Uncured coating can be removed with GSM Degreaser, Rosin Solvent, or MEK.

General-purpose coating. Good protection against oil, grease, most acids and alkalies, and most solvents. Strong solvents may cause swelling and softening with time. Concentrated acids eventually break down coating. Good salt-water immersion coating.

### CHARACTERISTICS

**Cure Requirements:**
Mixed pot life 30 minutes at +75°F [+24°C].

Normal cure in 24 hours at +75°F [+24°C].

To accelerate cure and improve properties, cure 2 hours at +130°F [+55°C].

**Operating Temperature Range:**
*Short Term:* –50° to +250°F [–45° to +120°C].
*Long Term:* –50° to +200°F [–45° to +95°C].

**Shelf Life:**
Minimum 5 months at +75°F [+24°C].

### PACKAGING OPTIONS

**M-Coat J-1:**
- 1 mixing dispenser [2 fl oz (59ml)]
- 1 piece M-Coat FT Teflon® Tape
  1 x 20 x 0.003in [25 x 500 x 0.08mm]

**M-Coat J-3:**
- 3 mixing dispensers [2 fl oz (59ml) ea]
- 3 pieces M-Coat FT Teflon® Tape
  1 x 20 x 0.003in [25 x 500 x 0.08mm]

Teflon is a Registered Trademark of DuPont.

VISHAY PRECISION GROUP

# Legal Disclaimer Notice

Vishay Precision Group

## Disclaimer

ALL PRODUCTS, PRODUCT SPECIFICATIONS AND DATA ARE SUBJECT TO CHANGE WITHOUT NOTICE.

Vishay Precision Group, Inc., its affiliates, agents, and employees, and all persons acting on its or their behalf (collectively, "Vishay Precision Group"), disclaim any and all liability for any errors, inaccuracies or incompleteness contained herein or in any other disclosure relating to any product.

The product specifications do not expand or otherwise modify Vishay Precision Group's terms and conditions of purchase, including but not limited to, the warranty expressed therein.

Vishay Precision Group makes no warranty, representation or guarantee other than as set forth in the terms and conditions of purchase. **To the maximum extent permitted by applicable law, Vishay Precision Group disclaims (i) any and all liability arising out of the application or use of any product, (ii) any and all liability, including without limitation special, consequential or incidental damages, and (iii) any and all implied warranties, including warranties of fitness for particular purpose, non-infringement and merchantability.**

Information provided in datasheets and/or specifications may vary from actual results in different applications and performance may vary over time. Statements regarding the suitability of products for certain types of applications are based on Vishay Precision Group's knowledge of typical requirements that are often placed on Vishay Precision Group products. It is the customer's responsibility to validate that a particular product with the properties described in the product specification is suitable for use in a particular application.

No license, express, implied, or otherwise, to any intellectual property rights is granted by this document, or by any conduct of Vishay Precision Group.

The products shown herein are not designed for use in life-saving or life-sustaining applications unless otherwise expressly indicated. Customers using or selling Vishay Precision Group products not expressly indicated for use in such applications do so entirely at their own risk and agree to fully indemnify Vishay Precision Group for any damages arising or resulting from such use or sale. Please contact authorized Vishay Precision Group personnel to obtain written terms and conditions regarding products designed for such applications.

Product names and markings noted herein may be trademarks of their respective owners.

# 404 ISOPHTHALIC RESIN

**Technical Description**

Polylite polyester resin 404 is a rigid, medium reactivity, premium chemical resistant, isophthalic based polyester. The resin is low viscosity, thixotropic and pre-promoted for room temperature cure with the addition of methyl ethyl ketone peroxide or benzoyl peroxide.

**Distinctive Properties**

Excellent Chemical Resistance
Low Water Absorption
High Heat Distortion Temp.
Stable Gel Time
Excellent Laminate Physicals
Versatility
SPC/SQC Controlled

**Product Specs**

Flash Point: 89F
Shelf Life, Minimum: 3 Months
Specific Gravity: 1.05-1.15
Weight per Gallon: 8.74-9.57lbs
% Styrene Monomer: 46-50
Viscosity, Brookfield LVF: 325-525cps
Thixotropic Index, Minimum: 1.5
Gel Time @ 1.25%: 20-24minutes
Color, Liquid: Purple Opaque

**Physical Properties**

Barcol Hardness: 38
Heat Distortion Temp: 106C

Specific Gravity: 1.19

Tensile Strength: 7,300

Tensile Modulus: 5.34

Tensile Elongation: 1.5

Flexural Strength: 15,250

Flexural Modulus: 6.27

Compressive Strength: 12,700

Water Absorption, 24hr Room Temp: .19%

Water Absorption, 2Hr Boiling: .51%

**Cure Conditions**

Clear casting with 1.25% MEK Peroxide, overnight room temperature cure, two hour post cure @250F

**LORD® 305 EPOXY ADHESIVE**

LORD TECHNICAL DATA

# LORD® 305 Epoxy Adhesive

## Description

LORD® 305 adhesive is a general purpose, medium viscosity, two-component epoxy adhesive system used for applications that require strong, durable, chemically and environmentally resistant bonds. This adhesive system provides excellent adhesion to prepared metals, fiberglass reinforced plastics (FRP), phenolic, wood, prepared rubber and other materials. It is also used to bond cured rubber to itself and rubber to metal, including gaskets, bushings, shock-absorbing devices and rubber rolls. LORD 305 adhesive can be either room temperature cured or heat cured for faster processing.

## Features and Benefits

***Durable*** – provides load bearing properties equal to or greater than the materials being bonded.

***Environmentally Friendly*** – contains no solvent, nonflammable and virtually odorless.

***Environmentally Resistant*** – resists moisture, sunlight and weathering.

***Temperature Resistant*** – performs at temperatures from -30 to +250°F (-34 to +121°C).

***Chemically Resistant*** – resists dilute acids, alkalis, solvents, greases and oils.

***Excellent Engineering Properties*** – provides low shrinkage, good creep properties and low water absorption.

## Application

***Surface Preparation*** – Remove soil, grease, oil, fingerprints, dust, mold release agents, rust and other contaminants from the surfaces to be bonded by solvent degreasing or alkaline cleaning.

On metal surfaces which are free of oxidation, use an isopropyl alcohol wipe. If necessary, use an abrasive material to remove tarnish. Always follow abrasion by a second cleaning to ensure removal of loose particles.

When bonding cured rubber, allow LORD 7701 adhesion enhancer/surface modifier to flash off before applying LORD 305 adhesive. Prime glass and ceramic surfaces with LORD AP-134 adhesion enhancer/surface modifier to promote adhesion.

Handle prepared surfaces carefully to avoid contamination. Assemble as soon as possible.

## Typical Properties*

| | 305-1 Resin | 305-2 Hardener |
|---|---|---|
| Appearance | Clear Amber Liquid | Blue Heavy Liquid |
| Viscosity, cP @ 77°F (25°C)<br>Brookfield HBF<br>Spindle 2, 10 rpm | 10,000-18,000 | 20,000-45,000 |
| Density | | |
| lb/gal | 9.4-10.0 | 7.75-8.35 |
| (kg/m³) | (1126-1198) | (928-1001) |
| Flash Point (Closed Cup), °F (°C) | >200 (>93) | >200 (>93) |

*Data is typical and not to be used for specification purposes.

LORD
Ask Us How™

# LORD TECHNICAL DATA

***Mixing*** – Thoroughly mix the proper amount of resin and hardener until uniform in color and consistency. Be careful not to whip excessive air into the adhesive system. Handheld cartridges will automatically dispense the correct volumetric ratio of each component.

Heat buildup due to an exothermic reaction between the two components will shorten the working time of the adhesive. Mixing smaller quantities will minimize heat buildup. Do not use any adhesive that has begun to cure.

***Applying*** – Apply the mixed adhesive to bond surfaces using automatic meter/mix/dispense equipment, hand-held cartridges or any convenient tool such as a stiff brush, spatula or trowel. For general use, a film thickness of approximately 0.02 inch (0.51 mm) is recommended. To control bondline thickness, a small amount of solid glass beads can be added into the mixed adhesive.

Join the parts in such a way as to avoid entrapped air. Apply only enough pressure to ensure good wetting of the adhesive on both surfaces. Squeezing a little adhesive out at the edges is usually a sign of proper assembly. It is not necessary to clamp the assembly unless movement during adhesive cure is likely.

Maximum adhesion will occur only with parts which mate well without the need for excessive clamping pressure during cure. Excessive clamping may squeeze too much adhesive from the bond area which can result in a poor bond.

***Curing*** – LORD 305 adhesive will cure to full strength in 24-48 hours, provided that the adhesive, substrates and ambient temperature are 65°F (18°C) or higher.

Higher temperatures will provide faster cure times; however, the bondline temperature should not exceed 325°F (162°C). Elevated temperature cure produces the highest bond strengths and impact resistance. Firm recommendations of cure times and temperatures depend on material composition and heating methods.

Once the adhesive has cured, it can be filed, sanded, machined or otherwise handled in the same way as a light metal. Paint, lacquers, enamels and other coatings can be applied to cured adhesive.

## Typical Properties* of Resin Mixed with Hardener

| | |
|---|---|
| Mix Ratio, Resin to Hardener | |
| General Purpose, -30 to 250°F (-34 to 121°C) | |
| Mixed Stress Joint Design | |
| by Volume | 1:1 |
| by Weight | 1.2:1 |
| High Temperature, 50-250°F (10-121°C) | |
| Shear Stress Joint Design | |
| by Volume | 2:1 |
| by Weight | 2.4:1 |
| Low Temperature, -40 to 100°F (-40 to 38°C) | |
| Peel Stress Joint Design | |
| by Volume | 1:2 |
| by Weight | 1:1.7 |
| Solids Content, % | 100 |
| Working Time, hr @ 75°F (24°C) | 1-2 |
| 54 g mass | |
| Time to Handling Strength, hr | 8-16 |
| Mixed Appearance | Blue Liquid |
| Cured Appearance | Translucent Blue |

*Data is typical and not to be used for specification purposes.

# LORD TECHNICAL DATA

## Typical Cured Properties

| | |
|---|---|
| Tensile Strength at Break, psi (MPa)<br>ASTM D882-83A, modified | 2490 (17.2) |
| Elongation, %<br>ASTM D882-83A, modified | 31 |
| Young's Modulus, psi (MPa)<br>ASTM D882-83A, modified | 108,500 (748) |
| Glass Transition Temperature, °F (°C)<br>ASTM E1640-99, by DMA | 141 (61) |

## Bond Performance

| Subtrates | Cold Rolled Steel to Cold Rolled Steel<br>Lap Shear<br>psi (MPa) | Aluminum to Aluminum<br>Lap Shear<br>psi (MPa) | SMC to SMC<br>Lap Shear<br>psi (MPa) | Natural Rubber to Cold Rolled Steel<br>45° Peel<br>pli (N/mm) | SBR to SBR<br>T-Peel<br>pli (N/mm) |
|---|---|---|---|---|---|
| Test @ Room Temperature | 2240 (15.4) | 1890 (13.0) | 820 (5.6) | 37 (6.5) | 84 (14.7) |
| Failure Mode | A | 36C/A | FT | 58R/A | R |
| Test @ Hot Strength, 180°F (82°C) | 1100 (7.6) | 1040 (7.2) | 490 (3.4) | 24 (4.2) | — |
| Failure Mode | A | A | 13FT/A | 44R/A | |
| Test after 7 days in $H_2O$ @ 130°F (54°C)<br>Test after 24 hours | 2630 (18.1) | 1840 (12.7) | 600 (4.1) | 33 (5.8) | 83 (14.5) |
| Failure Mode | A | A | FT | 13R/A | SB |
| Test after 14 days Salt Spray Exposure<br>Test Immediately | 2500 (17.2) | 1790 (12.3) | 610 (4.2) | — | 110 (19.3) |
| Failure Mode | A | A | 100FT | | 83R/SB |
| Test after 14 days @ 100°F (38°C), 100% RH<br>Test Immediately | 2740 (18.9) | 2010 (13.8) | 660 (4.5) | 41 (7.2) | 94 (16.5) |
| Failure Mode | A | A | FT | 50R/A | 83R/SB |
| Test @ -30°F (-34°C) | 2490 (17.1) | 1600 (11.0) | 720 (5.0) | 60 (10.5) | 78 (13.6) |
| Failure Mode | A | A | FT | 85R/A | R |

| Substrate | Surface Treatment |
|---|---|
| Cold Rolled Steel and Alumimum | MEK Wipe, Grit Blast, MEK Wipe |
| Sheet Molded Compound (SMC) | 320-grit Sandpaper, Dry Rag Wipe |
| Styrene Butadiene Rubber (SBR) | Primed with LORD 7701 Surface Treatment |
| Natural Rubber | Primed with LORD 7701 Surface Treatment |

| Bonded Parameters | Bond Area | Film Thickness | Cure | Mix Ratio |
|---|---|---|---|---|
| Metal Lap Shears | 1.0"x0.5" | 0.010" | 72 hr @ RT | 1:1 by Weight |
| SMC Lap Shears | 1.0"x1.0" | 0.030" | 72 hr @ RT | 1:1 by Weight |
| T-Peels | 1.0"x3.0" | 0.020" | 72 hr @ RT | 1:1 by Weight |
| 45° Peels | 1.0"x1.0" | 0.020" | 72 hr @ RT | 1:1 by Weight |

| Failure Mode Definition | Abbreviation |
|---|---|
| Adhesive Failure | A |
| Cohesive Failure | C |
| Fiber Tear | FT |
| Rubber Failure | R |
| Stock Break | SB |

# LORD TECHNICAL DATA

***Cleanup*** – Clean excess adhesive on the bonded assembly, as well as the equipment, prior to the adhesive cure with hot water and detergent or an organic solvent such as ketones. Once adhesive has cured, heat the adhesive to 400°F (204°C) or above to soften the cured adhesive. This allows the parts to be separated and the adhesive to be more easily removed. Some success may be achieved with commercial epoxy strippers.

## Shelf Life/Storage

Shelf life is two years from date of manufacture when stored at 40-80°F (4-27°C) in original, unopened container.

## Cautionary Information

Before using this or any LORD product, refer to the Material Safety Data Sheet (MSDS) and label for safe use and handling instructions.

*For industrial/commercial use only.* Must be applied by trained personnel only. Not to be used in household applications. Not for consumer use.



---

LORD provides valuable expertise in adhesives and coatings, vibration and motion control, and magnetically responsive technologies. Our people work in collaboration with our customers to help them increase the value of their products. Innovative and responsive in an ever-changing marketplace, we are focused on providing solutions for our customers worldwide ... Ask Us How.

**LORD Corporation**
**World Headquarters**
111 Lord Drive
Cary, NC 27511-7923
USA

**Customer Support Center** (In United States & Canada)
+1 877 ASK LORD (275 5673)

www.lord.com

For a listing of our worldwide locations, visit LORD.com/locations.



LORD
Ask Us How™

## DEFLECTION ACROSS SPECIMEN LENGTH

## CHAPTER 4 (TOP FRP PLATE)—SEGMENTAL

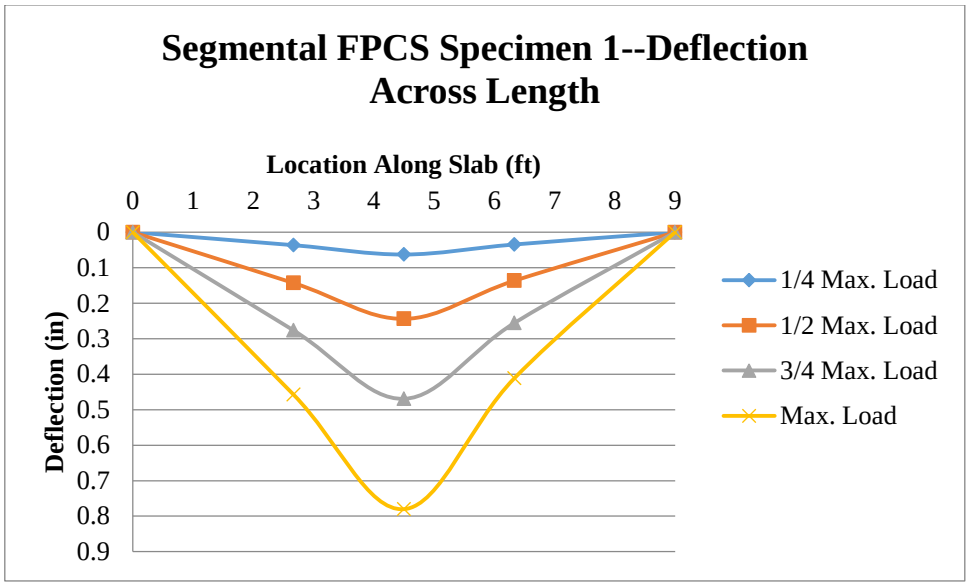


**Figure 180: Segmental FPCS Specimen 1—Deflection Across Sample Length**

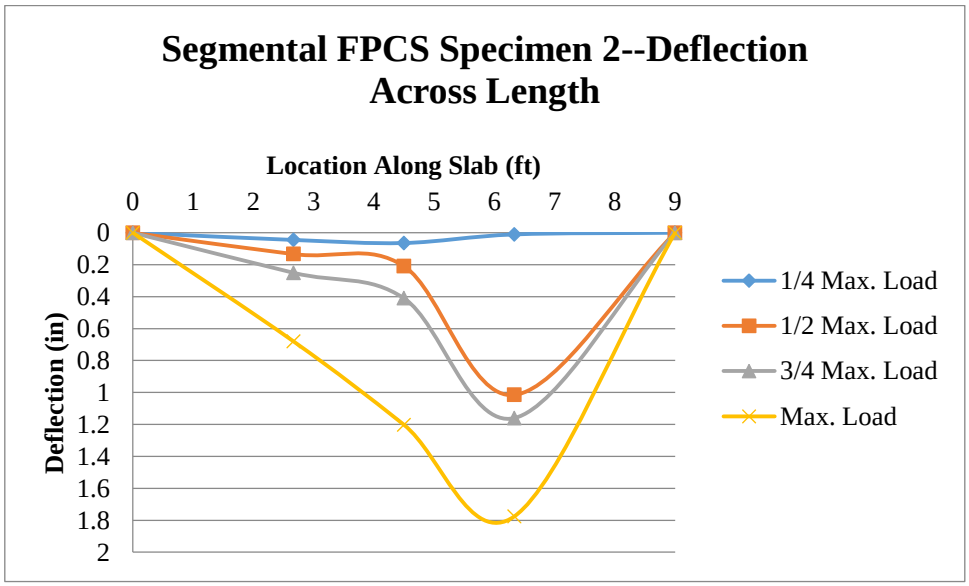


**Figure 181: Segmental FPCS Specimen 2—Deflection Across Sample Length**

# CHAPTER 4 (TOP FRP PLATE)—CONTINUOUS

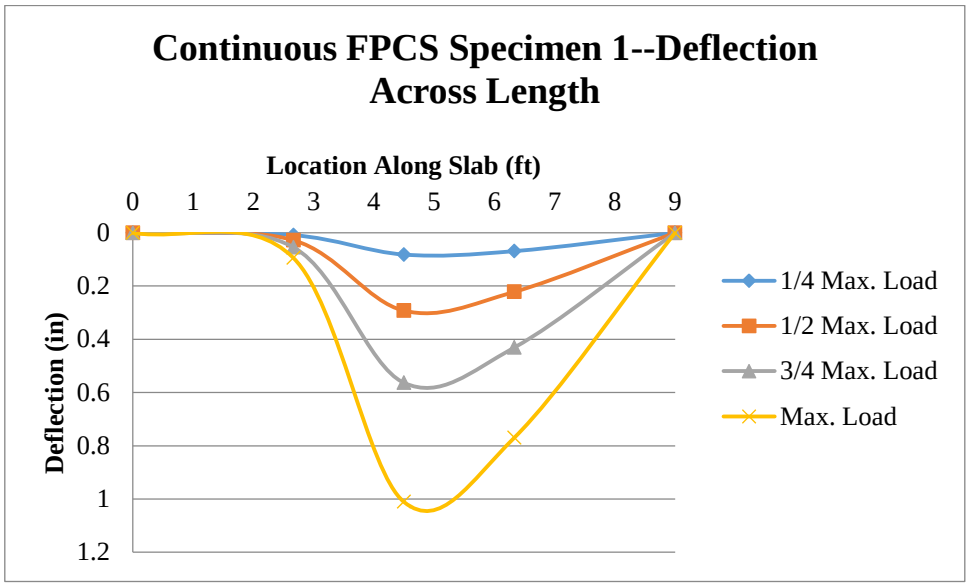


**Figure 182: Continuous FPCS Specimen 1—Deflection Across Sample Length**

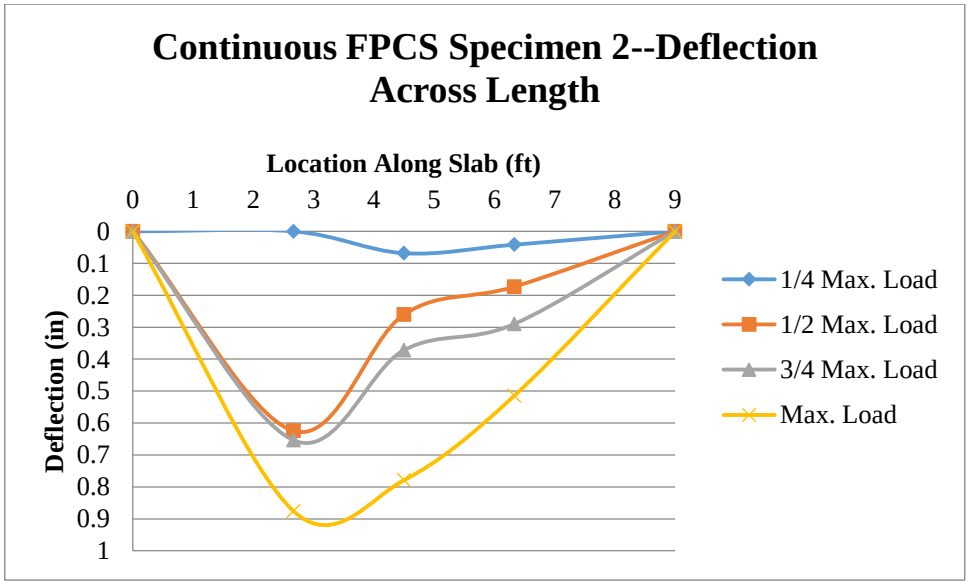


**Figure 183: Continuous FPCS Specimen 2—Deflection Across Sample Length**

# CHAPTER 4 (TOP & SIDE FRP PLATES)—8” FPCS

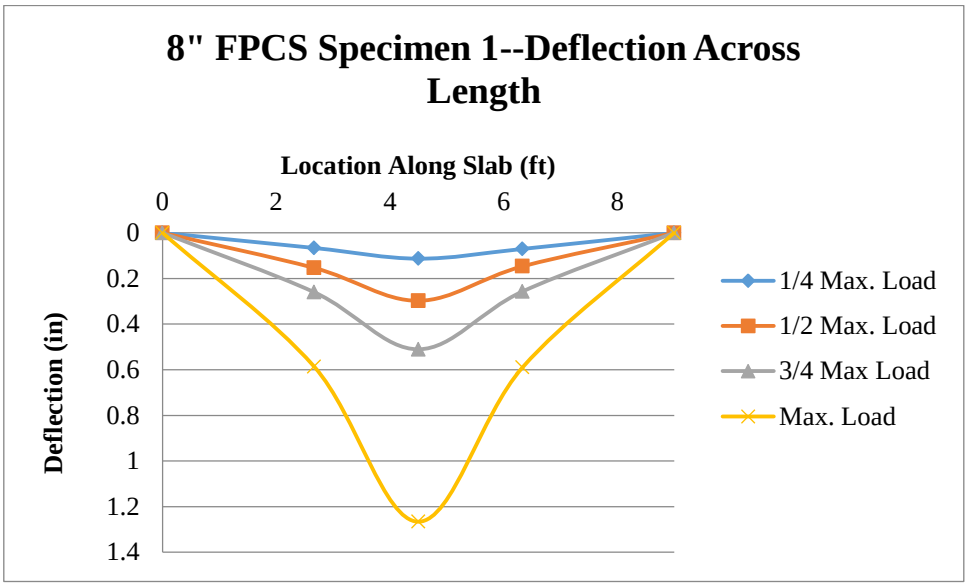


**Figure 184: 8" FPCS Specimen 1—Deflection Across Sample Length**

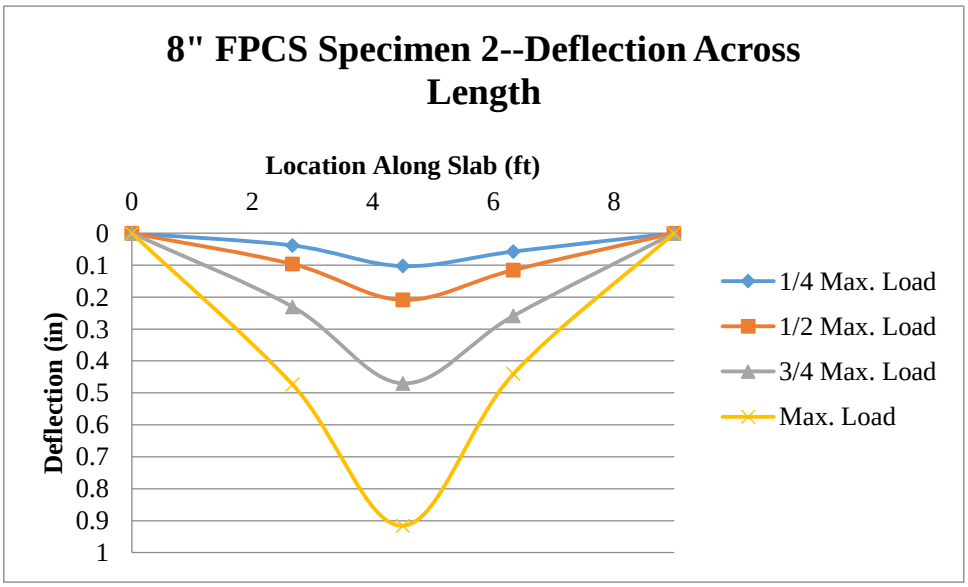


**Figure 185: 8" FPCS Specimen 2—Deflection Across Length**

# CHAPTER 4 (TOP & SIDE FRP PLATES)—10” FPCS

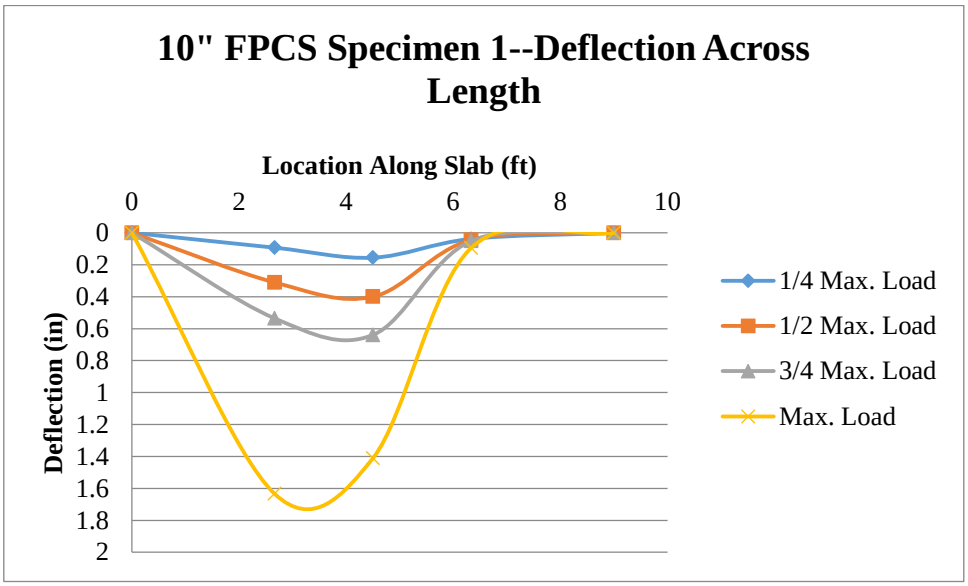


**Figure 186: 10” FPCS Specimen 1—Deflection Across Length**

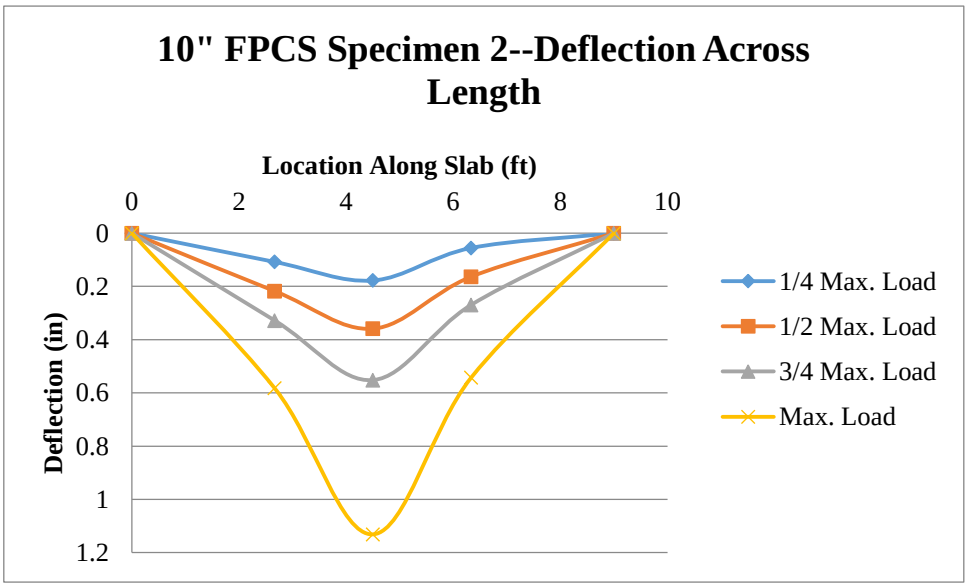


**Figure 187: 10” FPCS Specimen 2—Deflection Across Length**

# ADDITIONAL STRAIN DATA

## CHAPTER 4 (TOP FRP PLATE)—SEGMENTAL

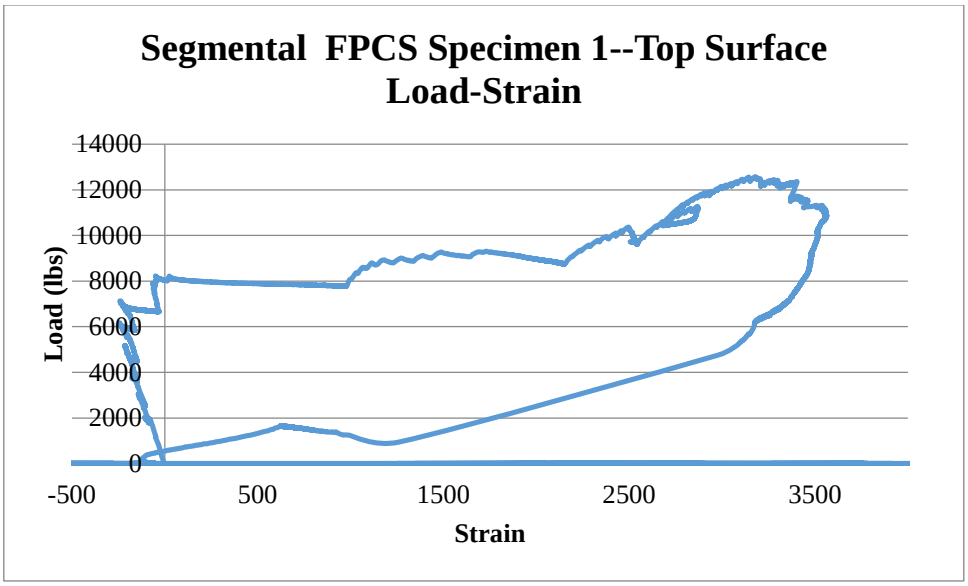


**Figure 188: Segmental FPCS Specimen 1—Top Surface Load-Strain**

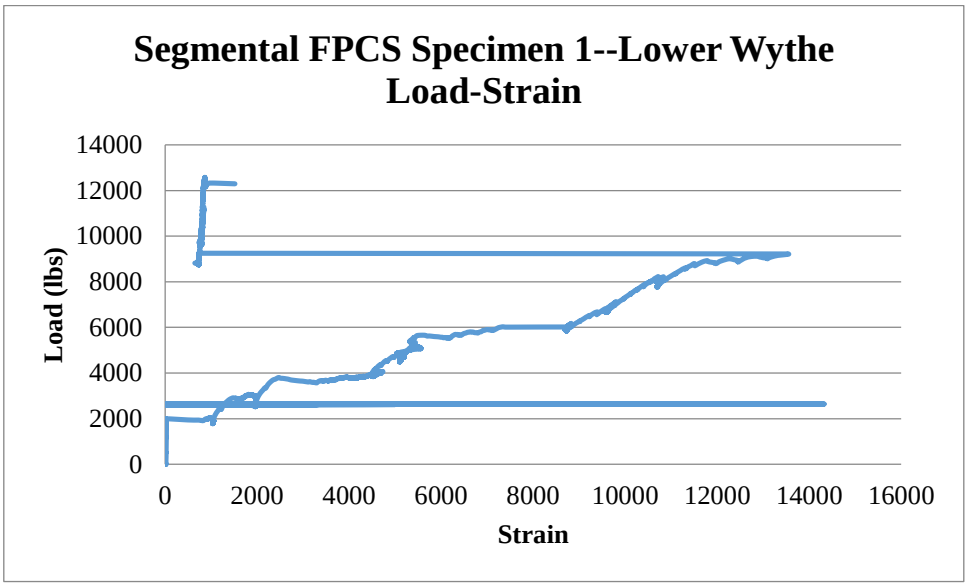


**Figure 189: Segmental FPCS Specimen 1—Lower Wythe Load-Strain**

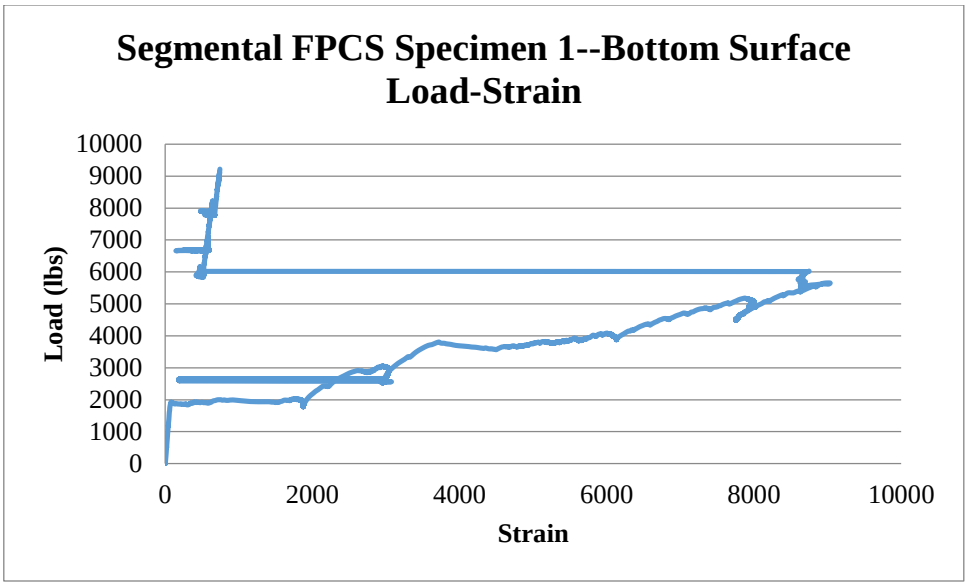


**Figure 190: Segmental FPCS Specimen 1—Bottom Surface Load-Strain**

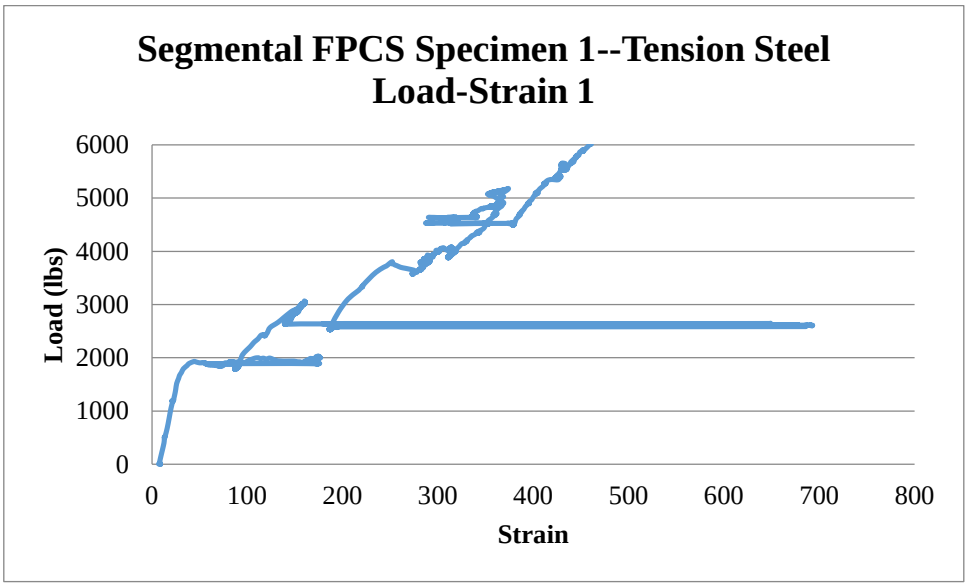


**Figure 191: Segmental FPCS Specimen 1—Tension Steel Load-Strain 1**

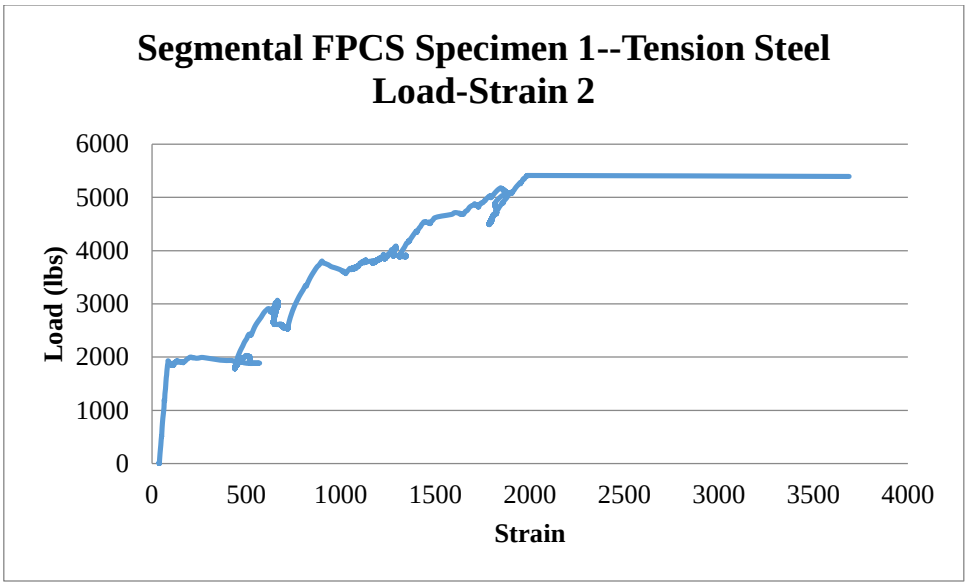


**Figure 192: Segmental FPCS Specimen 1—Tension Steel Load-Strain 2**

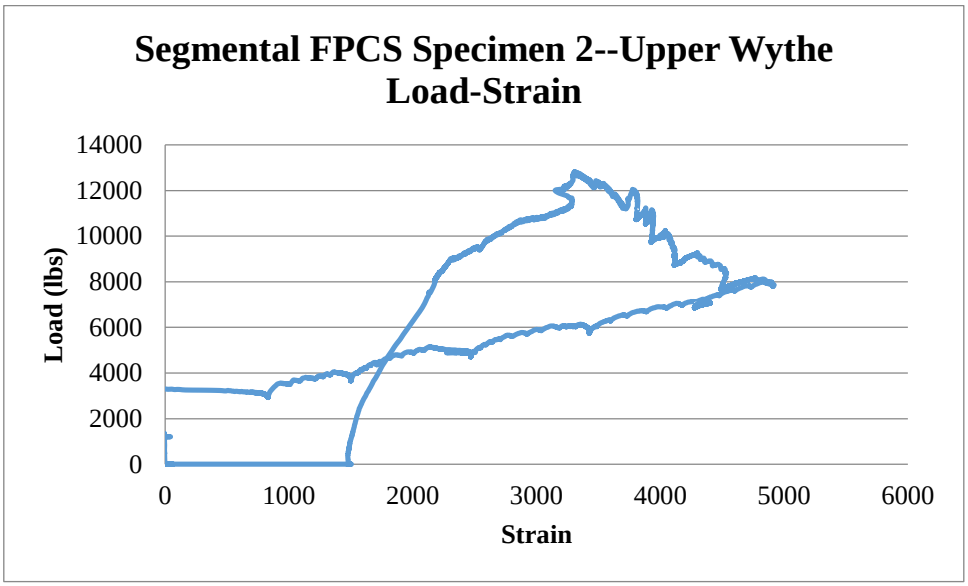


**Figure 193: Segmental FPCS Specimen 2—Upper Wythe Load-Strain**

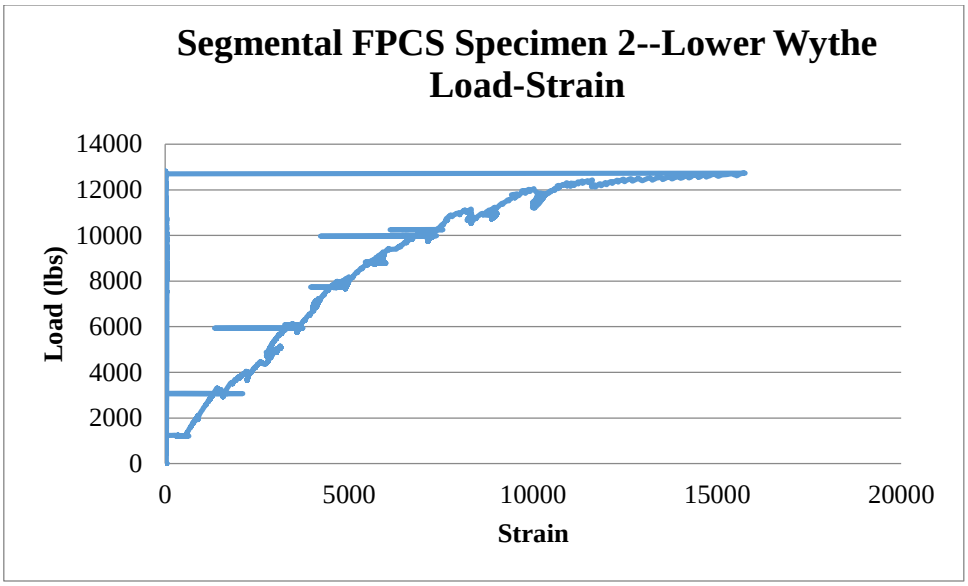


**Figure 194: Segmental FPCS Specimen 2—Lower Wythe Load-Strain**

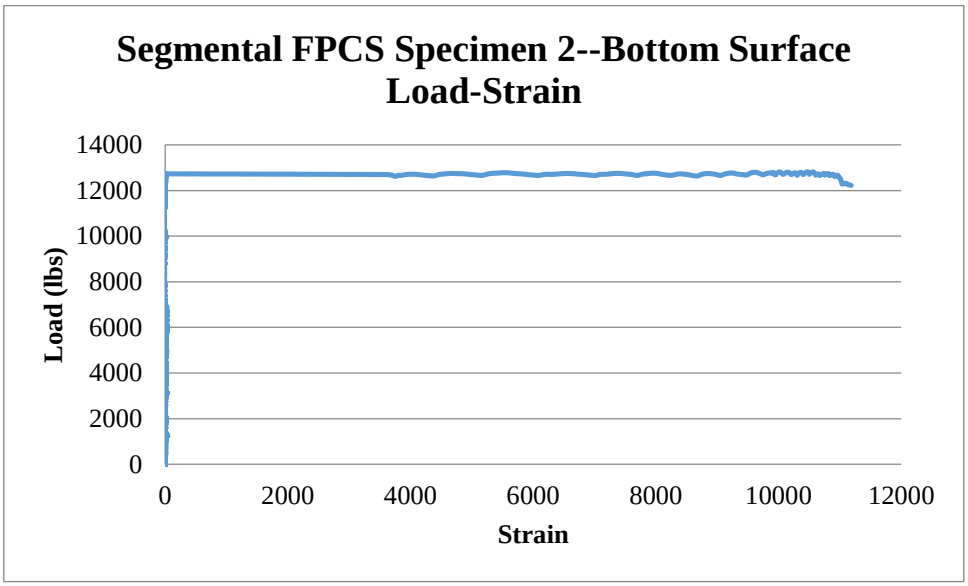


**Figure 195: Segmental FPCS Specimen 2—Bottom Surface Load-Strain**

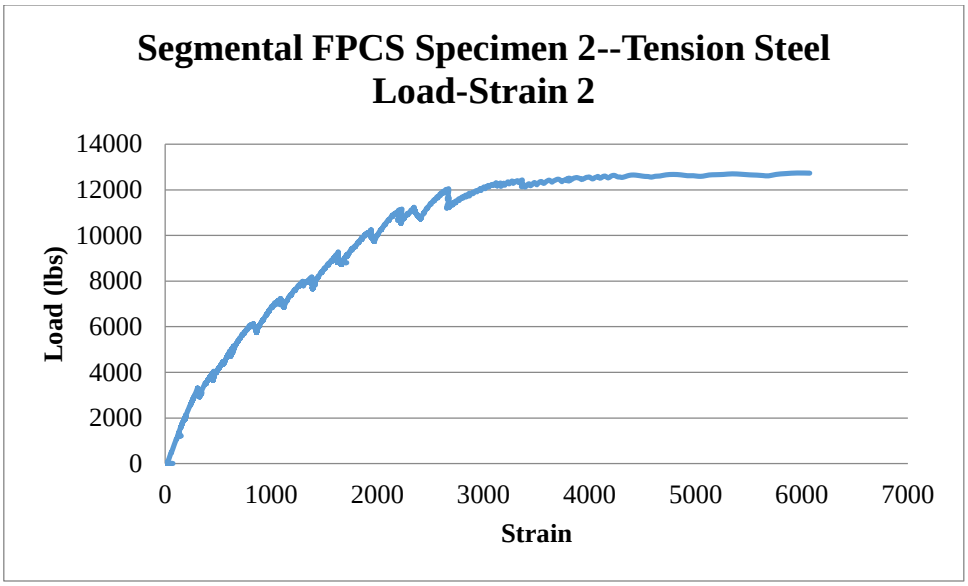


**Figure 196: Segmental FPCS Specimen 2—Tension Steel Load-Strain 2**

## CHAPTER 4 (TOP FRP PLATE)—CONTINUOUS

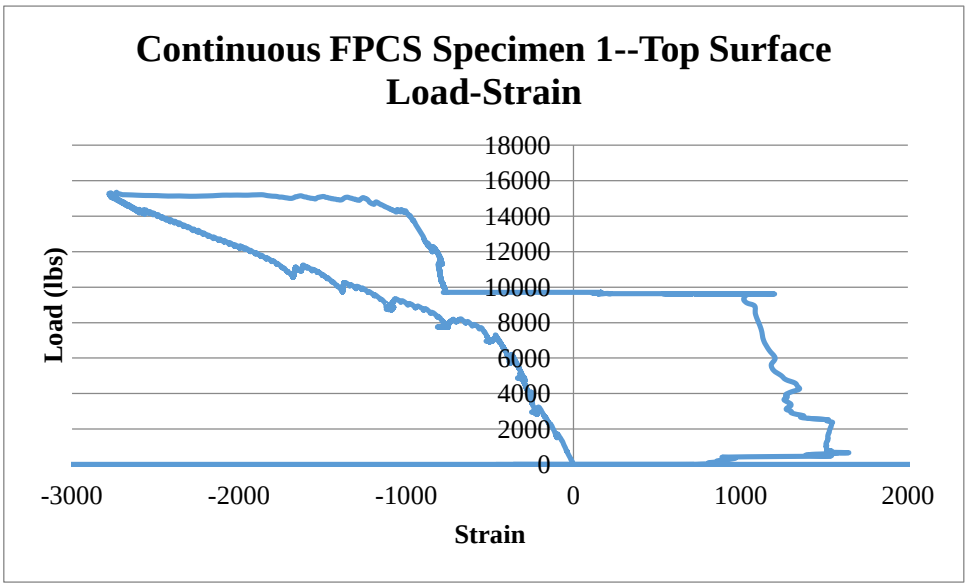


**Figure 197: Continuous FPCS Specimen 1—Top Surface Load-Strain**

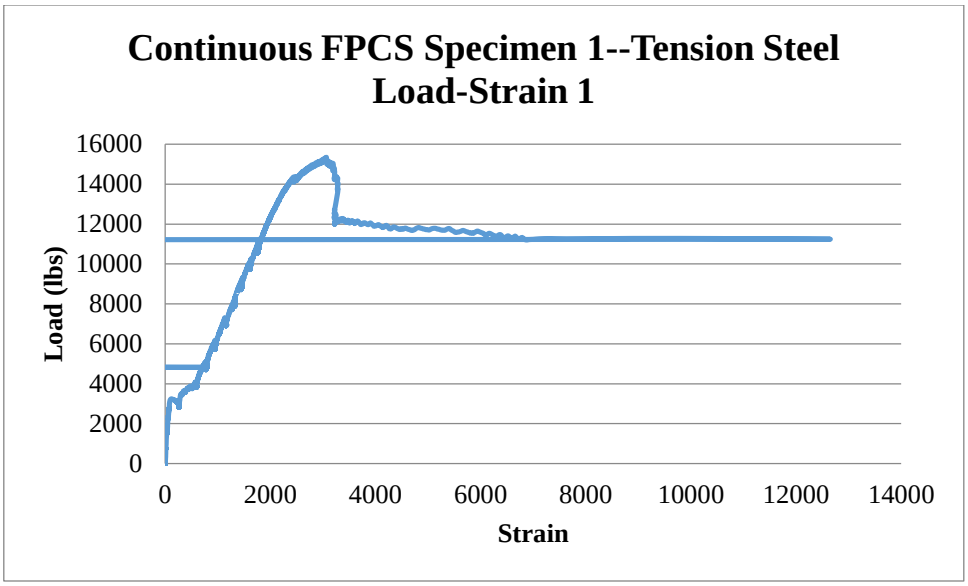


**Figure 198: Continuous FPCS Specimen 1—Tension Steel Load-Strain 1**

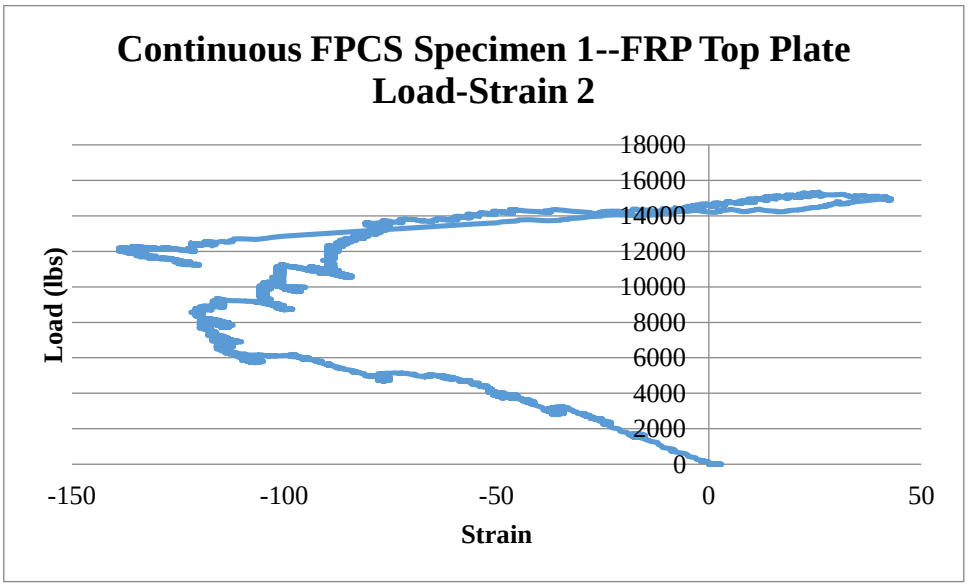


**Figure 199: Continuous FPCS Specimen 1—FRP Top Plate Load-Strain 2**

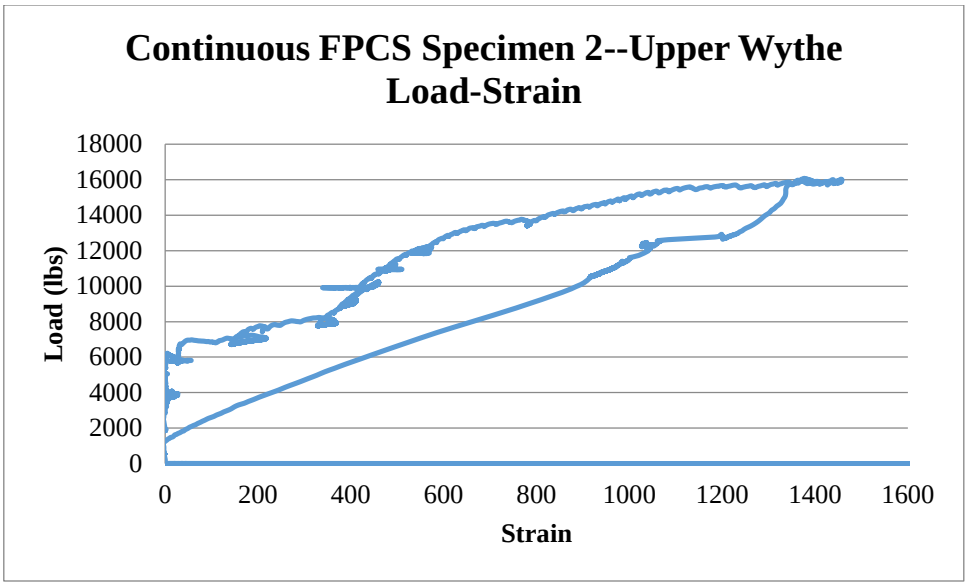


**Figure 200: Continuous FPCS Specimen 2—Upper Wythe Load-Strain**

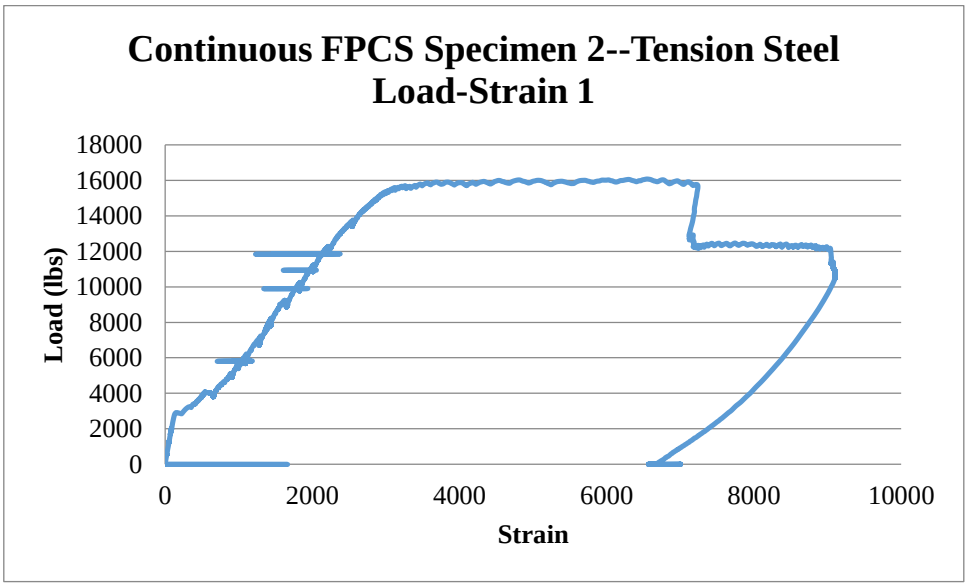


**Figure 201: Continuous FPCS Specimen 2—Tension Steel Load-Strain 1**

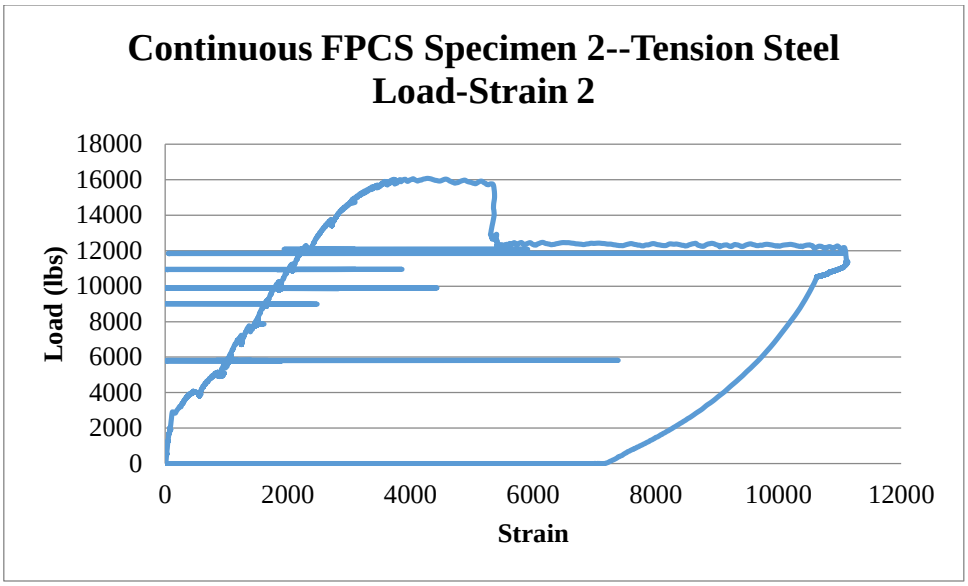


**Figure 202: Continuous FPCS Specimen 2—Tension Steel Load-Strain 2**

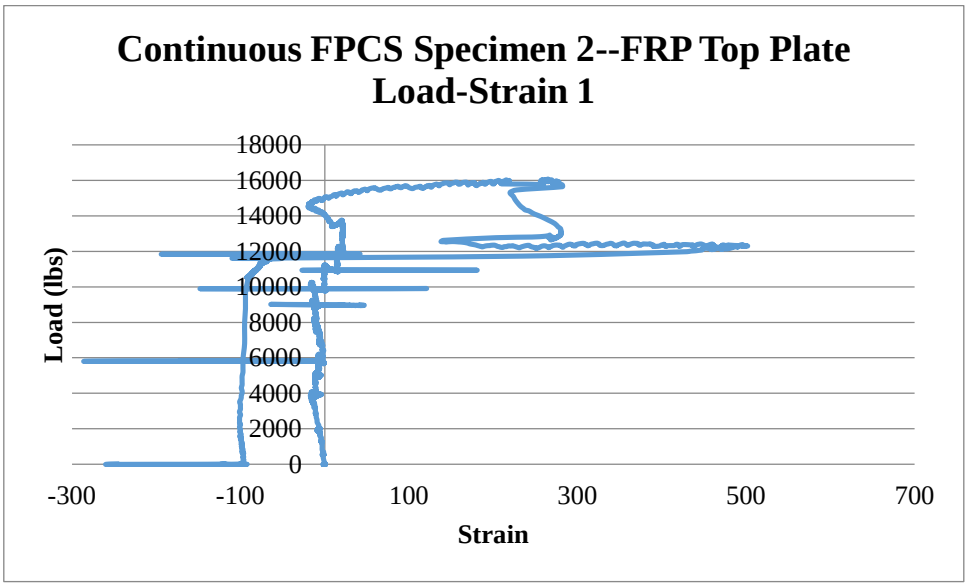


**Figure 203: Continuous FPCS Specimen 2—FRP Top Plate Load-Strain 1**

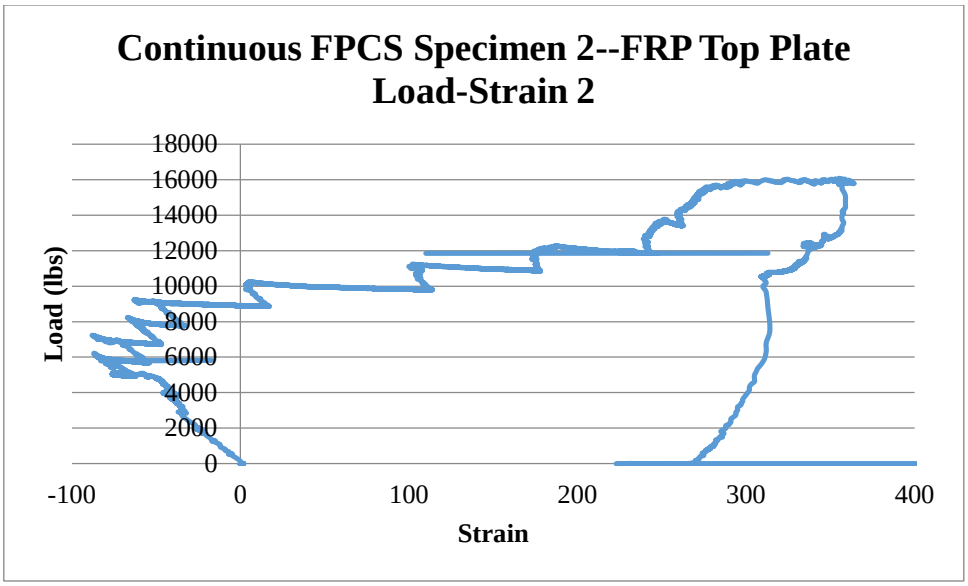


**Figure 204: Continuous FPCS Specimen 2—FRP Top Plate Load-Strain 2**

## CHAPTER 4 (TOP & SIDE FRP PLATES)—8” FPCS

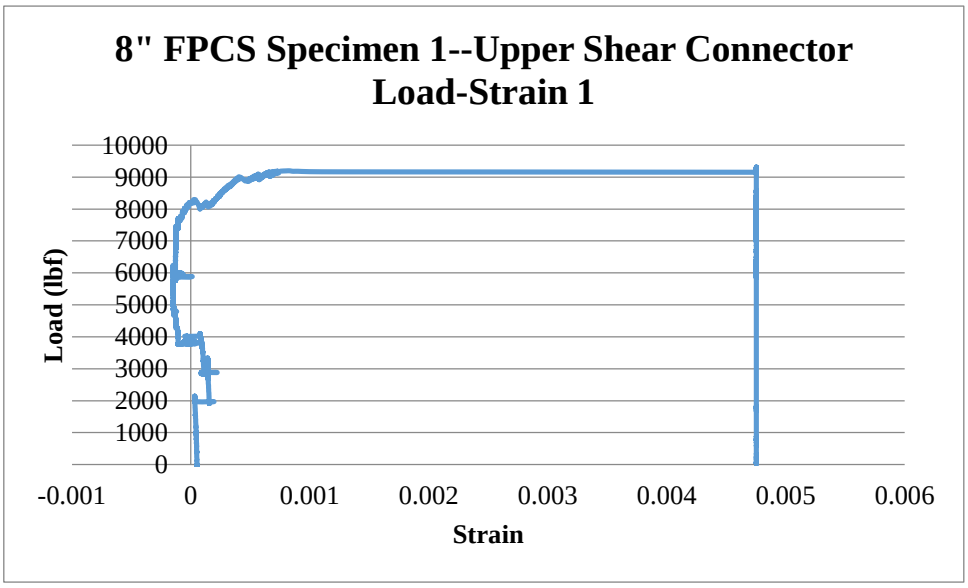


**Figure 205: 8" FPCS Specimen 1—Upper Shear Connector Load-Strain 1**

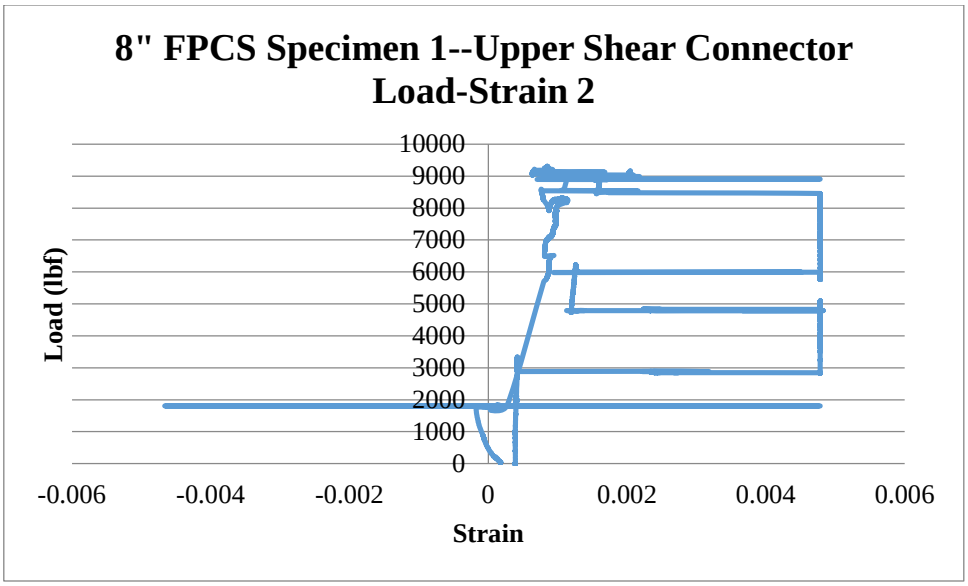


**Figure 206: 8" FPCS Specimen 1—Upper Shear Connector Load-Strain 2**

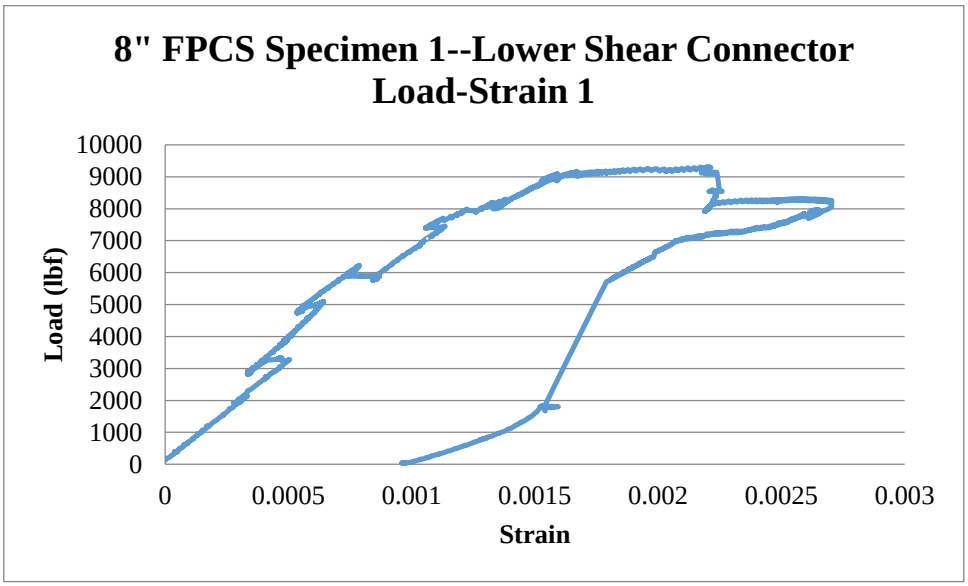


**Figure 207: 8" FPCS Specimen 1—Lower Shear Connector Load-Strain 1**

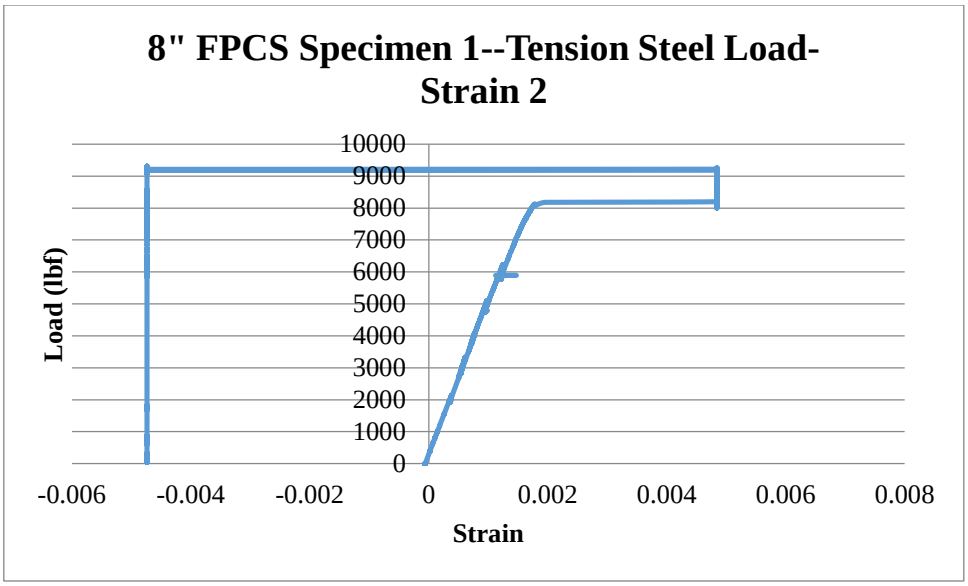


**Figure 208: 8" FPCS Specimen 1—Tension Steel Load-Strain 2**

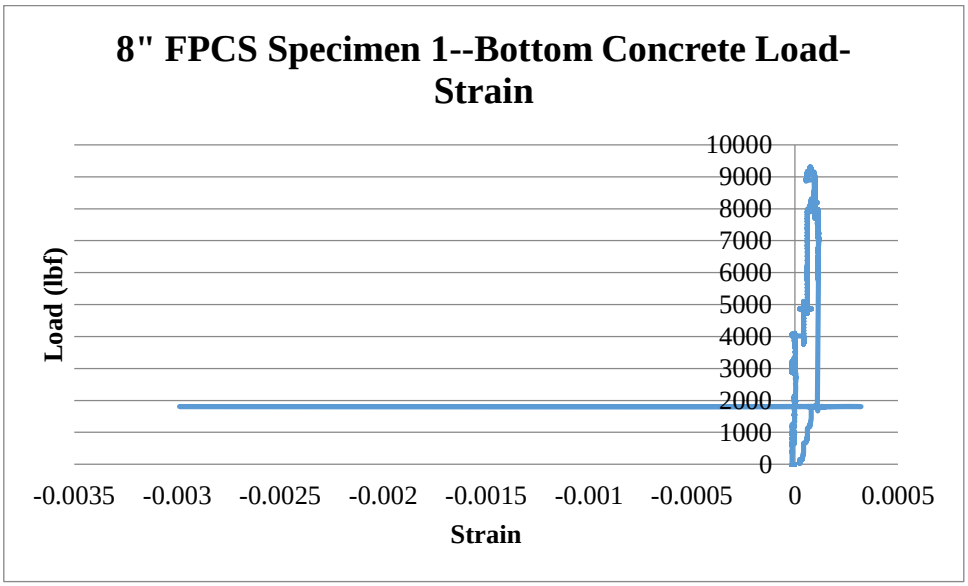


**Figure 209: 8" FPCS Specimen 1—Bottom Concrete Load-Strain**

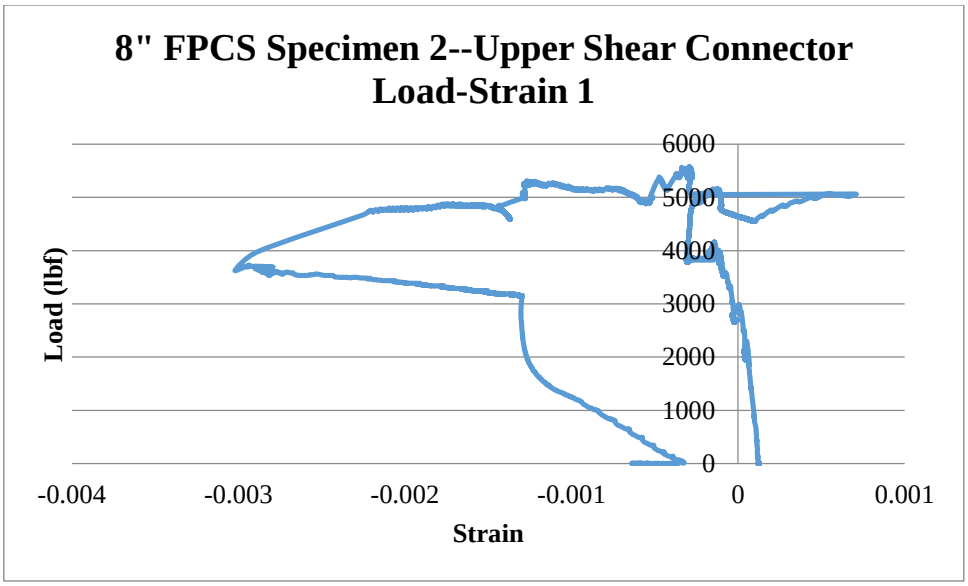


**Figure 210: 8" FPCS Specimen 2—Upper Shear Connector Load-Strain 1**

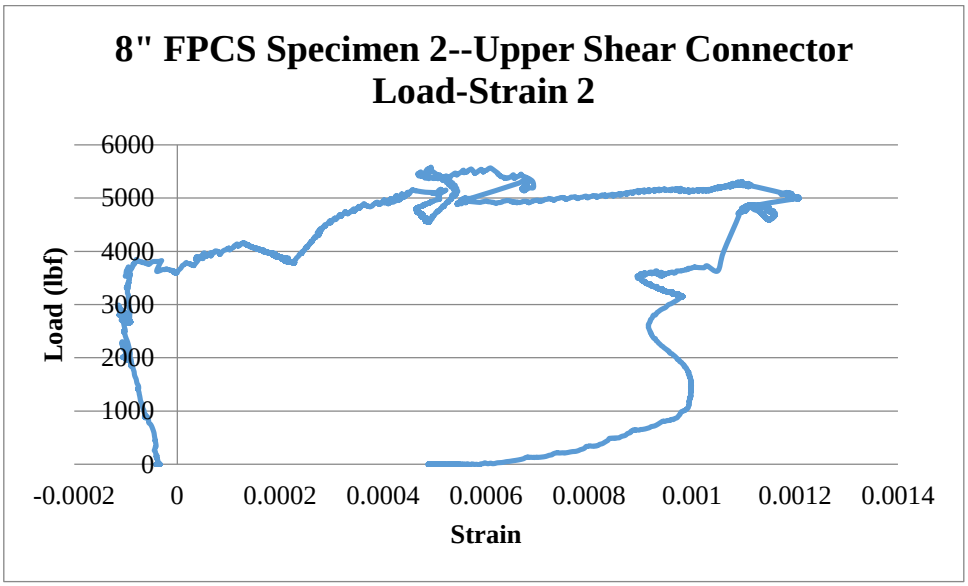


**Figure 211: 8" FPCS Specimen 2—Upper Shear Connector Load-Strain 2**

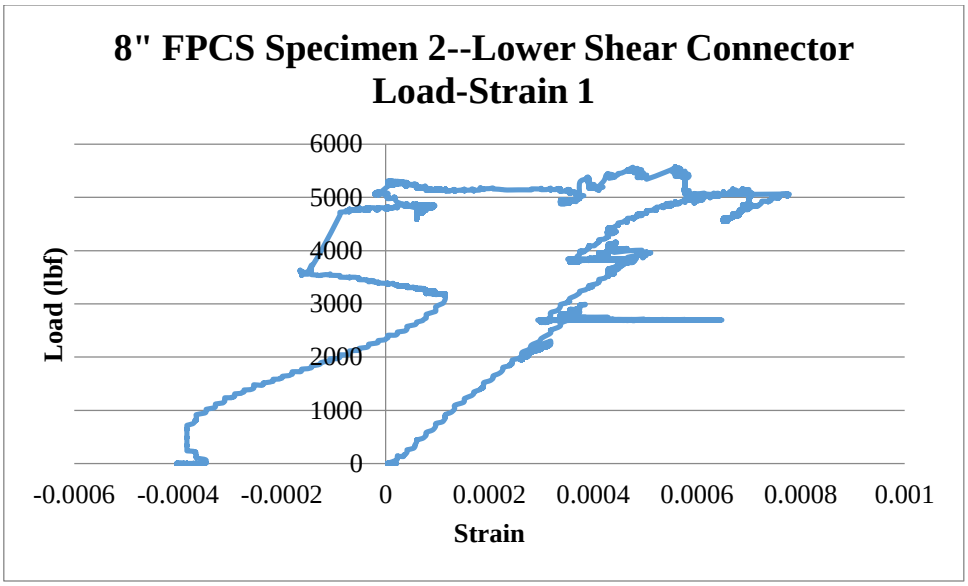


**Figure 212: 8" FPCS Specimen 2—Lower Shear Connector Load-Strain 1**

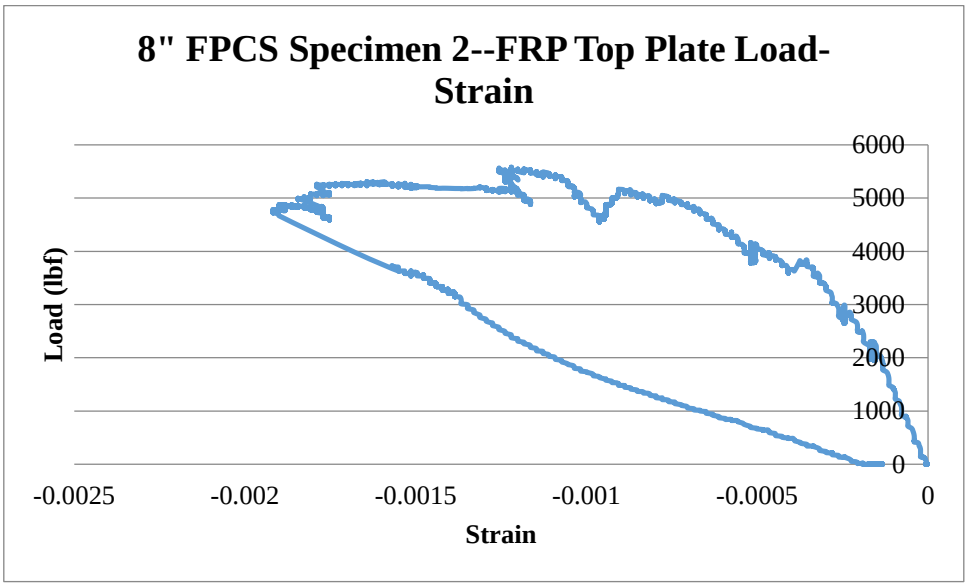


**Figure 213: 8" FPCS Specimen 2—FRP Top Plate Load-Strain**

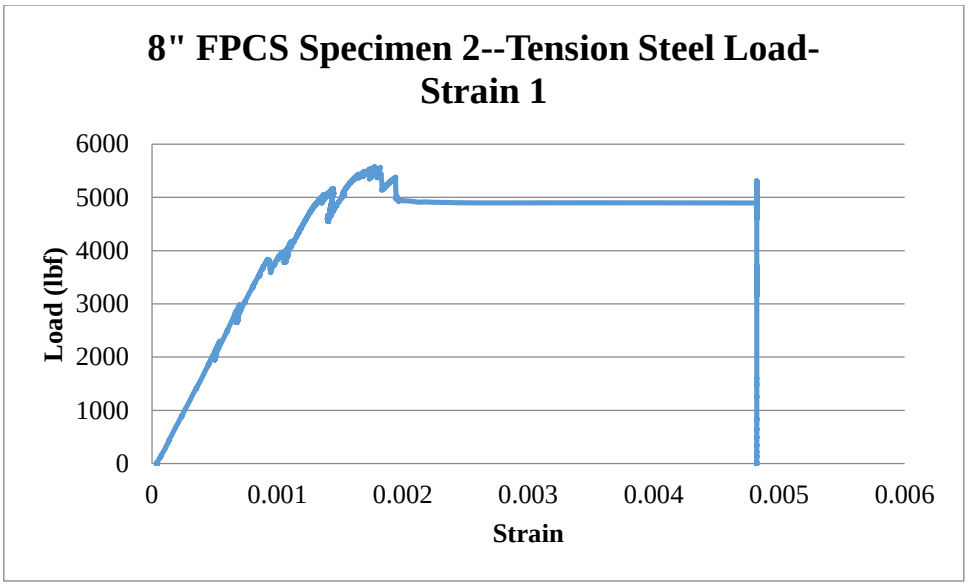


**Figure 214: 8" FPCS Specimen 2—Tension Steel Load-Strain 1**

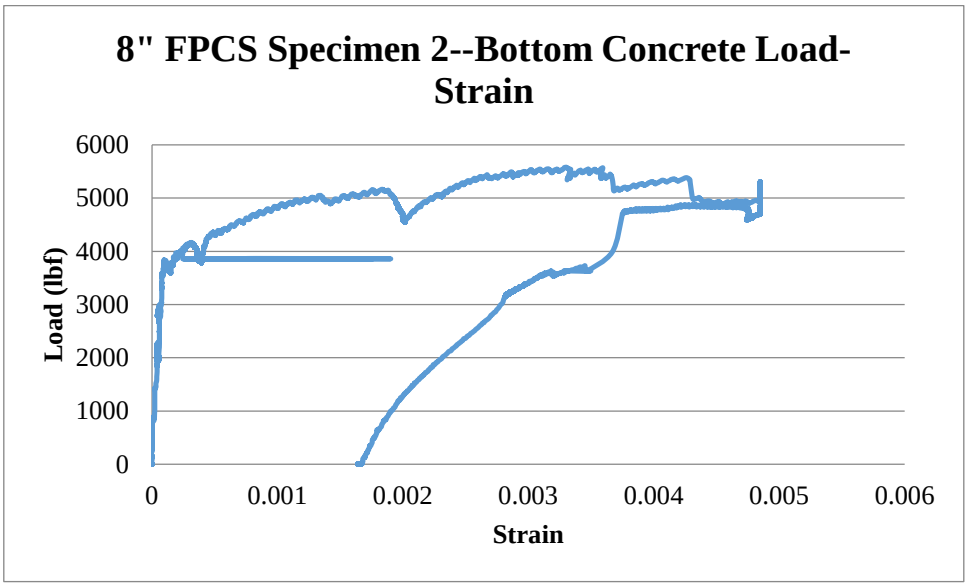


**Figure 215: 8" FPCS Specimen 2—Bottom Concrete Load-Strain**

# CHAPTER 4 (TOP & SIDE FRP PLATES)—10” FPCS

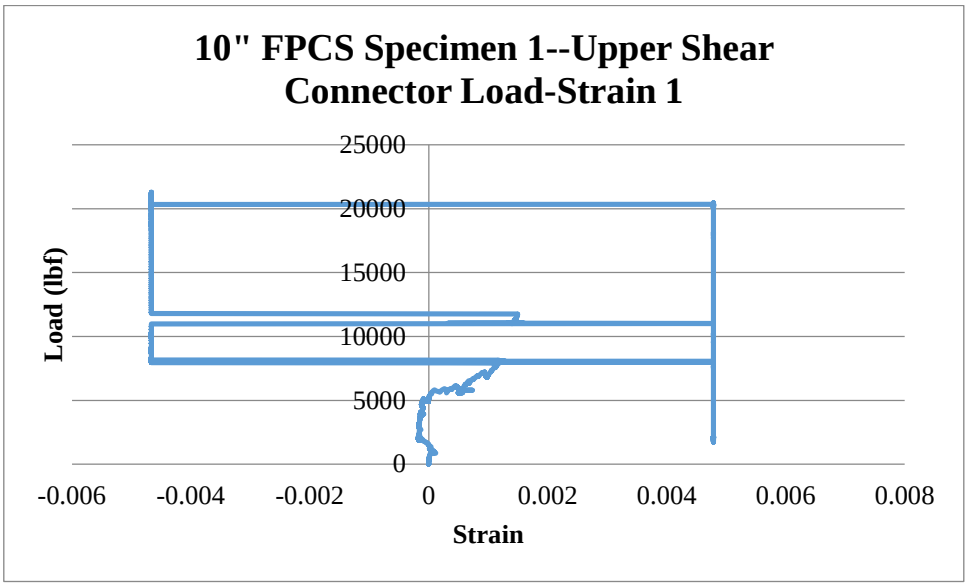


**Figure 216: 10” FPCS Specimen 1—Upper Shear Connector Load-Strain 1**

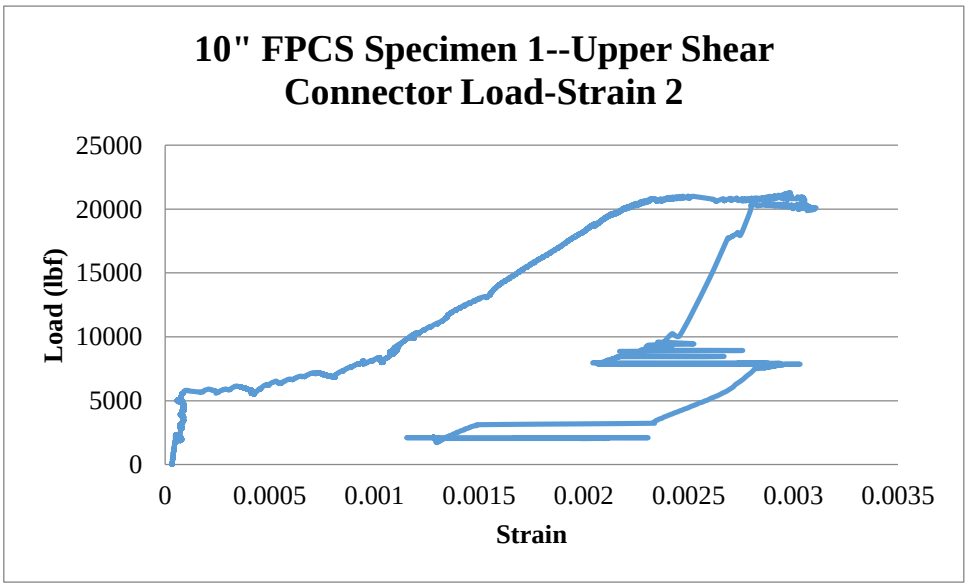


**Figure 217: 10” FPCS Specimen 1—Upper Shear Connector Load-Strain 2**

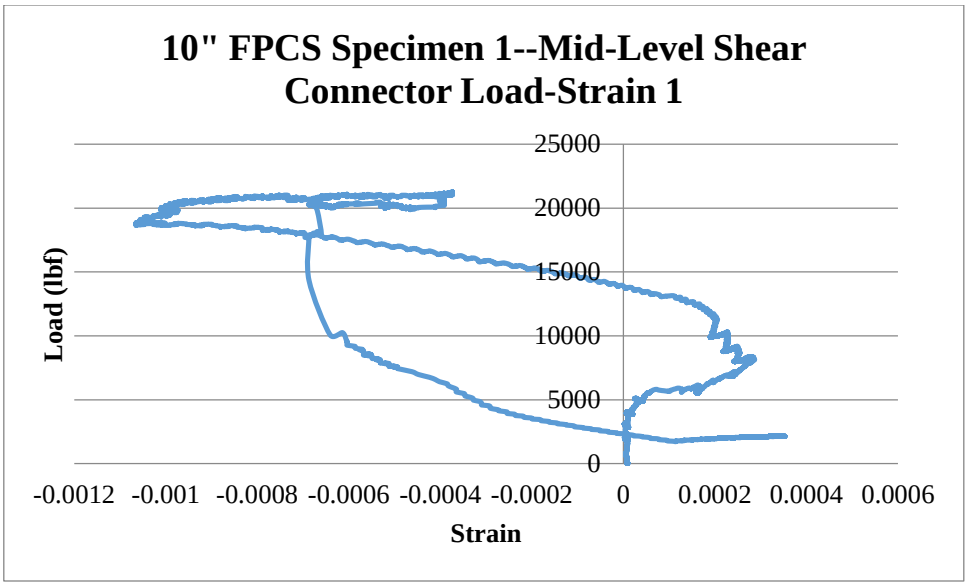


**Figure 218: 10" FPCS Specimen 1—Mid-Level Shear Connector Load-Strain 1**

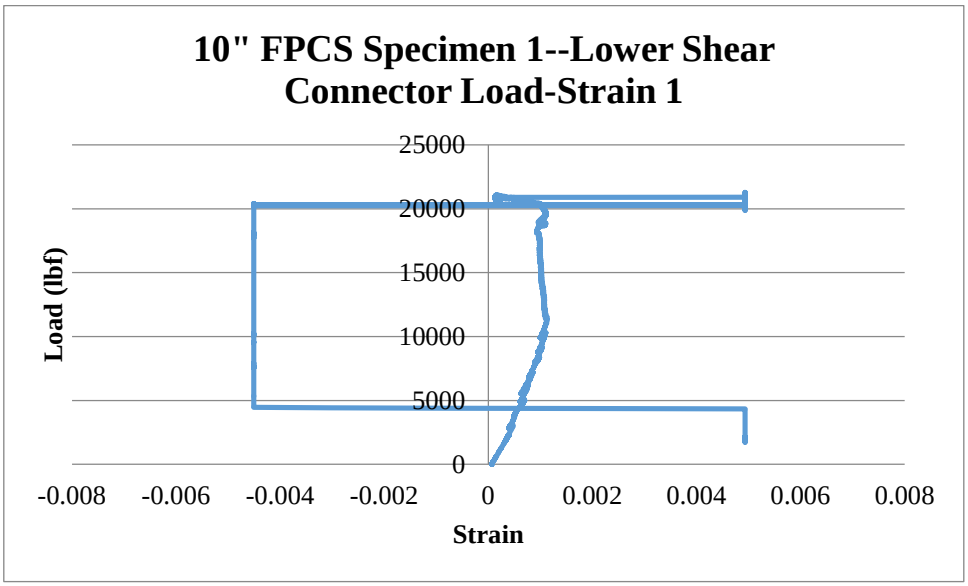


**Figure 219: 10" FPCS Specimen 1—Lower Shear Connector Load-Strain 1**

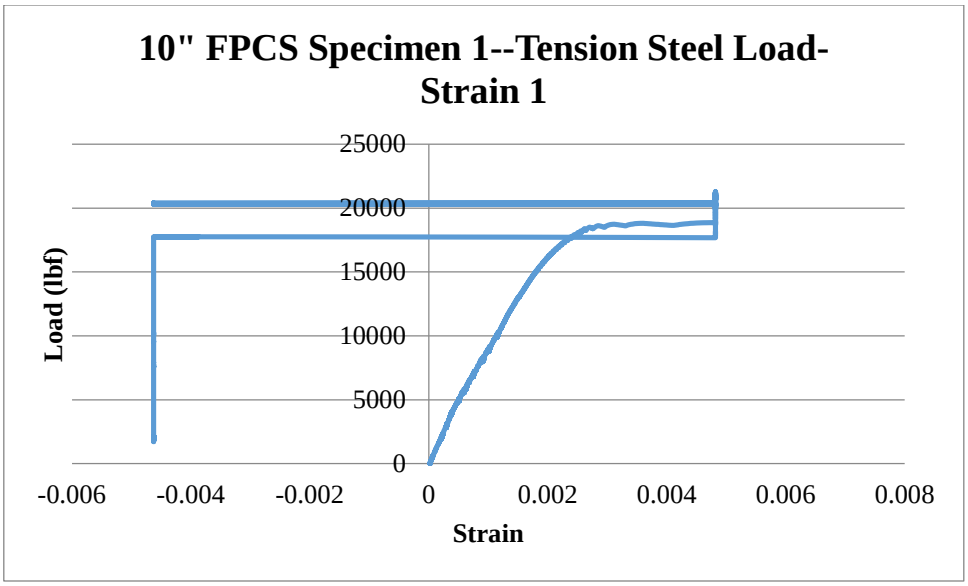


**Figure 220: 10” FPCS Specimen 1—Tension Steel Load-Strain 1**

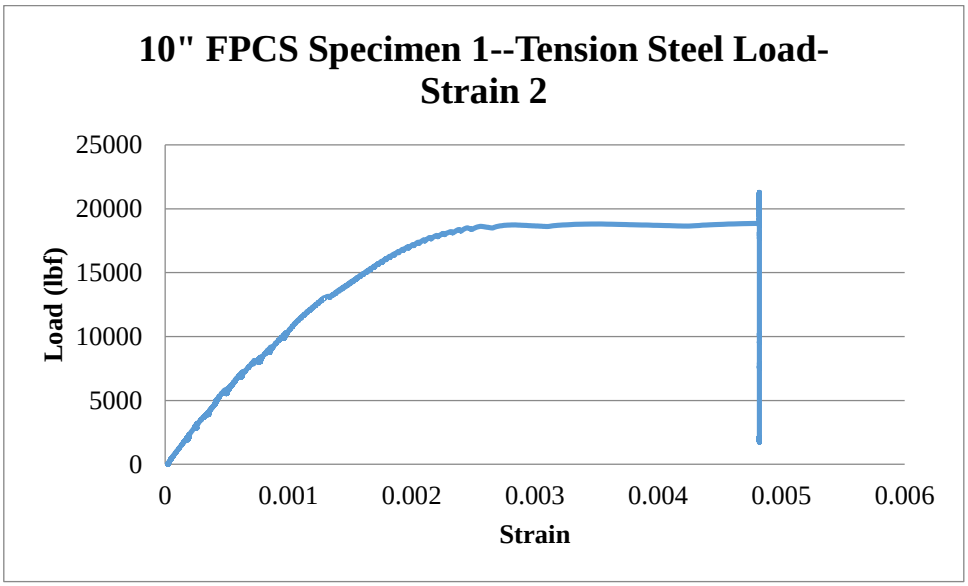


**Figure 221: 10” FPCS Specimen 1—Tension Steel Load-Strain 2**

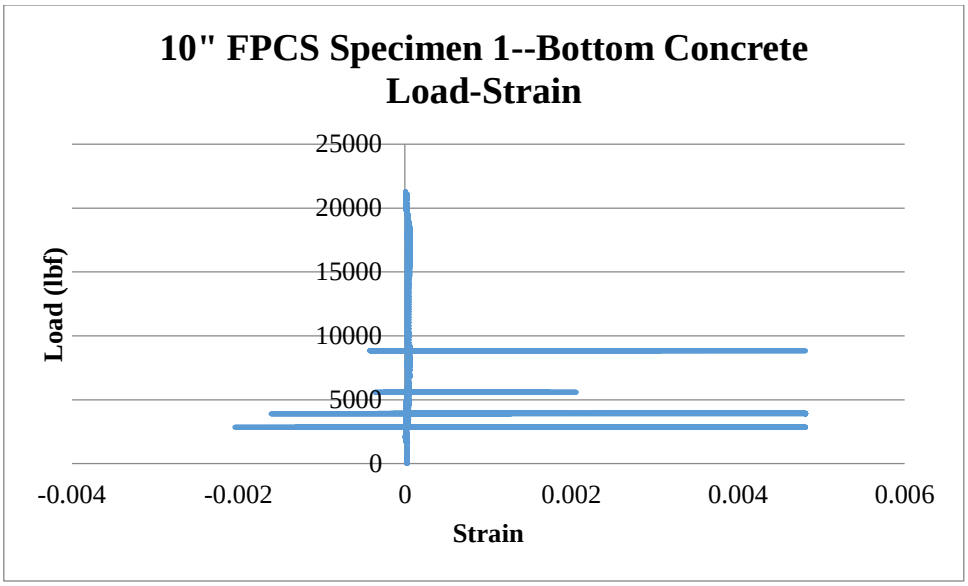


**Figure 222: 10” FPCS Specimen 1—Bottom Concrete Load-Strain**

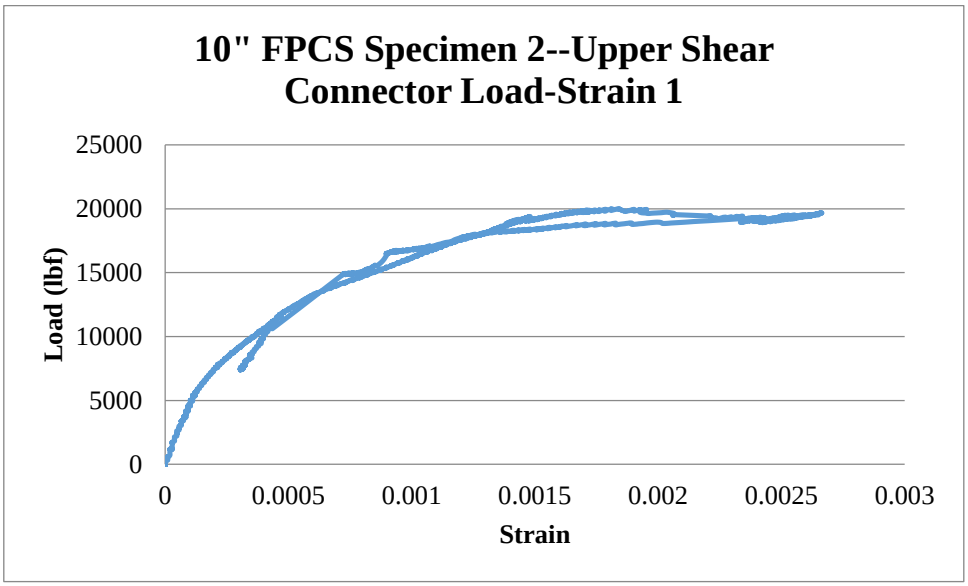


**Figure 223: 10” FPCS Specimen 2—Upper Shear Connector Load-Strain 1**

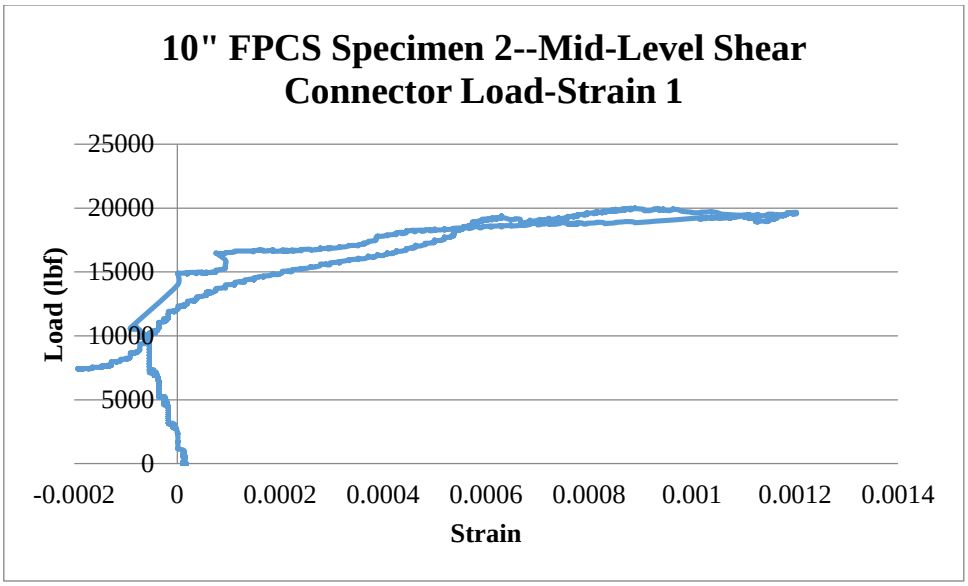


**Figure 224: 10" FPCS Specimen 2—Mid-Level Shear Connector Load-Strain 1**

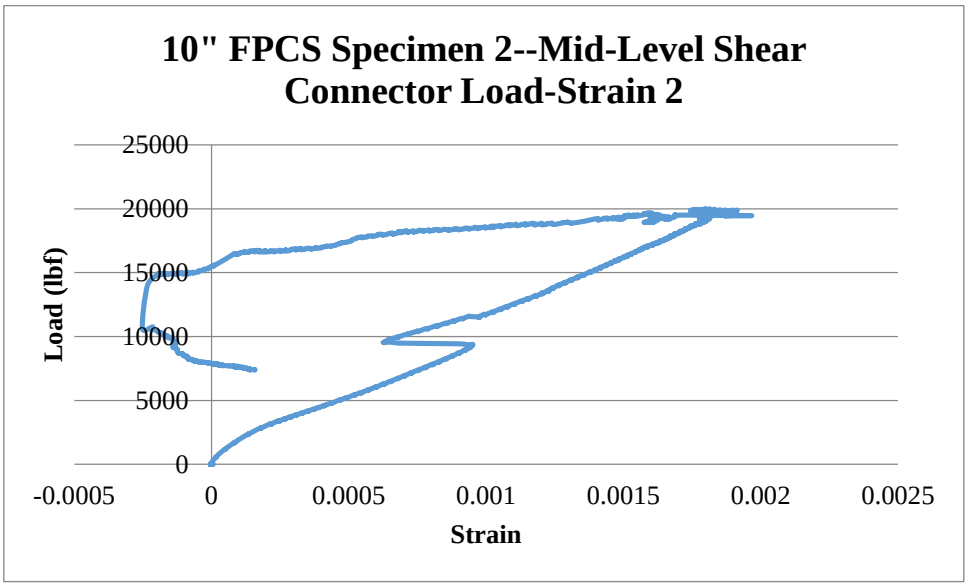


**Figure 225: 10" FPCS Specimen 2—Mid-Level Shear Connector Load-Strain 2**

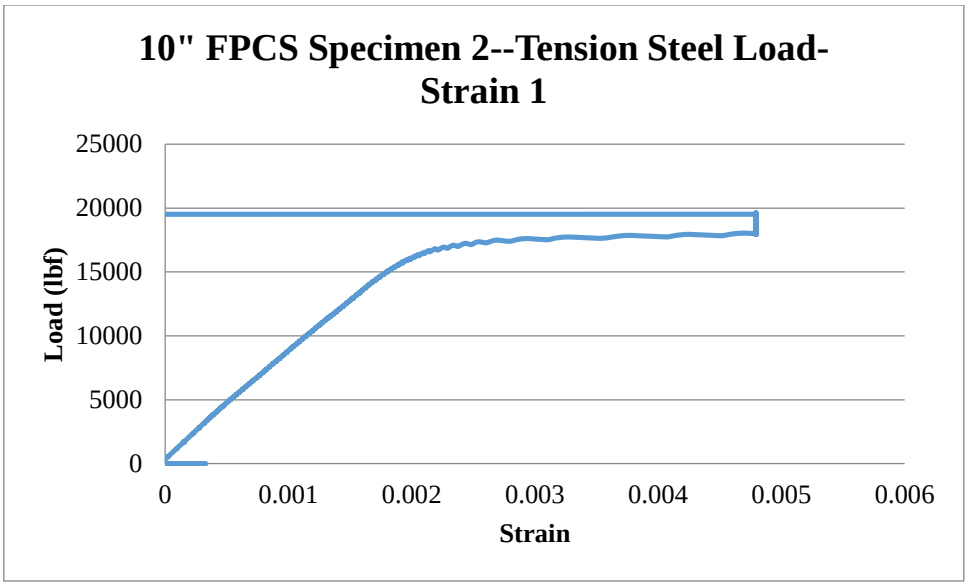


**Figure 226: 10” FPCS Specimen 2—Tension Steel Load-Strain 1**

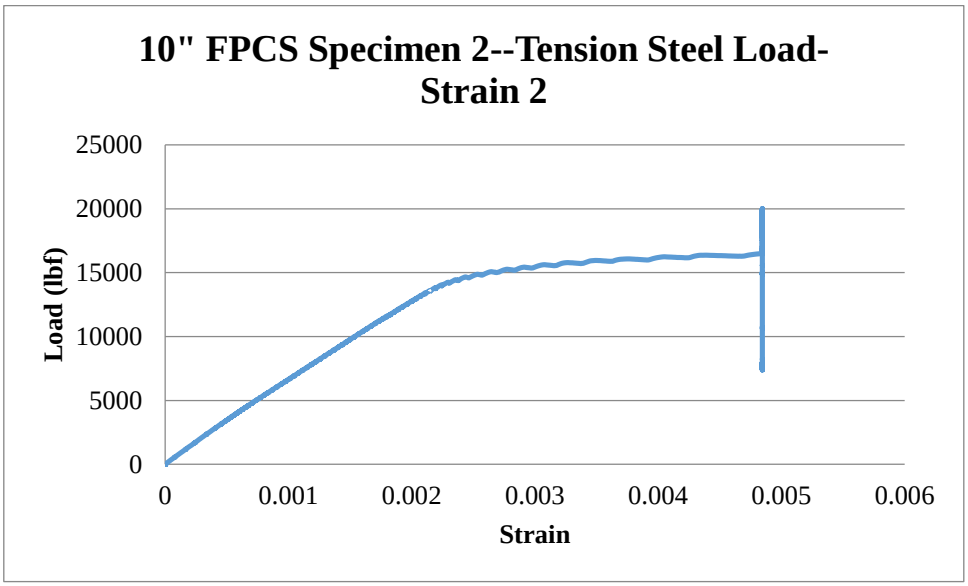


**Figure 227: 10” FPCS Specimen 2—Tension Steel Load Strain 2**

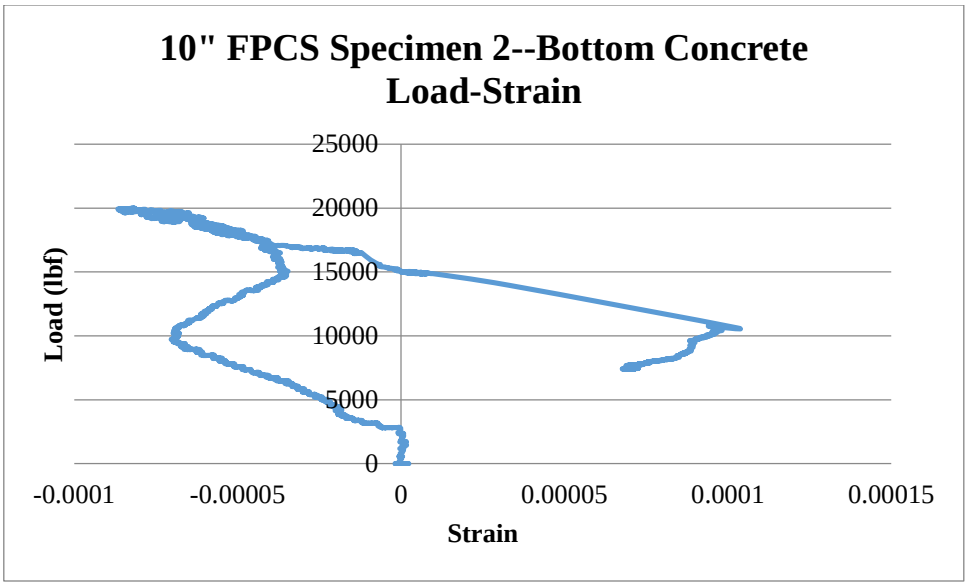


**Figure 228: 10” FPCS Specimen 2—Bottom Concrete Load-Strain**

# STRENGTH/STIFFNESS CORRECTIONS

**Given:** $A_s := 2\cdot(0.31in^2)$ $A_{sc} := 2\cdot(0.20in^2)$ $f_y := 60000psi$ $f_c := 4120psi$

$b := 24in$ $d := 8.9375in$ $d_{prime} := 1in$ $E_s := 29000ksi$

**Step 1:**

Determine the correction factor necessary to equate theoretical values to experimental results.

$$a := \frac{A_s\cdot f_y}{0.85\cdot f_c\cdot b} = 0.443\cdot in \qquad c := \frac{a}{0.85} = 0.521\cdot in$$

$$\varepsilon_s := 0.003\cdot\left(\frac{d_{prime} - c}{c}\right) = 2.761\times 10^{-3} \qquad f_s := E_s\cdot\varepsilon_s = 8.008\times 10^{4}\cdot psi$$

$$C_s := A_{sc}\cdot(f_s - 0.85\cdot f_c) = 30.631\cdot kip$$

$$C_c := 0.85\cdot f_c\cdot b\cdot a = 37.2\cdot kip$$

$$M_n := C_c\cdot\left(d - \frac{a}{2}\right) + C_s\cdot(d - d_{prime}) = 47.281\cdot kip\cdot ft$$

$$P_{cr} := \frac{2M_n}{4.5ft} = 21.014\cdot kip$$

$P_{experiment} := 20.5kip$

Correction Factor: $CF := \frac{P_{experiment}}{P_{cr}} = 0.976$

**Step 2:**

Determine the theoretical strength of a solid slab with $f_c'$=4860psi for both 8" and 10" thicknesses.

**8" Thick Specimen:**

**Given:** $A_s := 2\cdot(0.31in^2)$ $A_{sc} := 2\cdot(0.20in^2)$ $f_y := 60000psi$ $f_c := 4860psi$

$b := 24in$ $d := 6.9375in$ $d_{prime} := 1in$ $E_s := 29000ksi$

**Solution:**

$$a := \frac{A_s\cdot f_y}{0.85\cdot f_c\cdot b} = 0.375\cdot in \qquad c := \frac{a}{0.85} = 0.441\cdot in$$

$$\varepsilon_s := 0.003\cdot\left(\frac{d_{prime} - c}{c}\right) = 3.796\times 10^{-3} \qquad f_s := E_s\cdot\varepsilon_s = 1.101\times 10^{5}\cdot psi$$

$C_s := A_{sc}\cdot(f_s - 0.85\cdot f_c) = 42.383\cdot kip$

$C_c := 0.85\cdot f_c\cdot b\cdot a = 37.2\cdot kip$

$M_n := C_c\cdot\left(d - \frac{a}{2}\right) + C_s\cdot(d - d_{prime}) = 41.895\cdot kip\cdot ft$

$P_{cr} := \frac{2M_n}{4.5ft} = 18.62\cdot kip$

Critical Load with Correction Factor:

$P_{experiment} := P_{cr}\cdot CF = 18.165\cdot kip$

**10" Thick Specimen:**

**Given:** $A_s := 2\cdot(0.31in^2)$ $A_{sc} := 2\cdot(0.20in^2)$ $f_y := 60000psi$ $f_c := 4860psi$

$b := 24in$ $d := 8.9375in$ $d_{prime} := 1in$ $E_s := 29000ksi$

**Solution:**

$a := \frac{A_s\cdot f_y}{0.85\cdot f_c\cdot b} = 0.375\cdot in$ $c := \frac{a}{0.85} = 0.441\cdot in$

$\varepsilon_s := 0.003\cdot\left(\frac{d_{prime} - c}{c}\right) = 3.796\times 10^{-3}$ $f_s := E_s\cdot\varepsilon_s = 1.101\times 10^{5}\cdot psi$

$C_s := A_{sc}\cdot(f_s - 0.85\cdot f_c) = 42.383\cdot kip$

$C_c := 0.85\cdot f_c\cdot b\cdot a = 37.2\cdot kip$

$M_n := C_c\cdot\left(d - \frac{a}{2}\right) + C_s\cdot(d - d_{prime}) = 55.159\cdot kip\cdot ft$

$P_{cr} := \frac{2M_n}{4.5ft} = 24.515\cdot kip$

Critical Load with Correction Factor:

$P_{experiment} := P_{cr}\cdot CF = 23.916\cdot kip$

**Step 3:**
Determine the the theoretical deflection of the solid slab from Step 1 at the critical load to determine a deflection correction factor.

**Given:** $L := 9ft$ $E := 6.804 \times 10^{6} \cdot psi$ $I := 2000in^{4}$ $P := 1.4kip$ $\Delta_{ex} := 0.0027in$

**Solution**

$$\Delta := \frac{P \cdot L^{3}}{48 \cdot E \cdot I} = 2.7 \times 10^{-3} \cdot in$$

**No correction factor necessary**

**Step 4:**
Determine the theoretical deflection of a solid 8" slab using experimental data.

**Given:** $P := 1.4kip$ $E := 57000 \cdot \sqrt{4860} = 3.974 \times 10^{6}$ $I := 1024in^{4}$ $L := 9ft$

$E := 3.974\,10^{6} psi$

**Solution**

$$\Delta := \frac{P \cdot L^{3}}{48 \cdot E \cdot I} = 9.029 \times 10^{-3} \cdot in$$

**Apply this deflection to the stiffness equation for the 8" FPCS Panel**

**Step 5:**
Determine the theoretical deflection of a solid 10" slab using experimental data.

**Given:** $P := 1.4kip$ $E := 57000 \cdot \sqrt{4860} = 3.974 \times 10^{6}$ $I := 2000in^{4}$ $L := 9ft$

$E := 3.974\,10^{6} psi$

**Solution**

$$\Delta := \frac{P \cdot L^{3}}{48 \cdot E \cdot I} = 4.623 \times 10^{-3} \cdot in$$

**Apply this deflection to the stiffness equation for the 10" FPCS Panel**

# APPENDIX 3

This appendix presents all corrections, material properties, calculations and additional graphs/figures pertaining to Chapter 5.

## DEFLECTION ACROSS SPECIMEN LENGTH

### FULL SCALE—8” FPCS

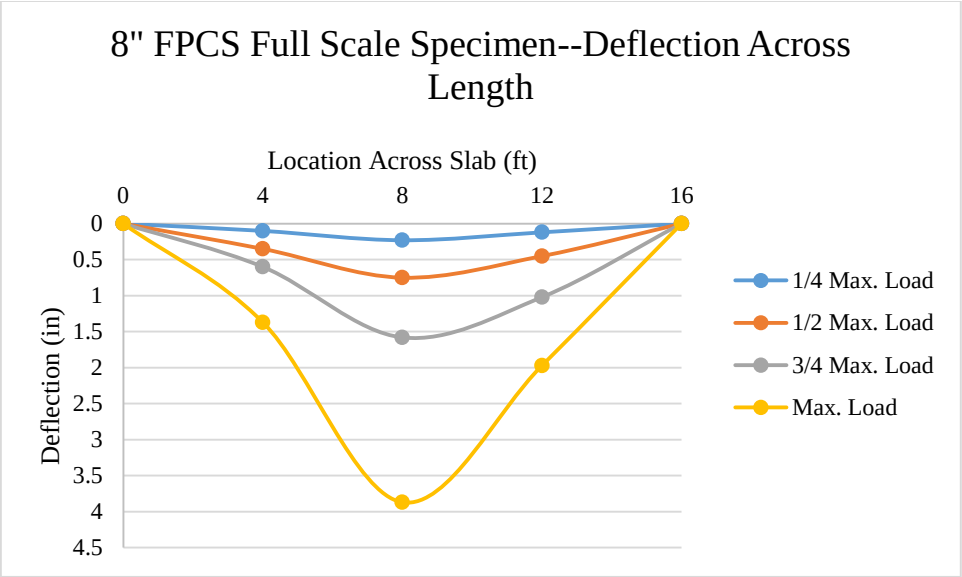


### FULL SCALE —10” FPCS

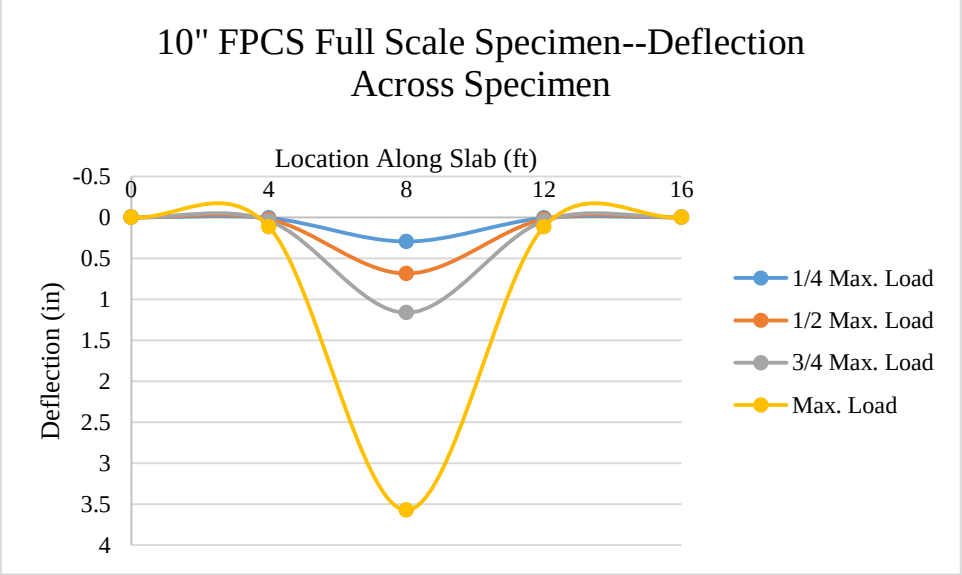

# ADDITIONAL STRAIN DATA

## FULL SCALE —8" FPCS

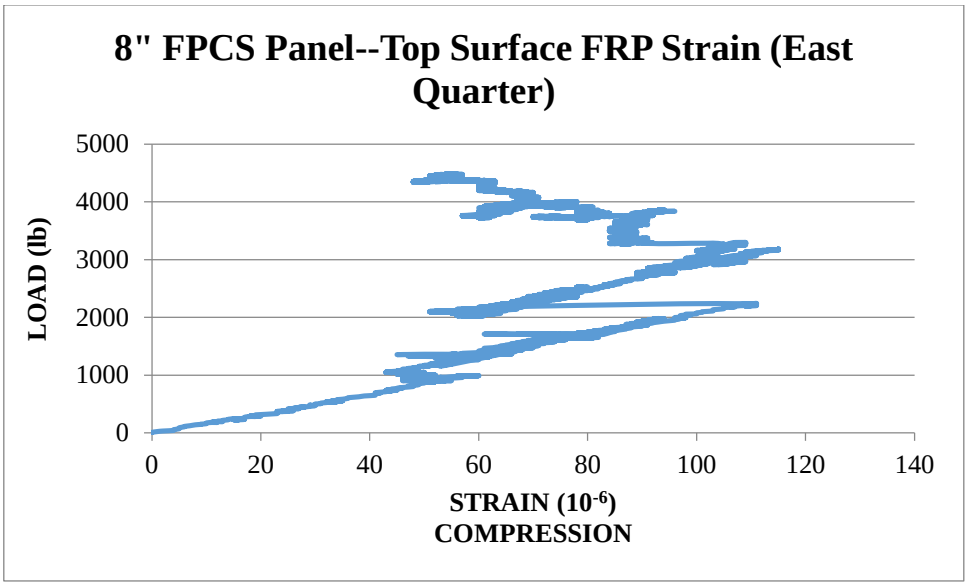


**Figure 229: 8" FPCS Panel--Top Surface FRP Strain (East Quarter)**

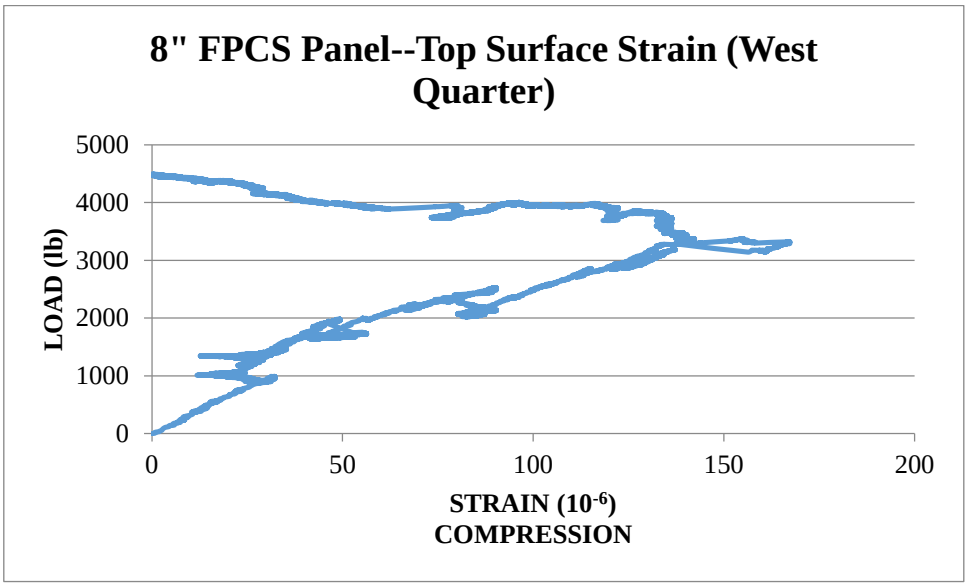


**Figure 230: 8" FPCS Panel--Top Surface Strain (West Quarter)**

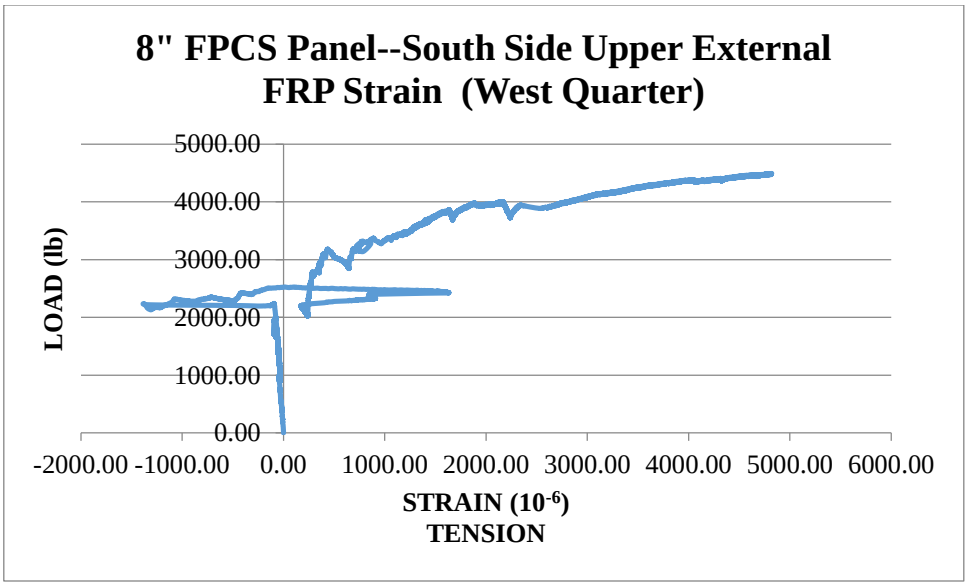


**Figure 231: 8" FPCS Panel--South Side Upper External FRP Strain (West Quarter**

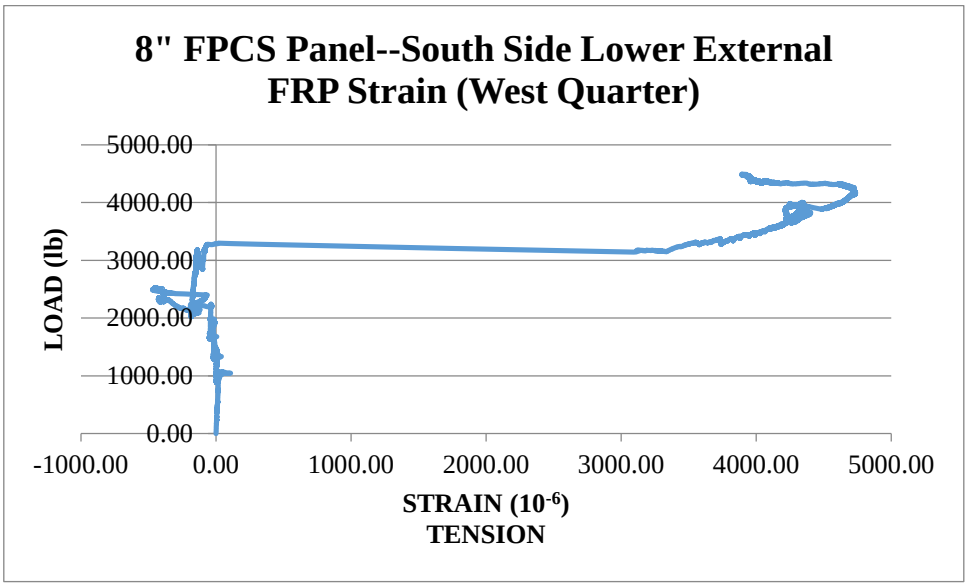


**Figure 232: 8" FPCS Panel--South Side Lower External FRP Strain (West Quarter)**

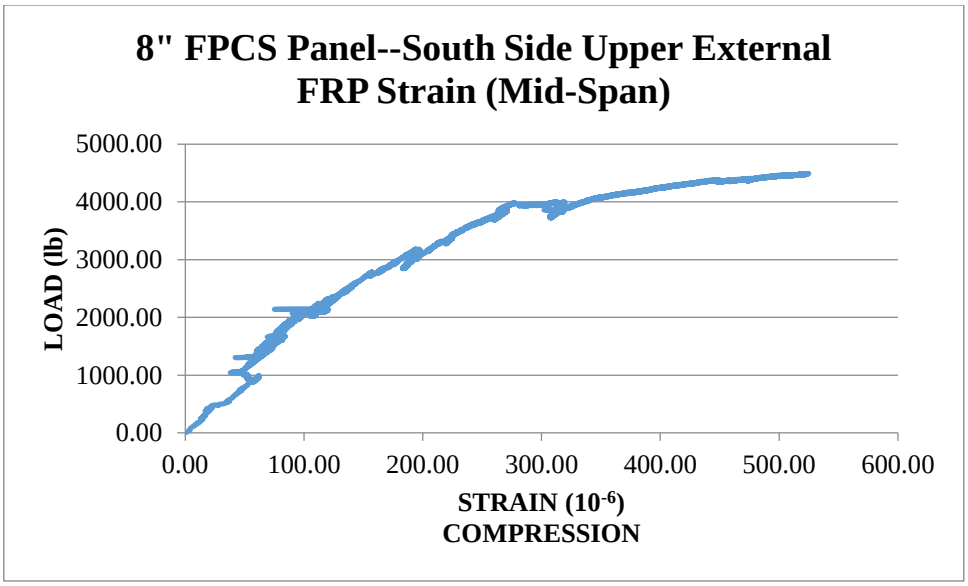


**Figure 233:8" FPCS Panel--South Side Upper External FRP Strain (Mid-Span**

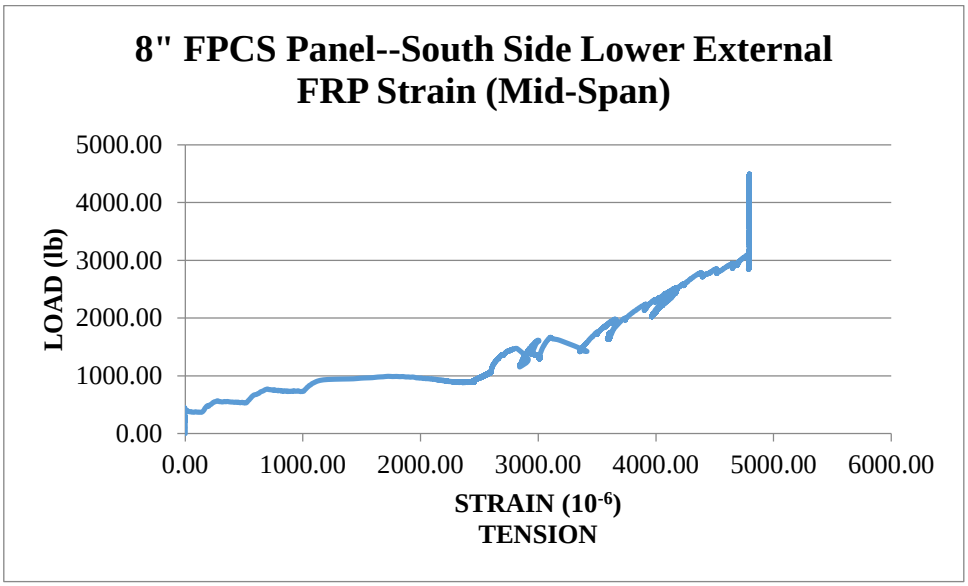


**Figure 234: 8" FPCS Panel--South Side Lower External FRP Strain (Mid-Span)**

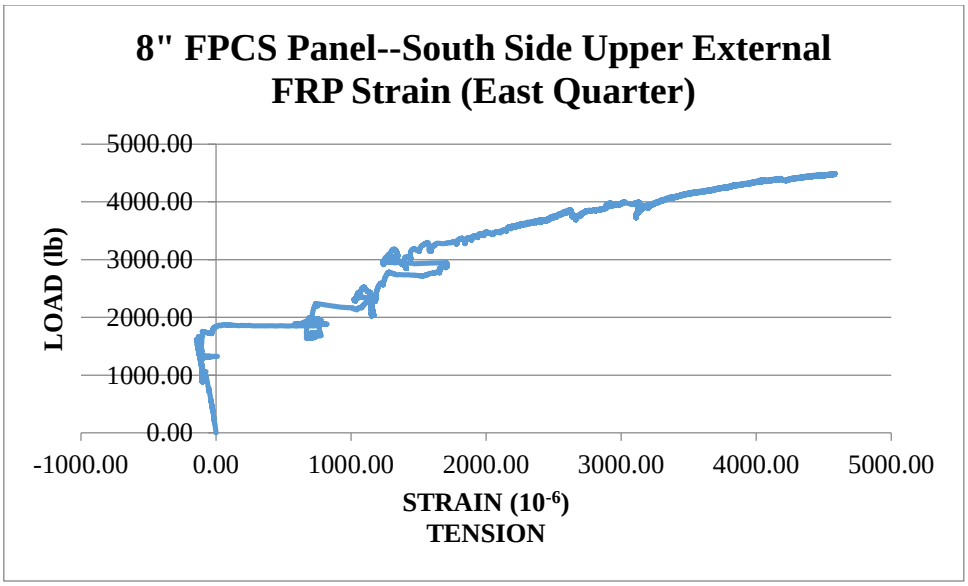


**Figure 235: 8" FPCS Panel--South Side Upper External FRP Strain (East Quarter)**

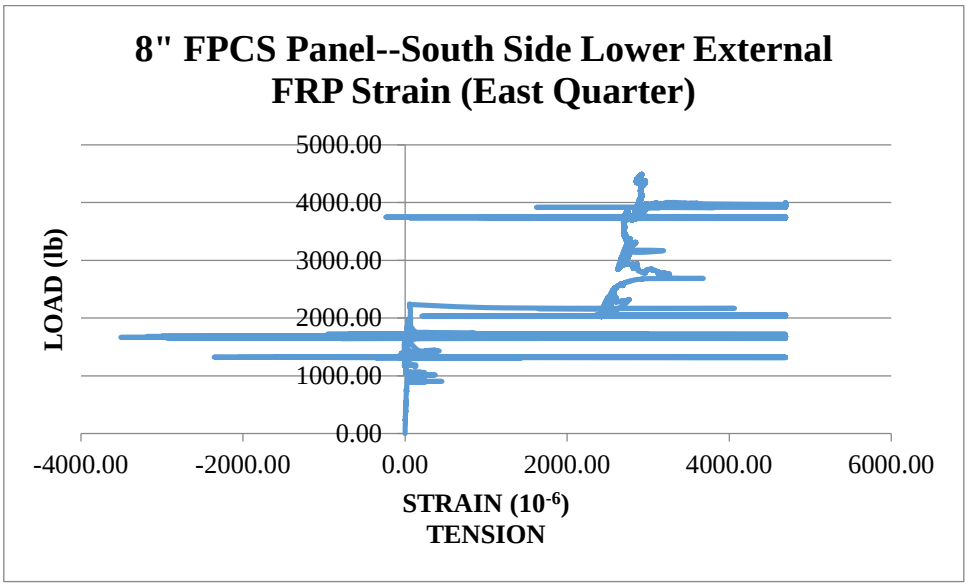


**Figure 236: 8" FPCS Panel--South Side Lower External FRP Strain (East Quarter)**

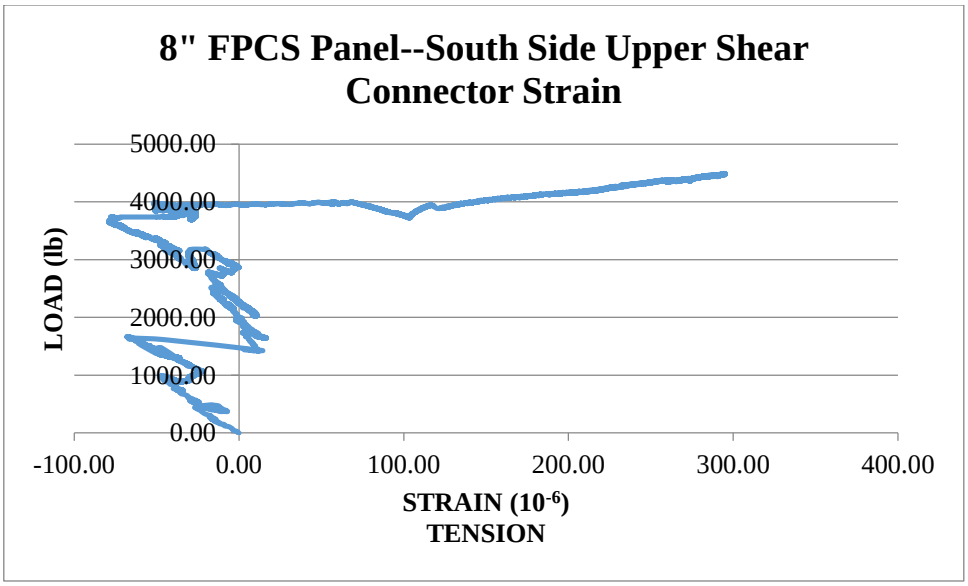


**Figure 237: 8" FPCS Panel--South Side Upper Shear Connector Strain**

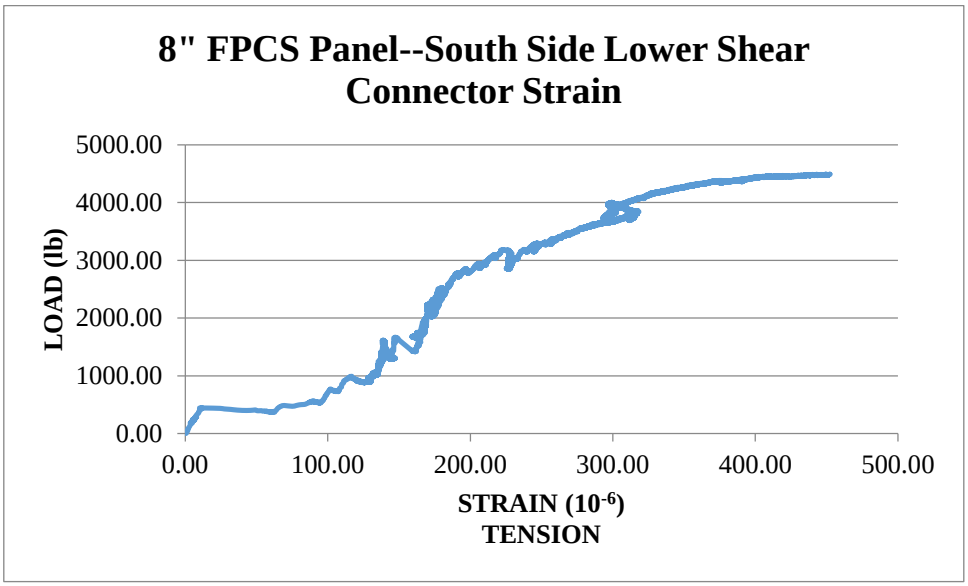


**Figure 238: 8" FPCS Panel--South Side Lower Shear Connector Strain**

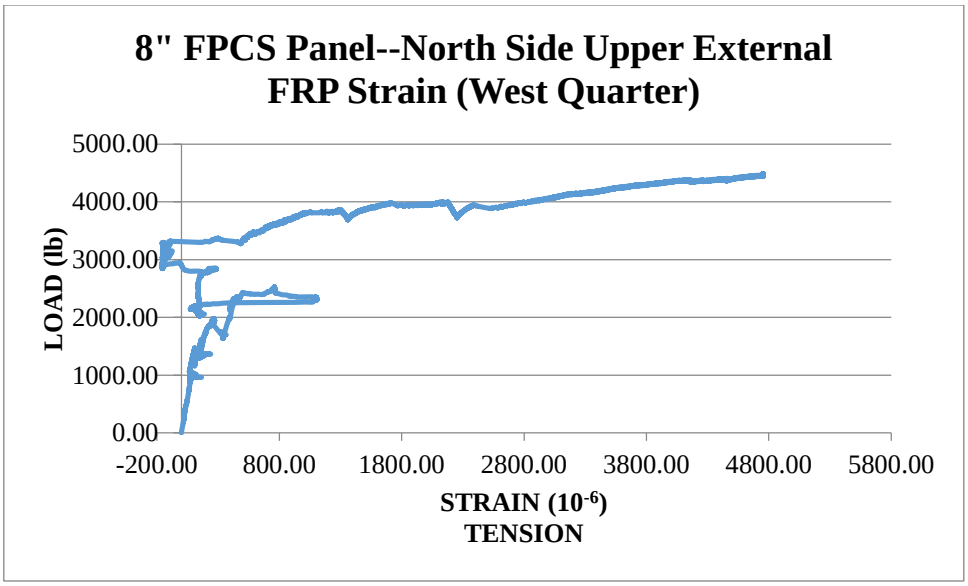


**Figure 239: 8" FPCS Panel--North Side Upper External FRP Strain (West Quarter)**

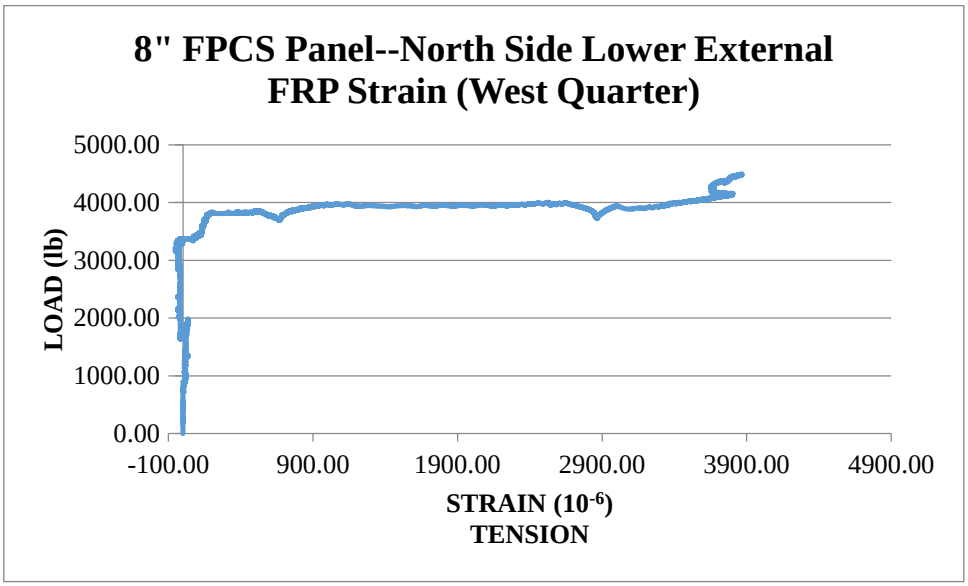


**Figure 240: 8" FPCS Panel--North Side Lower External FRP Strain (West Quarter)**

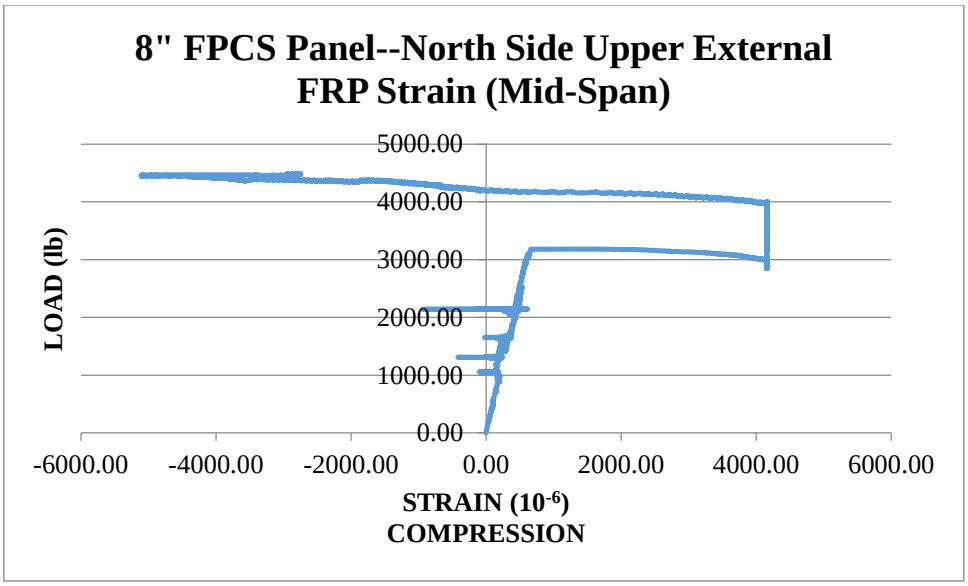


**Figure 241: 8" FPCS Panel--North Side Upper External FRP Strain (Mid-Span)**

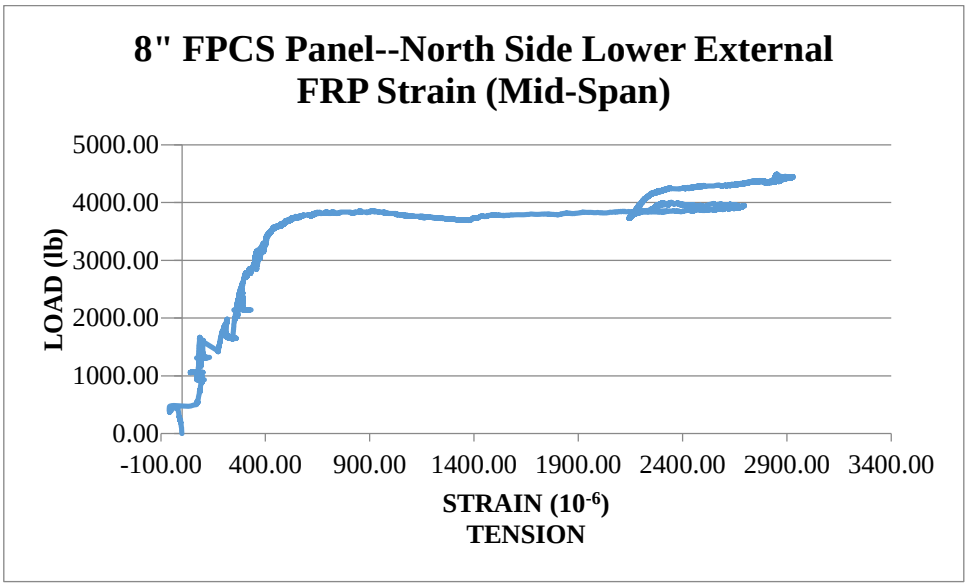


**Figure 242: 8" FPCS Panel--North Side Lower External FRP Strain (Mid-Span)**

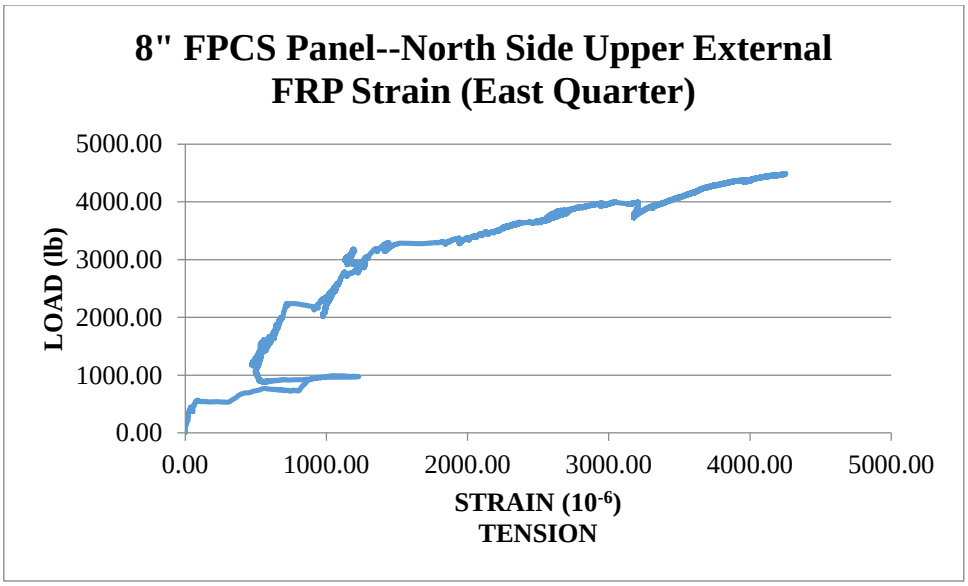


**Figure 243: 8" FPCS Panel--North Side Upper External FRP Strain (East Quarter)**

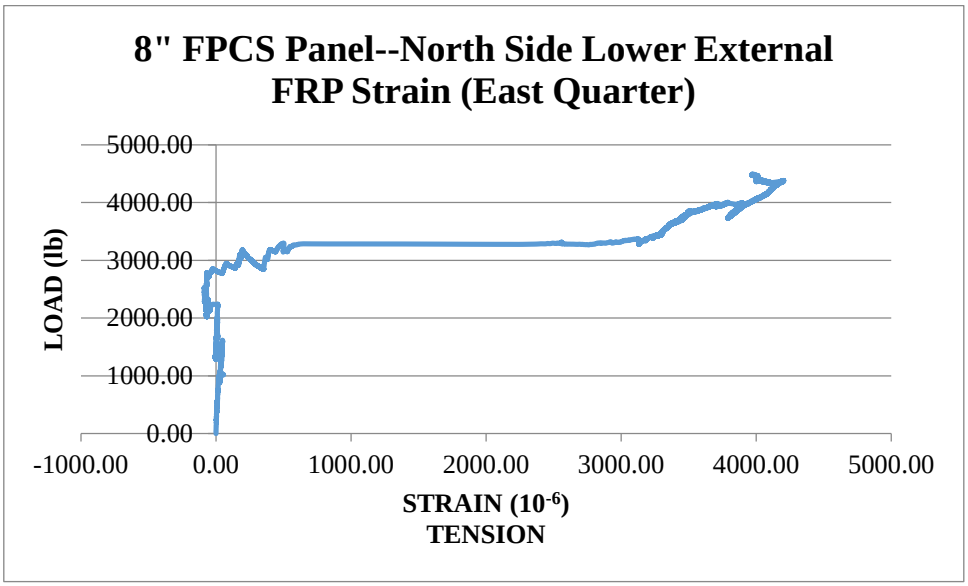


**Figure 244: 8" FPCS Panel--North Side Lower External FRP Strain (East Quarter)**

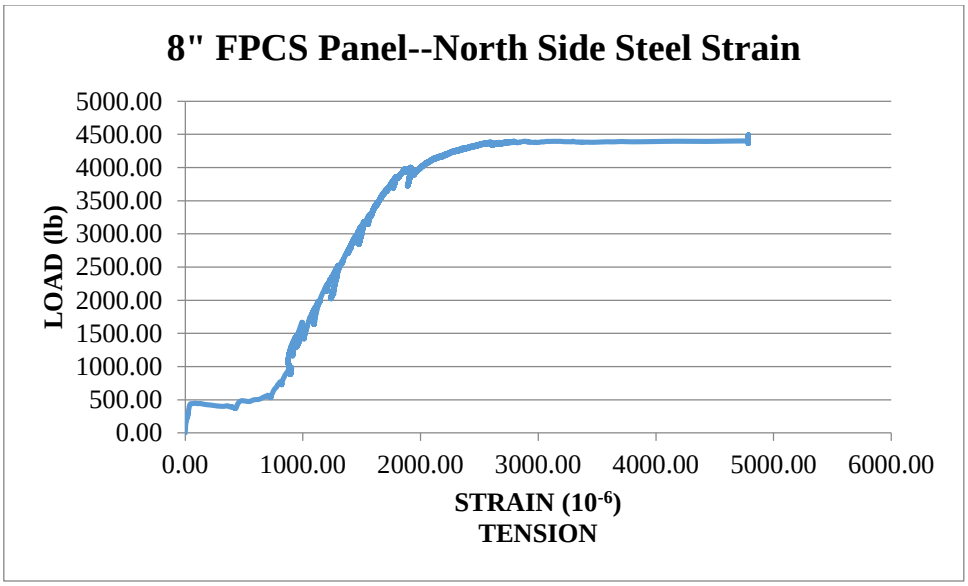


**Figure 245: 8" FPCS Panel--North Side Steel Strain**

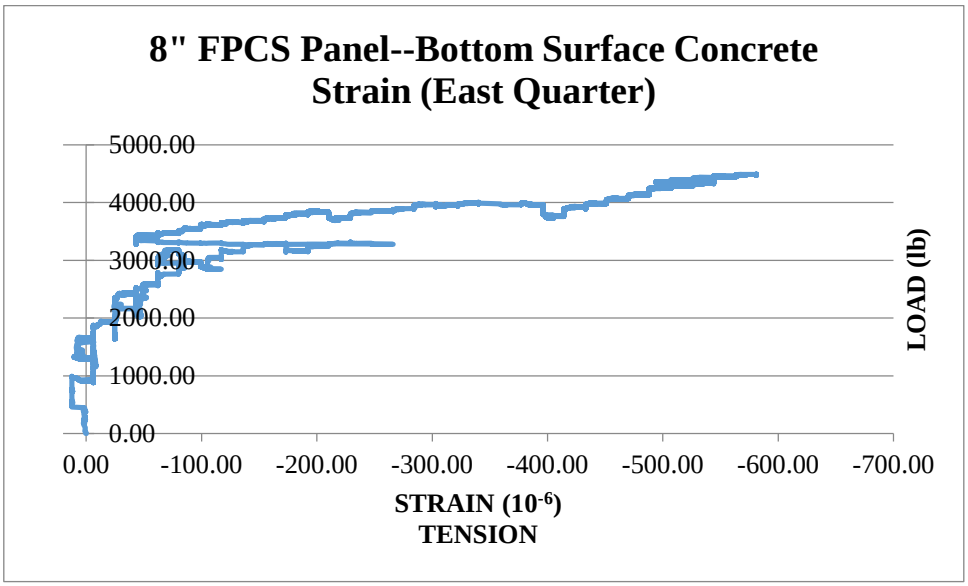


**Figure 246: 8" FPCS Panel--Bottom Surface Concrete Strain (East Quarter)**

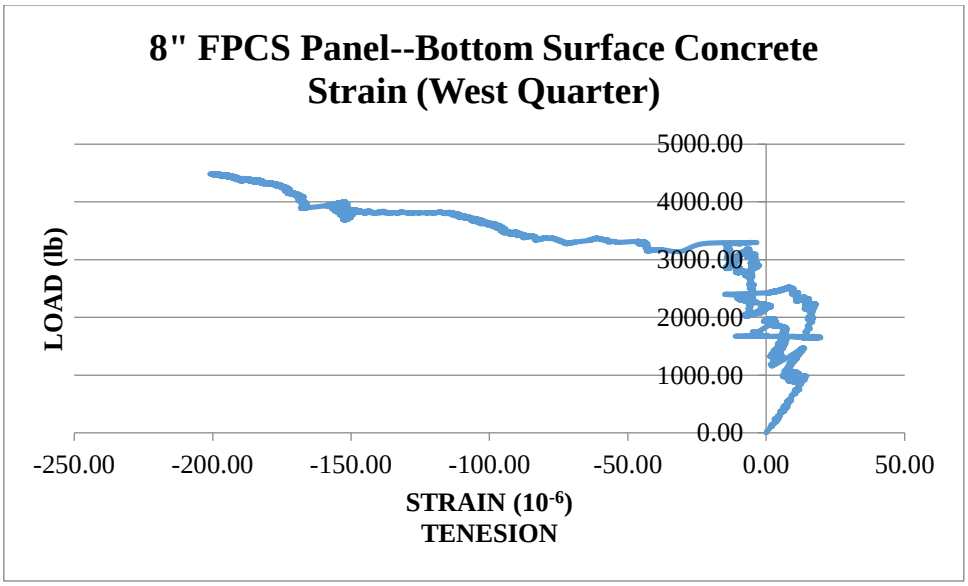


**Figure 247: 8" FPCS Panel--Bottom Surface Concrete Strain (West Quarter)**

## FULL SCALE —10" FPCS

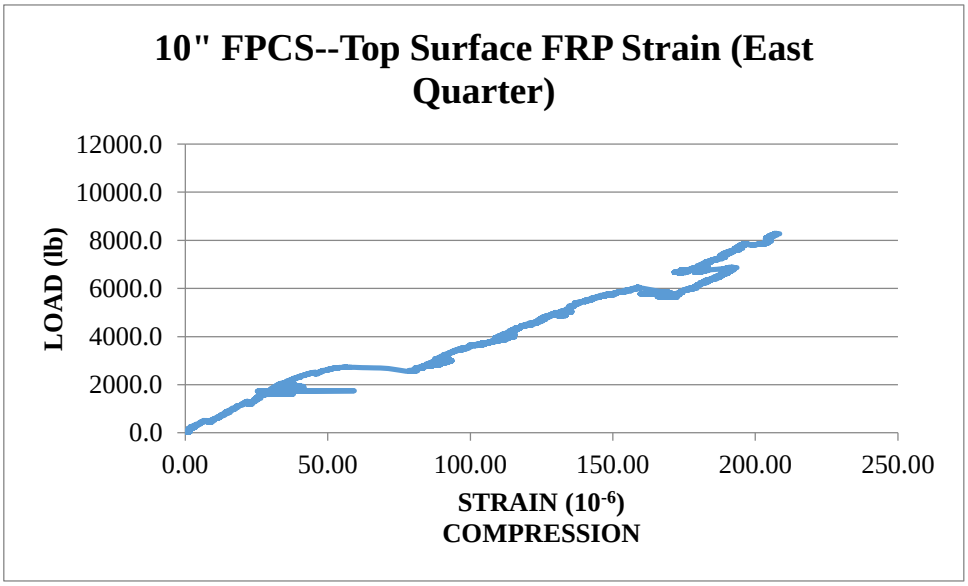


**Figure 248: 10" FPCS--Top Surface FRP Strain (East Quarter)**

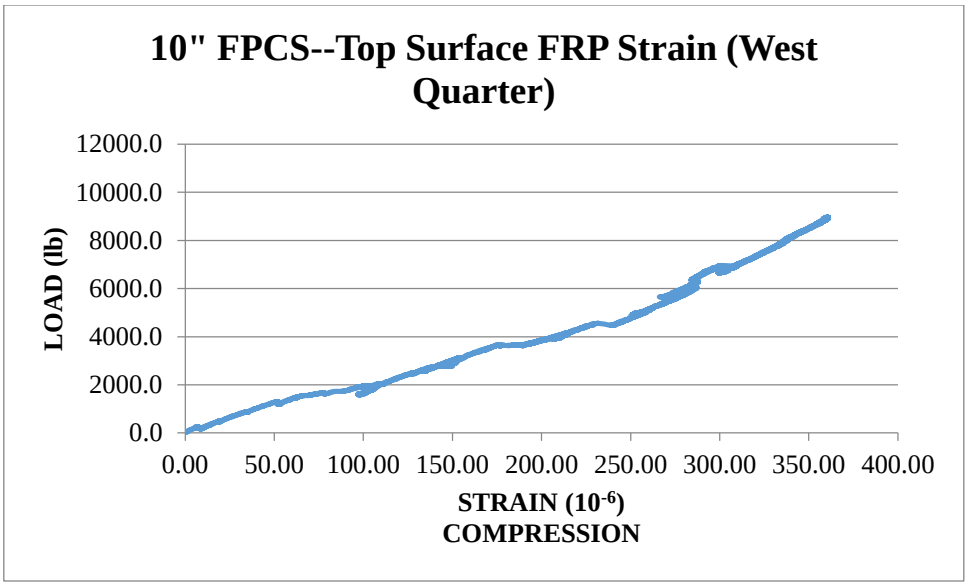


**Figure 249: 10" FPCS--Top Surface FRP Strain (West Quarter)**

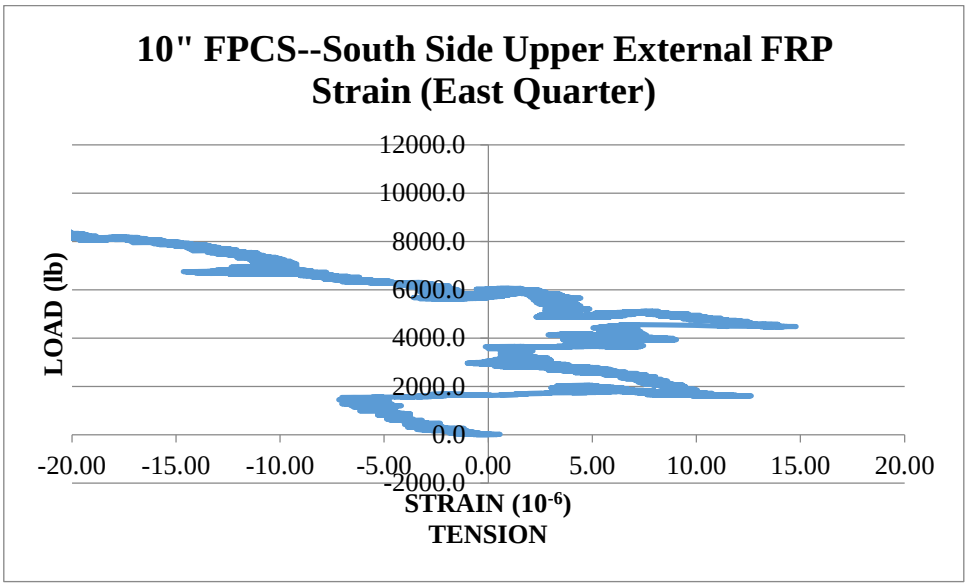


**Figure 250: 10" FPCS--South Side Upper External FRP Strain (East Quarter)**

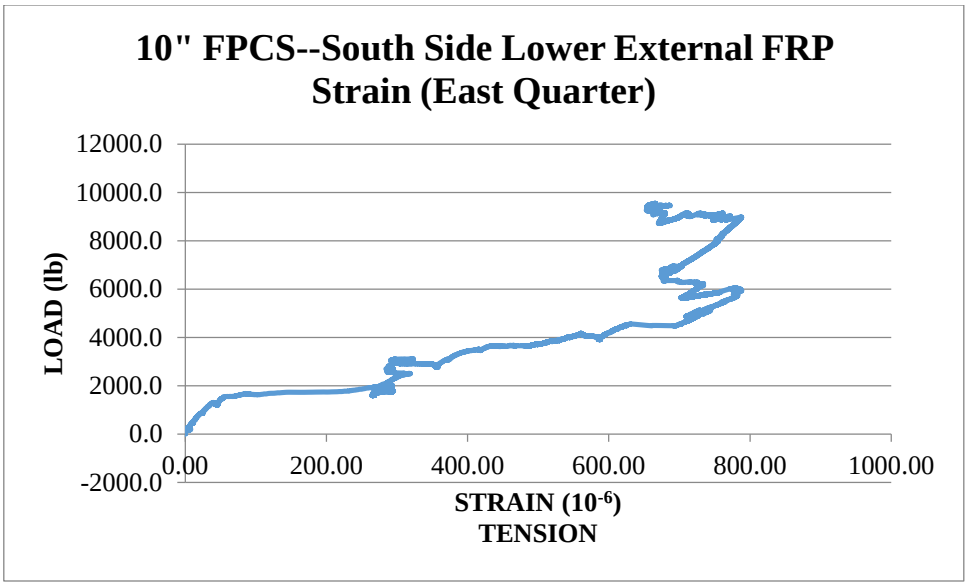


**Figure 251: 10" FPCS--South Side Lower External FRP Strain (East Quarter)**

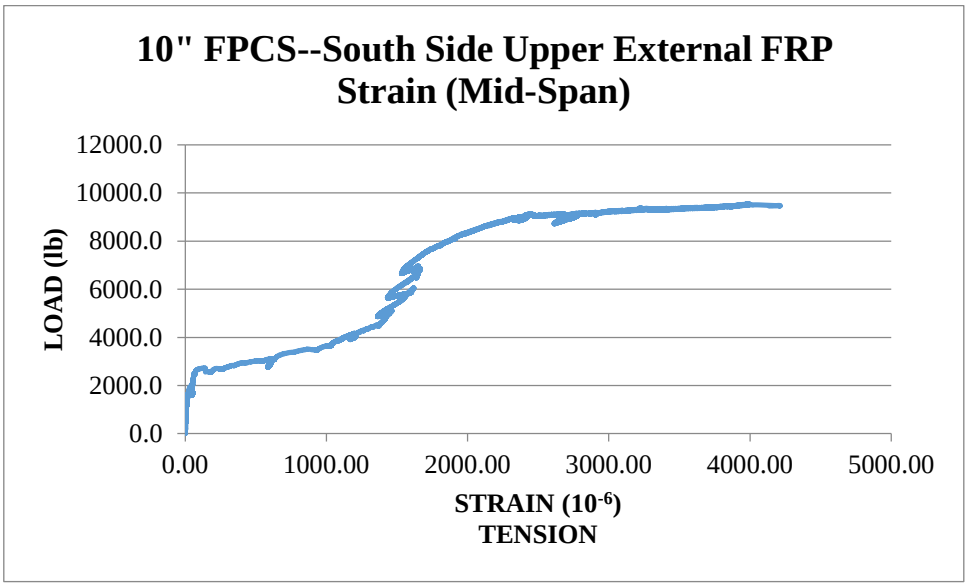


**Figure 252: 10" FPCS--South Side Upper External FRP Strain (Mid-Span)**

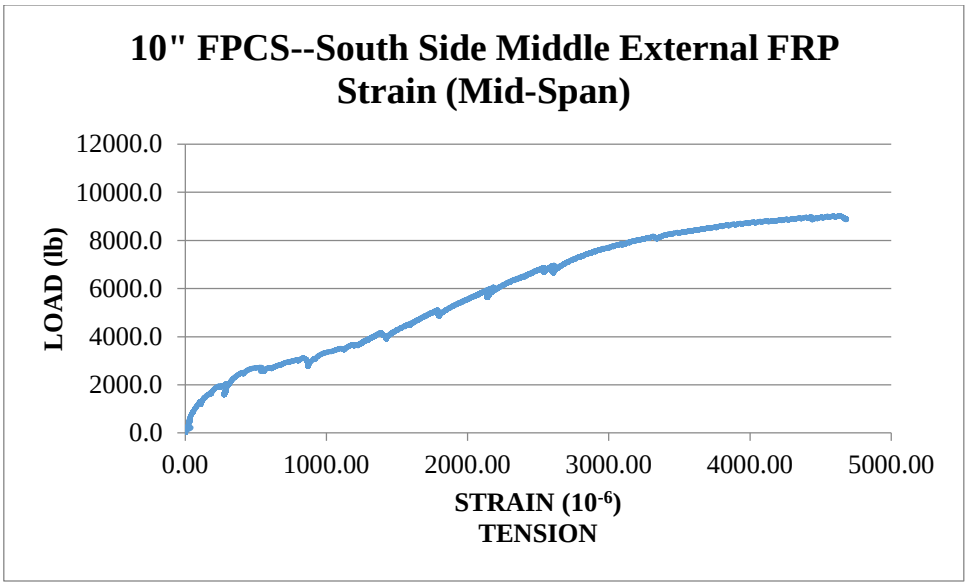


**Figure 253: 10" FPCS--South Side Middle External FRP Strain (Mid-Span)**

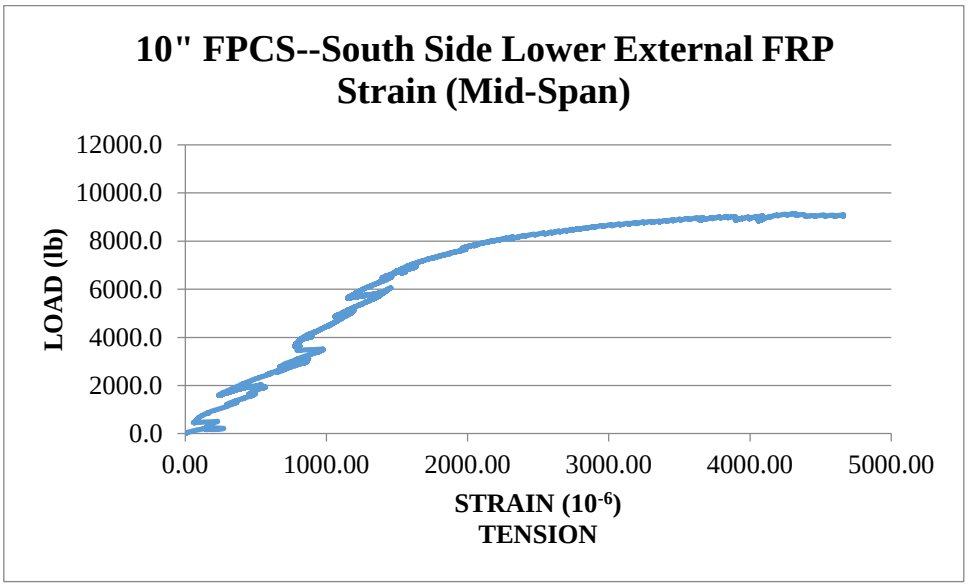


**Figure 254: 10" FPCS--South Side Lower External FRP Strain (Mid-Span)**

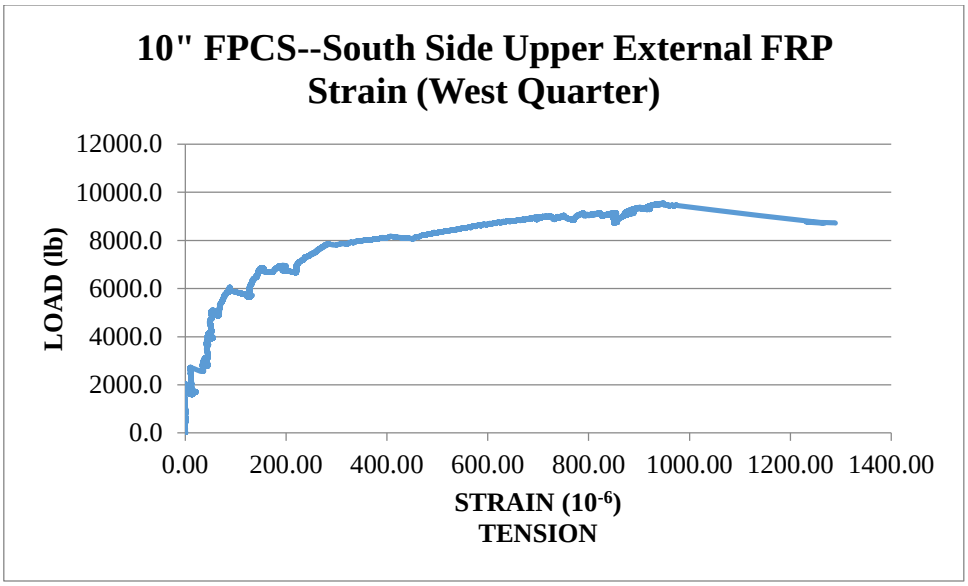


**Figure 255: 10" FPCS--South Side Upper External FRP Strain (West Quarter)**

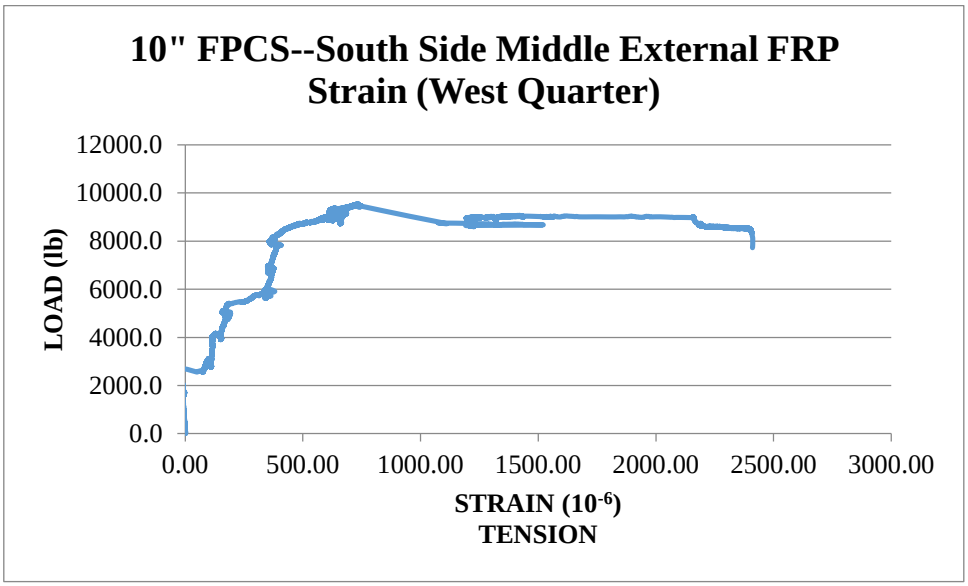


**Figure 256: 10" FPCS--South Side Middle External FRP Strain (West Quarter)**

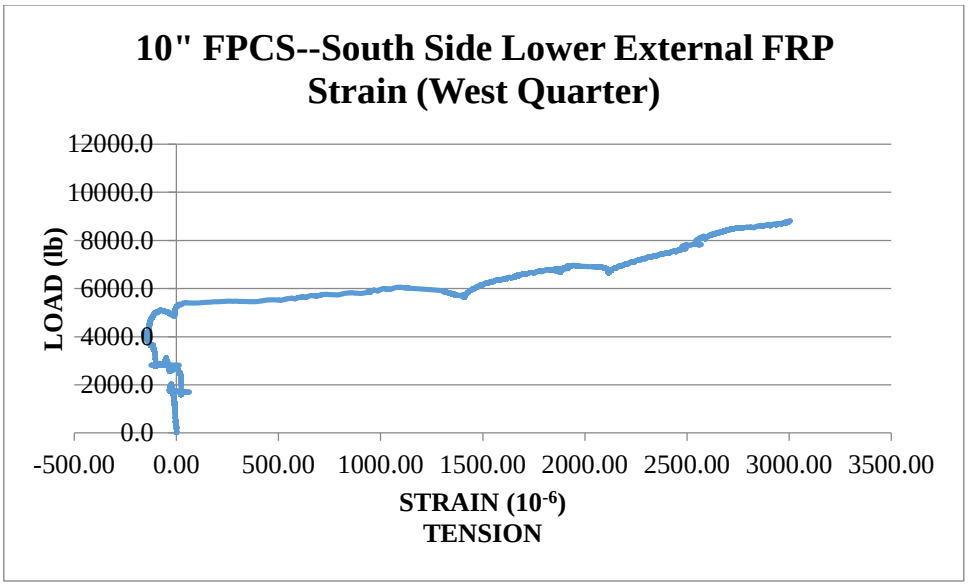


**Figure 257: 10" FPCS--South Side Lower External FRP Strain (West Quarter)**

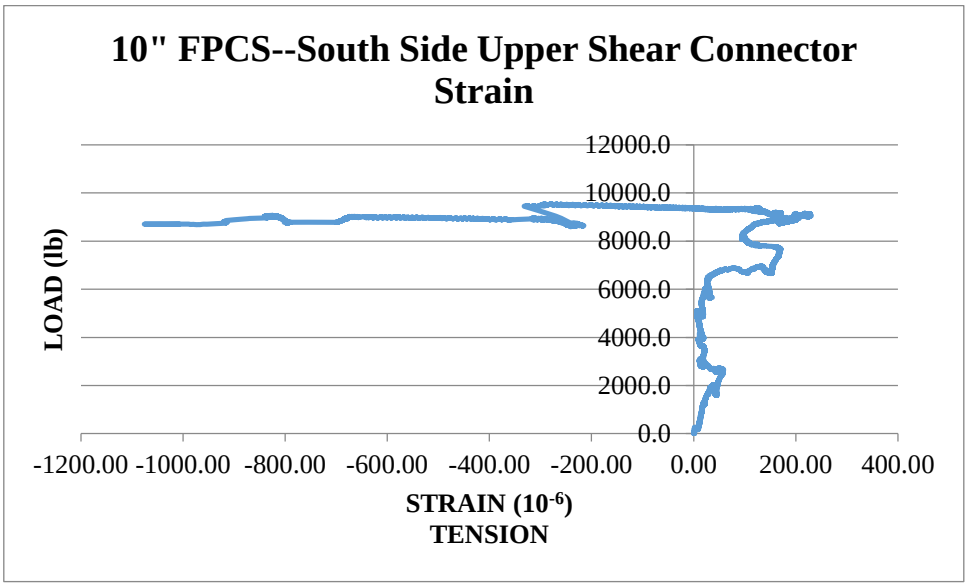


**Figure 258: 10" FPCS--South Side Upper Shear Connector Strain**

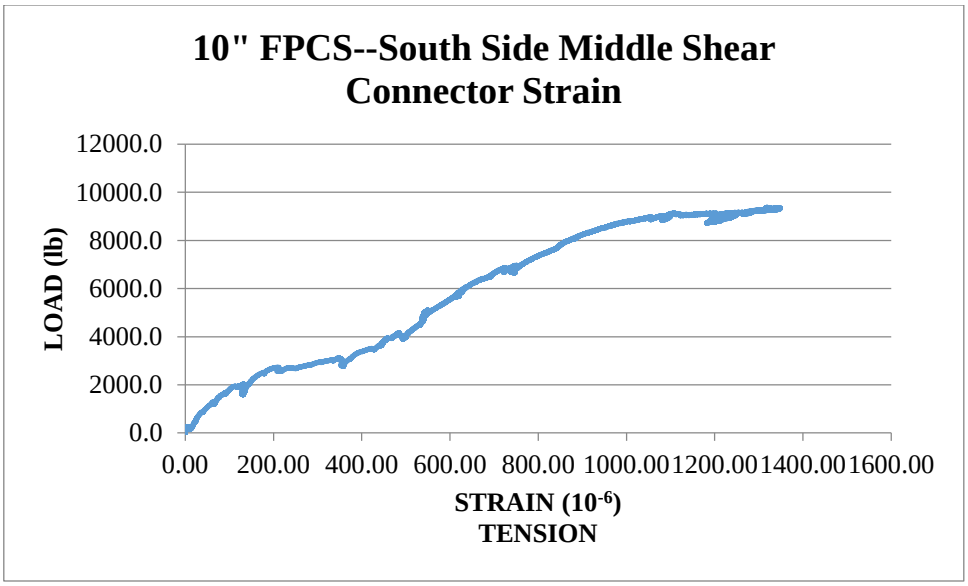


**Figure 259: 10" FPCS--South Side Middle Shear Connector Strain**

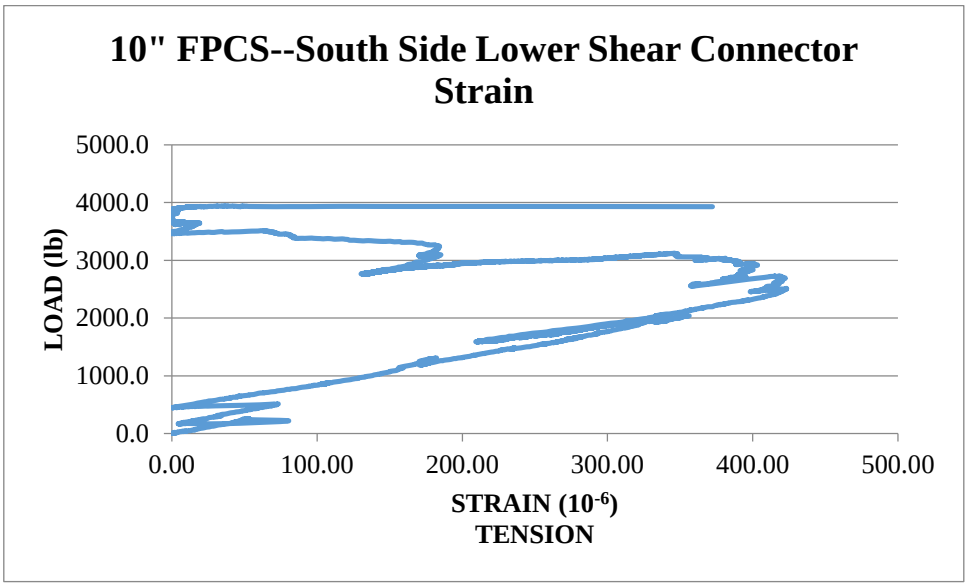


**Figure 260: 10" FPCS--South Side Lower Shear Connector Strain**

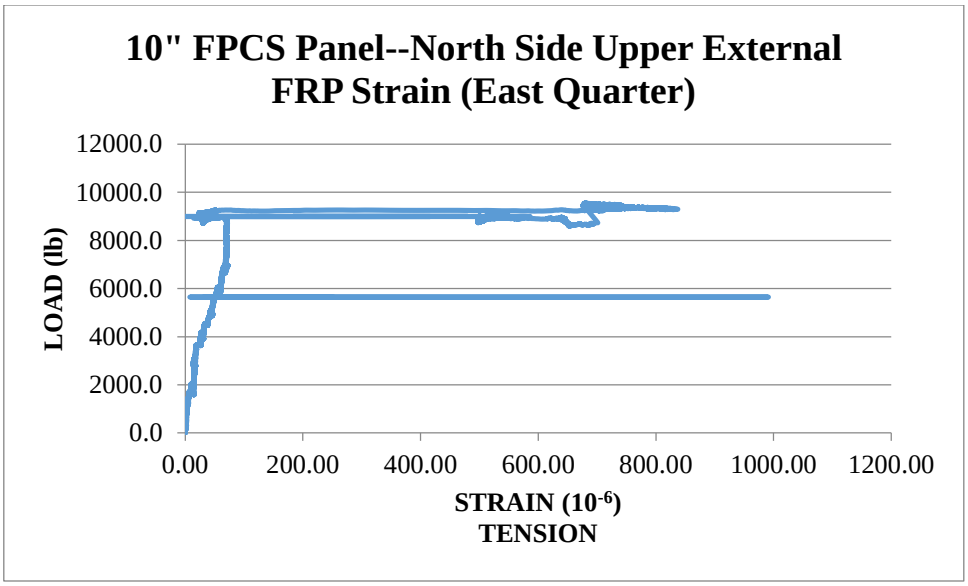


**Figure 261: 10" FPCS Panel--North Side Upper External FRP Strain (East Quarter)**

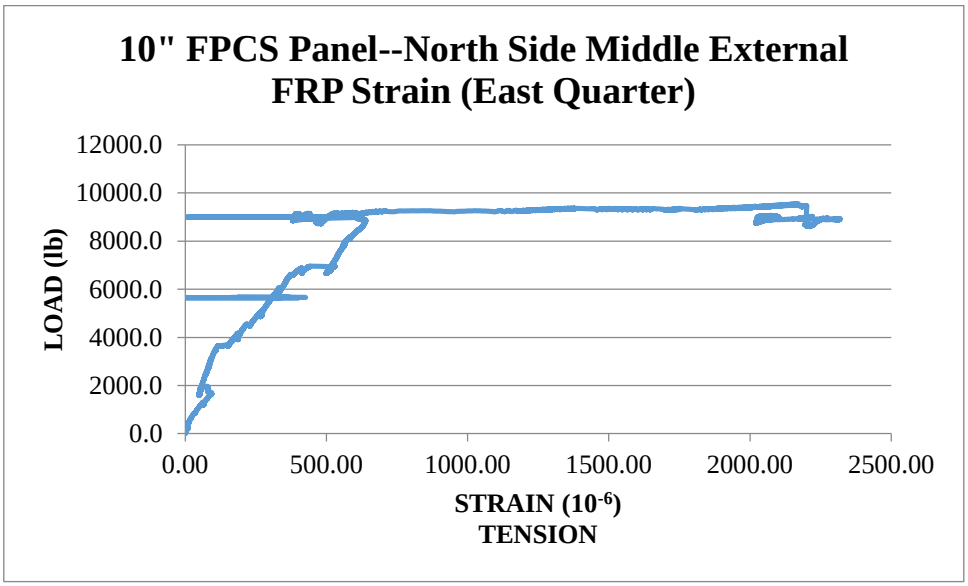


**Figure 262: 10" FPCS Panel--North Side Middle External FRP Strain (East Quarter)**

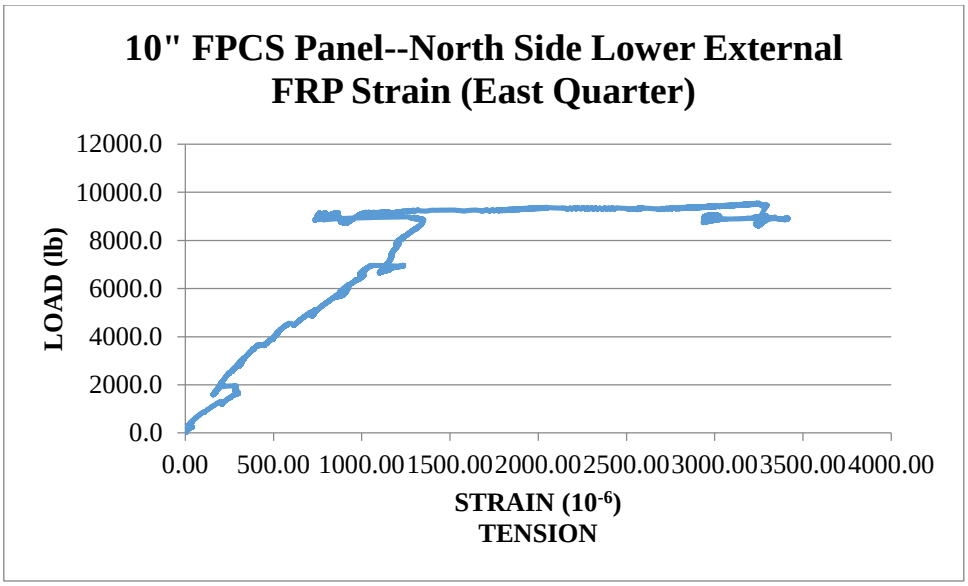


**Figure 263: 10" FPCS Panel--North Side Lower External FRP Strain (East Quarter)**

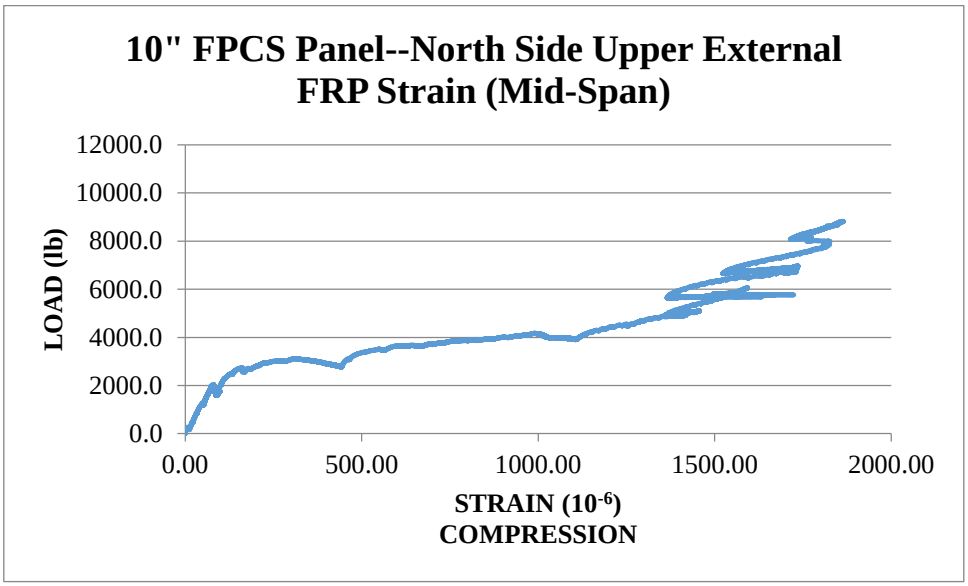


**Figure 264: 10" FPCS Panel--North Side Upper External FRP Strain (Mid-Span)**

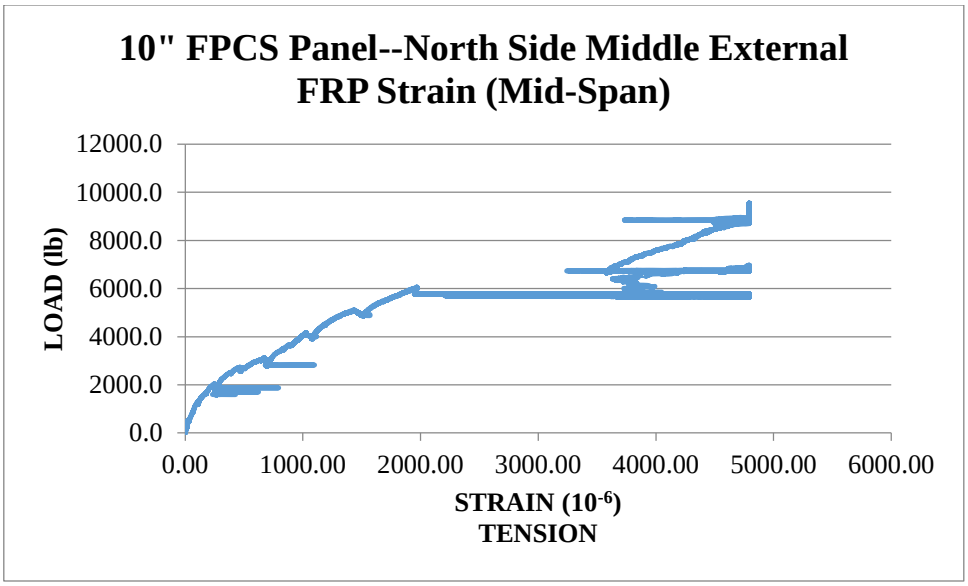


**Figure 265: 10" FPCS Panel--North Side Middle External FRP Strain (Mid-Span)**

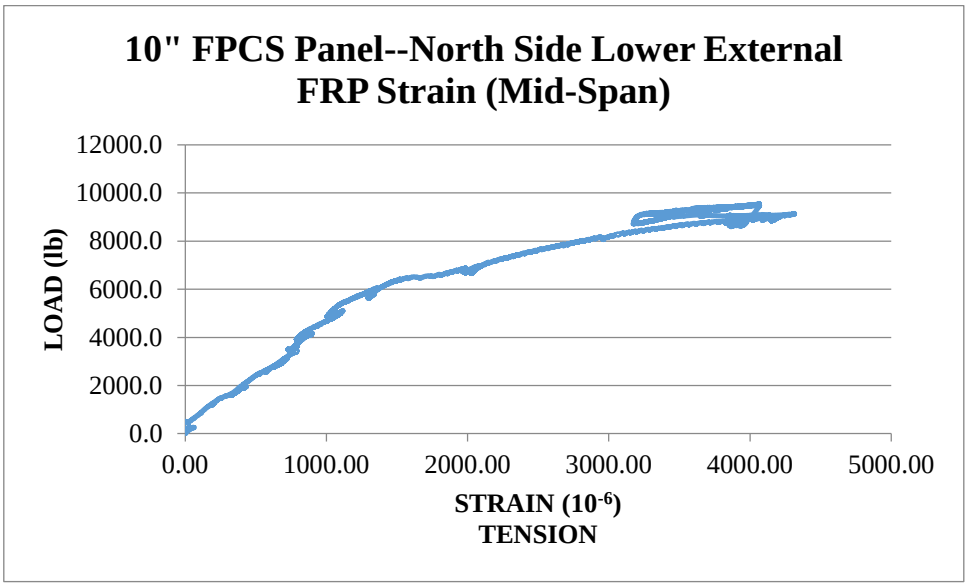


**Figure 266: 10" FPCS Panel--North Side Lower External FRP Strain (Mid-Span)**

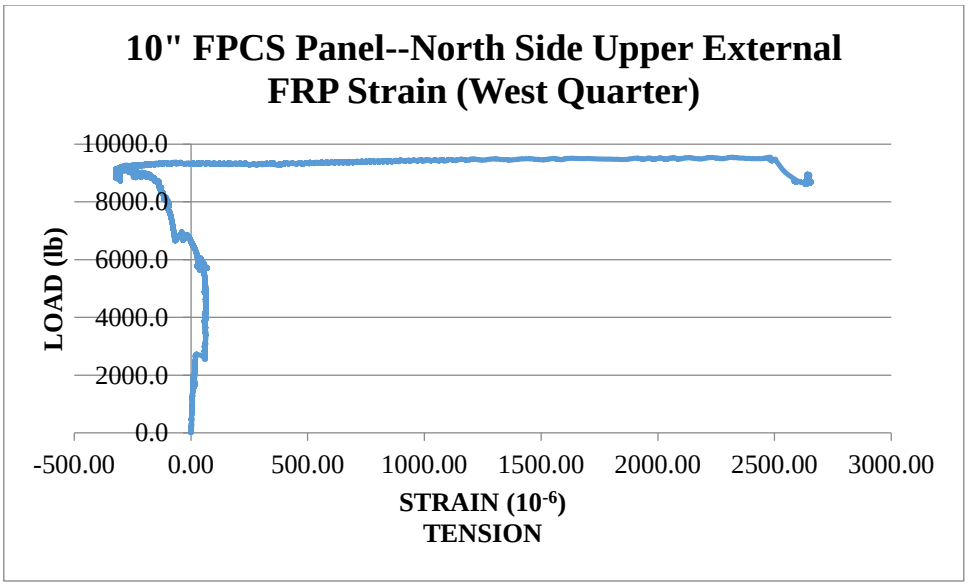


**Figure 267: 10" FPCS Panel--North Side Upper External FRP Strain (West Quarter)**

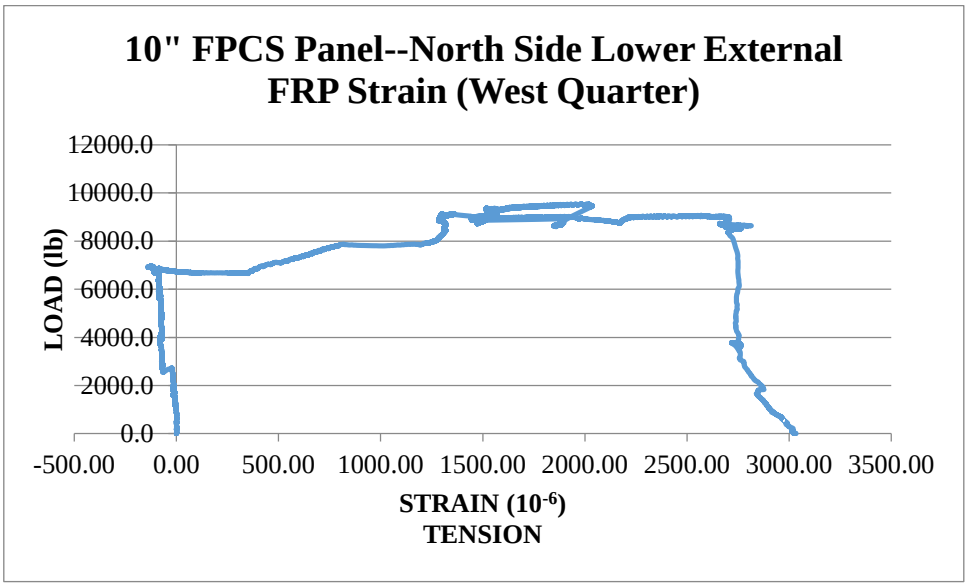


**Figure 268: 10" FPCS Panel--North Side Lower External FRP Strain (West Quarter)**

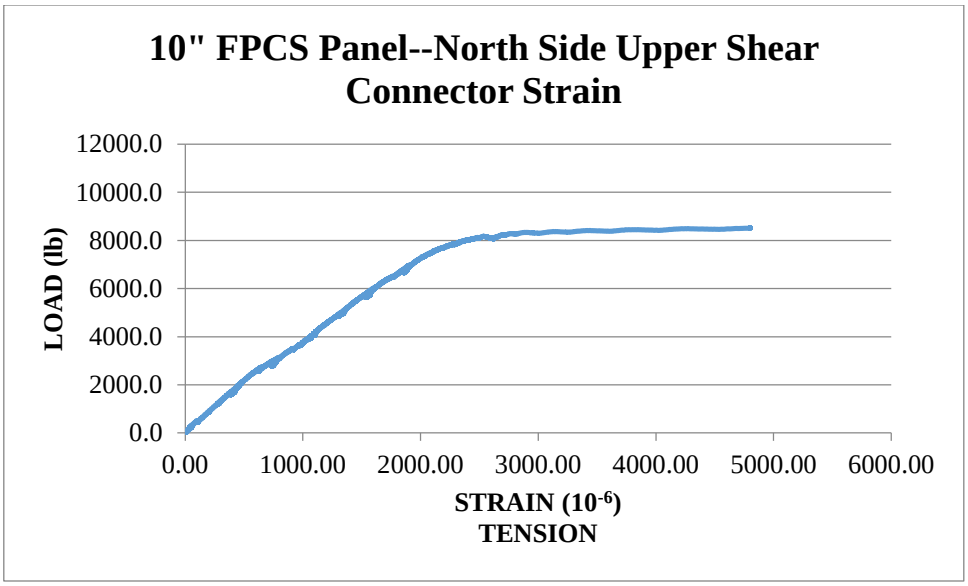


**Figure 269: 10" FPCS Panel--North Side Upper Shear Connector Strain**

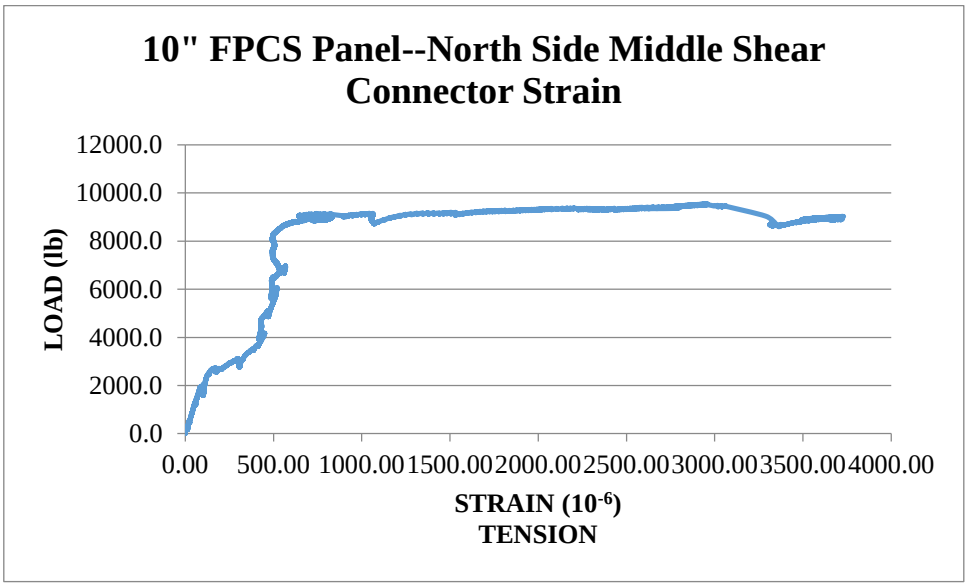


**Figure 270: 10" FPCS Panel--North Side Middle Shear Connector Strain**

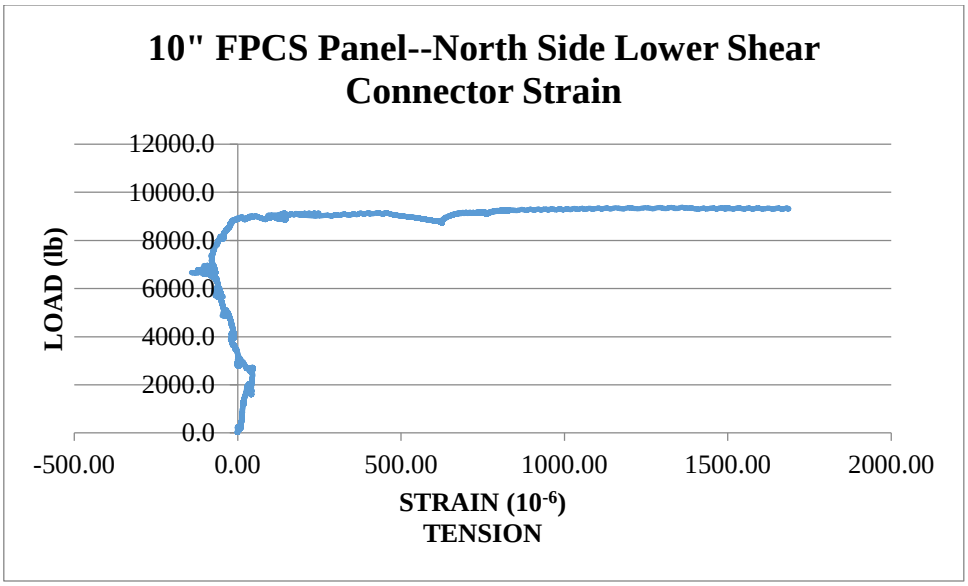


**Figure 271: 10" FPCS Panel--North Side Lower Shear Connector Strain**

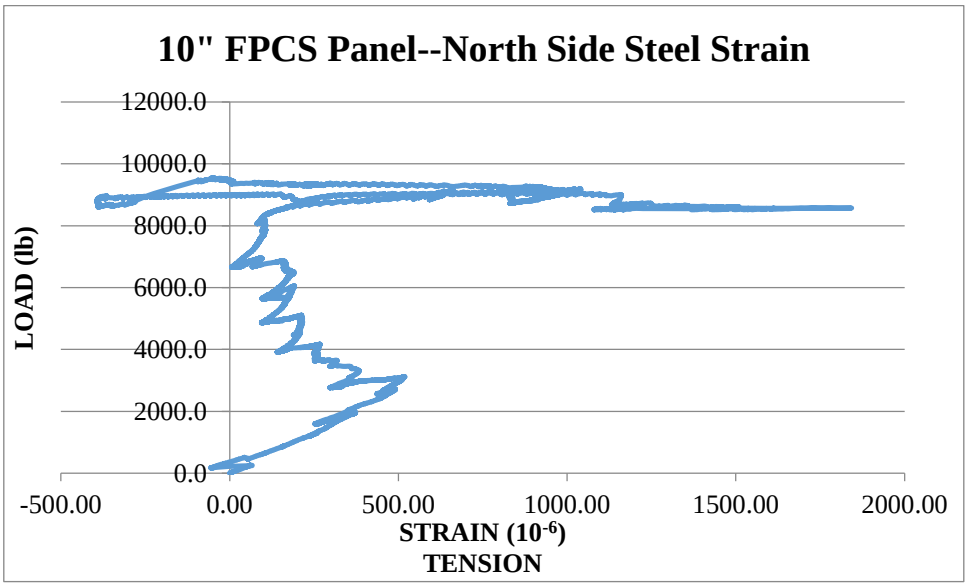


**Figure 272: 10" FPCS Panel--North Side Steel Strain**

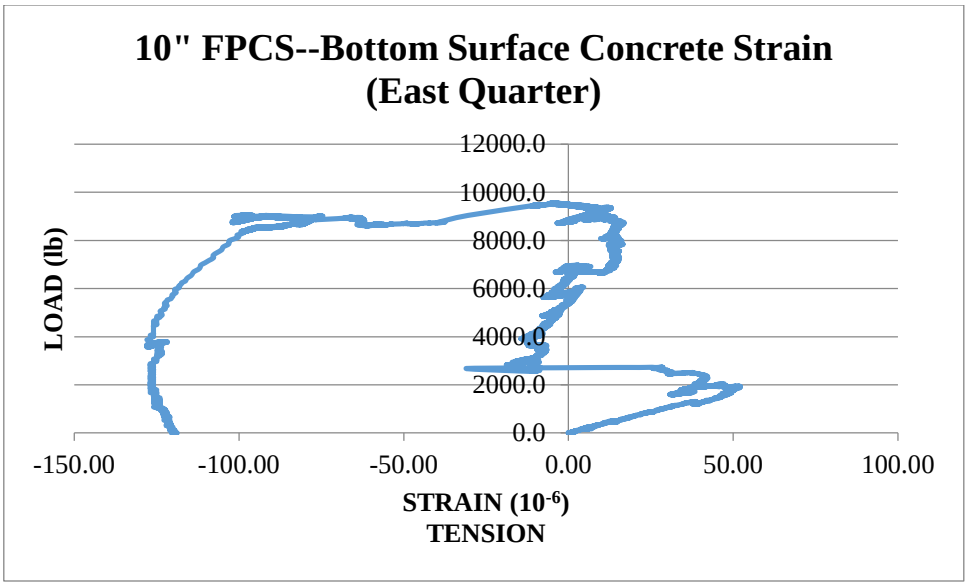


**Figure 273: 10" FPCS--Bottom Surface Concrete Strain (East Quarter)**

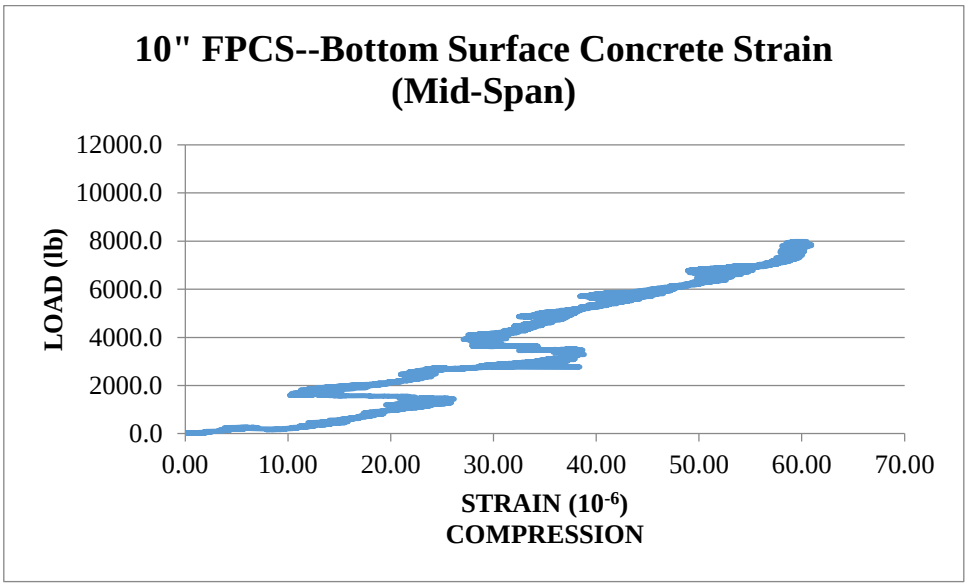


**Figure 274: 10" FPCS--Bottom Surface Concrete Strain (Mid-Span)**

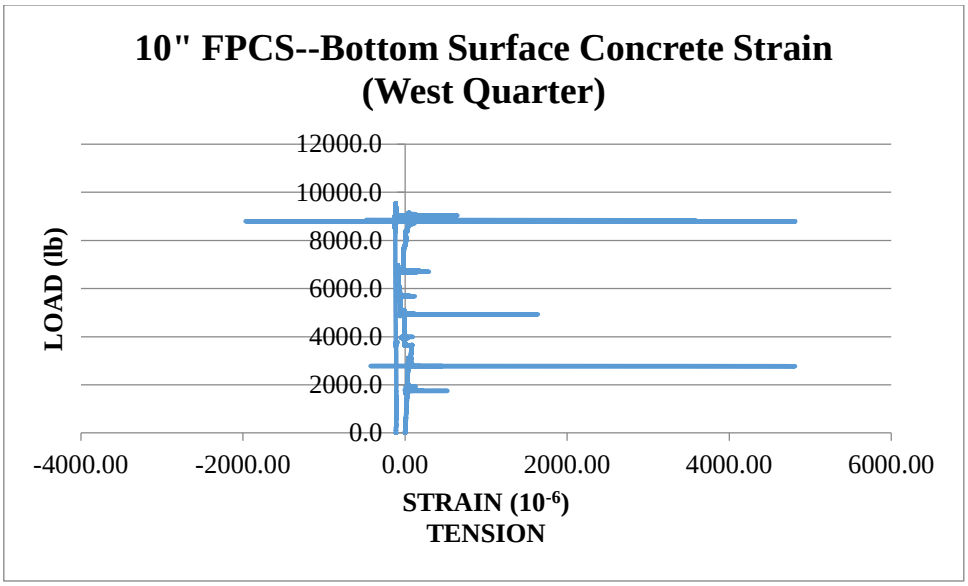


**Figure 275: 10" FPCS--Bottom Surface Concrete Strain (West Quarter)**

# STRENGTH/STIFFNESS CORRECTION

**Given:** $A_s := 2\cdot(0.31in^2)$ $A_{sc} := 2\cdot(0.20in^2)$ $f_y := 60000psi$ $f_c := 4120psi$

$b := 24in$ $d := 8.9375in$ $d_{prime} := 1in$ $E_s := 29000ksi$

**Step 1:**

Determine the correction factor necessary to equate theoretical values to experimental results.

$$a := \frac{A_s\cdot f_y}{0.85\cdot f_c\cdot b} = 0.443\cdot in \qquad c := \frac{a}{0.85} = 0.521\cdot in$$

$$\varepsilon_s := 0.003\cdot\left(\frac{d_{prime} - c}{c}\right) = 2.761\times 10^{-3} \qquad f_s := E_s\cdot\varepsilon_s = 8.008\times 10^{4}\cdot psi$$

$$C_s := A_{sc}\cdot(f_s - 0.85\cdot f_c) = 30.631\cdot kip$$

$$C_c := 0.85\cdot f_c\cdot b\cdot a = 37.2\cdot kip$$

$$M_n := C_c\cdot\left(d - \frac{a}{2}\right) + C_s\cdot(d - d_{prime}) = 47.281\cdot kip\cdot ft$$

$$P_{cr} := \frac{2M_n}{4.5ft} = 21.014\cdot kip$$

$P_{experiment} := 20.5kip$

Correction Factor: $CF := \frac{P_{experiment}}{P_{cr}} = 0.976$

**Step 2:**

Determine the theoretical strength of a solid slab with $f_c' = 2815psi$ for the 8" and $f_c' = 4807.5psi$ for the 10" thicknesses.

**8" Thick Specimen:**

**Given:** $A_s := 2\cdot(0.31in^2)$ $A_{sc} := 2\cdot(0.20in^2)$ $f_y := 60000psi$ $f_c := 2815psi$

$b := 24in$ $d := 6.9375in$ $d_{prime} := 1in$ $E_s := 29000ksi$

**Solution:**

$$a := \frac{A_s\cdot f_y}{0.85\cdot f_c\cdot b} = 0.648\cdot in \qquad c := \frac{a}{0.85} = 0.762\cdot in$$

$$\varepsilon_s := 0.003\cdot\left(\frac{d_{prime} - c}{c}\right) = 9.365\times 10^{-4} \qquad f_s := E_s\cdot\varepsilon_s = 2.716\times 10^{4}\cdot psi$$

$C_s := A_{sc} \cdot (f_s - 0.85 \cdot f_c) = 9.906 \cdot kip$

$C_c := 0.85 \cdot f_c \cdot b \cdot a = 37.2 \cdot kip$

$M_n := C_c \cdot \left(d - \frac{a}{2}\right) + C_s \cdot (d - d_{prime}) = 25.403 \cdot kip \cdot ft$

$P_{cr} := \frac{2M_n}{8ft} = 6.351 \cdot kip$

Critical Load with Correction Factor:

$P_{experiment} := P_{cr} \cdot CF = 6.196 \cdot kip$

**10" Thick Specimen:**

**Given:** $A_s := 2 \cdot (0.31in^2)$ $A_{sc} := 2 \cdot (0.20in^2)$ $f_y := 60000psi$ $f_c := 4807.5psi$

$b := 24in$ $d := 8.9375in$ $d_{prime} := 1in$ $E_s := 29000ksi$

**Solution:**

$a := \frac{A_s \cdot f_y}{0.85 \cdot f_c \cdot b} = 0.379 \cdot in$ $c := \frac{a}{0.85} = 0.446 \cdot in$

$\varepsilon_s := 0.003 \cdot \left(\frac{d_{prime} - c}{c}\right) = 3.723 \times 10^{-3}$ $f_s := E_s \cdot \varepsilon_s = 1.08 \times 10^5 \cdot psi$

$C_s := A_{sc} \cdot (f_s - 0.85 \cdot f_c) = 41.549 \cdot kip$

$C_c := 0.85 \cdot f_c \cdot b \cdot a = 37.2 \cdot kip$

$M_n := C_c \cdot \left(d - \frac{a}{2}\right) + C_s \cdot (d - d_{prime}) = 54.601 \cdot kip \cdot ft$

$P_{cr} := \frac{2M_n}{8ft} = 13.65 \cdot kip$

Critical Load with Correction Factor:

$P_{experiment} := P_{cr} \cdot CF = 13.317 \cdot kip$

**Step 3:**
Determine the theoretical deflection of a solid 8" slab using experimental data.

**Given:** $P := 1.4kip$ $E := 57000\cdot\sqrt{2815} = 3.024 \times 10^{6}$ $I := 1024in^{4}$ $L := 16ft$

$E := 3.024 \times 10^{6}psi$

**Solution**

$$\Delta := \frac{P\cdot L^{3}}{48\cdot E\cdot I} = 0.067\cdot in$$

**Apply this deflection to the stiffness equation for the Full Scale 8" FPCS Panel**

**Step 4:**
Determine the theoretical deflection of a solid 10" slab using experimental data.

**Given:** $P := 1.4kip$ $E := 57000\cdot\sqrt{4807.5} = 3.952 \times 10^{6}$ $I := 2000in^{4}$ $L := 16ft$

$E := 3.952 \times 10^{6}psi$

**Solution**

$$\Delta := \frac{P\cdot L^{3}}{48\cdot E\cdot I} = 0.026\cdot in$$

**Apply this deflection to the stiffness equation for the Full Scale 10" FPCS Panel**

# ALLOWABLE LOAD/DEFLECTION CALCULATIONS

**Given:** $I_{10} := 2000in^4$ $E_{10} := 3.952 \times 10^6 psi$ $L := 16ft$

$I_8 := 1024in^4$ $E_8 := 3.024 \times 10^6 psi$

**Step 1:**
Determine the maximum deflection permitted for a solid slab given the effective length.

$$\Delta_{max} := \frac{L}{360} = 0.533 \cdot in$$

**Step 2:**
Collect the maximum load applied to produce the maximum allowable deflection.

8" FPCS Panel: $P_{cr8} := 1.864kip$

10" FPCS Panel: $P_{cr10} := 3.845kip$

**Step 3:**
Using the test data, determine the equivalent distributed load which can be safely applied to each specimen and remain within the allowable maximum deflection.

Point Load: $\Delta = \frac{P \cdot L^3}{48 \cdot E \cdot I}$ Distributed Load: $\Delta = \frac{5 \cdot w \cdot L^4}{384 \cdot E \cdot I}$

Therefore: $w = \frac{384 \cdot P}{240 \cdot L}$

Solve Distributed Load Equivalents:

8" FPCS Panel: $w_8 := \frac{384 \cdot P_{cr8}}{240 \cdot L} = 0.186 \cdot \frac{kip}{ft}$

10" FPCS Panel: $w_{10} := \frac{384 \cdot P_{cr10}}{240 \cdot L} = 0.385 \cdot \frac{kip}{ft}$

Because this occurs over a width of 2-feet, therefore, the following calculations can be made:

8" FPCS Panel: $Allowable\_Load_{8in} := \frac{w_8}{2ft} = 93.2 \cdot \frac{lbf}{ft^2}$

10" FPCS Panel: $Allowable\_Load_{10in} := \frac{w_{10}}{2ft} = 192.25 \cdot \frac{lbf}{ft^2}$

**Step 4:**

Using the test data, determine the equivalent distributed load which will result in the failure of the specimens.

Failure Loads (from experiments):

8" FPCS Panel: $P_{cr8} := 4.493kip$

10" FPCS Panel: $P_{cr10} := 9.553kip$

Point Load: $\Delta = \frac{P \cdot L^3}{48 \cdot E \cdot I}$ Distributed Load: $\Delta = \frac{5 \cdot w \cdot L^4}{384 \cdot E \cdot I}$

Therefore: $w = \frac{384 \cdot P}{240 \cdot L}$

Solve Distributed Load Equivalents:

8" FPCS Panel: $w_8 := \frac{384 \cdot P_{cr8}}{240 \cdot L} = 0.449 \cdot \frac{kip}{ft}$

10" FPCS Panel: $w_{10} := \frac{384 \cdot P_{cr10}}{240 \cdot L} = 0.955 \cdot \frac{kip}{ft}$

Because this occurs over a width of 2-feet, therefore, the following calculations can be made:

8" FPCS Panel: $Failure\_Load_{8in} := \frac{w_8}{2ft} = 224.65 \cdot \frac{lbf}{ft^2}$

10" FPCS Panel: $Failure\_Load_{10in} := \frac{w_{10}}{2ft} = 477.65 \cdot \frac{lbf}{ft^2}$

# APPENDIX 4

This appendix presents all corrections, material properties, calculations and additional graphs/figures pertaining to Chapter 6.

# ALLOWABLE CREEP DEFLECTION (6 MONTHS)

**Given:** $b := 24in$ $h_1 := 10in$ $h_2 := 8in$ $A'_s := 0.40in^2$ $L := 9ft$

**Required:** Determine the sustained load factor for both 10" and 8" solid slabs.

## Solution

Sustained Load Correction Factor (ACI 318-11, EQ 9-11): $\lambda_\Delta = \frac{\xi}{1 + 50 \cdot \rho'}$

Assuming a six month period: $\xi := 1.2$

Determine ρ' for 10" Solid Slab: $\rho'_1 := \frac{A'_s}{b \cdot h_1} = 1.667 \times 10^{-3}$

Determine ρ' for 8" Solid Slab: $\rho'_2 := \frac{A'_s}{b \cdot h_2} = 2.083 \times 10^{-3}$

Determine Correction Factor for 10" Solid Slab: $\lambda_{\Delta 1} := \frac{\xi}{1 + 50 \cdot \rho'_1} = 1.108$

Determine Correction Factor for 8" Solid Slab: $\lambda_{\Delta 2} := \frac{\xi}{1 + 50 \cdot \rho'_2} = 1.087$

Determine the Maximum Allowable Creep Deflection:

10" Solid Slab: $\Delta_{10in} := \frac{L}{360} \cdot \lambda_{\Delta 1} = 0.332in$

8" Solid Slab: $\Delta_{8in} := \frac{L}{360} \cdot \lambda_{\Delta 2} = 0.326in$

The creep specimen will be analyzed to determine if they are within these requirements.

## ADDITIONAL DEFLECTION DATA

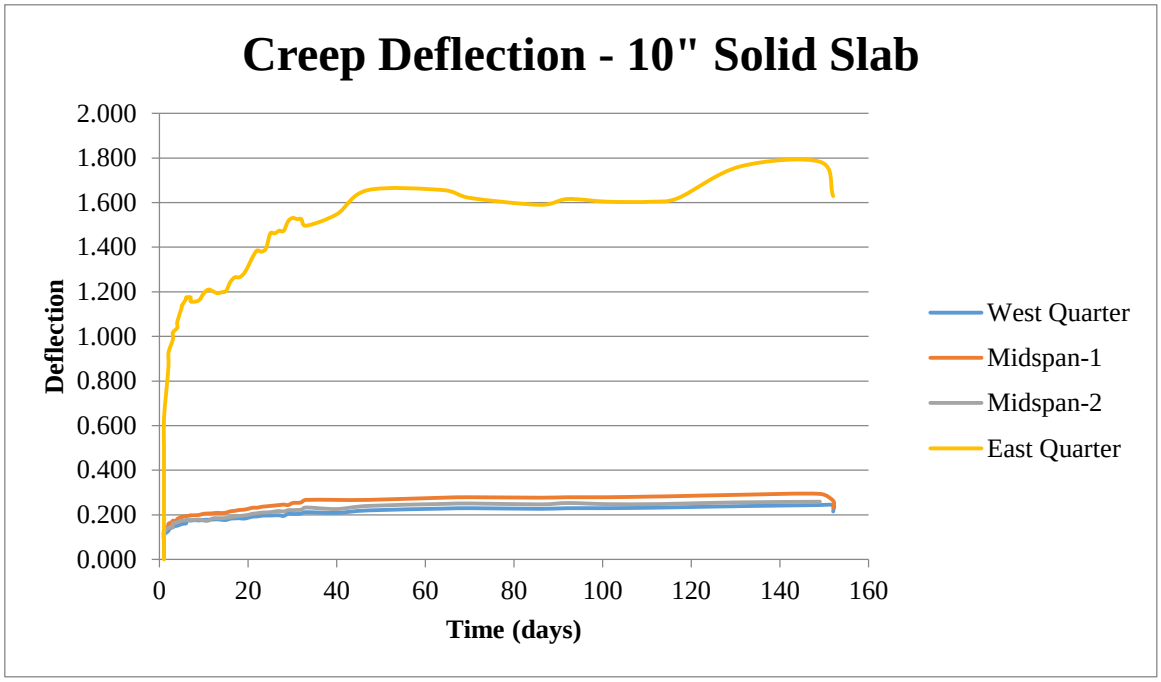


**Figure 276: Creep Deflection—10” Solid Slab**

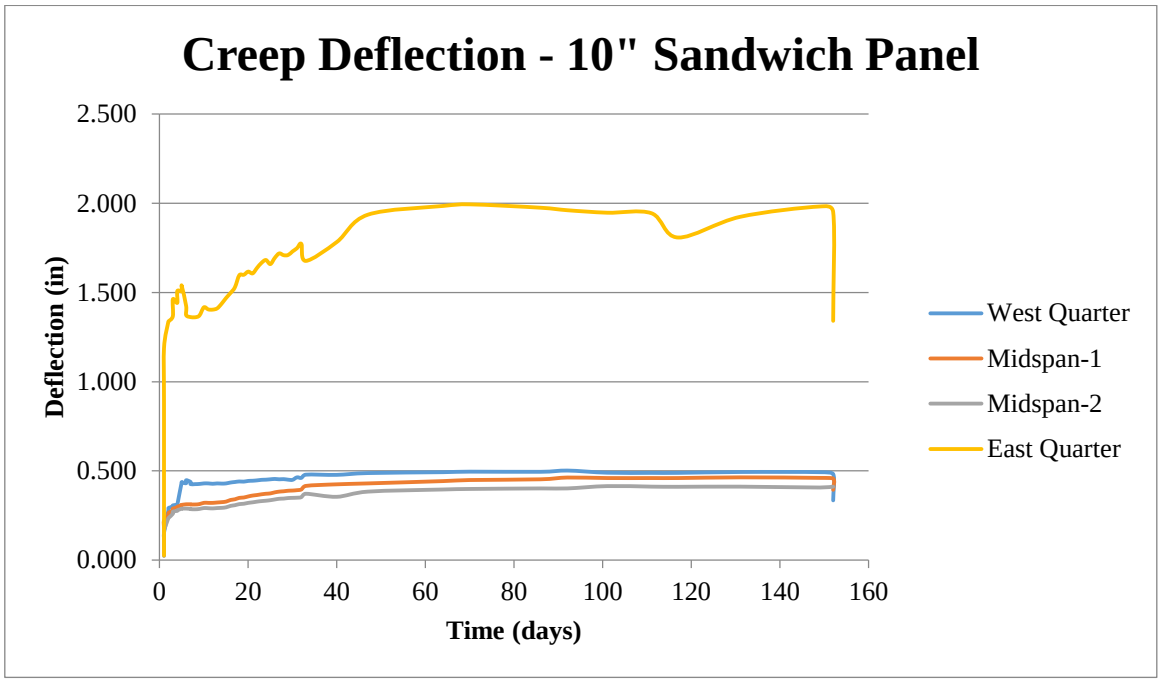


**Figure 277: Creep Deflection—10” Sandwich Panel**

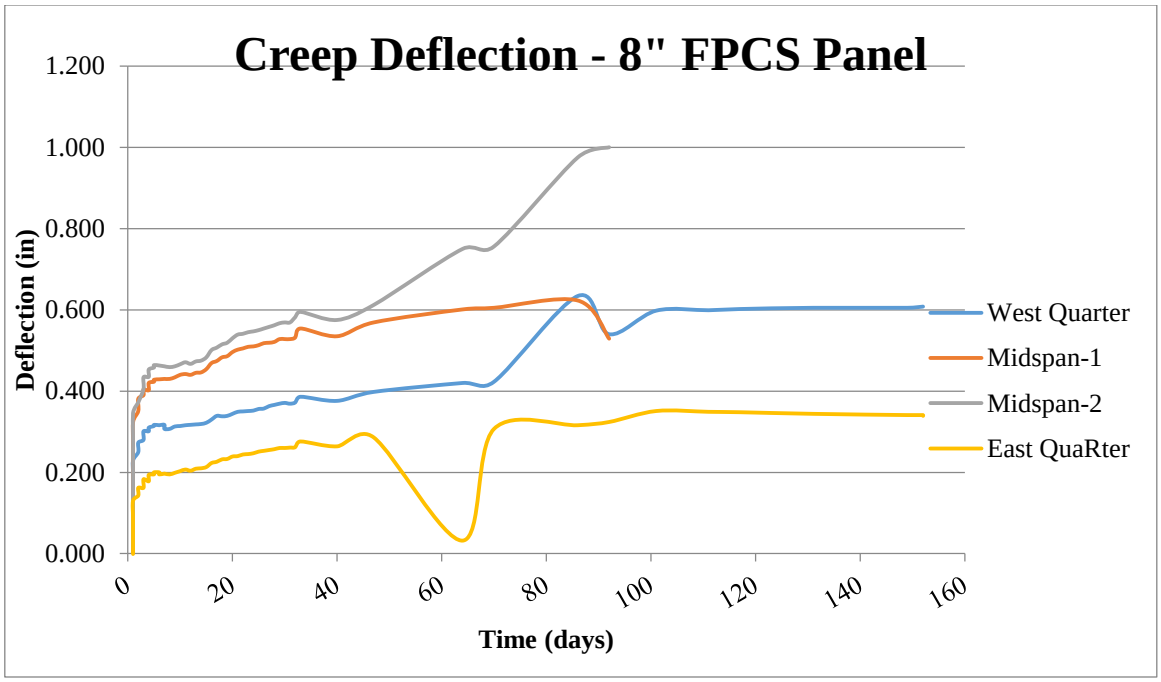


**Figure 278: Creep Deflection—8" FPCS Panel**

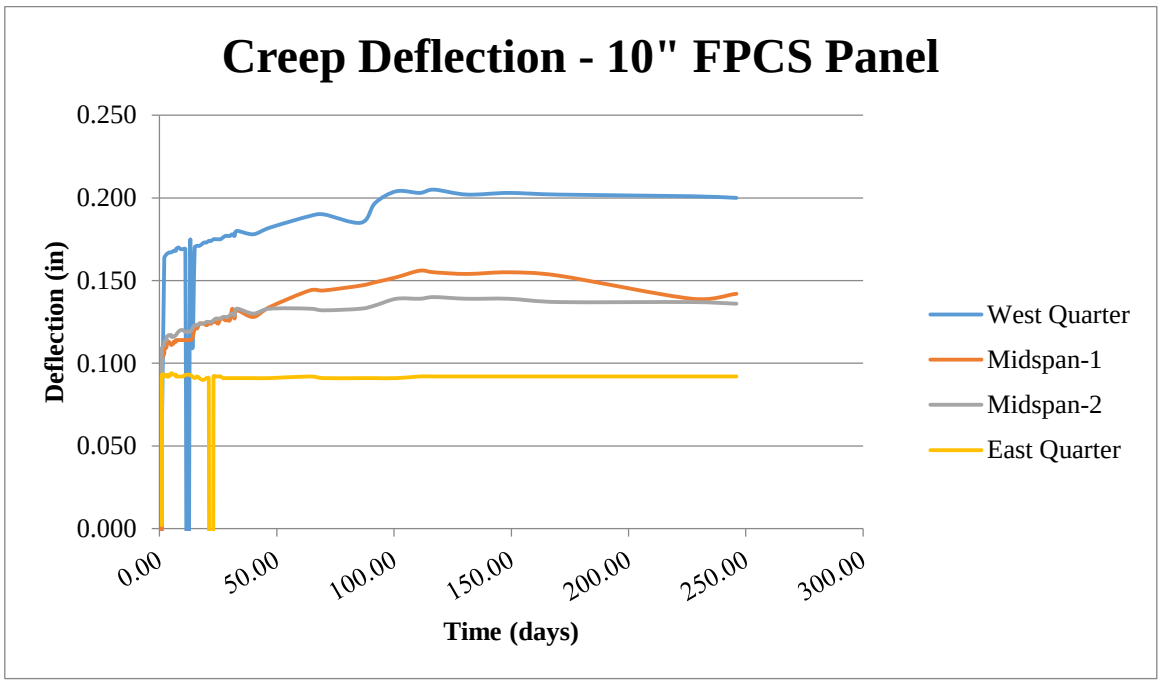


**Figure 279:Creep Deflection—10" FPCS Panel**

# ADDITIONAL STRAIN DATA

## SOLID SLAB

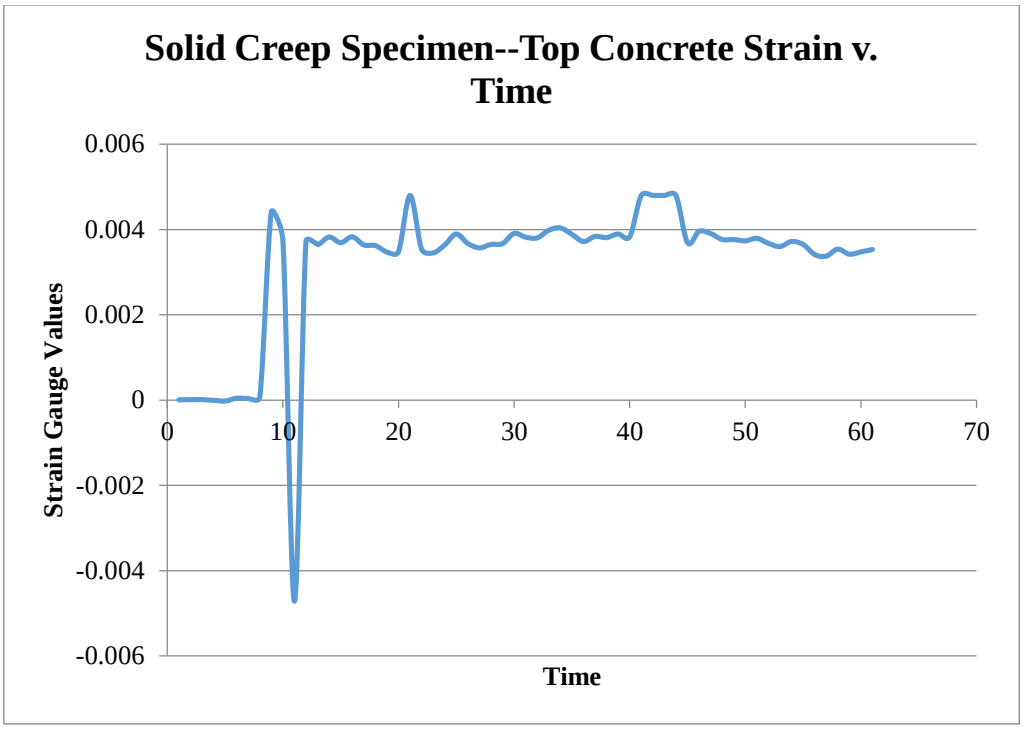


**Figure 280: Solid Creep Specimen—Top Concrete Strain v. Time**

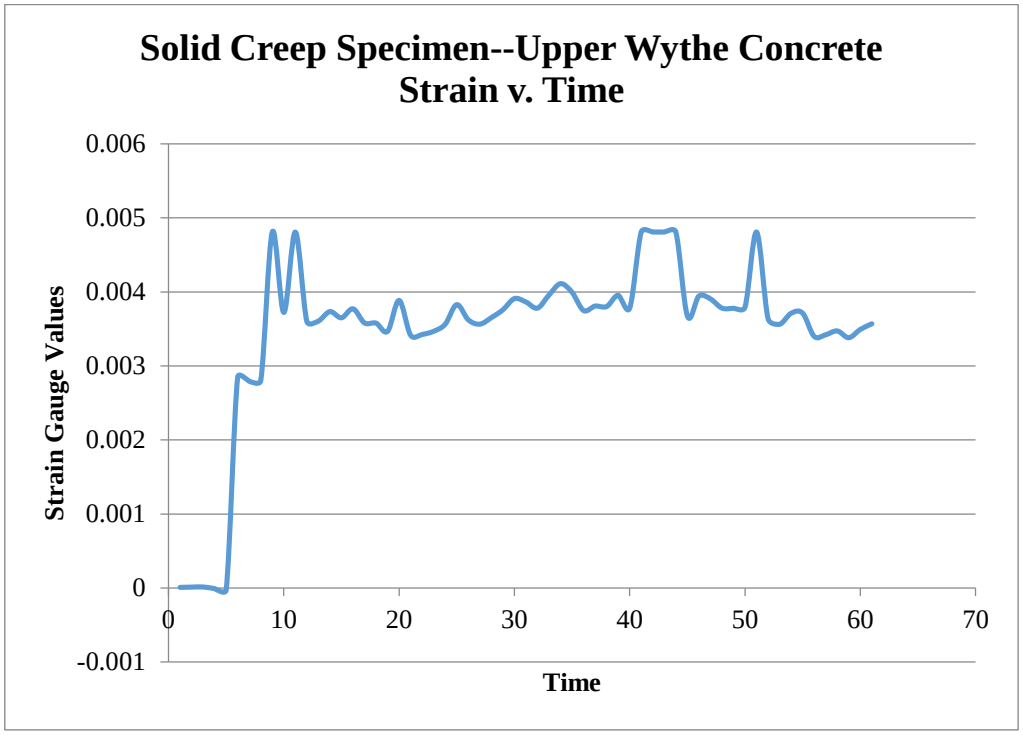


**Figure 281: Solid Creep Specimen—Upper Wythe Concrete Strain v. Time**


**Figure 282: Solid Creep Specimen—Tension Steel Strain v. Time**

## 10” SANDWICH PANEL

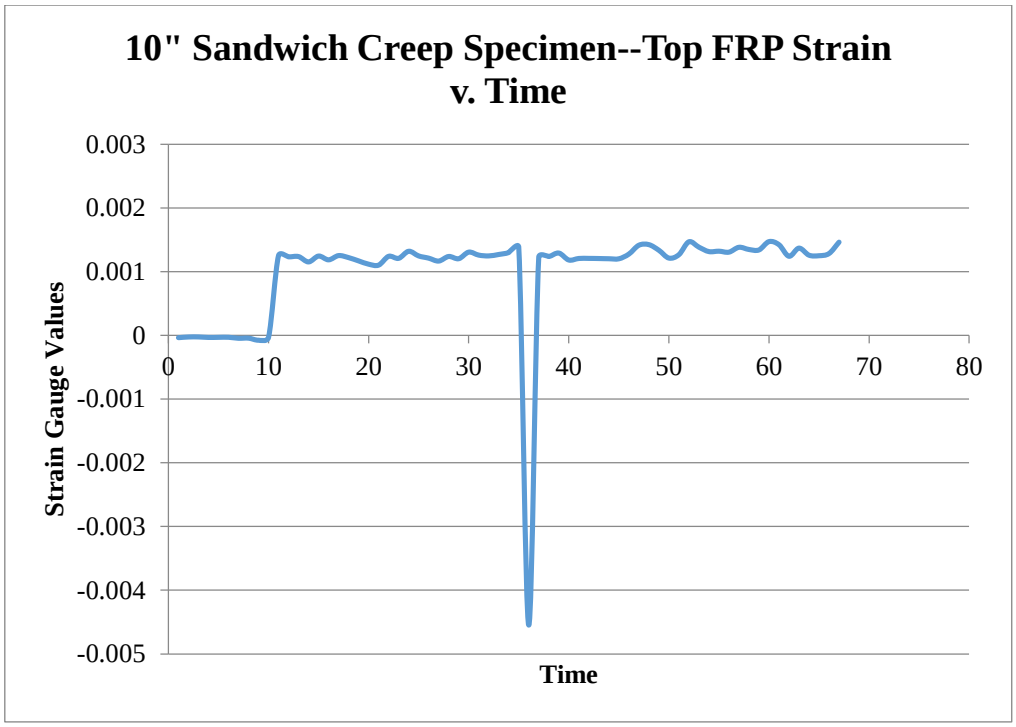


**Figure 283: 10” Sandwich Creep Specimen—Top FRP Strain v. Time**

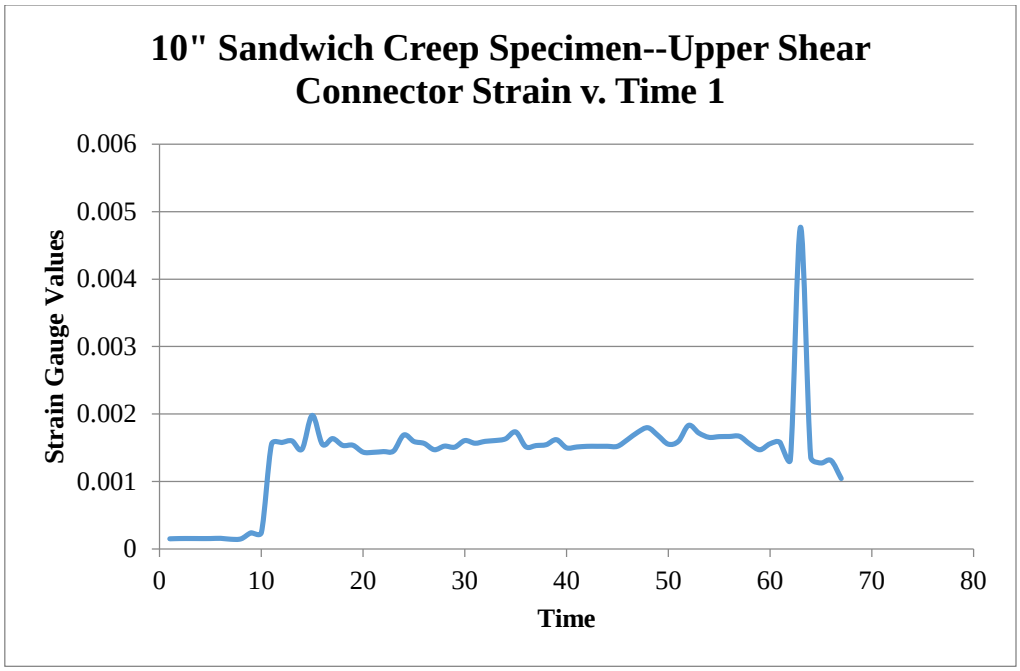


**Figure 284: 10" Sandwich Creep Specimen—Upper Shear Connector Strain v. Time 1**

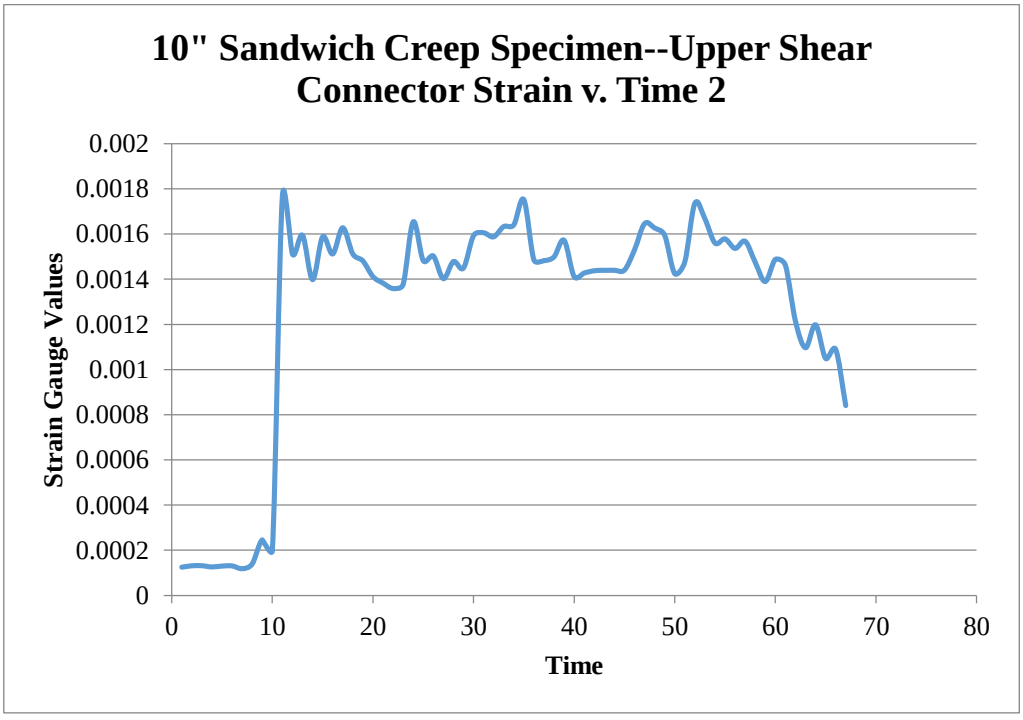


**Figure 285: 10" Sandwich Creep Specimen—Upper Shear Connector Strain v. Time 2**

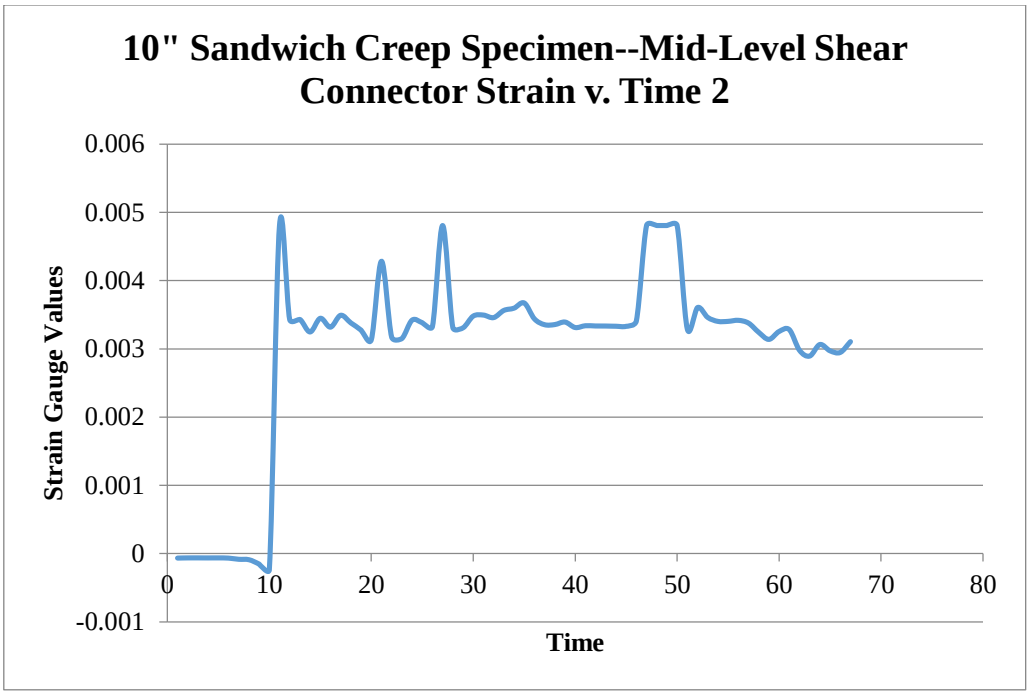


**Figure 286: 10" Sandwich Creep Specimen—Upper Shear Connector Strain v. Time 2**

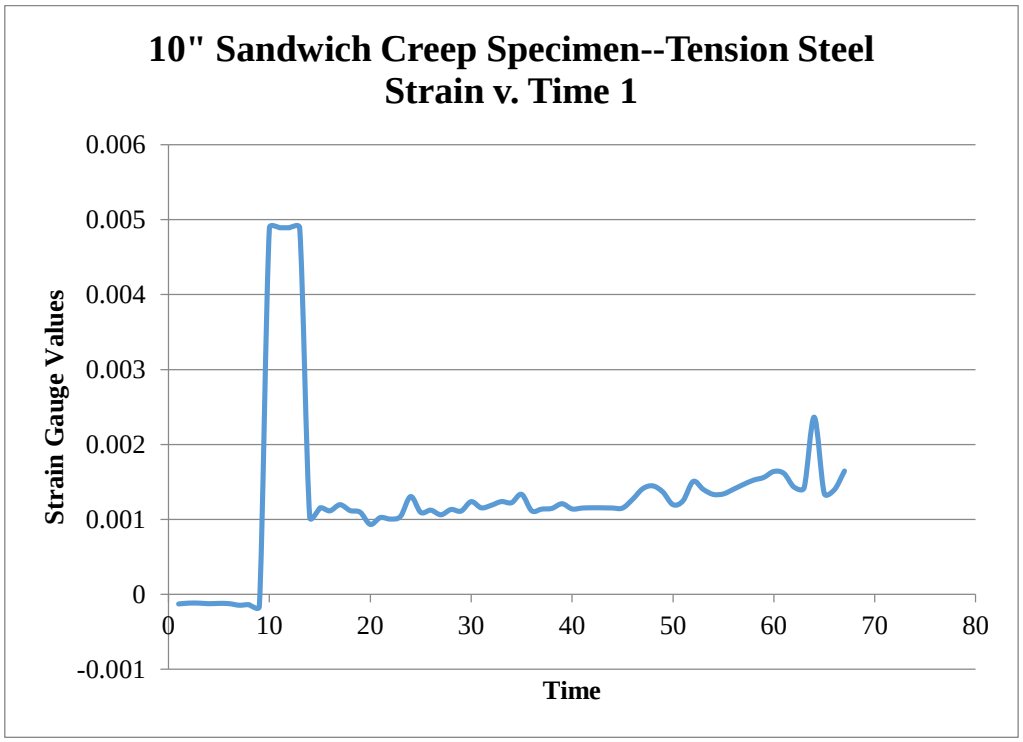


**Figure 287: 10" Sandwich Creep Specimen—Tension Steel Strain v. Time 1**

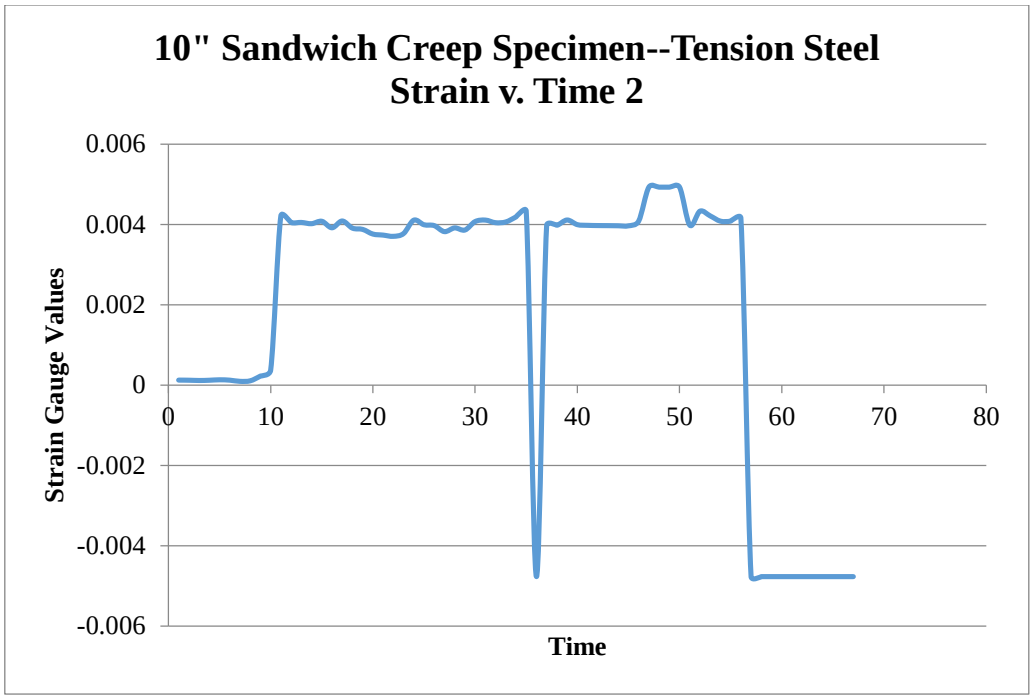


**Figure 288: 10" Creep Specimen—Tension Steel Strain v. Time 2**

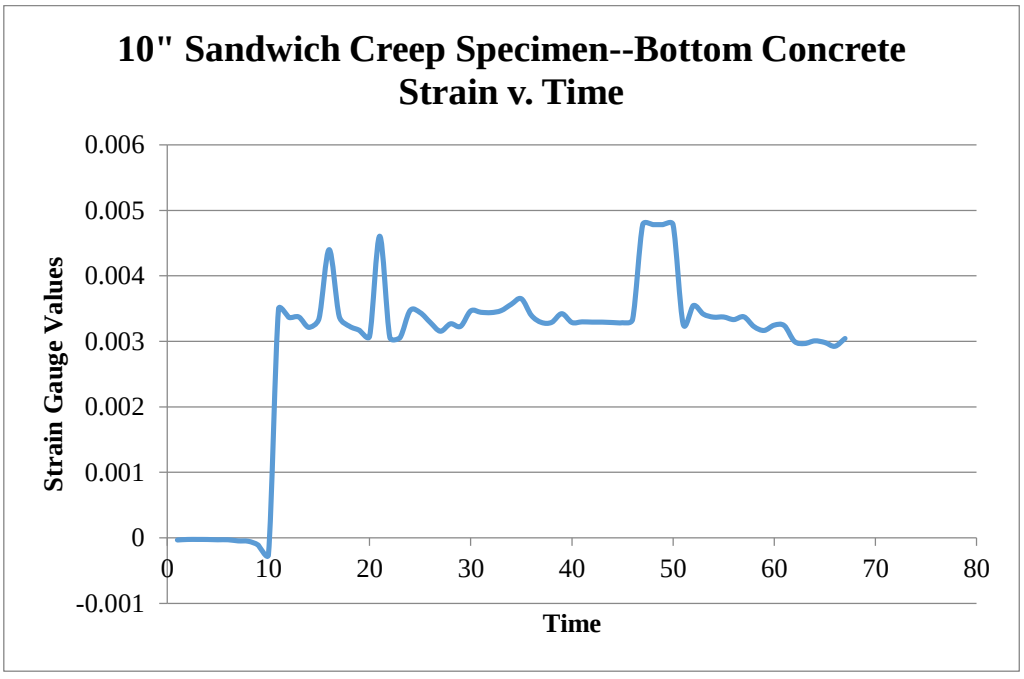


**Figure 289: 10" Sandwich Creep Specimen—Bottom Concrete Strain v. Time**

## 8” FPCS

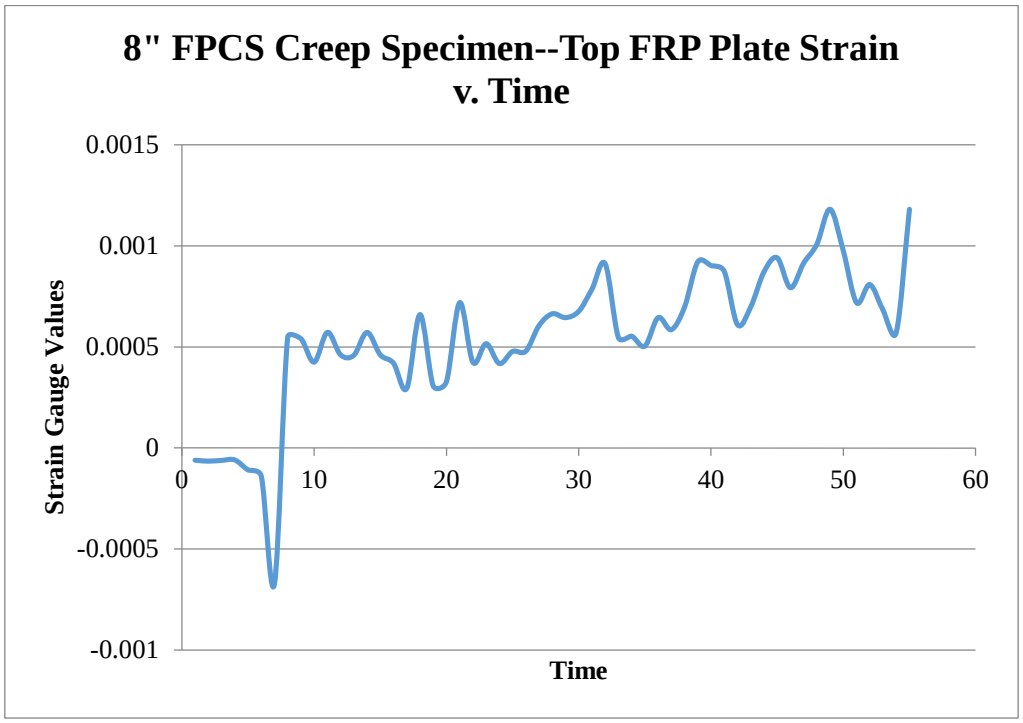


**Figure 290: 8” FPCS Creep Specimen—Top FRP Plate Strain v. Time**

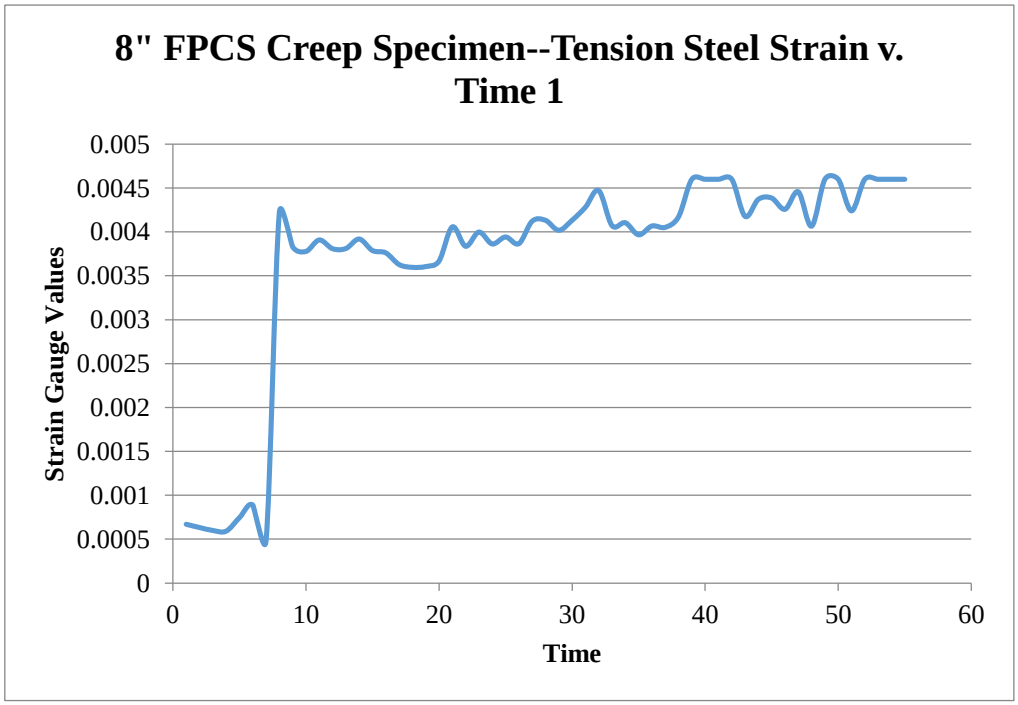


**Figure 291: 8”FPCS Creep Specimen—Tension Steel Strain v. Time 1**

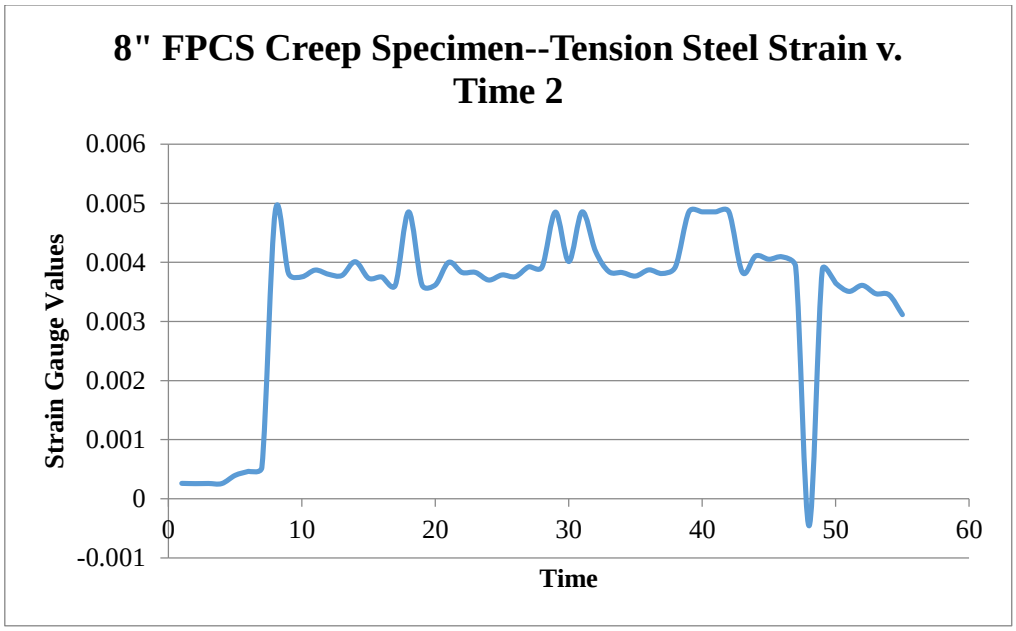


**Figure 292: 8" FPCS Creep Specimen—Tension Steel Strain v. Time 2**

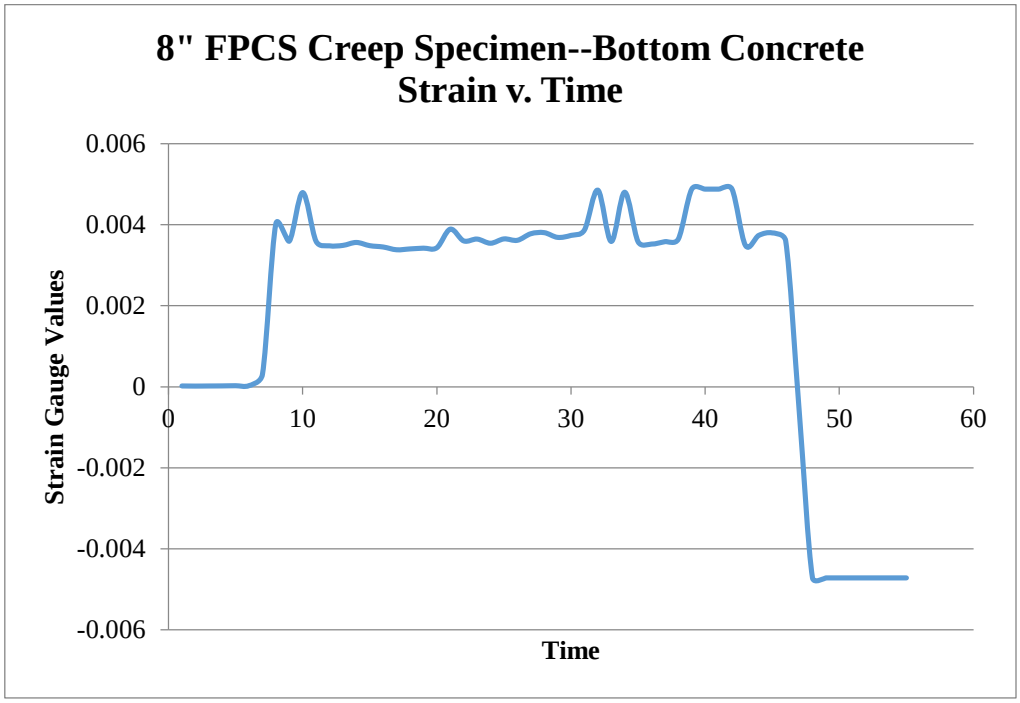


**Figure 293: 8" FPCS Creep Specimen—Bottom Concrete Strain v. Time**

## 10” FPCS

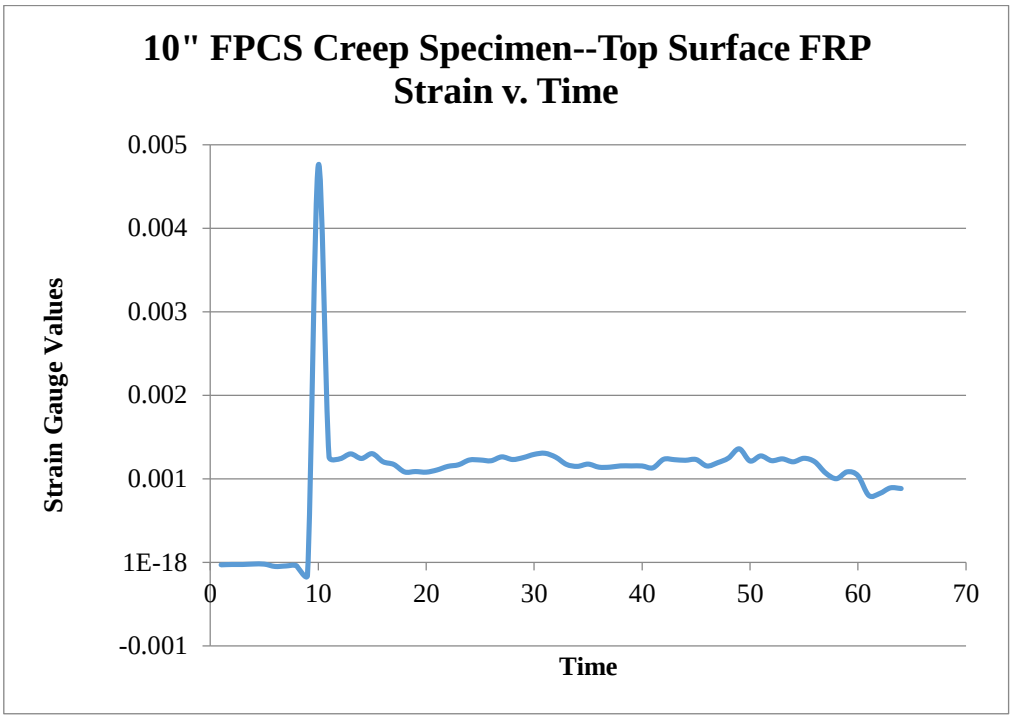


**Figure 294: 10” FPCS Creep Specimen—Top Surface FRP Strain v. Time**

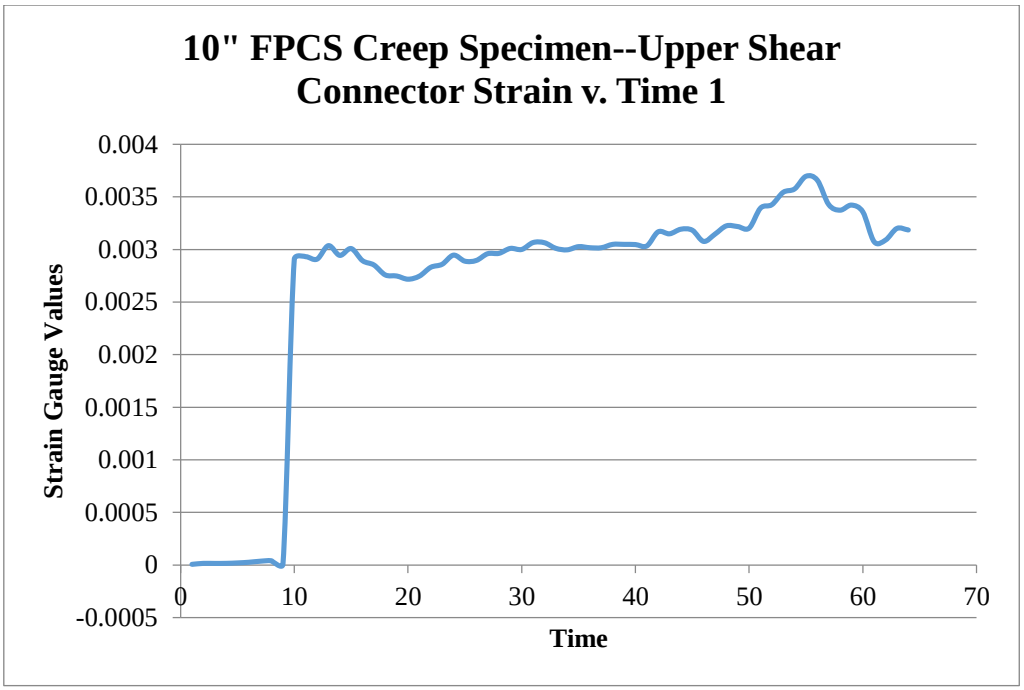


**Figure 295: 10” FPCS Creep Specimen—Upper Shear Connector Strain v. Time 1**

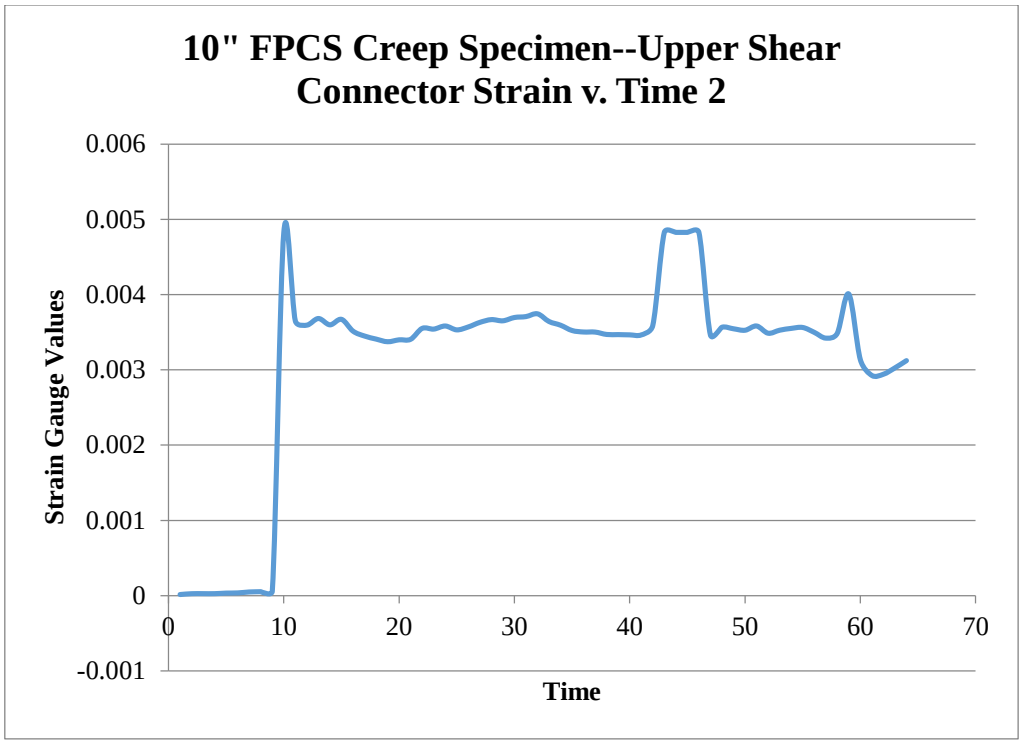


**Figure 296: 10" FPCS Creep Specimen—Upper Shear Connector Strain v. Time 2**

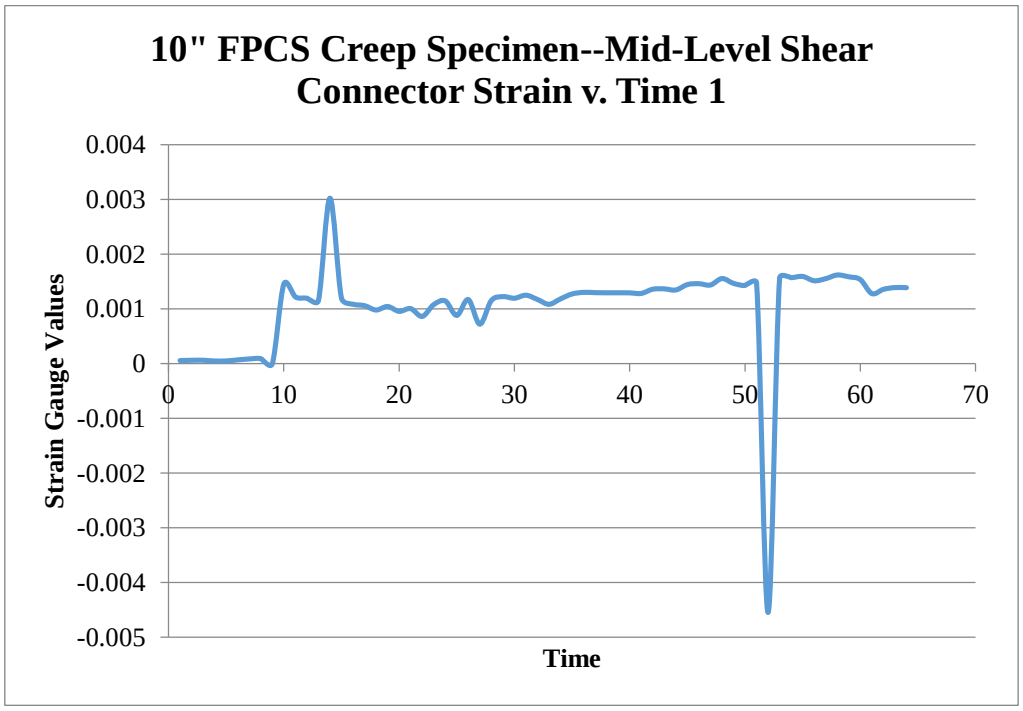


**Figure 297: 10" FPCS Creep Specimen—Mid-Level Shear Connector Strain v. Time 1**

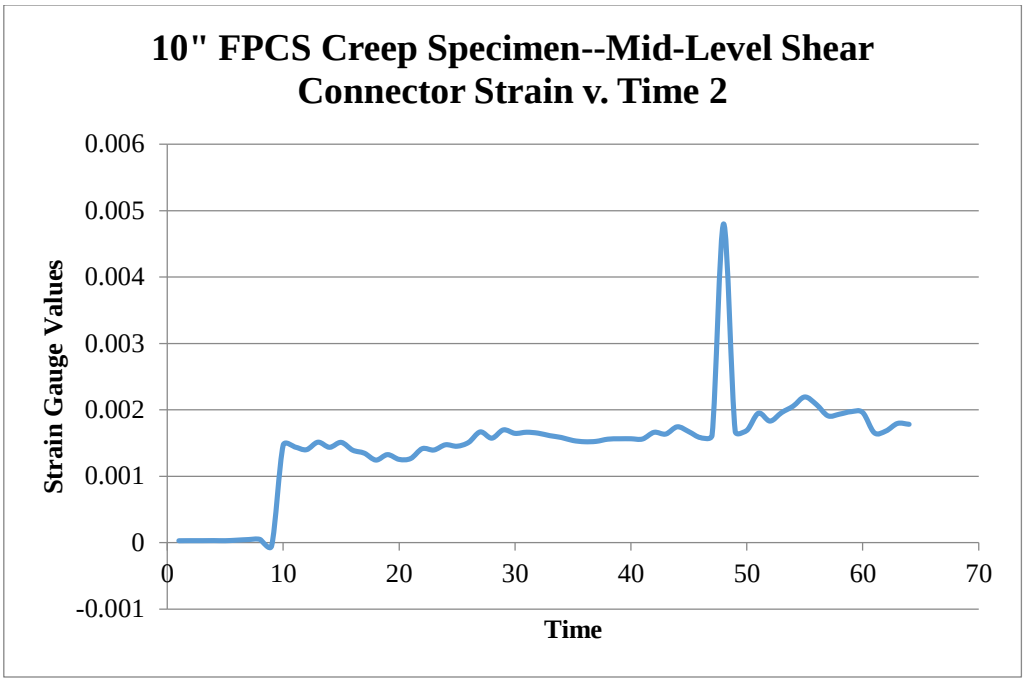


**Figure 298: 10” FPCS Creep Specimen—Mid-Level Shear Connector Strain v. Time 2**

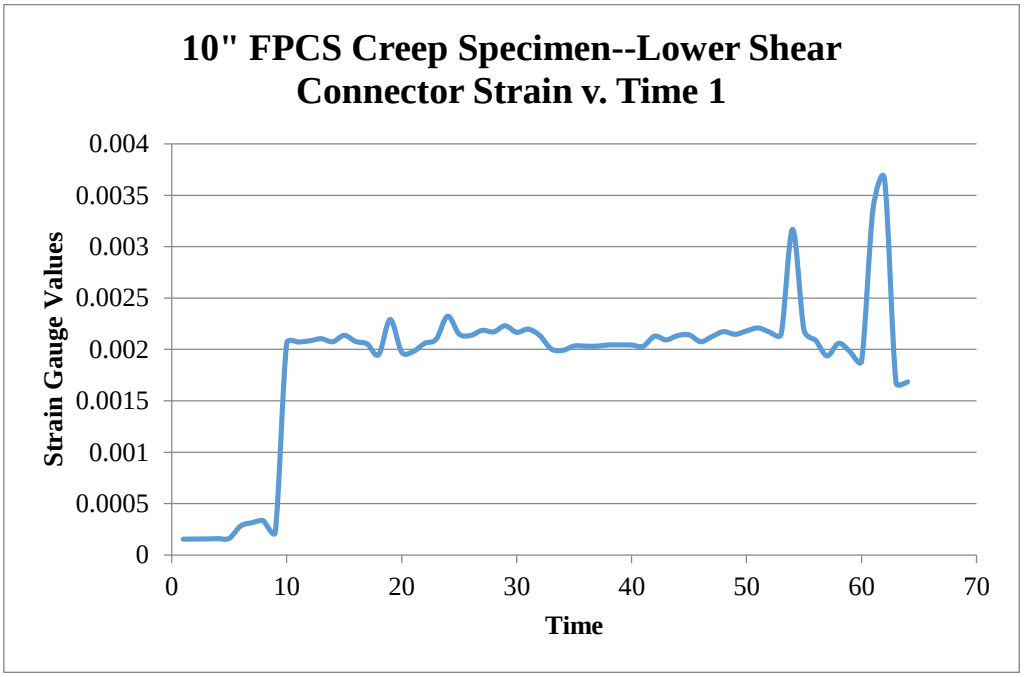


**Figure 299: 10” FPCS Creep Specimen—Lower Shear Connector Strain v. Time 1**

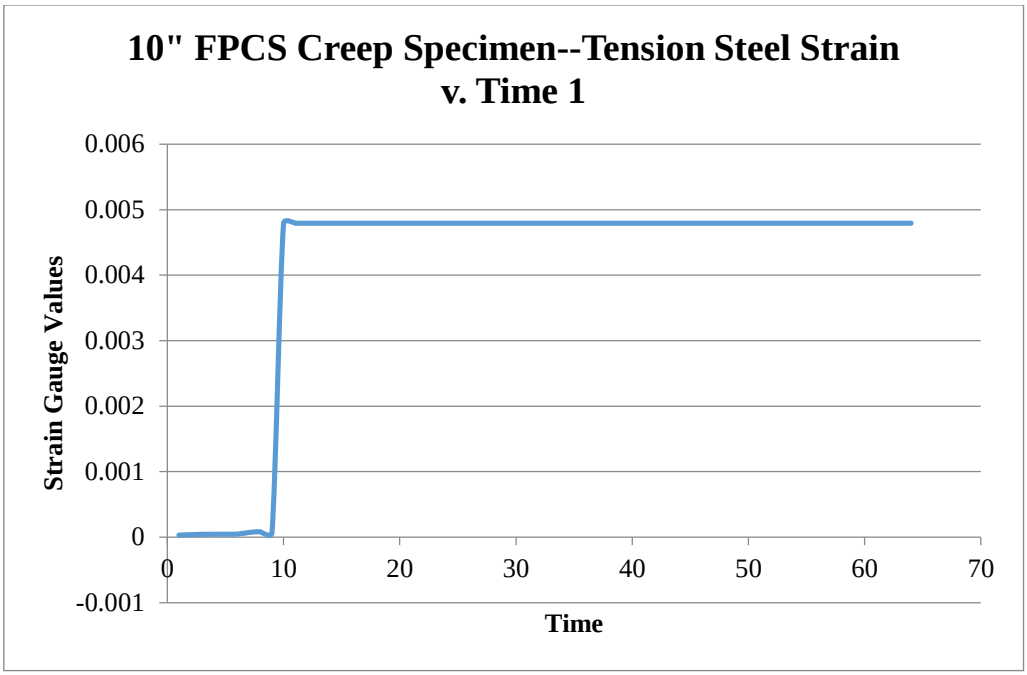


**Figure 300: 10" FPCS Creep Specimen—Tension Steel Strain v. Time 1**

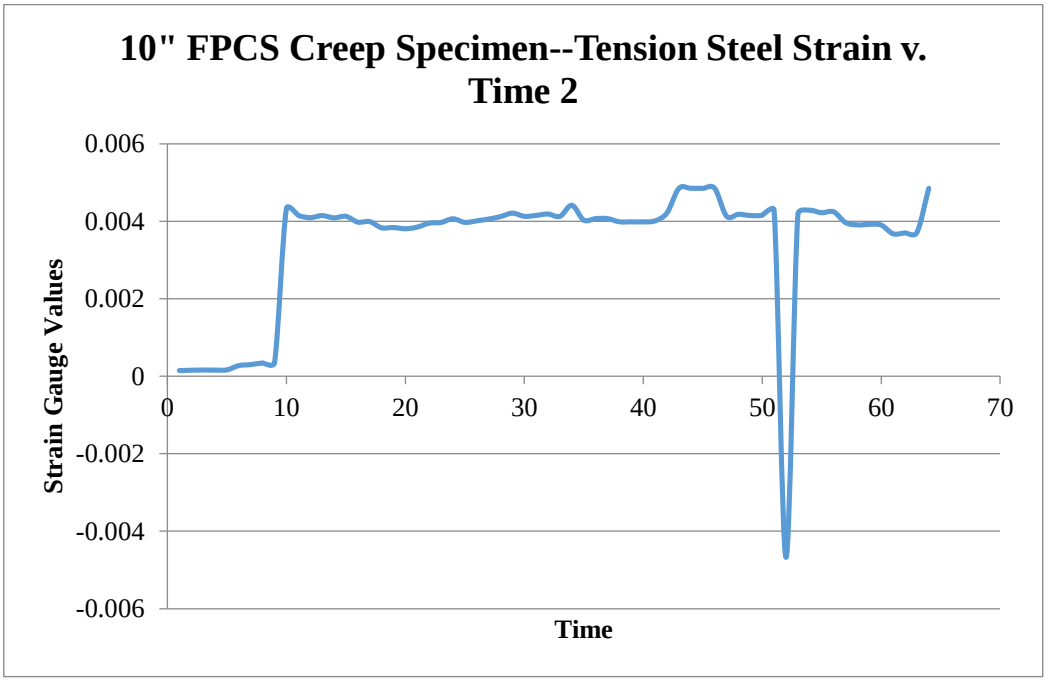


**Figure 301: 10" FPCS Creep Specimen—Tension Steel Strain v. Time 2**

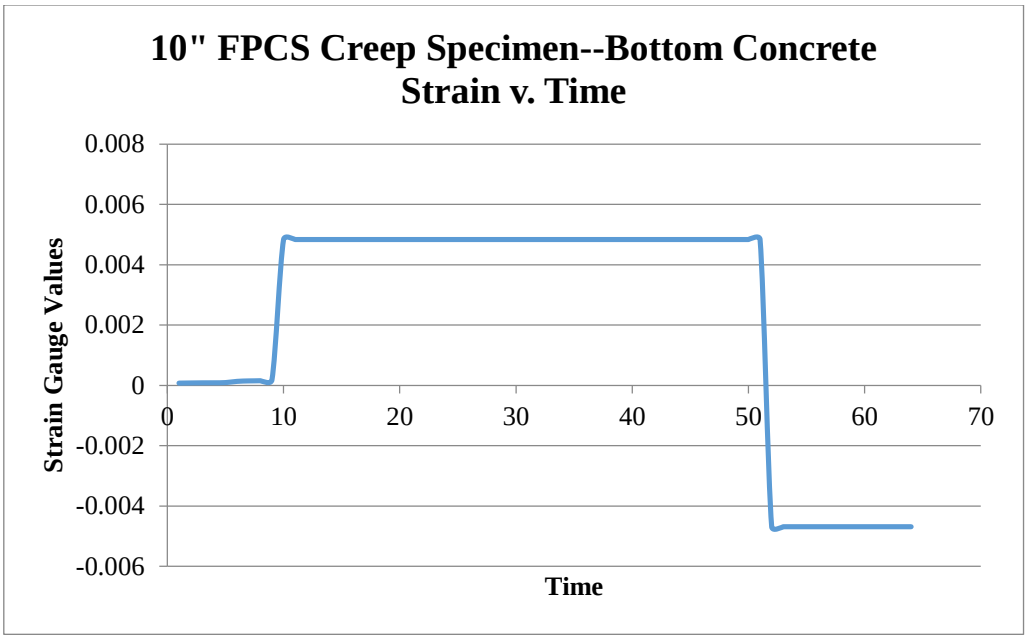


**Figure 302: 10" FPCS Creep Specimen—Bottom Concrete Strain v. Time**